Computational chemistry of organometallic and inorganic species

Thomas J. Davin

A Thesis submitted for the degree of Doctor of Philosophy

UNIVERSITY OF GLASGOW

DEPARTMENT OF CHEMISTRY

Submitted February 2009

Abstract

This thesis presents computational investigations of problems related to redox processes and structural rearrangement in inorganic systems. Density functional theory has been used to gain insight into the origin and nature of such reactions. The work presented concerns two main topics: hydrogenase-like systems containing an Fe_2 core and carbon-phosphorus cluster compounds. In chapters II and III, we describe the impact of reduction, an important phenomenon in the H_2 production catalytic cycle, on a hydrogenase-like model. In collaboration with Talarmin and co-workers who have conducted careful electrochemical studies, we have used DFT to identify structures of species observed in cyclic voltammetry. We have also studied the binding of a proton to similar systems and, through the calculation of chemical shifts and coupling constants, confirmed the structures of iron hydrides observed by ^{1}H NMR spectroscopy. In chapter V we focus on carbon-phosphorus systems that can exist in 2 or more isomeric forms. We address first the case of a system of formula $C_6H_4P_3$ which has the right valence configuration to exist either as a planar structure or as a 3-dimensional cluster (*nido* according to Wade's rules). We then examine whether it is possible to control the preferred conformation by the addition of substituents on the phenyl ring. Finally, we look at the rearrangement of a planar diphosphene into a cage isomer and try to understand the mechanism and in particular the role of the protonation in the conversion from planar to 3-dimensional structure.

Contents

Abstract i
List of figures ix
List of tables xi
Acknowledgements xii
Author's declaration xiii

Introduction **1**

Chapter I Elements of theory **5**

1 Hartree-Fock theory (HF) 9
2 Electron correlation 11
3 Density Functional Theory (DFT) 13
4 Functionals 17
5 Basis sets 21
6 Software 24
Bibliography 25

Chapter II Hydrogenase enzymes and their models: biological and chemical studies **27**

Bibliography 44

Chapter III Computational studies of hydrogenase-like models 49

Introduction . . . 49

1 Our work . . . 55

2 Validation of methodology . . . 58

Results . . . 60

1 Reduction of the Fe-Fe core . . . 62

a Reduction of [(Fe(CO)$_3$)$_2$(μ−(SRS))] . . . 62

b Impact of the solvation on the computational model . . . 66

c Use of NHC as an electron-donating ligand . . . 68

2 Electronic structure of the dianion in isomer C . . . 72

a AIM calculations . . . 74

3 Conclusion . . . 77

Bibliography . . . 79

Chapter IV Characterisation of iron hydride complexes through the computation of NMR parameters 81

Introduction . . . 81

1 Experimental basis . . . 81

2 Structures . . . 82

3 Development of the methodology for the calculation of NMR parameters . . . 86

a Brief overview of the theoretical background . . . 86

b Previous calculations of chemical shifts . . . 88

c Previous calculations of coupling constant . . . 92

4 Methodology . . . 96

Results . . . 98

1 Basis set choice . . . 98

2 Chemical shifts for isomers A, B, C and D 98
3 Coupling constants for A, B, C and D 101
4 Conclusion 105
Bibliography 106

Chapter V Carbon Phosphorus chemistry **109**

Introduction 109
1 P/C isolobal analogy 110
2 Multiple bonding in main group heavy elements 111
3 Multiple bonds to phosphorus 113
4 Theories of cluster bonding 122
Results 124
1 2D vs 3D isomerisation in P/C rings 124
a The aim of our work 124
b Validation of methodology 125
c Influence of substitution 127
d Conclusion 130
2 Rearrangement of P=P bonds 131
a Validation of methodology 132
b Mechanism in absence of proton 135
c Mechanism in presence of proton 137
d Solvation 137
e Conclusion 139
Bibliography 140

Appendix: Publications submitted up to this date **143**

List of Figures

Chapter I Elements of theory 5

I-1 SCF cycle involved in the Hartree-Fock method 11

I-2 Possible repartition of the electrons for the **S**ingle, **D**ouble and **T**riple virtual excitations 12

Chapter II Hydrogenase enzymes and their models: biological and chemical studies 27

II-1 X-ray structure of the *Desulfovibrio Desulfuricans* [Fe]only-hydrogenase enzyme. 30

II-2 The H-cluster in the *Clostridium pasteurianum* bacteria. 31

II-3 Catalytic cycle of the production/oxidation of H_2 as presented by Armstrong *et al.* and completed by Pachter and Trohalaki. 32

II-4 Different Fe-Fe model compounds synthesised by Rauchfuss (**I**, **V**, **VI**), Talarmin (**II**), Adams (**III**), Pickett (**IV**) and Song (**VII**) and their co-workers. 34

II-5 Asymmetry created in the molecule by the replacement of two CO ligands by a chelating dppe ligand. 36

II-6 S-to-S linking groups as synthesised by Pickett (**I**), Talarmin (**II**), Sun (**III**) and Rauchfuss (**IV**, **V** and **VI**) and their co-workers. . . . 38

II-7 "Rotated" and "unrotated" structures. 38

II-8 Oxidation states of the iron centres during the catalytic process as proposed by Darensbourg and co-workers. 40
II-9 Two examples of hypothetical catalytic cycles for the formation/oxidation of H_2 42

Chapter III Computational studies of hydrogenase-like models 49

III-1 Proposed computed Catalytic cycle summarised from De Gioia *et al.*, Liu and Hu, Fan and Hall and Zampella *et al.* work. 50
III-2 Reduction of the Fe-Fe bond due to the reduction of the hydrogenase-like system. 52
III-3 Computational models of Hall and Hu which match closely the experimental data for H_{ox}^{inact}, H_{ox} and H_{red} forms of the $[Fe_2S_2]_H$ cluster. 53
III-4 Influence of the presence of the N as a bridgehead for the channeling of hydrogen. 54
III-5 The possible positioning of the dppe di-chelating ligand: apical-basal and basal-basal. 54
III-6 Structures studied by Talarmin and Rauchfuss and their respective co-workers. 55
III-7 Cyclic voltammetry of complexes $Fe_2(CO)_6(\mu-SRS)$ in MeCN-$[NBu_4]$-$[PF_6]$ under CO at 40 $V.s^{-1}$ scan rate (**III**, R=$CH_2N((CH_2)_2OMe)$-CH_2 and **I**, R=$(CH_2)_3$). 56
III-8 Reduction reaction and the side products. 57
III-9 $[Fe_2(CO)_6(\mu-CO)(\mu-S(CH_2)_3SH)]^-$ as observed by Pickett *et al.* with IR. 57
III-10 Comparison of different possible bridgeheads for the neutral species. 61
III-11 Comparison of different possible bridgehead for the anion and dianion species. 63
III-12 The isomers **A**, **B** and **C** of $Fe_2(CO)_6(\mu-SCH_2N((CH_2)_2OMe)CH_2S)$. 64

III-13 Comparison of the energies of $[Fe_2(CO)_6(\mu{-}SCH_2N((CH_2)_2OMe)CH_2S)]$ (**III**) for different isomers and redox states. 65
III-14 Structure of $[Fe_2(CO)_5L_{NHC}(\mu{-}pdt)]$ with L_{NHC} = 2,4,6-trimethylphenyl, methyl or H. 68
III-15 Comparison of structural parameters for isomers **A**, **B** and **C** for the dianion species of compounds **I**, **II** and **III** where one of the CO is replaced by a NHC ligand (bond lengths in Å). 70
III-16 Calculation of $[Fe_2(CO)_6(\mu{-}SH)]^-$ singlet and triplet for the CO-bridged and non-CO-bridged compounds. 73
III-17 Evolution of the Fe-Fe bond length and the energy of the system with the increase of the Fe-O bond length. 75
III-18 AIM analysis of the Cr-Cr bond in the two Cr-C simple bond plan . 76
III-19 AIM analysis of the Fe-Fe bond in the Fe-$C_{(bonding)}$-Fe plan and in the Fe-S-Fe plan 77

Chapter IV Characterisation of iron hydride complexes through the computation of NMR parameters 81

IV-1 Conformations induced by the replacement of 2 CO by a dppe. . . . 82
IV-2 NMR spectra obtained by Schollhammer and co-workers and corresponding proposed structures (at 223K). 83
IV-3 Systems for which hydride NMR chemical shift have been calculated by Best *et al.*. 91
IV-4 Compounds for which $J_{H\text{-}H}$ coupling constants have been calculated by Autschbach and Mort. 94
IV-5 Comparison of the stabilities between the two possible isomers for **C**: basal-basal and basal-apical. 101
IV-6 Two iron hydrides with two different groups in trans synthesised and resolved by NMR spectroscopy by Duckett and co-workers. . . . 104

IV-7 Comparison of the chemical shift of hydrides in trans of a CO or P group between experiment done by Duckett *et al.* and our calculations. 105

Chapter V Carbon Phosphorus chemistry 109

V-1 Frontier molecular orbitals of P, CH, CH_2 and CH_3 fragments. . . . 110

V-2 Description of planar and trans-bent structures. 111

V-3 Comparison of H_2XXH_2 structures for X=C and M=Si,Ge,Sn. . . . 112

V-4 Orbital diagram presenting the switch from alkene (D_{2h}) to disilene (D_{2h} or C_{2h} for $H_2Si{=}SiH_2$) species. 114

V-5 Orbital diagram presenting the switch from alkyne ($D_{\infty h}$) to disilyne (C_{2h}) species. 115

V-6 Donor-acceptor system to describe the Si≡Si triple bond as proposed by Frenking *et al.*. 115

V-7 Two possible conformations a silene can adopt. 116

V-8 The three possible isomers that a compound of formula P_2H_2 can adopt. 116

V-9 Comparison of frontier orbitals for double bond between same elements of group 15 (N=N and P=P). 117

V-10 Highest occupied molecular orbitals of imine and phosphaethylene as described by Lacombe *et al.*. 118

V-11 Comparison of the HOMOs and LUMOs for structurally close double bonded systems. 119

V-12 Potential isomeric structures for benzene and phosphinine structures: Benzene (**B**), Benzvalene (**V**), Dewar benzene (**D**), Prismane (**P**) and Bicycloprpenyl (**C**). 120

V-13 The pyramidal and planar phospholes conformations (R= $CH_2(C_6H_5)$ or $CH(CH_3)_2$). 121

V-14 Borane examples of *closo*, *nido* and *arachno* deltahedra. 122

V-15 Isolobality between organic and organometallic fragments. 123

V-16 Pyramidal and planar structure of $[H_2C_2P_3]^+$ and $[C_6H_4P_3]^+$. . . . 124

V-17 The total potential energy surface for the isomerisation of $C_6H_4P_3$. . 126
V-18 Distortion mechanism of the original structure, **B** and the potential positions for substituents (position 3 and 4). 127
V-19 Optimised structures of substituted species $[R{-}C_6H_3P_3]^+$ (PBE1PBE/6-311G(2df) on P and 6-311G(d) on other). 129
V-20 Conversion of **1** (**1-H**$^+$) into **3** (**3-H**$^+$). 131
V-21 Mechanism proposed by Russell *et al.*. 132
V-22 Potential energy surface of the rearrangement reaction. 134
V-23 Proposed mechanism of the potential rearrangement from compound **1** to **3**. 135
V-24 Representation of the HOMO-1 (C_1, C_2 and C_3 delocalisation) and the LUMO (localisation on the P_{12}) for the compound **2** in absence of H^+. 135
V-25 Evolution of the $C_3{-}C_6$ and $C_{10}{-}P_{12}$ bond lengths during the transition state between **2** and **3**. 136
V-26 Possible rearrangement from **1** to **3** deduced from calculations. . . . 137
V-27 Comparison between solvated and gas phase pathway including the non-protonated starting and ending compound. 138

List of Tables

Chapter I Elements of theory 5

Chapter II Hydrogenase enzymes and their models: biological and chemical studies 27

Chapter III Computational studies of hydrogenase-like models 49

III-1 Basis set/functional comparison for $[Fe_2(CO)_6(\mu-pdt)]$. 59

III-2 Energies of the different isomers of $Fe_2(CO)_6(\mu-SCH_2N((CH_2)_2OMe)-CH_2S-)$ (**A**, **B** and **C**) for different charges (anion and dianion) and different bridgeheads ($N(CH_2)_2OMe$, NH and CH_2). 64

III-3 Relative energies of anion and dianion for the different isomers (**A**, **B** and **C**) solvated. 67

III-4 Comparison of the stabilisation of the dianion species for different bridgehead by replacing a CO by a NHC ligand. 69

III-5 Bond length comparison for $[Fe_2(CO)_5L(\mu-SCH_2RCH_2S)]^{2-}$. 71

III-6 Effects of the reduction/elongation of the Fe-O bond. 74

Chapter IV Characterisation of iron hydride complexes through the computation of NMR parameters 81

IV-1 Energies of the different di-iron model isomers (B3LYP and SDD(Fe) / SVP (others)). 83

IV-2 Comparison between bond lengths obtained computationally and experimentally. 85

IV-3 Comparison of Experimental and calculated chemical shift for transition metal hydrides as proposed by Ziegler and Jolibois and their respective co-workers. 90

IV-4 Participation of the Fermi-contact part in the ^{2}J coupling constant as reported in Elguero and Alkorta review. 93

IV-5 Calculated coupling constants, $J_{H\text{-}H}$ compared to experimental data for hydrogen and hydride ligands as presented by Autschbach and Mort. 94

IV-6 NMR calculations with different basis sets compared to experimental NMR spectra. 100

IV-7 Effect of bond and angle change on the NMR parameters calculated for isomer **B**. 103

Chapter V Carbon Phosphorus chemistry 109

V-1 Comparison of the stability of different possible conformation for P_2H_2 as calculated by Allen *et al.*. 116

V-2 Stability comparison between the different potential isomer for phosphinines and benzene species. 120

V-3 Comparison of the bond length obtained through computational optimisation with experimental results for compound **3**. 133

Acknowledgements

I want above everybody else, to thank my supervisor, professor John McGrady, without who nothing would have been possible. I would like to thank him for all the help and the advice he provided me as well as for his patience and the efforts he put into bringing me where I am now. I would also like to thank Dimitrios Pantazis for all his advice and for all the help he generously provided me. I am also thankful to the people of John McGrady's group, past and present, and Hans Martin Senn's group who have all brought something to help me in my progresses (Anna Anastasi, Charlotte Elkington, Evdokyia "Eva" Salamanova, Vihar Georgiev). I would also like to acknowledge the person without who, I would never have been able to obtain this PhD: Dr. Karine Costuas, who also continued to help me during my PhD. I would also like to thank Professor Abdou Boucekhine, who made me discover computational chemistry and appreciate it.

Finally, I would also like to thank the persons who are not related to the chemistry world but whose presence has contributed to my work and to where I am today. They all brought something to me during these three years which helps me overcome the obstacles raised during my PhD. I would like to start to thank my parents who have always been of great advice and always there to support me. Many times they made me realise that things where not as bad as I may have first thought. I am also thankful to sensei Holland, sensei Kearney and the University of Glasgow aikido club members as well as sensei MacKay of the University of Glasgow karate club, who have helped me to develop myself and become who I am today. They kept me sane, released my frustration and kept me smiling when things at work were not great. Last but not least, I would like to thank a thousand times Tracy "pokey" Cooper for her help, her advice and to have always been there when I needed it the most.

It is thanks to all these people that these three years were, for me, a personal achievement.

Author's declaration

The work presented in this thesis is the original work of the author, except where references have been made to other sources. No part of this work has previously been submitted for any other degree.

Thomas J. Davin

Pour mes parents, Béatrice et Myrian DAVIN.

INTRODUCTION

In this thesis, we describe computational studies of organometallic and inorganic systems which undergo redox process, structural rearrangement and/or protonation. More precisely, we use quantum chemical methods in order to investigate the structural modifications of systems resulting from reduction, protonation or the addition of substituents. Although the use of computational methods for most of these calculations is now to a certain extent fairly common, it always necessitates an adaptation of the techniques to the problem at hand coupled with the search for an efficient treatment of the system. Over the last decade, density functional theory, has proved to be an effective tool for exploring inorganic reaction mechanisms. Recent development of methods and computer architectures have allowed the modelling of more and more complex and larger and larger systems which were considered intractable a decade ago. The modern implementation of density functional theory forms the basis of all the computational studies presented in this thesis.

In chapter I, we give a brief review of the theoretical methods most often used in computational studies. Starting from the Schrödinger equation we establish the basis of Hartree-Fock and Density Functional Theory and the description of functionals and basis sets associated with the use of these methods. After this brief overview of the theoretical methods, the topics covered in this thesis will be presented in four chapters, the first three being linked to the structures of di-iron systems. The

last chapter is independent from the previous ones, and deals with isomerisms in carbon-phosphorus systems. The chapters are organised as follows:

In Chapter II, we give a brief overview of the hydrogenase active core in its biological environment because it will be the focus of the next two chapters. We describe the distribution, structure and biochemical role of the hydrogenase enzymes, focussing on their active core, the "H-cluster" and more particularly, its organometallic part which is the centre of the catalytic process. We survey the possible composition of its active site and then discuss the proposed biological pathway for the catalysis of H_2 production. Then we review experimental studies on model compounds similar to the hydrogenase active core $[Fe_2S_2]_H$ cluster. We then review the electrochemical studies done on these systems, considering first the behaviour of iron centres during the reduction, then the positioning of the protons on the structure. Finally, we describe the reversible catalytic pathways that have been proposed for the production/oxidation of H_2.

Chapter III describes our computational studies on the Fe_2 model systems. We first review computational studies done over the last decade starting by the proposed catalytic cycles that have emerged from these studies. Then we focus on computational studies regarding the reduction of this system and on the studies done on the three most important states of the catalyst during the catalytic pathway.

We then present our results, done in collaboration with the Talarmin group, in Brest, who have conducted detailed electrochemical measurements. We present first a Fe_2 compound and discuss the outcome of 1- and 2-electron reduction. Somewhat surprisingly, we do not observe cleavage of the Fe-Fe bond, but rather a more complex structural rearrangement introducing a Fe-S bond cleavage. This work has been published in the *New Journal of Chemistry*.

In chapter IV we present a description of experimental studies done by Schollhammer and co-workers, in Brest, on systems similar to those seen in the previous two chapters. They have synthesised and protonated an asymmetric Fe_2 model species and observed, using NMR spectroscopy, a number of isomeric hydride species. We use theory to validate and, in some cases, challenge the structures proposed by Schollhammer *et al.* based on these NMR studies. By computing energies, ^{1}H chemical shifts and $^{31}P-^1H$ coupling constants, we are able to systematically evaluate various candidate structures.

Finally, in chapter V we present a short overview of multiple bonding in group 14 and 15 elements. The results in this chapter are divided into two distinct projects, both of which have been done in collaboration with the Russell group in Bristol.

The first part describes an analysis of structural preferences in carbon-phosphorus systems. The systems in question have the correct valence electron configuration to adopt either a planar structure or a 3-dimensional cluster geometry (*nido* cluster by Wade's rules). We explore the factors that determine the structural preference, and the impact of substitution on it.

The second project is an investigation of the rearrangement of a planar diphosphene, $Me_5C_5P{=}PC_5Me_5$ into a 3-dimensional cage. We explore the critical role of protonation in catalysing this rearrangement. This has been published in the *European Journal of Inorganic Chemistry*.

Chapters I and V are self-contained, while Chapters II, III and IV are related. Chapter II stands as a general introduction for Chapter III and IV. All chapters, except Chapters I and II, contain a detailed introduction to the particular topic which provides general background information and more specific details concerning studies done previously on the same topic. It is followed by the description of the methodological choices for the particular studies presented in each chapter. Finally,

a complete review of the researches we have done is presented and results are given as well as discussions and conclusions drawn from them.

CHAPTER I

Elements of theory

The foundation of theoretical chemistry is the Schrödinger equation:

$$\widehat{H}\,\Psi \;=\; E\,\Psi \tag{I-1}$$

where $\widehat{H}$ is the Hamiltonian operator, Ψ is the wavefunction (eigenfunction for a given Hamiltonian) and E is the energy of the system. The wavefunction Ψ describes the system and takes as variables the positions of electrons and nuclei in the system, leading to the following equation:

$$\widehat{H}\,\Psi_i(\vec{x_1},\ldots,\vec{x_N},\vec{R_1},\ldots,\vec{R_M}) \;=\; E\,\Psi_i(\vec{x_1},\ldots,\vec{x_N},\vec{R_1},\ldots,\vec{R_M}) \tag{I-2}$$

$\vec{x_N}$ describing the positions of the electrons, N and $\vec{R_M}$ describing the positions of the nuclei, M. A knowledge of Ψ allows the properties of the system to be deduced.

The wavefunctions is chosen to be orthogonal and normalised (orthonormal) over all space, i.e.:

$$<\Psi_i\,|\,\Psi_j>=\;\delta_{ij} \tag{I-3}$$

where δ_{ij} is the Kronecker symbol and takes for value:

$$\delta_{ij} = 1 \quad \text{if} \quad i = j \tag{I-4}$$

$$\delta_{ij} = 0 \quad \text{if} \quad i \neq j \tag{I-5}$$

The first step for solving the Schrödinger equation is to establish the form of the Hamiltonian operator.

$$H = T_e + T_n + V_{ne} + V_{ee} + V_{nn} \tag{I-6}$$

where T_e and T_n are the kinetic energy terms for the electrons and the nuclei respectively; V_{ne} represents the attractive potential between electrons and nuclei, and V_{ee} and V_{nn} the inter-electronic and inter-nuclear repulsion potentials. The different terms of this equation can be developed as following:

$$\widehat{T}_e = -\frac{1}{2}\sum_{i=1}^{N}\nabla_i^2 \quad ; \quad \widehat{T}_n = -\frac{1}{2}\sum_{A=1}^{M}\frac{1}{M_A}\nabla_A^2$$

$$\widehat{V}_{ne} = -\sum_{i=1}^{N}\sum_{A=1}^{M}\frac{Z_A}{r_{iA}}$$

$$\widehat{V}_{ee} = \sum_{i=1}^{N}\sum_{j>i}^{N}\frac{1}{r_{ij}} \quad ; \quad \widehat{V}_{nn} = \sum_{A=1}^{M}\sum_{B>A}^{M}\frac{Z_A Z_B}{R_{AB}}$$

So H can now be written :

$$H = -\frac{1}{2}\sum_{i=1}^{N}\nabla_i^2 - \frac{1}{2}\sum_{A=1}^{M}\frac{1}{M_A}\nabla_A^2 - \sum_{i=1}^{N}\sum_{A=1}^{M}\frac{Z_A}{r_{iA}} + \sum_{i=1}^{N}\sum_{j>i}^{N}\frac{1}{r_{ij}} + \sum_{A=1}^{M}\sum_{B>A}^{M}\frac{Z_A Z_B}{R_{AB}} \tag{I-7}$$

where A and B denote the M nuclei and i and j the N electrons of the system.

The Born-Oppenheimer approximation

As noted previously, the wavefunctions Ψ are functions of the position of both the nuclei and the electrons of the system. However, since a nucleus is much heavier than an electron (approximately 1900 times more), its movements compared to the

electrons are negligible. In this case, they can be considered to be frozen and their kinetic energy set to zero but they still contribute to the potential energy of the system. Ψ is now only dependent on the kinetic energy of the electrons (T_e), the electron-nuclear attraction (V_{ne}) and the electron-electron repulsion (V_{ee}), so the Hamiltonian becomes:

$$\widehat{H} = -\frac{1}{2}\sum_{i=1}^{N}\nabla_i^2 - \sum_{i=1}^{N}\sum_{A=1}^{M}\frac{Z_A}{r_{iA}} + \sum_{i=1}^{N}\sum_{j>i}^{N}\frac{1}{r_{ij}} + V_{nn} \tag{I-8}$$

where V_{nn} represents the nucleus-nucleus repulsion and is a constant. We see that **I-8** is factorisable.

$$\widehat{H}_{elec} = \sum_i \left(-\frac{1}{2}\nabla_i^2 - \sum_A \frac{Z_A}{r_{iA}} + \sum_{j>i}\frac{1}{r_{ij}} \right) \tag{I-9}$$

And the wavefunction depends now only on the electronic coordinates:

$$H_{elec}\,\Psi_{i(elec)}(\vec{x_1},\vec{x_2},\ldots,\vec{x_i},\vec{x_j},\ldots,\vec{x_N}) = E_{elec}\,\Psi_{i(elec)}(\vec{x_1},\vec{x_2},\ldots,\vec{x_i},\vec{x_j},\ldots,\vec{x_N}) \tag{I-10}$$

The electrons are also described by their spin quantum number. This spin can take two values, $-1/2$ or $1/2$, that are defined by the alignment of the spin with respect to an arbitrary axis. These two types of spin are called α and β (by convention α and β are the spinfunctions for $m_s = +1/2$ and $-1/2$, respectively) and are orthonormalised:

$$< \alpha \,|\, \alpha > = < \beta \,|\, \beta > = 1$$

$$< \alpha \,|\, \beta > = < \beta \,|\, \alpha > = 0$$

The wavefunction is described by both a spatial component and a spin component:

$$\Psi(\vec{x}) = \psi(\vec{r}).\sigma \quad \sigma = \alpha \,\text{or}\, \beta \tag{I-11}$$

The Slater determinant

The antisymmetry principle The wavefunction Ψ is not observable itself but the expression

$$\left|\Psi(\vec{x_1},\vec{x_2},\ldots,\vec{x_N})\right|^2 d\vec{x_1}d\vec{x_2}\ldots d\vec{x_N} \tag{I-12}$$

where $d\vec{x_1}d\vec{x_2}\ldots$ is a small volume represents the probability of finding an electron at a given point in space. The electrons being indistinguishable, the exchange of two electrons doesn't change the probability:

$$\left|\Psi(\vec{x_1},\vec{x_2},\ldots,\vec{x_i},\vec{x_j},\ldots,\vec{x_N})\right|^2 = \left|\Psi(\vec{x_1},\vec{x_2},\ldots,\vec{x_j},\vec{x_i},\ldots,\vec{x_N})\right|^2 \tag{I-13}$$

However, the exchange of two electrons leads to a change of sign of the wavefunction, i.e. Ψ is antisymmetric with respect to electron change. This represents the quantum-mechanical generalisation of the Pauli's exclusion principle ('no two electrons can occupy the same state').

The exact wavefunction is unknown, so it is necessary to generate a trial wavefunction which obeys this antisymmetry principle. To do so, the N-electron wavefunction is expressed as an antisymmetric product of N one-electron wavefunctions $\chi_i(\vec{x_i})$. This product is denoted Φ_{SD} and is referred to as Slater determinant:

$$\Phi_{SD} = \frac{1}{\sqrt{N!}}\begin{vmatrix} \chi_1(\vec{x_1}) & \chi_2(\vec{x_1}) & \ldots & \chi_N(\vec{x_1}) \\ \chi_1(\vec{x_2}) & \chi_2(\vec{x_2}) & \ldots & \chi_N(\vec{x_2}) \\ \vdots & \vdots & \ddots & \vdots \\ \chi_1(\vec{x_N}) & \chi_2(\vec{x_N}) & \ldots & \chi_N(\vec{x_N}) \end{vmatrix} \tag{I-14}$$

The columns are single electron wavefunctions (orbitals), $\chi(\vec{x})$ while the rows are the electron indices.

Variational method

To solve equation **I-10** the variational method (Rayleigh-Ritz variational method) is used.

The variational theorem states that the value calculated for the total energy of a trial wavefunction can only be greater than or equal to the ground-state energy, E_0.

$$E = < \Psi | H | \Psi > \geq E_0 \tag{I-15}$$

This method provides a criterion for establishing the "best" wavefunction, subject to a given set of constants. From now, the two methods based on the variational method (the Hartree-Fock method and Density functional theory) will be described.

1 - Hartree-Fock theory (HF)

In the Hartree-Fock method, the Hamiltonian can be divided into two parts: a core Hamiltonian H_i^c describing the kinetic energy and the electron-nuclei attraction potential and a part describing the electron-electron repulsion:

$$H = \sum_i \left[H^c(i) + \sum_{j>i} \frac{1}{r_{ij}} \right] \qquad \text{with } H^c(i) = -\frac{1}{2}\nabla_i^2 - \sum_A \frac{Z_A}{r_{iA}} \tag{I-16}$$

The core Hamiltonian can be solved exactly whereas the electron-electron repulsion part can only be treated in an average way, i.e. each electron is considered to be moving independently of the others in an average field created by the other electrons.

By applying the variational method to a single Slater determinant, Φ_{SD}, the calculation of the lowest possible energy is possible through the optimisation of the orbitals χ_i. The equations formed are called Hartree-Fock equations, and their

solution determines the best spin orbitals for which E will reach its lowest value.

$$\widehat{f}_i\,\chi_i \;=\; \epsilon_i\,\chi_i \tag{I-17}$$

χ_i is an eigenfunction of the operator $\widehat{f}$, also known as Fock operator and ϵ_i is the corresponding energy and represents the orbital energy. The negative of the eigenvalue of the Fock operator associated with this spin orbital, $-\epsilon_i$, corresponds to the ionisation potential according to Koopmans.

The Fock operator is an effective one-electron operator which has the form:

$$\widehat{f}_i \;=\; -\frac{1}{2}\,\nabla_i^2 \;-\; \sum_A \frac{Z_A}{r_{iA}} \;+\; V_{HF}(i) \tag{I-18}$$

$V_{HF}(i)$ is the Hartree-Fock potential. It represents the average repulsive potential experienced by each electron due to the other N-1 electrons. This replaces the more complex $\frac{1}{r_{ij}}$ repulsion operator which was too complex to be solved. By assimilating the electronic repulsions of different electrons into an average potential, the equation is now solvable. V_{HF} is composed of two terms:

$$V_{HF}(\vec{x_1}) \;=\; \sum_j \left(\widehat{J}_j(\vec{x_1}) \;-\; \widehat{K_j}(\vec{x_1})\right) \tag{I-19}$$

$$\widehat{J}_j(\vec{x_1}) \;=\; \int |\chi_j(\vec{x_2})|^2\;\frac{1}{r_{12}}\,d\vec{x_2} \tag{I-20}$$

$$\widehat{K_j}(\vec{x_1})\,\chi_i(\vec{x_1}) \;=\; \int \chi_j^*(\vec{x_2})\,\frac{1}{r_{12}}\,\chi_i(\vec{x_2})\,d\vec{x_2}\,\chi_j(\vec{x_1}) \tag{I-21}$$

The operator $\widehat{J}_j$ represents the potential experienced by an electron at position $\vec{x_1}$ due to the average charge distribution of another electron in the spin orbital χ_j. On the other hand, the second term, $\widehat{K_j}$, has no classical interpretation. It leads to an exchange of the variables in the two spin orbitals.

To finally solve the Hartree-Fock equation two methods can be used depending on the situation faced. If the system contains an even number of electrons, all of

them paired, the system is solved using the RHF formalism (Restricted Hartree-Fock) or if there is an odd number of electrons or an even number but with some electrons unpaired, then the UHF formalism (Unrestricted Hartree-Fock) can be used. In the first case, RHF, the equations of Roothan-Hall are used to resolve the equation, whereas in the second case, UHF, the equation is resolved using the Berthier-Pople-Nesbert equations.

In order to calculate V_{HF} it is necessary to know χ. Therefore we need an iterative method known as the SCF (Self-Consistent Field method). From an initial guess for V_{HF}, χ is calculated and used to generate a new V_{HF}. This process continues until the cycle converges, i.e. until successive potentials are identical.

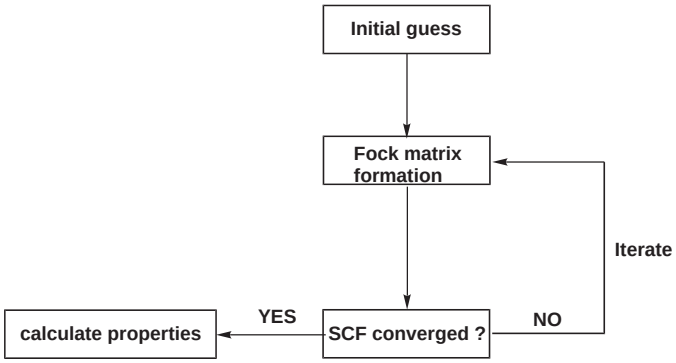

Figure I-1: SCF cycle involved in the Hartree-Fock method

2 - Electron correlation

The main problem emerging from the solutions obtained through the HF method is that the total energy obtained is always higher than the real energy. This is principally due to the fact that in the Hartree-Fock method the electrons are considered to move in an average electronic field, so the correlated motion of each electron with the others is omitted. The difference between the real energy and the HF energy is

designated as the correlation energy.

$$E_{correlation} = E_{total} - E_{HF} \tag{I-22}$$

This gap represents the electronic correlation energy. The correlation constitutes, in most cases, approximately 1% of the total energy but this 1% can have a large influence on the properties calculated for the system. The usual way to introduce the correlation is to take into account the excitation of one or more electrons from one or more occupied orbitals to one or more virtual orbitals higher in energy.

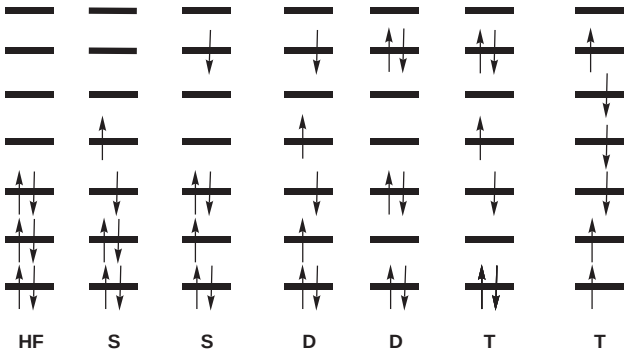

Figure I-2: Possible repartition of the electrons for the **S**ingle, **D**ouble and **T**riple virtual excitations

Each state is described by a Slater determinant, and the combination of them gives the new trial function which should be closer to the real system than the original determinant.

$$\Psi = c_0\Phi_{HF} + \sum_{i=1} c_i\Phi_i \tag{I-23}$$

where the sum is over all the possible "excited" states and c_i are the coefficients defining the contribution of each exited state to the wavefunction.

3 - Density Functional Theory (DFT)

The electron density ρ

In contrast to Hartree-Fock theory, DFT theory is based on the electron density, rather than on wavefunctions. Electron density can be easily found experimentally *via* X-ray diffraction as well as from theory. By using electron density associated with the correct Hamiltonian operator, the energy of the system can be completely described.

Hohenberg and Kohn theorems

In 1964, Hohenberg and Kohn established two fundamental theorems that marked the beginning of modern DFT.[1] Their first theorem states that the external potential $V_{ext}(\vec{r})$ applied on the system (V_{ext} is an external potential to the system which is due to the presence of the nuclei) is defined as a unique functional of the electronic density, $\rho(r)$. One particular external potential can be defined by one and only one particular electron density and vice versa. In turn V_{ext} fixes $\widehat{H}$ which is therefore a unique functional of $\rho(\vec{r})$.

$$\rho_0 \Longrightarrow \{N, Z, R\} \Longrightarrow V_{ext} \Longrightarrow \widehat{H} \Longrightarrow \Psi_0 \Longrightarrow E_0 \tag{I-24}$$

where the "$_0$" index represents the system in its ground state. So, for the ground state, the energy of the system is written:

$$E_0 = T[\rho_0] + E_{ee}[\rho_0] + E_{Ne}[\rho_0] \tag{I-25}$$

The $T[\rho]$ and $E_{ee}[\rho]$ part of the equation are independent of the variables N, R and Z (respectively: number of electrons, electron-nucleus distance and the nuclear

charge) whereas E_{Ne} is dependent upon those variables. So the previous equation can be re-written as following:

$$E_0[\rho_0] = \underbrace{T[\rho_0] + E_{ee}[\rho_0]}_{\text{universally valid}} + \underbrace{\int \rho_0(\vec{r})\, V_{Ne}\, d(\vec{r})}_{\text{system dependent}} \tag{I-26}$$

The independent parts are gathered into a new quantity: the Hohenberg-Kohn functional:

$$F_{HK}[\rho] = T[\rho] + E_{ee}[\rho] \tag{I-27}$$

If the functional F_{HK} was known exactly, it would allow the calculation of E_0. However the explicit forms of the two terms which compose this functional are unknown. The E_{ee} term can be separated in two terms: a Coulomb part and a term containing all the non-classical contributions to the electron-electron interaction.

$$E_{ee}[\rho] = J[\rho] + E_{ncl}[\rho] \tag{I-28}$$

The second Hohenberg-Kohn theorem is simply the use of the variational theory applied to the electronic density. When an approximate electronic density $\tilde{\rho}(\vec{r})$, associated with an external potential V_{ext}, is used, the resulting energy, as in HF, will always be greater than or equal to the exact ground state energy:

$$E[\tilde{\rho}] = T[\tilde{\rho}] + E_{Ne}[\tilde{\rho}] + E_{ee}[\tilde{\rho}] \geq E_{exact} \tag{I-29}$$

The Kohn-Sham approach

As seen in the previous section the Hohenberg-Kohn theorems lies at the heart of modern DFT but a problem appears in the Hohenberg-Kohn orbital-free model: it yields a poor representation of the kinetic energy. In 1965,[2] Kohn and Sham realised that most of the problems are connected with the way the kinetic energy is described. So, they proposed to resolve the problem by introducing the idea of

a fictitious system built from a set of orbitals (one electron functions) where the electrons are non interacting, i.e. each electron is submitted to an average repulsion field coming from the other electrons. They divided the total energy in the following parts:

$$E[\rho] \;=\; T_S[\rho] \;+\; \int [\widehat{V}_{ext}(r) \;+\; \widehat{J}(r)]\,\rho(r)\,dr \;+\; E_{XC}[\rho] \tag{I-30}$$

$T_S[\rho]$ corresponds to the electron kinetic energy for the hypothetical system, with ρ equivalent to the real system but for non-interacting electrons. $\widehat{J}(r)$ represents the classical Coulomb interaction between electrons and $\widehat{V}_{ext}$, as stated previously, is the potential arising from the nuclei:

$$\widehat{J}(r) \;=\; \int \frac{\rho(r')}{|r'-r|}\,dr' \tag{I-31}$$

$$\widehat{V}_{ext} \;=\; \sum_A \frac{Z_A}{|R_A - r|} \tag{I-32}$$

r and r' represent the coordinates of the 2 electrons. The computation of the kinetic energy can be expressed in terms of one electron function:

$$T_S[\rho] \;=\; -\frac{1}{2}\sum_{i=1}^{N} <\varphi_i|\nabla^2|\varphi_i> \tag{I-33}$$

Finally, E_{XC} is a term which encompasses all the other contributions to the energy which are not accounted for in the previous terms such as electron exchange, correlation energy and correction for the self-interaction included in the Coulomb term and the portion of the kinetic energy which corresponds to the differences between the non-interacting and the real system.

A new Hamiltonian can be created by taking into account only the non-interacting system:

$$\widehat{H}_S \;=\; -\frac{1}{2}\sum_i^N \nabla_i^2 \;+\; \sum_i^N V_{S(\vec{r_i})} \tag{I-34}$$

One-electron functions are reintroduced in density functional theory in the form

of Kohn-Sham orbitals, φ_i. As for HF, these orbitals are determined by:

$$\widehat{f}^{KS}\,\varphi_i \;=\; \epsilon_i\,\varphi_i \tag{I-35}$$

$$\text{with}\quad \widehat{f}^{KS} \;=\; -\tfrac{1}{2}\,\nabla^2 \;+\; V_S(\vec{r}) \tag{I-36}$$

where $\widehat{f}^{KS}$ is a one-electron operator, called the Kohn-Sham operator and the corresponding orbitals are called Kohn-Sham orbitals. $V_S(\vec{r})$ describes the effective potential of the non-interacting reference system. The non-interacting system is related to the real system by choosing an effective potential, V_S such that:

$$\rho_S(\vec{r}) \;=\; \sum_i^N \,|\varphi_i(\vec{r})|^2 \;=\; \rho_0(\vec{r}) \tag{I-37}$$

Then we come back to the original system:

$$E_{DFT}[\rho] \;=\; T_S[\rho] \;+\; E_{Ne}[\rho] \;+ J[\rho] \;+\; E_{XC}[\rho] \tag{I-38}$$

where:

$$E_{XC}[\rho] \;=\; (T[\rho] \;-\; T_S[\rho]) \;+\; (E_{ee}[\rho] \;-\; J[\rho]) \;=\; T_C[\rho] \;+\; E_{ncl}[\rho] \tag{I-39}$$

In this way, it becomes possible to compute the major part of the kinetic energy (the rest being merged with the non-classical electron-electron repulsion). The Hohenberg-Kohn functional then becomes:

$$F[\rho(\vec{r})] \;=\; T_S[\rho(\vec{r})] \;+\; J[\rho(\vec{r})] \;+\; E_{XC}[\rho(\vec{r})] \tag{I-40}$$

where $\mathrm{E_{XC}}$ contains the residual kinetic energy as well as the repulsion terms.

As stated previously, $\mathrm{E_{XC}}$ is the only unknown term of the equation. To model it, it is necessary to approximate it. In the next section the different approximation methods used to modeled the functional will be described.

4 - Functionals

Exchange-correlation functional (E_{xc})

As noted earlier, the $E_{XC}[\rho]$ functional contains the non-classical contributions to the potential energy due to the electron-electron interaction and the difference between the kinetic energy of the real system and the kinetic energy related to the non-interacting system. The "functionals" described here represent different approximations to this exchange-correlation functional. Development of new functionals is an ongoing and active area of research.

LDA: Local Density Approximation

This is the base for most of the exchange-correlation functionals, and it is defined using the electronic density of an uniform electron gas. The constant value of the electronic density does not reflect the rapid variation of densities in a molecule. Although LDA is a rough approximation, it is the only system for which the density is defined by $\rho = \frac{N}{V}$ (N represents the number of electrons and V represents the volume of the gas), and the form of the exchange and correlation energy functionals are known exactly or to a very high accuracy. In the case of open-shell systems the electronic density, ρ is replaced by the spin electronic densities, ρ_α and ρ_β such as, $\rho = \rho_\alpha + \rho_\beta$. This approximation is called local spin-density approximation: LSDA. A famous example of a LDA functional is the one developed by Vosko, Wilk and Nusair (VWN) based on high-level quantum Monte Carlo calculations for uniform electron gases.[3] The use of LDA gives more accurate results for the determination of molecular properties (structures, vibrational frequencies, charge moments, elastic moduli) than the HF method but shows some flaws in the case of energetics details

(bond energies, energy barriers in chemical reaction) which are poorly characterised by using this type of functional.

GGA: Generalised Gradient Approximation

The LDA can be considered as a zeroth order approximation, but LDA describes the energies rather badly so a new type of functional was introduced: the generalised gradient approximation. These functionals include the gradient of the electron density, $\nabla\rho$. This use of the electron density gradient describes the non-homogeneity of the true electron density rather better.

The GGA is usually divided into exchange and correlation terms that can, then, be solved individually.

$$E_{XC}^{GGA} = E_X^{GGA} + E_C^{GGA} \tag{I-41}$$

Here is a non exhaustive list of some of the most efficient GGA functionals commonly used in computational chemistry.

- **B** is an exchange functional developed by Becke.[4] It is a gradient correction to the LSDA exchange energy. It includes a single parameter fitted on known atomic data from the rare gas atoms.

- **P86** is a correlation functional developed by Perdew.[5] It is a popular gradient correction to LSDA which includes one empirical parameter fitted for the neon atom.

- **PW91** is an exchange-correlation functional developed by Perdew then Perdew, Wang and Burke.[6,7] It is a modification of the P86 functional.

- **B95** is a correlation functional (for meta-GGA) developed by Becke,[8] does not contain any empirical parameters and treats better the self-interaction error.
- **PBE** is an exchange-correlation functional developed by Perdew, Burke and Ernzerhof.[9]
- **LYP** is a correlation functional developed by Lee, Yang and Parr.[10] It is the most extensively used GGA correlation functional. It contains four empirical parameters fitted to the helium atom.

From the previous GGA functionals a combination between exchange and correlation functionals is made so as to try to describe completely the systems. Some of the most common combinations are: BLYP, BP86 and BPW91.

meta-GGA The meta-GGA functionals are an expansion of the normal GGA. Contrary to the GGA, the meta-GGA includes the laplacian of the electron density or the local kinetic energy density, $\nabla^2\rho$. Common meta-GGA functionals include BB95[11] and PBEKCIS.[12]

Hybrid functionals

The previous functional types all present a problem because the exchange part is very poorly described due to a problem of electronic self-interaction. On the other hand, the exchange part in HF is defined exactly. So an alternative approach would be to use a mix of DFT and HF to describe the exchange energy. However, taking the correlation part from DFT and the exchange part from HF gives poor results (worse than GGA). A first approach to this problem would be to regroup the exchange and correlation parts, so a functional that describes the system better than the GGA functionals can be obtained.[13] The final solution to this problem is the

use of a combination of HF, GGA and LSDA functionals to describe the exact exchange and correlation part of the hybrid functional. Usually hybrid functionals are composed of a mixture of exact and DFT exchange. The main element of these functionals come from GGA functionals, so they are often called GGA hybrid functionals.

- **B3** contains exact exchange, and is an exchange functional developed by Becke.[14] It is a combination of LSDA and GGA functionals.
- **PBE0** also called PBE1PBE, has been developed by Adamo and Barone.[15] It is a combination of 75% PBE GGA exchange functional and 25% of HF exchange.
- **B97** and **B98** were developed first by Becke (B97),[16] then modified by Becke and Schmider (B98).[17] Unlike PBE0 and B3 functionals, B98 and B97 are meta-GGA hybrid functionals instead of GGA hybrids. They contain an exchange part taken from HF method.

To describe correctly the exchange-correlation term, it is necessary to combine exchange and correlation functionals to obtain an hybrid functional such as: B1B95,[11] B1LYP[18] or B3P86.[19]

A famous example of exchange and correlation combination is the most often used hybrid functional: B3LYP.[20] The B3LYP functional is a mix between LDA and GGA functionals taken from the DFT and HF methods, to a certain extent, as shown below:

$$E_{XC}^{B3LYP} = E_{XC}^{LDA} + a_0\,(E_X^{HF} - E_X^{LDA}) + a_X\,(\underbrace{E_X^{GGA}}_{B88(B)} - E_X^{LDA}) + a_C\,(\underbrace{E_C^{GGA}}_{LYP} - E_C^{LDA}) \tag{I-42}$$

where $a_0 = 0.20$, $a_X = 0.72$ and $a_C = 0.81$ are three empirical parameters determined by fitting the predicted values to a set of atomisation energies, ionisation

potentials, proton affinities, and total atomic energies.

5 - Basis sets

Basis functions are used to create the atomic orbitals (AO) or molecular orbitals and are usually expanded as a linear combination of such functions with the coefficients to be determined. These basis functions can be classified into two main types:

- Slater-type orbitals, also called STOs, have the exponential dependence: $e^{-\zeta r}$ and are very close in their mathematical expression to the real AO:

$$\eta^{\mathrm{STO}} \;=\; N\, r^{n-1}\, e^{-\zeta\, r}\, Y_{lm}(\Theta, \phi) \tag{I-43}$$

  where N is a factor of normalisation, ζ is the exponent. r, Θ and ϕ are spherical coordinates and Y_{lm} is the angular momentum part (function describing the "shape"). Finally n, l and m are the classical quantum numbers: principal, angular momentum and magnetic, respectively.

- the Gaussian-type orbitals, also known as GTOs, which have the exponential dependence: $e^{-\alpha r^2}$:

$$\eta^{\mathrm{GTO}} \;=\; N\, x^{l}\, y^{m}\, z^{n}\, e^{-\alpha\, r^2} \tag{I-44}$$

  where N is, as previously, a normalisation factor, x, y and z are Cartesian coordinates.

The STOs describe very closely the behaviour of hydrogen atomic orbitals because they feature a cusp at r=0 and a good exponential decay for bigger values of r. The GTOs, in contrast, do not show a cusp at r=0 and decrease too rapidly for large values of r. Despite those problems the GTOs are a better compromise due

to the fact that the product of two GTOs centred on two different atoms is a third one situated between them. This is not the case for STOs, which are therefore very difficult to handle computationally because the four-centre-two-electron integrals are very time consuming. A number of GTOs can be combined to **approximate** a STO, and this often proves to be more efficient than using the STO itself.

The degree of complexity, and thus precision, of a basis set is defined by the number of contracted functions (CGF) employed to represent each atomic orbital, the minimum being one contracted function to describe a basis function. For example the STO-3G basis set (where G indicates a combination of contracted Gaussian functions) is formed by a linear combination of three CGF for each basis function so as to resemble an STO. For more precision and better description of the system, two or more functions can be used to describe each type of orbital, usually double-zeta and triple-zeta basis sets give a good precision.

The valence electrons are the ones that change most in chemical reactions, so it is most important to have a flexible description of these electrons. Such basis sets, where the core and valence orbitals are treated differently, are called split valence basis sets. The most used example of a split valence basis set is the 6-31G basis set. The nomenclature of this type of basis set: **X**-**YZ**G is:

- X represents the number of primitives GTOs used to describe one single contracted Gaussian function of the core.
- Y and Z (more can be added for a better precision) represent the number of primitives GTOs describing the valence orbitals. In the case of 6-31G, it is composed of two functions, one containing three primitives and the other only one.

Additions can be made to the basis sets using polarisation functions and/or diffuse functions. Bonding between atoms induces a deformation of the electronic

cloud around each atom, called polarisation. To allow this, functions with higher angular momentum are added to the basis set. For example, the addition of a p function to H allows polarisation. In the same way a d-function can be added to a basis set containing p valence orbitals, f-functions for d-valence orbitals. For more precise results the polarisation functions included can be defined better: for example for a hydrogen atom with 6-31G basis set p and d polarisation functions can be added, the basis set becoming 6-31G(pd). The diffuse functions, represented by a "+" (for example 6-31+G or 6-31++G), describe the part of atomic orbitals distant from the nuclei that can have a very important role when considering anions or diffuse electronic clouds in second or third row transition metals for example.

Another fact to take into account is that for transition metals the inner core of these atoms is very large and so the number of basis functions used to describe it would be very big. To resolve this problem, those basis functions can be replaced by an *Effective Core Potential* (ECP). The ECP will model the effects of the nucleus and the electrons from the inner shell on the valence electrons as an average effect. This allows not only the reduction of big computational calculations but can include some relativistic effects on the system studied because these basis functions are generated from relativistic atomic calculations.

Functionals/basis sets performances

Recent studies[21,22] have compared different functionals from HF to hybrid-meta-GGA associated with different basis sets. They compare experimental properties with those found computationally and make an average of the degree of error observed. The functional/basis sets are used to study different compounds from purely organic molecules (mainly based on C, O, P, H, N,...) to those containing a sin-

gle first row transition metal. The main conclusions which can be extracted from these reviews are that hybrid-GGA and hybrid-meta-GGA, described by Perdew as "fourth rung over five of the Jacob's ladder", i.e. high level of computational efficiency, are the best choice for accurate computational calculations today. To a lesser extent some GGA (second rung) and meta-GGA (third rung) can be considered as being efficient for the calculation of certain properties. The use of LSDA functionals is to be avoided due to their poor performance compared to modern functionals.

For systems containing transition metals, Jensen and co-workers have tested five common GGA and hybrid-GGA functionals (B3LYP, BP86, PBE0, PBE, and BLYP) on their efficiency to calculate the properties of a series of diatomic systems containing a first-row transition metal (Sc, Ti, V, Cr, Mn, Fe, Co, Ni, Cu or Zn) and an organic element (H, F, Cl, Br, N, C, O or S). They compared the results they obtained for different properties to the data found experimentally. This work allowed them to classify the functionals from the most efficient to the less efficient as such: PBE0 > B3LYP > PBE $\sim$ BP86 > BLYP.[23]

6 - Software

All the calculations described in this thesis have been performed using Gaussian03 series of programs.[24]

Bibliography

[1] Hohenberg, P.; Kohn, W. *Phys. Rev.*, **1964**, *136*, B864.

[2] Kohn, W.; Sham, L. J. *Phys. Rev.*, **1965**, *140*, A1133.

[3] Vosko, S. J.; Wilk, L.; Nusair, M. *Can. J. Chem.*, **1980**, *58*, 1200.

[4] Becke, A. D. *Phys. Rev. B*, **1988**, *38*, 3098.

[5] Perdew, J. P. *Phys. Rev. B*, **1986**, *33*, 8822.

[6] Perdew, J. P.; Wang, Y. *Phys. Rev. B*, **1992**, *45*, 13244.

[7] Perdew, J. P.; Chevary, J. A.; Vosko, S. H.; Jackson, K. A.; Pederson, M. R.; Singh, D. J.; Fiolhais, C. *Phys. Rev. B*, **1992**, *46*, 6671.

[8] Becke, A. D. *J. Chem. Phys.*, **1996**, *104*, 1040.

[9] Perdew, J. P.; Burke, K.; Ernzerhof, M. *Phys. Rev. Lett.*, **1996**, *77*, 3865.

[10] Lee, C.; Yang, W.; Parr, R. G. *Phys. Rev. B*, **1988**, *37*, 785.

[11] Becke, A. D. *J. Chem. Phys.*, **1996**, *104*, 1040.

[12] Perdew, J. P.; Burke, K.; Ernzerhof, M. *Phys. Rev. Lett.*, **1996**, *77*, 3865.

[13] Perdew, J. P.; Ernzerhof, M.; Burke, K. *J. Chem. Phys.*, **1996**, *105*, 9982.

[14] Becke, A. D. *J. Chem. Phys.*, **1993**, *98*, 5648.

[15] Adamo, C.; Barone, V. *Chem. Phys. Lett.*, **1998**, *298*, 113.

[16] Becke, A. D. *J. Chem. Phys.*, **1997**, *107*, 8554.

[17] Schmider, H. L.; Becke, A. D. *J. Chem. Phys.*, **1998**, *108*, 9624.

[18] Adamo, C.; Barone, V. *Chem. Phys. Lett.*, **1997**, *274*, 242.

[19] Perdew, J. P. *Phys. Rev. B*, **1986**, *33*, 8822.

[20] Lee, C.; Yang, W.; Parr, R. G. *Phys. Rev. B*, **1988**, *37*, 785.

[21] Riley, K. E.; Op't Holt, B. T.; Merz, K. M. J. *J. Chem. Theory Comput.*, **2007**, *3*, 407.

[22] Sousa, S. F.; Fernandes, P. A.; Ramos, M. J. *J. Phys. Chem. A*, **2007**, *111*, 10439.

[23] Jensen, K. P.; Roos, B. O.; Ryde, U. *J. Chem. Phys.*, **2007**, *126*, 014103.

[24] *Gaussian03, D.02*: Frisch, J. A.; Trucks, G. W.; Schlegel, H. B.; Scuseria, G. E.; Robb, M. A.; Cheeseman, J. R.; Montgomery, J. A. Jr; Vreven, T.; Kudin, K. N.; Burant, J. C.; Millan, J. M.; Iyengar, S. S.; Tomasi, J.; Barone, V.; Mennucci, B.; Cossi, M.; Scalmani, G.; Rega, N.; Peterson, G. A.; Nakatsuji, H.; Hada, M.; Ehara, M.; Toyota, K.; Fukuda, R.; Hasegawa, J.; Ishida, M.; Nakajima, T.; Honda, Y.; Kitao, O.; Nakai, H.; Klene, M.; Li, X.; Knox, J. E.; Hratchian, H. P.; Cross, J. B.;

Adamo, C.; Jaramillo, J.; Gomperts, R.; Stratmann, R. E.; Yazyev, O.; Austin, A. J.; Cammi, R.; Pomelli, C.; Ochterski, J. W.; Ayala, P. Y.; Mrokuma, K.; Voth, G. A.; Salvador, P.; Dannenberg, J. J.; Zakrzewski, V. G.; Dapprich, S.; Daniels, A. D.; Strain, M. C.; Farkas, O.; Malick, D. K.; Rabuck, A. D.; Raghavachari, K.; Foresman, J. B.; Ortiz, J. V.; Cui, Q.; Baboul, A. G.; Clifford, S.; Cioslowski, J.; Stefanov, B. B.; Liu, G.; Liashenko, A.; Piskorz, P.; Komaromi, I.; Martin, L. R.; Fox, D. J.; Keith, T.; Al-Laham, M. A.; Peng, C. Y.; Nanayakkara, A.; Challacombe, M.; Gill, P. M. W.; Johnson, B.; Chen, W.; Wong, M. W.; Gonzalez, C.; Pople, J. A. Gaussian, Inc. Pittsburgh, 2003.

CHAPTER II

Hydrogenase enzymes and their models: biological and chemical studies

The hydrogenase systems catalyse the conversion of H^+ to H_2 and vice versa. Their activity can be summarised *via* the following reversible equation:

$$H_2 \rightleftarrows 2H^+ + 2e^-$$

These enzymes arouse a lot of interest in different domains which encompass the replacement of fossil fuels by renewable energies and the creation of catalytic systems as a source of cheap chemical production of dihydrogen.[1,2] One of the main reasons is their intense catalytic activity with a number of turnover from 6000 to 9000 s^{-1}.[3–5] This introductory chapter is an overview of the biological system itself and its chemical models.

The hydrogenase enzyme was discovered by Stephenson and Stickland in 1931[6] and is found in a variety of bacteria (methanogenic, acetogenic, nitrate and sulfate reducing bacterias,[7] anaerobic archaea, rhizobia, protozoa), anaerobically adapted algae and fungi.[8] These bacteria and archaea live in anaerobic and/or dark places and/or sulfurous atmospheres, mainly in water-containing volcanic areas such as terrestrial solfataric fields, hot springs and shallow and abyssal submarine hydrothermal environments. Certain of those bacteria grow optimally even in places where the temperature is above 80°C.[9] Another category of hydrogenase appears also in green

algae which are present in anaerobic domains exposed to light.[10,11] The most commonly studied hydrogenase enzymes come from the *Desulfovibrio* (*desulfuricans*, *vulgaris*, *gigas*), *Clostridium pasteurianum* or *Trichomonas vaginalis* bacteria families.[12–14]

Three main categories of hydrogenases exist, which are differentiated by the composition of their active site, called the "H-cluster", which contains two components: a $[Fe_4{-}S_4]_H$ cubane cluster and a bimetallic $[M_2S_2]_H$ cluster (see Figure II-2). The function of the enzymes is most of the time closely related to the composition of its active site and more precisely to the metals in the bimetallic cluster,[15] i.e. a [Fe-Ni] centre will usually catalyse the oxidation of H_2 while a [Fe-Fe] centre will usually catalyse its production. In certain rare cases the hydrogenase centre can catalyse both reactions.

- The [Fe-Ni] hydrogenases[2] are among the most studied and the most numerous hydrogenase enzymes in nature. Some variants have the capacity to catalyse the oxidation of dihydrogen, where others can catalyse reversible dihydrogen production/oxidation. These enzymes can be found in *Desulfovibrio Gigas* and *Desulfovibrio Vulgaris* bacteria.[14,16]

- The [Fe-Fe] hydrogenases (iron-only hydrogenases)[17] are 10 to 100 times more efficient in catalysis than [Ni-Fe] hydrogenases. This class is the most studied hydrogenase for industrial applications and also mechanistic studies.[7] This system principally catalyses the reduction of protons leading to the formation of dihydrogen. This enzyme can be found for example in *Clostridium Pasteurianum* and *Desulfovibrio Desulfuricans* bacteria.[14,18]

- The [Fe] hydrogenases (iron-sulfur cluster-free hydrogenases) which are found in methanogenic bacteria. The most famous example, studied extensively by Thauer *et al.*, is methylenetetrahydromethanopterin dehydrogenase.[19–23]

- The metal-free and Ni-Fe-Se hydrogenases, a minor group of the hydrogenase

family, are principally found in methanogenic organisms.[15] The [Ni-Fe-Se] hydrogenases have the advantage of being less O_2 sensitive than the other metallic hydrogenases.

Hydrogenase enzymes, generating H_2 from electrons and H^+, fulfil (for a certain number of living entities) the same function as respiratory enzymes which use O_2 to oxidise nutritive elements leading to the production of energy. Other ones using H_2 as a source of electrons, replicating the role of oxygen-evolving complex in photosynthetic organisms, which normally use H_2O as a substrate.[15] Hydrogenases also play a major role in the fermentation of biological substances to CH_4 and in microbial phosphorylation, where H_2 can serve as an energy source or be generated as the product of reductive processes.[24]

In their natural environment, hydrogenases, like other enzymes, are composed of an active centre surrounded by protein layers. The protein system surrounding the core is a very complex network of residues and is different from one enzyme to the other. Some recent examples about this subject are reported in Gärtner, Lubitz, Matias, Fontecilla-Camps or Meyer work.[12,13,17,25–28] An example of the global structure of an enzyme, in this case the *Desulfovibrio Desulfuricans*, is given in Figure II-1.[25]

In some cases, different categories of hydrogenases are found in the same organism, for example in *Clostridium Pasteurianum*, where the hydrogenase I catalyses both oxidation and formation of H_2 while hydrogenase II catalyses only the oxidation.[29]

The hydrogenase systems that will be the focus of the rest of this chapter are those containing two irons in their core. It was only in 1998 that Peters *et al.*[18] characterised the first structure of a Fe-only hydrogenase from *Clostridium pasteurianum*, by X-ray diffraction. The active centre of the enzyme is composed of two iron atoms covalently bonded together and also linked by two thiolato bridges, where the sulphur atoms are linked together by an organic chain. The coordination spheres of

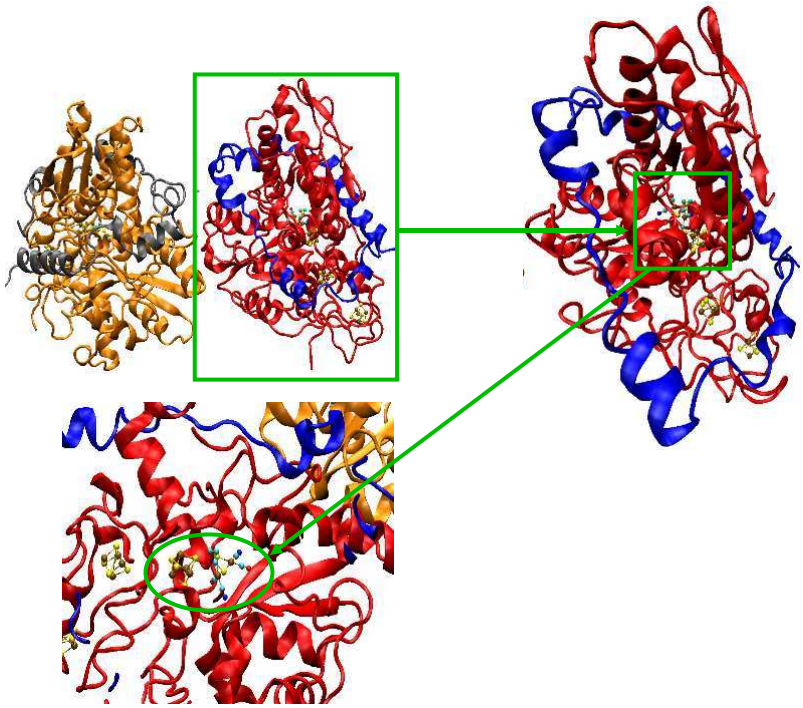

Figure II-1: X-ray structure of the *Desulfovibrio Desulfuricans* [Fe]only-hydrogenase enzyme.

the two metals are completed by COs and a CN ligand on each metal. The presence of CO and CN is highly unusual in enzymes because they are usually considered to be highly toxic in biology. One of the metallic centres (the distal centre) may also have a H_2O ligand, whereas the other centre (proximal centre) is linked by a thiolato bridge to the $[Fe_4{-}S_4]$cubane cluster (see Figure II-2).[8,30] The thiolato bridge linking the Fe_4 cluster and the bimetallic compound is part of a cysteine residue. The active site, the $[Fe_2S_2]_H$ cluster and the cubane cluster are linked to the protein backbone by four cysteines.

We will from now on focus exclusively on the bimetallic part of the H-cluster which is the site of the redox events.[31] The Fe_4S_4 cluster, which plays the role of electron donor in the catalytic process and is not directly involved in the reaction with H_2 or H^+, will not be discussed further.[32]

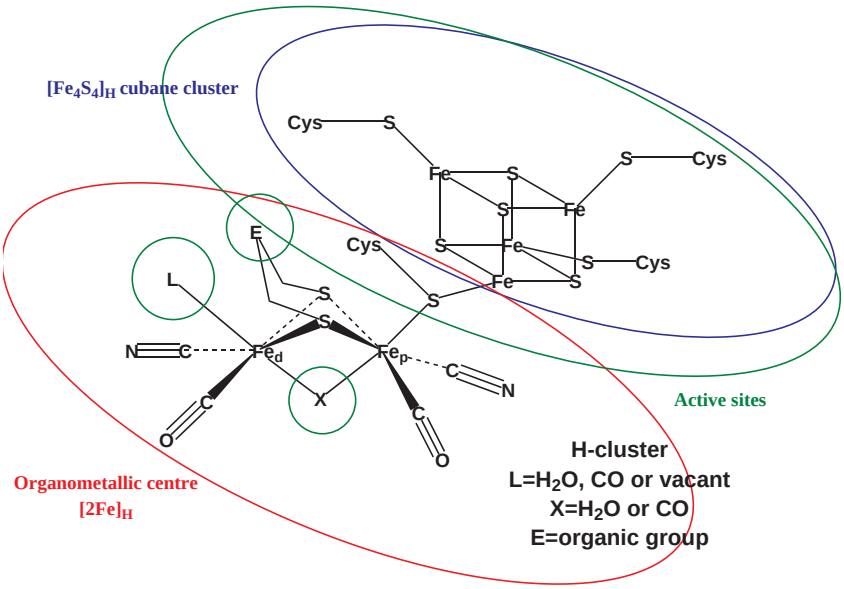

Figure II-2: The H-cluster in the *Clostridium pasteurianum* bacteria.

To conclude this overview of the biological system, it is interesting to consider a possible catalytic cycle involving an hydrogenase, first presented by Armstrong and co-workers in 2004[33] and explored in 2007 by Trohalaki and Pachter using DFT methods.[34] The catalytic cycle is presented in Figure II-3. The first steps (compounds **1** to **5**) involve the introduction of electrons into the $[Fe_2S_2]_H$ cluster (coming from the Fe_4S_4 cluster) and the loss of the H_2O ligand, opening a vacant site on the distal iron which in turn allows the displacement of the bridging CO to a terminal position, generating an empty site between the two irons. On compound **5** a proton is added (as well as an electron), to one of the cyanide ligands and it gives compound **6**. The addition of a second hydrogen (and the necessary electron) occurs on the bridging position. The two hydrogens (placed in two site close to each other) are then bonded together (compounds **8** and **9**) and finally the dihydrogen formed is ejected from the molecule and the compound, after addition of a new hydrogen (and an electron), come back to its mono-hydrogenated state (compound **6**).

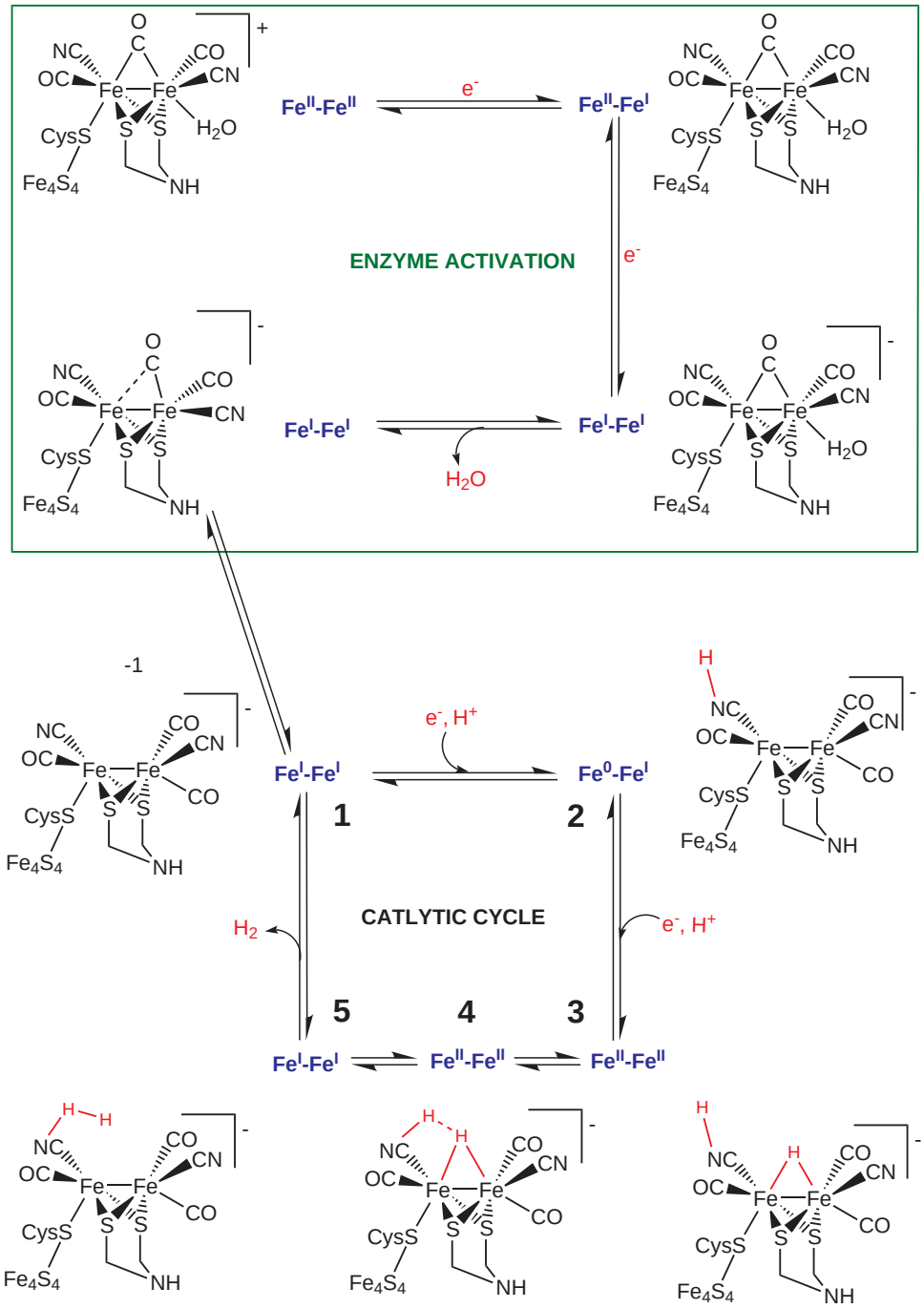

Figure II-3: Catalytic cycle of the production/oxidation of H_2 as presented by Armstrong *et al.* and completed by Pachter and Trohalaki[34] (electrons are provided by the $[Fe_4S_4]$ cluster; $[Fe_4S_4]$ cluster has been shown experimentally to be charged 2+).

The biological systems studied have inspired many research teams to find a simplified chemical model possessing the same properties of the hydrogenase enzyme active core and today many different iron-iron based compounds have been developed to mimic the hydrogenase core. The first examples of this class of compound appeared in literature as far back as 1929: $[(NO)_2FeSC_2H_5]_2$, $[Fe(CO)_3SC_2H_5]_2$ and $[Fe(-O-N=N-O-)SC_2H_5]_2$. However, no analytical methods available at this time could confirm the structures.[35] In 1965 a similar compound, synthesised by Hieber *et al.*,[36] $Fe_2S_2(CO)_6$, was identified as an intermediate of a reaction producing $Fe_3S_2(CO)_9$, another iron carbonyl chalcogenide. The compound was characterised by infrared spectra by the same group and then by Dahl and coworkers using X-ray diffraction.[37] Finally a first fully described synthetic pathway leading to this sort of compound was developed, in 1979 by Seyferth and Henderson.[38] The resulting compound was composed of two iron centres linked by two thiolato bridges, and each iron centre was surrounded by three carbonyl ligands. The two sulphurs constituting the thiolato bridges were either bridged or directly bonded together. A propyl bridge between the two sulphur atoms was added later by Winter *et al.*.[39] and is now often used as a generic parent model of the Fe-only hydrogenase core: $(\mu-pdt)Fe_2(CO)_6(pdt=-S(CH_2)_3S-)$. As noted previously, Peters *et al.*[18] characterised for the first time the structure of the Fe-only hydrogenase contained in the *Clostridium pasteurianum* enzyme and in 1999 Darensbourg *et al.* compared the X-ray structure also obtained from a Fe-only hydrogenase extracted from the *Clostridium pasteurianum* enzyme with the structure of the $[Fe_2(CO)_6(\mu-SCH_2CH_2CH_2S)]$ compound synthesised by Winter *et al.*.[39] By superimposing the two structures they observed that the Fe-Fe distance in the model complex is 0.1 Å shorter than those reported for the di-iron site in the protein structures. They also saw that the match between the iron and the sulphur positions is very close as well as the electron density match of the pdt-bridged di-iron site, and the overall coordination of the irons. The only difference appearing in the pdt units is on the central CH_2 group.[40] Once the similarity between the biological and synthetic compounds had been established, many teams started to synthesise similar molecules. In Figure II-4

are summarised some of the different compounds synthesised which are representative of the large volume of work done in this domain:[41–47] more than 300 different structures based on the $[Fe_2(L)_6(SR)_2]^x$ hydrogenase core-like unit can be found in the Cambridge database, more than 250 of which have a CO or CN group as a ligand which illustrates the great interest aroused by such systems.

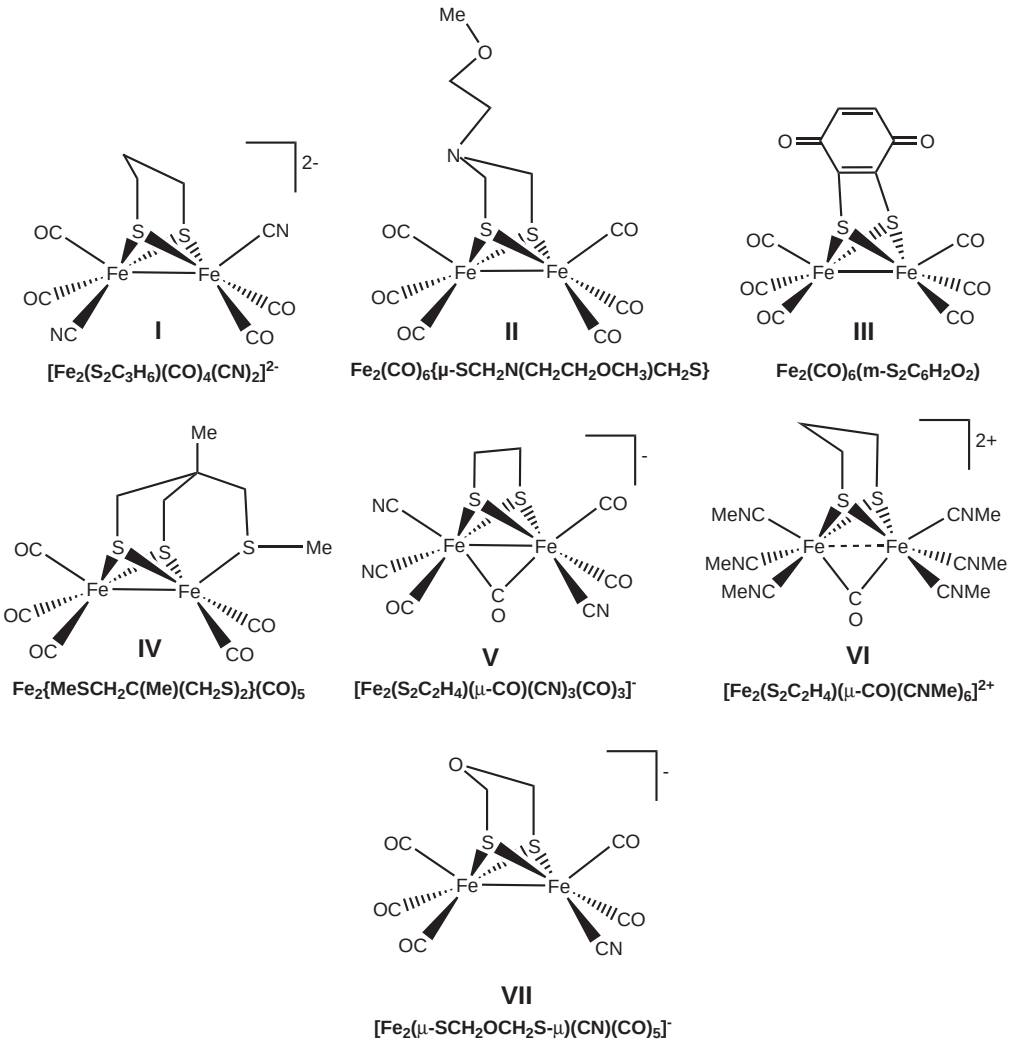

Figure II-4: Different Fe-Fe model compounds synthesised by Rauchfuss (**I**,[48] **V**,[49] **VI**[50]), Talarmin (**II**[32]), Adams (**III**[51]), Pickett (**IV**[52]) and Song (**VII**[53]) and their co-workers.

As noted earlier, hydrogenases are remarkable in their ability to catalyse the reversible oxidation of H_2 to provide electrons at a low potential, the bonding of H_2 to the cluster framework serving to reduce the barrier to H-H bond cleavage.[54] Hy-

drogenases have been widely characterised by X-ray diffraction and IR spectroscopy, and both techniques have shed important clues on the possible mechanisms of action. Diffraction affords accurate structural information on the hydrogenase active site, allowing one to speculate on binding sites. IR spectroscopy, in contrast, brings information about the ligands inside the molecule and, through their vibrations, information on the nature of ligation and on the oxidation state of the metals. Different mechanisms have been proposed for the catalytic cycle on the basis of these experiments. This being said, it is interesting to look firstly more closely at the components of the active site and their impact on the structure.

The ligands surrounding each metal centre have a non negligible influence on the molecule. In the enzyme, these ligands are usually carbonyl and cyanide groups. However, by synthesising compounds containing a different number of these ligands and/or ligands of different nature, one can control the properties and the catalytic efficiency of the new synthesised system.[31,55,56] Compounds containing only CO ligands, being easier to synthesise, were synthesised first following the method developed by Seyferth.[38] The CN^- ligands are usually added afterwards by exchange with CO under excess of CN^-.[48] Compounds containing CN ligands are often made because the CN have the ability to stabilise the molecule more than the CO alone. Their ability to serve as an anchor for the hydrogens (see Figure II-3) is also another non negligible property. However, the overall structures of systems containing six CO and four CO/2 CN^- are very similar with few geometrical differences.[40] CN is one of the most used ligands to replace CO ligands but a number of groups have also used phosphorus related ligands in place of CO. This class of compounds include mono- (e.g. PMe_3[57]) and bi-dentate ligands (e.g. DiPhenyl-Phosphino-Ethane (dppe)[58]) and recently, the use of a dppe as ligand has shown promise in the creation of dihydrogen catalysts, because it involves an asymmetrical coordination environment, hence directing the protonation and the reduction.[59]

Among the three types of ligands mainly used to coordinate iron centres, the CN^- and phosphorus-derived ligands appear to be most effective for proton reduc-

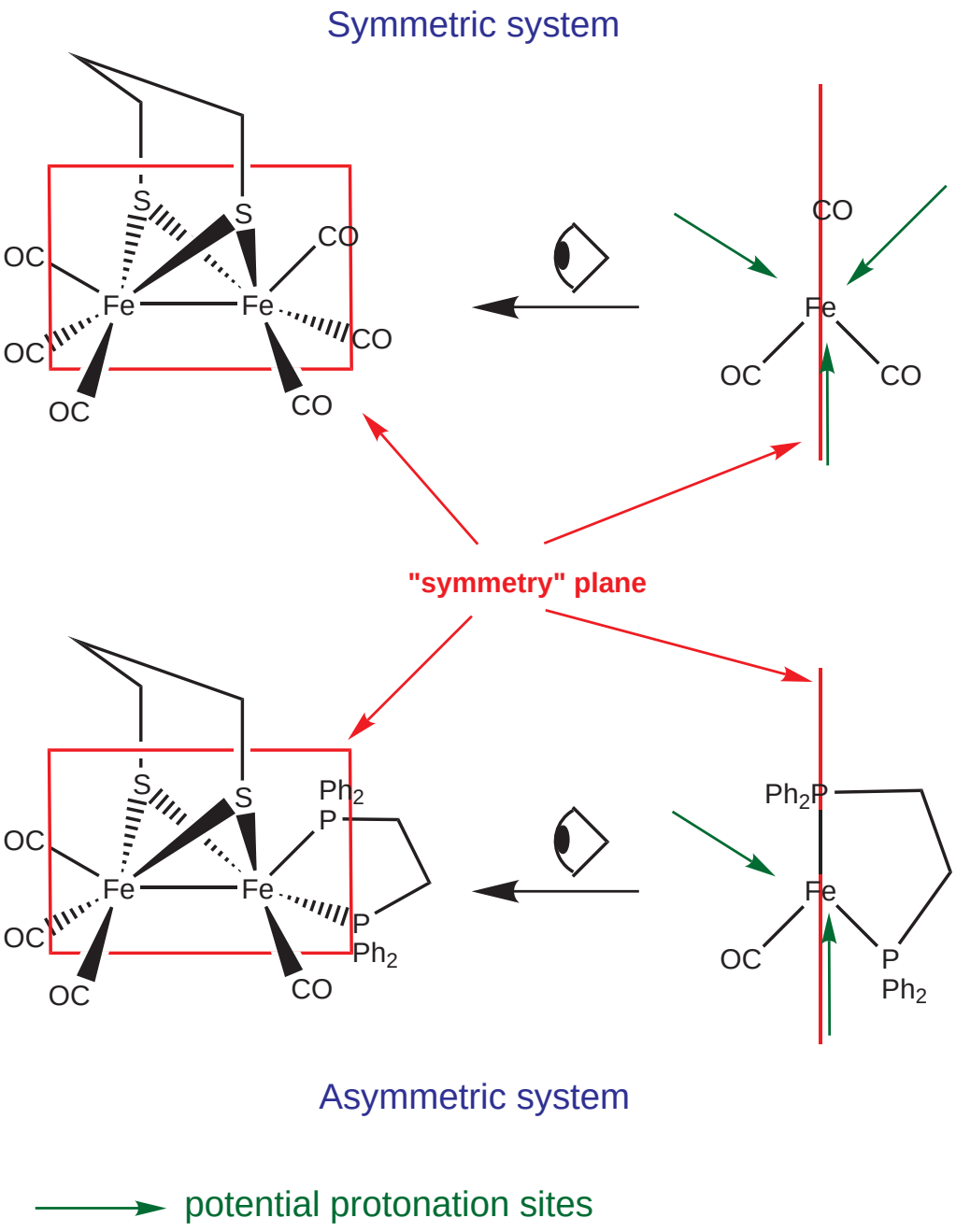

Figure II-5: Asymmetry created in the molecule by the replacement of two CO ligands by a chelating dppe ligand.

tion. The ability of the CN^- ligand to activate proton reduction may be due to its ability to attract a proton thanks to their negative charge, as noted by Rauchfuss and co-workers.[57,60] On the other hand, the bi-dentate phosphorus-derived systems increase the basicity of the site where protons will be bound[61] and induce an asymmetry in the compound, a key feature in the structure of the natural site as shown by Hall *et al.*.[62] Other 2-electron donor ligands have been used, including CNMe,[63] $P(OMe_3)$[64] or NHC (N-heterocyclic carbene).[65] Sun and co-workers have shown that the asymmetrisation of the Fe_2 core, discussed earlier, appears to be important in its catalytic role,[66] and a number of recent studies have focused on the asymmetrisation of the complex to control the site of protonation on the compound (see Figure II-5).[58,59,62,67,68]

The S-to-S linker is another part of the molecule which has attracted much interest from the chemistry community. In the enzyme, it has been proposed to be a $CH_2{-}X{-}CH_2$ group where X can be either C-, O- or N-based and was, after re-examination, confirmed to be a $\mu{-}SCH_2NHCH_2S$ group by Fontecilla-Camps *et al.*.[13,69] Since then, many S-to-S linkers of different length and composition have been synthesised, with different bridgehead substituents (Figure II-6). Rauchfuss *et al.* found that the dithiolate bridge has no electronic role for a variety of compounds,[70] a hypothesis confirmed by Darensbourg and co-workers, who showed that different linkers have a similar effect on the CO ligands (studies based on the CO vibrational bands).[55] One possible role of the linker can be to introduce a heteroatom capable of binding to a metal centre during the catalytic cycle (see compounds **I** and **II** on Figure II-6). Other modifications of the S-to-S linker have been made to enhance the system, for example a light switch for the catalytic system (**III**) or elements facilitating the approach of hydrogens (**V** and **VI**).

As shown In Figure II-2, in nature the compounds possess usually another bridging ligand (usually CO or H_2O) between the two irons in addition to the two thiolates. However, many of the model compounds synthesised don't share this feature, although a few recent studies have focused on the presence of a CO bridge linking

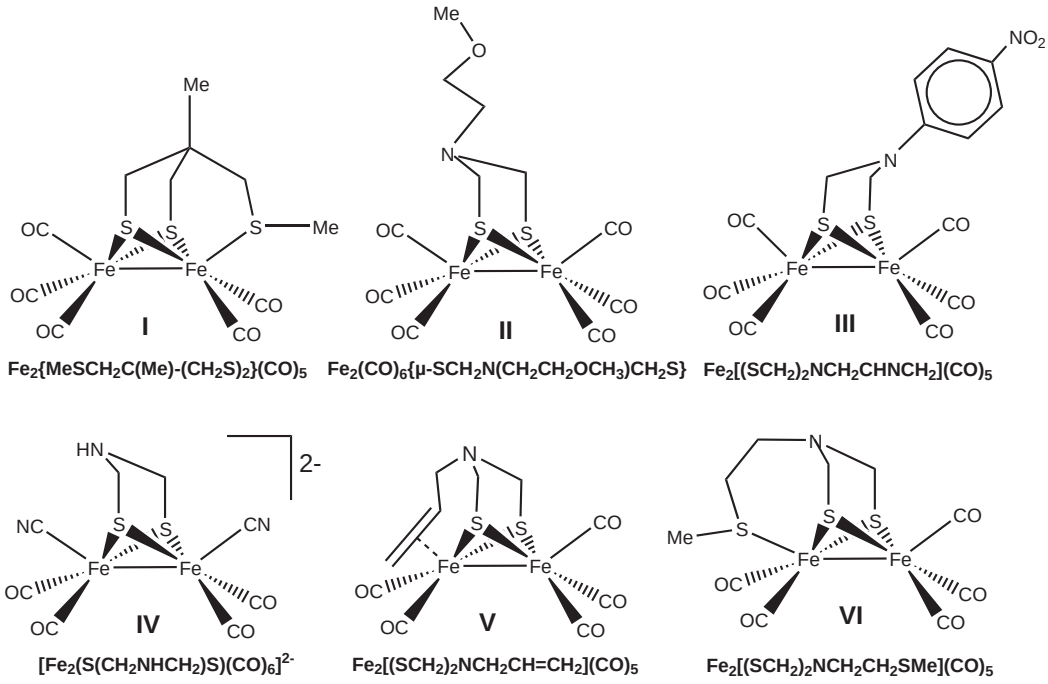

Figure II-6: S-to-S linking groups as synthesised by Pickett (**I**[71]), Talarmin (**II**[32]), Sun (**III**[72]) and Rauchfuss (**IV**,[73] **V**[44] and **VI**[44]) and their co-workers.

the two irons.[49] Isomerism between systems featuring bridged and terminal COs can be achieved by rotating one $Fe(CO)_3$ fragment.The relationship between "bridged" and "non-bridged" isomers has been described by Hall *et al.*, who describe them as "rotated" and "unrotated" isomers (see Figure II-7).[62] One possible role for this "rotation" is to open an empty site on one of the irons to allow the bonding of a proton. Rauchfuss and co-workers have shown that this bridging CO ligand can be tuned by the ligands surrounding one of the Fe centres.[49]

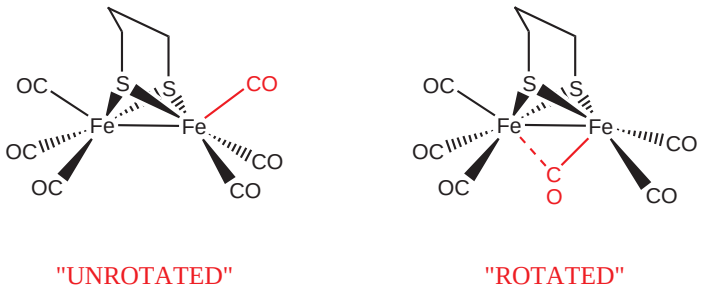

Figure II-7: "Rotated" and "unrotated" structures.

To know the structure of a compound and understand the impact of its different components is important, but the purpose of this work is to understand the catalytic process, and so confirm the design of di-iron compounds to mimic the function of the H-cluster (active core of the hydrogenase enzyme). As seen in the previous section, the $[Fe_2S_2]_H$ cluster part of the H-cluster in the biological system is linked to a Fe_4S_4 cluster whose role is to deliver electrons to the di-iron part. The reduction is an important part of the catalytic cycle because it induces protonation, which leads to the formation of H_2. A number of experiments focusing on the behaviour of the di-iron compound at different levels of oxidation or reduction have been reported, the aim being to describe what happens to the compound during the catalytic cycle, which necessarily involves different oxidation levels of the $[Fe_2S_2]_H$ cluster.[8] In these studies electrodes replace the electron-donor $[Fe_4S_4]$cubane cluster present in the biological system.[32]

The reduction of Fe_2 is the key point of H_2 production[31] and as such it has been extensively studied using electrochemistry.[32,70,74–80] Darensbourg *et al.*[55] proposed that the oxidation state of the iron cores is $Fe^I{-}Fe^I$ for the initial complex, and then present potential reduction cycles as shown in the left part of Figure II-8.[55] The first possible pathway shows two successive electron additions and the resulting oxidation state becomes $[Fe^0{-}Fe^0]^{2-}$ (*via* a $[Fe^0{-}Fe^I]^-$ intermediate). From this oxidation state two protons are added successively (*via* a $[(H)Fe^{II}{-}Fe^0]^-$ intermediate) and the $Fe^I{-}Fe^I$ is regenerated when the H_2 formed is released. The second possible catalytic pathway is similar to the first with the difference that a proton is added immediately after each addition of a single electron. On another hand Zampella and co-workers[81] have proposed that the initial state possesses a $Fe^{II}{-}Fe^I$ oxidation state (see right part of Figure II-8). An electron is then added generating an oxidation state of $[Fe^I{-}Fe^I]^-$ followed by the addition of the first proton (iron cores become $(H)Fe^{II}{-}Fe^I$). Similarly an electron and then a proton are added a second time giving $[(H_2)Fe^{II}{-}Fe^I]$ (*via* a $[(H)Fe^{II}{-}Fe^I]^-$ intermediate). The initial species is then regenerated by release of the dihydrogen molecule formed.

Both propositions are present in the biological catalytic processes and are dependent of the activation process of the enzyme.

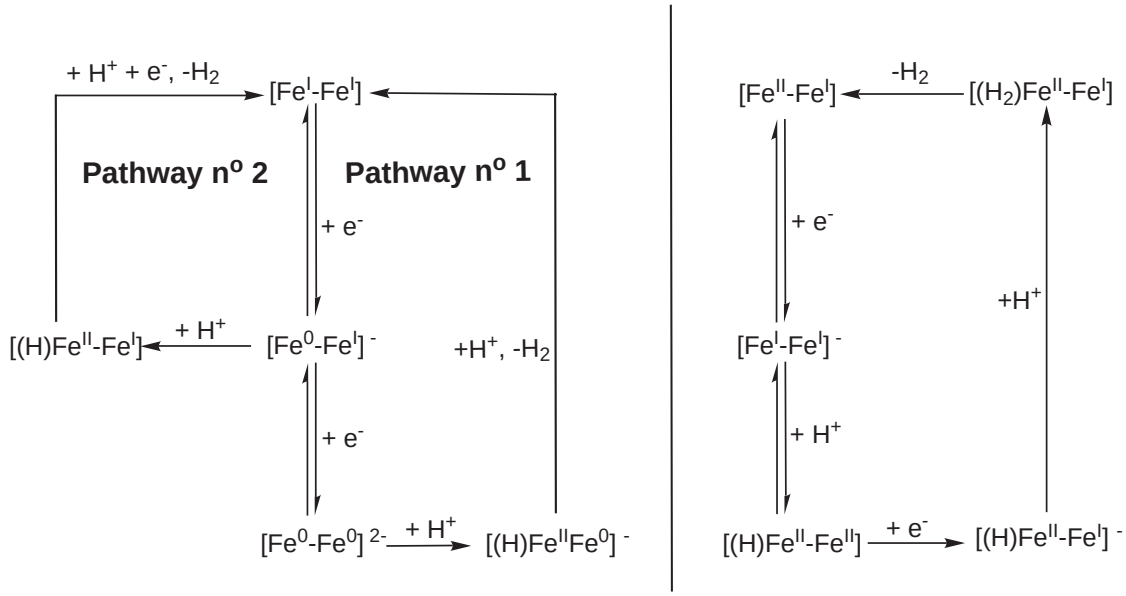

Figure II-8: Oxidation states of the iron centres during the catalytic process as proposed by Darensbourg[55] (left side) and Zampella[81] (right side) and their respective co-workers.

The addition of electrons (reduction of the Fe_2 core) is generally directly followed by the addition of a proton. Talarmin and co-workers[32] have shown that the reduction pathway is a successive addition of two electrons, and so two protons, in two distinctive steps but the anchor points of the protons in the molecule is still an open question.[82,83] There is, however, only a limited number of possible sites available to bind a proton on the complex. The possible sites found to play this role are: *(i)* directly on one iron,[84] *(ii)* at the bridging position between the two Fe,[76,85] *(iii)* on the N bridgehead (if DTMA S-to-S linker used)[76,84,85] or other entity with an appropriate basicity, *(iv)* on the iron thiolato bridge sulphurs, *(v)* on one of the CN^- ligands[60] or, finally, *(vi)* on the S of the modelled thiolato bridge linking the $[Fe_2S_2]_H$ cluster to the $[Fe_4S_4]$ cubane cluster in nature. The binding of a proton on one or both of the iron centres appears to be a recurrent choice in many studies.[76,84,85] A

number of studies have already tried to deal with the question of the site of proton binding and proposed some possible pathways. For example the first proton may be bonded to the distal iron and the second on the N belonging to the S-to-S linker (in the case of a DTMA bridge).[13,17,86] It is clear that the number of possible sites described earlier for protonation increases the number of possible pathways.[57,87] As an example of this diversity, the studies done by Gloaguen and co-workers can be cited. They argue that the first proton is placed as a bridge between the two iron centres and the second proton binds to one of the CN^- ligands.[60] There is another structural feature which seems to play an important role in the proton approach: the bridgehead ligand.[82,83,88] The presence of a basic functional group on the bridgehead position can extend the number of proton binding sites.

Two examples of catalytic cycles are presented in Figure II-9. They are simplified examples of hypotheses proposed in the literature.[55,83,89,90] The first cycle involves six distinct compounds, **1**-**6**. Species **1** is the starting catalyst, and need to be reduced first (species **2**) to coordinate H^+ at the distal iron (species **3**). Reduction of the compound (species **4**) and addition of a second proton yields **5**, where the two hydrogen atoms are attached to Fe and S. After rearrangement of the protons (species **6**), dihydrogen is released regenerating the starting complex **1**. The cycle being reversible, the oxidation of H_2 follows the opposite pathway. The second catalytic cycle is only slightly different to the first. The difference comes from the presence of an amino group on the bridgehead position (DTMA bridge) instead of a CH_2 group. This difference induces a change in the sites of protonation; the first hydrogen will be bound to the distal iron as in the first cycle but the second proton will be bound to the nitrogen atom of the DTMA bridge, this time, which is the main difference with the first catalytic cycle described.

In chapter 3, we describe a series of calculations performed in collaboration with the group of Professor Jean Talarmin in Brest, who have synthesised and studied an unusual Fe_2 species with a pendant OMe group attached to the bridgehead nitrogen

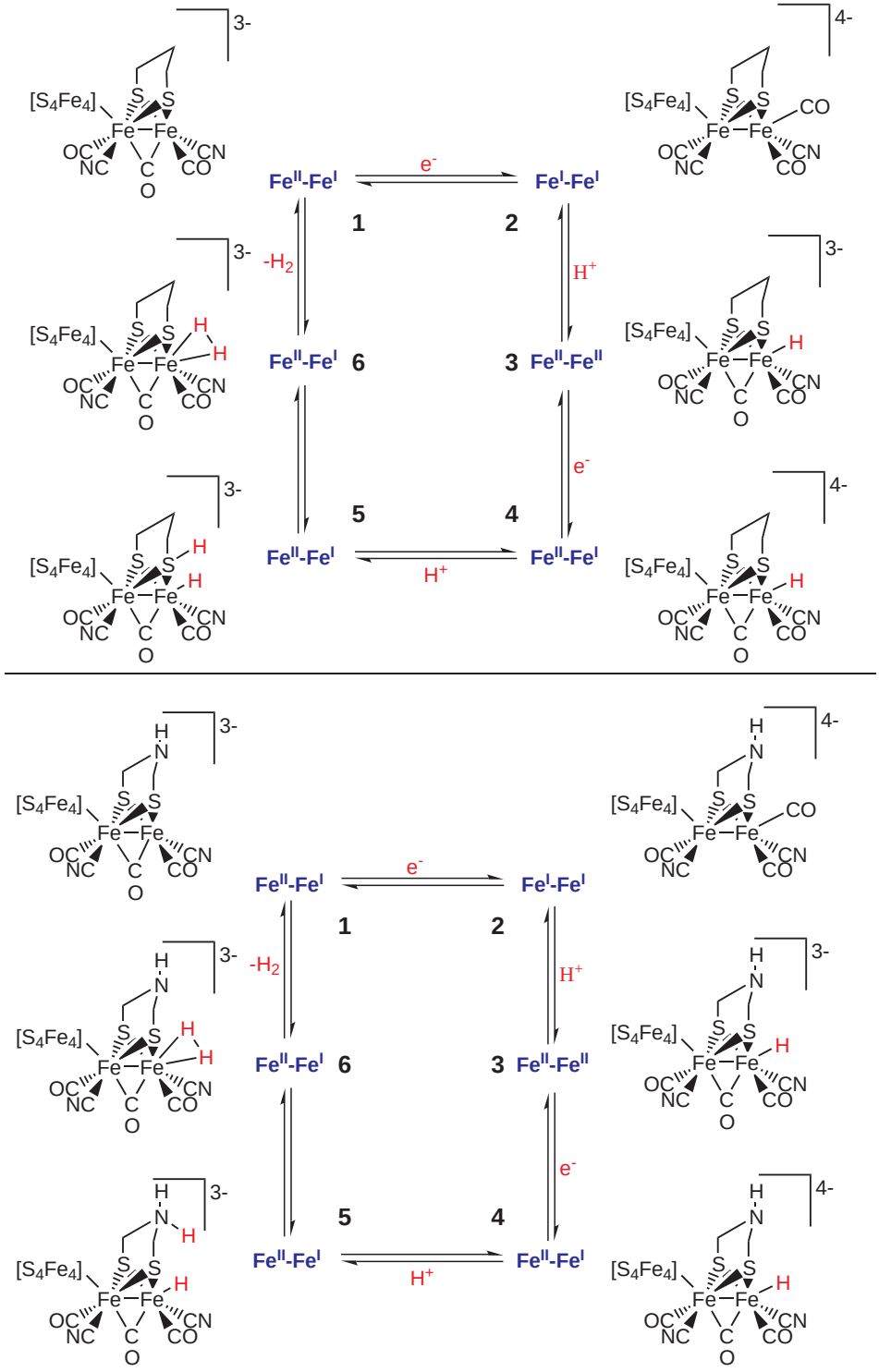

Figure II-9: Two examples of hypothetical catalytic cycles for the formation/oxidation of H_2

(Figure II-4 (II)). The purpose was to explore the potential role of this group as a donor to the metal centre, and the influence of this coordination on the catalytic cycle.

In chapter 4, we extend this work to consider the site of protonation at a dinuclear Fe_2 site, which has been characterised by Schollhammer and co-workers in Brest using NMR Spectroscopy. By computing NMR parameters (δ, J), we have been able to validate and, in some cases refine the structural assignments made in their original work.

Bibliography

[1] Weaver, P. F.; Lien, S.; Seibert, M. *Solar Energy*, **1980**, *24*, 3.

[2] Albracht, S. P. J. *Biochim. Biophys. Acta*, **1994**, *1188*, 167.

[3] Pershad, H. R.; Duff, J. L. C.; Heering, H. A.; Duin, E. C.; Albracht, S. P. J.; Armstrong, F. A. *Biochemistry*, **1999**, *38*, 8992.

[4] Vincent, K. A.; Cracknell, J. A.; Parkin, A.; Armstrong, F. A. *Dalton Trans.*, **2005**, 3397.

[5] Hallenbeck, P. C.; Benemann, J. R. *Int. J. Hydrogen Energy*, **2002**, *27*, 1185.

[6] Stephenson, M.; Stickland, L. H. *Biochem. J.*, **1930**, *25*, 205.

[7] Darensbourg, M. Y.; Lyon, E. J.; Smee, J. J. *Coord. Chem. Rev.*, **2000**, *206-207*, 533.

[8] Evans, D. J.; Pickett, C. J. *Chem. Soc. Rev.*, **2003**, *32*, 268.

[9] Hedderich, R.; Klimmek, O.; Kröger, A.; Dirmeier, R.; Keller, M.; Stetter, K. O. *Microbio. Rev.*, **1999**, *22*, 353.

[10] Gaffron, H. *Nature*, **1939**, *143*, 204.

[11] Gaffron, H.; Rubin, J. *J. Gen. Physiol.*, **1942**, *26*, 219.

[12] Matias, P. M.; Pereira, I. A. C.; Soares, C. M.; Carrondo, M. A. *Progress in Biophysics and Molecular Biology*, **2005**, *89*, 292.

[13] Nicolet, Y.; Piras, C.; Legrand, P.; Hatchikian, C. E.; Fontecilla-Camps, J. C. *Structure*, **1999**, *7*, 13.

[14] Vignais, P. M.; Billoud, B.; Meyer, J. *FEMS Microbiol. Rev.*, **2001**, *25*, 455.

[15] Das, D.; Dutta, T.; Nath, K.; Kotay, S. M.; Das, A. K.; Veziroglu, T. *Current Science*, **2006**, *90*, 1627.

[16] Volbeda, A.; Charon, M.-H.; Piras, C.; Hatchikian, E. C.; Frey, M.; Fontecilla-Camps, J. C. *Nature*, **1995**, *373*, 580.

[17] Nicolet, Y.; Cavazza, C.; Fontecilla-Camps, J. C. *J. Inorg. Biochem.*, **2002**, *91*, 1.

[18] Peters, J. W.; Lanzilotta, W. N.; Lemon, B. J.; Seefeldt, L. C. *Science*, **1998**, *282*, 1853.

[19] Zirngibl, C.; Hedderich, R.; Thauer, R. K. *FEBS Lett.*, **1990**, *261*, 112.

[20] Schwörer, B.; Fernández, V. M.; Zirngibl, C.; Thauer, R. K. *Eur. J. Biochem.*, **1993**, *212*, 255.

[21] Hartmann, G. C.; Santamaria, E.; Fernández, V. M.; Thauer, R. K. *J. Biol. Inorg. Chem.*, **1996**, *1*, 446.

[22] Korbas, M.; Vogt, S.; Meyer-Klaucke, W.; Bill, E.; Lyon, E. J.; Thauer, R. K.; Shima, S. *J. Biol. Chem.*, **2006**, *281*, 30804.

[23] Shima, S.; Thauer, R. K. *The Chemical Record*, **2007**, *7*, 37.

[24] Kentemich, T.; Haverkamp, G.; Bothe, H. *Naturwissenschaften*, **1995**, *77*, 12.

[25] Tosatto, S. C. E.; Giacometti, G. M.; Valle, G.; Costantini, P. *Biochem. and Biophys. Research Com.*, **2006**, *339*, 277.

[26] Agrawal, A. G.; Voordouw, G.; Gärtner, W. *Antonie van Leeuwenhoek*, **2006**, *90*, 281.

[27] Schröder, O.; Bleijlevens, B.; de Jongh, T. E.; Chen, Z.; Li, T.; Fischer, J.; Förster, J.; Friedrich, C. G.; Bagley, K. A.; Albracht, S. P. J.; Lubitz, W. *J. Biol. Inorg. Chem.*, **2007**, *12*, 212.

[28] Meyer, J. *Cell. Mol. Life Sci.*, **2007**, *64*, 1063.

[29] Adams, M. W. W.; Mortenson, L. E. *J. Biol. Chem.*, **1984**, *259*, 7045.

[30] Démentin, S.; Belle, V.; Bertrand, P.; Guigliarelli, B.; Adryanczyk-Perrier, G.; De Lacey, A. L.; Fernadez, V. M.; Rousset, M.; Léger, C. *J. Am. Chem. Soc.*, **2006**, *128*, 5209.

[31] Capon, J.-F.; Gloaguen, F.; Schollhammer, P.; Talarmin, J. *Coord. Chem. Rev.*, **2005**, *249*, 1664.

[32] Capon, J.-F.; Ezzaher, S.; Gloaguen, F.; Pétillon, F. Y.; Schollhammer, P.; Talarmin, J.; Davin, T. J.; McGrady, J. E.; Muir, K. W. *New J. Chem.*, **2007**, *31*, 2052.

[33] Armstrong, F. A. *Curr. Opin. Struct. Biol.*, **2004**, *8*, 133.

[34] Trohalaki, S.; Pachter, R. *Energy & Fuels*, **2007**, *21*, 2278.

[35] Reihlen, H.; Gruhl, A.; Hessling, G. *Liebigs Ann. Chem.*, **1929**, *472*, 268.

[36] von Hieber, W.; Gruber, J. *Z. anorg.allgem. Chem.*, **1958**, *296*, 91.

[37] Dahl, L. F.; Wei, C. H. *Inorg. Chem.*, **1965**, *4*, 1.

[38] Seyferth, D.; Henderson, R. S. *J. Am .Chem. Soc.*, **1979**, *101*, 508.

[39] Winter, A.; Zsolnai, L.; Huttner, G. *Z. Naturforsch. B*, **1982**, *37*, 1430.

[40] Lyon, J. E.; Georgakaki, L. P.; Reibenspies, J. H.; Darensbourg, M. Y. *Angew. Chem. Int. Ed.*, **1999**, *38*, 3178.

[41] Song, L.-C.; Lu, G.-L.; Hu, Q.-M.; Fan, H.-T.; Chen, Y.; Sun, J. *Organometallics*, **1999**, *18*, 3258.

[42] Westmeyer, M. D.; Rauchfuss, T. B.; Verma, A. K. *Inorg. Chem.*, **1996**, *35*, 7140.

[43] Song, L.-C.; Tang, M.-Y.; Su, F.-H.; Hu, Q.-M. *Angew. Chem. Int. Ed.*, **2006**, *45*, 1130.

[44] Lawrence, J. D.; Li, H.; Rauchfuss, T. B. *Chem. Comm.*, **2001**, 1481.

[45] Han, J.; Huang, M.; Coucouvanis, D. *Polyhedron*, **2002**, *21*, 2523.

[46] Broadhurst, P. V.; Johnson, B. F. G.; Lewis, J.; Raithby, P. R. *Chem. Commun.*, **1982**, 140.

[47] Song, L.-C.; Qin, X.-D.; Hu, Q.-M.; Huang, X.-Y. *Organometallics*, **1998**, *17*, 5437.

[48] Schmidt, M.; Contakes, S. M.; Rauchfuss, T. B. *J. Am. Chem. Soc.*, **1999**, *121*, 9736.

[49] Boyke, C. A.; van der Vlugt, J. I.; Rauchfuss, T. B.; Wilson, S. R.; Zampella, G.; De Gioia, L. *J. Am. Chem. Soc.*, **2005**, *127*, 11010.

[50] Boyke, C. A.; Rauchfuss, T. B.; Wilson, S. R.; Rohmer, M.-M.; Bénard, M. *J. Am. Chem. Soc.*, **2004**, *126*, 15151.

[51] Adams, R. D.; Miao, S. *Inorg. Chem.*, **2004**, *43*, 8414.

[52] Razavet, M.; Davies, S. C.; Hughes, D. L.; Pickett, C. J. *Chem. Commun.*, **2001**, 847.

[53] Song, L.-C.; Yang, Z.-Y.; Bian, H.-Z.; Hu, Q.-M. *Organometallics*, **2004**, *23*, 3082.

[54] Marr, A. C.; Spencer, D. J. E.; Schröder, M. *Coord. Chem. Rev.*, **2001**, *219-221*, 1055.

[55] Chong, D.; Georgakaki, I. P.; Mejia-Rodriguez, R.; Sanabria-Chinchilla; Soriaga, M. P.; Darensbourg, M. Y. *Dalton Trans.*, **2003**, 4158.

[56] Lyon, E. J.; Georgakaki, I. P.; Reibenspies, J. H.; Darensbourg, M. Y. *J. Am. Chem. Soc.*, **2001**, *123*, 3268.

[57] Gloaguen, F.; Lawrence, J. D.; Rauchfuss, T. B. *J. Am. Chem. Soc.*, **2001**, *123*, 9476.

[58] Ezzaher, S.; Capon, J.-F.; Gloaguen, F.; Pétillon, F. Y.; Schollhammer, P.; Talarmin, J.; Pichon, R.; Kervarec, N. *Inorg. Chem.*, **2007**, *46*, 3426.

[59] Justice, A. K.; Zampella, G.; De Gioia, L.; Rauchfuss, T. B.; Van der Vlugt, J. I.; Wilson, S. R. *Inorg. Chem.*, **2007**, *46*, 1655.

[60] Gloaguen, F.; Lawrence, J. D.; Rauchfuss, T. B.; Bénard, M.; Rohmer, M.-M. *Inorg. Chem.*, **2002**, *41*, 6573.

[61] Dowa, J. R.; Zanoti, V.; Facchin, G.; Angelici, R. J. *J. Am. Chem. Soc.*, **1992**, *114*, 160.

[62] Tye, J. W.; Darensbourg, M. J.; Hall, M. B. *Inorg. Chem.*, **2006**, *45*, 1552.

[63] Lawrence, J. D.; Rauchfuss, T. B.; Wilson, S. R. *Inorg. Chem.*, **2002**, *41*, 6193.

[64] van der Vlugt, J. I.; Rauchfuss, T. B.; Wilson, S. R. *Chem. Eur. J.*, **2006**, *12*, 90.

[65] Morvan, D.; Capon, J.-F.; Gloaguen, F.; Le Goff, A.; Marchivie, M.; Michaud, F.; Schollhammer, P.; Talarmin, J.; Yaouanc, J.-J.; Pichon, R.; Kervarec, N. *Organometallics*, **2007**, *26*, 2042.

[66] Duan, L.; Wand, M.; Li, P.; Na, Y.; Wang, N.; Sun, L. *Dalton Trans.*, **2007**, 1277.

[67] Hogarth, G.; Richards, I. *Inorg. Chem. Commun.*, **2007**, *10*, 66.

[68] Gao, W.; Ekström, J.; Liu, J.; Chen, C.; Eriksson, L.; Weng, L.; Åkermark, B.; Sun, L. *Inorg. Chem.*, **2007**, *46*, 1981.

[69] Nicolet, Y.; de Lacey, A. L.; Vernède, X.; Fernandez, V. M.; Hatchikian, E. C.; Fontecilla-Camps, J. C. *J. Am. Chem. Soc.*, **2001**, *123*, 1596.

[70] Gloaguen, F.; Lawrence, J. D.; Schmidt, M.; Wilson, S. R.; Rauchfuss, T. B. *J. Am. Chem. Soc.*, **2001**, *123*, 12518.

[71] Razavet, M.; Davies, S. C.; Hughes, D. L.; Barclay, J. E.; Evans, D. J.; Fairhurst, S. A.; Liu, X.; Pickett, C. J. *Dalton Trans.*, **2003**, 586.

[72] Liu, T.; Wang, M.; Shi, Z.; Cui, H.; Dong, W.; Chen, J.; Åkermark, B.; Sun, L. *Chem. Eur. J.*, **2004**, *10*, 4474.

[73] Li, H.; Rauchfuss, T. B. *J. Am. Chem. Soc.*, **2002**, *124*, 726.

[74] Guiral-Brugna, M.; Giudici-Orticoni, M.-T.; Bruschi, M.; Bianco, P. *J. Electroanalytical Chem.*, **2001**, *510*, 136.

[75] Wang, Z.; Liu, J.-H.; He, C.-J.; Jiang, S.; Åkermark, L.-C. Sun. *J. Organomet. Chem.*, **2007**, *692*, 5501.

[76] Capon, J.-F.; Ezzaher, S.; Gloaguen, F.; Pétillon, F. Y.; Schollhammer, P.; Talarmin, J. *Chem. Eur. J.*, **2008**, *14*, 1954.

[77] Hambourger, M.; Gervaldo, M.; Svedruzic, D.; King, P. W.; Gust, D.; Ghirardi, M.; Moore, A. L.; Moore, T. A. *J. Am. Chem. Soc.*, **2008**, *130*, 2015.

[78] Gao, S.; Fan, J.; Sun, S.; Peng, X.; Zhao, X.; Hou, J. *Dalton Trans.*, **2008**, 2128.

[79] Yu, Z.; Wang, M.; Li, P.; Dong, W.; Wang, F.; Sun, L. *Dalton Trans.*, **2008**, 2400.

[80] Li, P.; Wang, M.; Pan, J.; Chen, L.; Wang, N.; Sun, L. *J. Inorg. Biochem.*, **2008**, *102*, 952.

[81] Zampella, G.; Greco, C.; Fantucci, P.; De Gioia, L. *Inorg. Chem.*, **2006**, *45*, 4109.

[82] Henry, R. M.; Shoemaker, R. K.; DuBois, D. L.; DuBois, M. R. *J. Am. Chem. Soc.*, **2006**, *128*, 3002.

[83] Liu, X.; Ibrahim, S. K.; Tard, C.; Pickett, C. J. *Coord. Chem. Rev.*, **2005**, *249*, 1641.

[84] Barton, B. E.; Rauchfuss, T. B. *Inorg. Chem.*, **2008**, *47*, 2261.

[85] Löscher, S.; Schwartz, L.; Stein, M.; Ott, S.; Haumann, M. *Inorg. Chem.*, **2007**, *46*, 11094.

[86] Nicolet, Y.; Lemon, B. J.; Fontecilla-Camps, J. C.; Peters, J. W. *Trends Biochme. Sci.*, **2000**, *25*, 138.

[87] Borg, S. J.; Tye, J. W.; Hall, M. B.; Best, S. P. *Inorg. Chem.*, **2007**, *46*, 384.

[88] Ott, S.; Kritikos, M.; Åkemark, B.; Sun, L.; Lomoth, R. *Angew. Chem. Int. Ed.*, **2004**, *43*, 1006.

[89] Best, S. P. *Coord. Chem. Rev.*, **2005**, *249*, 1536.

[90] Borg, S. J.; Behrsing, T.; Best, S. P.; Razavet, M.; Liu, X.; Pickett, C. J. *J. Am. Chem. Soc.*, **2004**, *126*, 16988.

CHAPTER III

Computational studies of hydrogenase-like models

Introduction

In the previous chapter, an overview of the biological and chemical aspects of hydrogenase and hydrogenase-like systems has been presented. In this chapter, we present a computational study of the consequences of 1- and 2-electron reduction of a model Fe_2 compound. This work was performed in collaboration with Professor Jean Talarmin at the University of Brest, and has been published in the *New Journal of Chemistry* in 2007.

In order to place this work into context, previous computational studies of Fe_2 systems, performed in the context of hydrogenase activity, are reviewed.

Over the past decade, the development of density functional theory has provided quantitative insight into the structures and properties of transition metal systems which has helped significantly in the understanding of hydrogenase and many other metalloenzymes. In most cases computational chemistry is used as a tool to assess experimental results and, in complement to the experiments, to understand the properties of a specific molecule. Experimental studies of H_2 production/oxidation catalysis are in their early stages, but the use of computational chemistry is a powerful tool to predict possible catalytic cycles and so guide future experiments. The

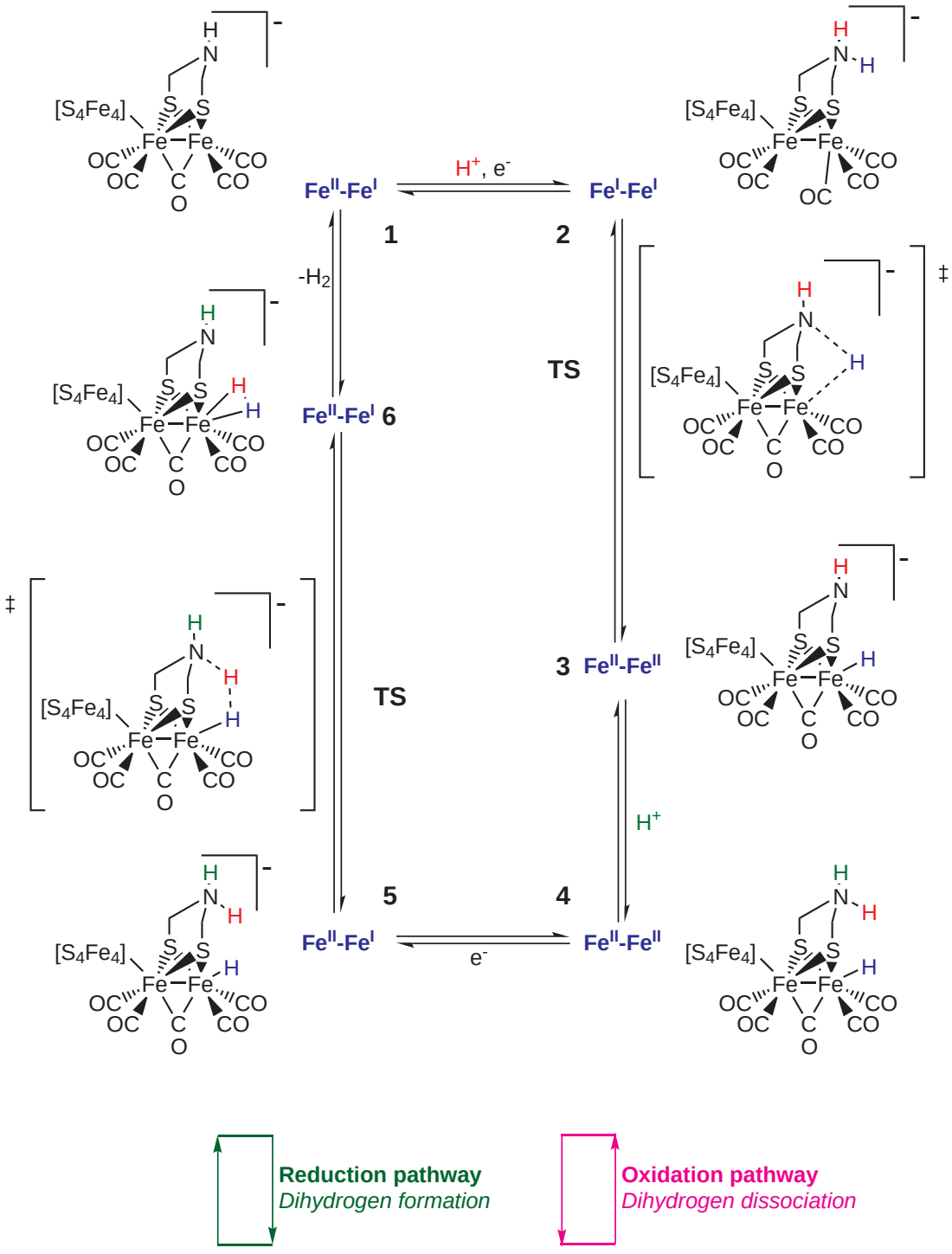

Figure III-1: Proposed computed Catalytic cycle, summary of De Gioia *et al.*,[11] Liu and Hu,[2] Fan and Hall[4] and Zampella *et al.*[8] work.

catalytic cycle summarising the computational studies of De Gioia *et al.*, Liu and Hu, Fan and Hall and Zampella *et al.* presented in Figure III-1, is a good illustration of how theory has been used to inform experiment.[2,4,8,11]

In Figure III-1, the catalytic pathway is initiated by the reduction of the metal centres. This process has been considered by Popescu *et al.* to involve Fe^{III}–Fe^{III}, Fe^{III}–Fe^{II} and Fe^{II}–Fe^{II} oxidation levels.[3] However, later studies done by Cao and Hall using DFT calculations show that these oxidation states are not compatible with experimental IR data and that the cycle is more likely to involve Fe^{I}–Fe^{I}, Fe^{II}–Fe^{I} and Fe^{II}–Fe^{II} (structure **2**, **1** and **3**, respectively, in Figure III-1).[16] The impact of the reduction process on the di-thiolato di-iron systems' structure is the elongation of the Fe-Fe bond (see Figure III-2). Computational results obtained by Ziegler and co-workers confirm that the impact of the two step reduction is directly felt by the Fe-Fe bond which is elongated.[5] By optimising the different reduction steps, De Gioia *et al.* also found that the Fe-Fe bond is elongated from 2.71 for the neutral to 3.74 Å for the dianion species.[6] This is easily explained by the fact that the HOMO and LUMO of the system are the Fe-Fe σ and σ^* orbitals as shown by Hsu and co-workers.[7] Naturally, the reduction of the system is done *via* the filling of the Fe-Fe σ^* orbital, which obviously leads to the breaking of the iron bond (see Figure III-2).

De Gioia and co-workers have suggested that the oxidation pathway (from **6** to **1** in Figure III-1) might differ from the reduction pathway by the presence of an additional Fe^{III}–Fe^{II} intermediate.[8]

Hu and co-workers (and also Hall *et al.*) have also argued that although the Fe^{II}–Fe^{I} oxidation state can not bind a proton, it is an important precursor to the proton reduction. Later, Brunold *et al.* have shown that this Fe^{II}–Fe^{I} oxidation state (**6**) is valence localised: Fe_p^{2+}–Fe_d^{+} and that the Fe^{II}–Fe^{II} state (**4**), in contrast, is an inactive species which is stable in normal conditions but needs to be activated to start the catalytic cycle.[9] The model structures proposed by Hu and Hall and their respective co-workers for each oxidation state are described more pre-

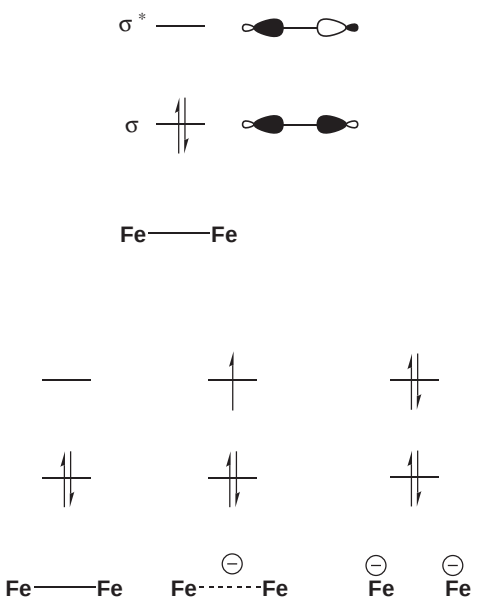

Figure III-2: Reduction of the Fe-Fe bond due to the reduction of the hydrogenase-like system.

cisely in Figure III-3. The three oxidation states presented fit the three oxidation states observed in the biological catalytic cycle (Figure II-3): a completely reduced (catalytically inactive) form, $[Fe^{I}-Fe^{I}]$, H_{ox}^{inact} (also called H_{ox}^{air}), a partially oxidised form (active state of the catalyst), $[Fe^{II}-Fe^{I}]$, H_{ox}^{cat} (or H_{ox}) and a totally oxidised form of the $[Fe_2S_2]_H$ cluster, $[Fe^{II}-Fe^{II}]$, H_{red}.[10,11]

A certain number of computational studies have also shown that the presence of a bridging ligand between the two iron centres (usually a CO) changes the impact exerted by the addition of electrons. The Fe-Fe bond breaking discussed previously is replaced here by the displacement of the bridging CO from its initial position to a position closer to one of the iron centres.[8,12–14]

Hu and Hall's DFT calculations on hydrogenase-like models containing different S-to-S bridges ($-CH_2NHCH_2-$ for Hu and $-CH_2CH_2CH_2-$ for Hall) (see Figure III-3) have shown that a change in S-to-S bridge does not change the oxidation states of H_{ox}^{inact}, H_{ox} and H_{red} oxidation states.[1,2] The optimisation of structures possessing different bridgeheads also suggests that the S-to-S bridge (which can be electron

acceptor or donor) has no effect on the stabilisation of the molecule and so does not favour one geometry over another.[15]

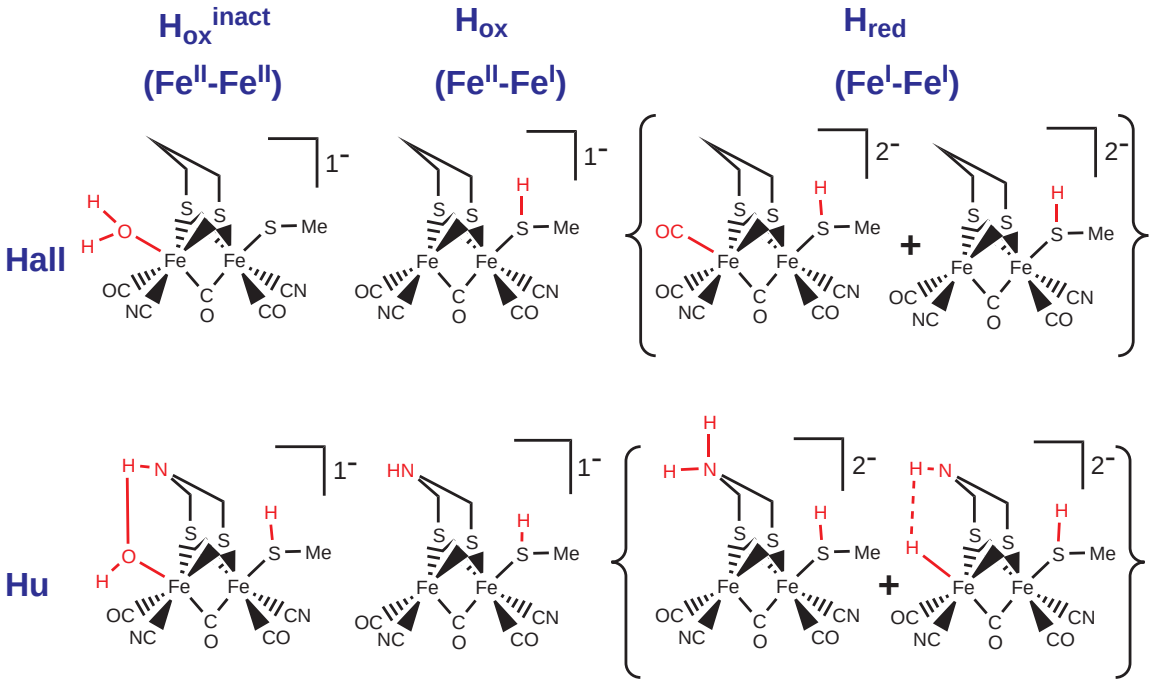

Figure III-3: Computational models of Hall[4,16,17] and Hu[1,2] which match closely the experimental data for H_{ox}^{inact}, H_{ox} and H_{red} forms of the $[Fe_2S_2]_H$ cluster.

However, the bridge between the two sulphur atoms is a structural feature which has an important influence on the catalytic properties of the compound. As mentioned in the previous chapter, the S-to-S linker can, indeed, affect the rotation of the iron fragment[18] and also influences the pathway of dihydrogen cleavage/production.

For example, the possible role of a nitrogen group at the bridgehead position has been described by a number of groups.[1,2,4] Sun *et al.* have shown, using electrochemical reduction, that the protonation on the nitrogen atom can play a significant role in catalysis by shifting the reduction potential of the diiron subunit to more positive values.[19,20] Calculations reported by Hall and Cao and by De Gioia suggest that the presence of such a basic group reduces the calculated barrier for H-H cleavage substantially (6.53 kcal/mol for DTMA versus 17.4 kcal/mol for PDT bridge).[4,11,16] In the reductive cycle, the bridge also plays a key role in directing the site of protonation. For example, De Gioia *et al.* have agreed that the nitrogen centre directs the

first proton towards the iron closest to the bridgehead position. The second proton then binds directly to the nitrogen, in close proximity to the first, thereby reducing the entropic barrier to H-H bond formation by 25 kcal/mol (see Figure III-4).[21,22]

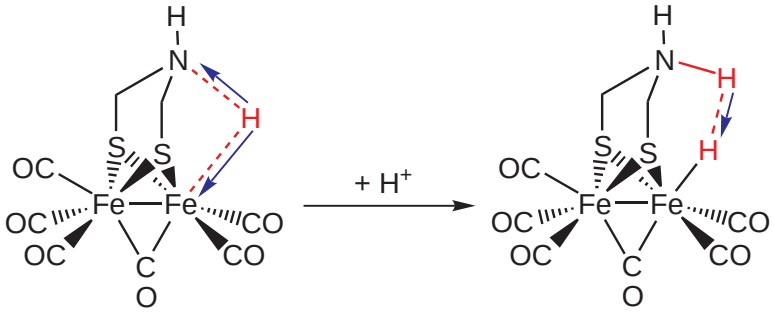

Figure III-4: Influence of the presence of the N as a bridgehead for the channeling of hydrogen.

Car and co-workers have confirmed that the presence of a NH group in the centre of the S-to-S bridge influences the approach of hydrogen due to the nitrogen's basicity.[23]

Beyond the catalytic reactions, the nature of the bridge can also play a role in defining the orientation of ligands around the iron centres. For example, in the dppe system, $Fe_2(CO)_4(\mu{-}SRS)(dppe)$, a DTMA bridge favours the basal-basal isomer while a $-(CH_2)_3-$ bridge stabilises the basal-apical structure (see Figure III-5).[24]

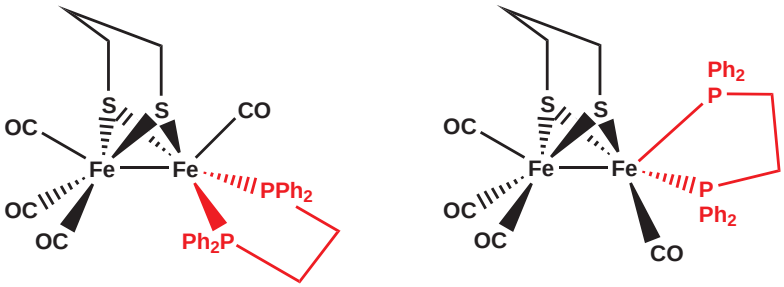

Figure III-5: The possible positioning of the dppe di-chelating ligand: apical-basal and basal-basal.

1 - Our work

Talarmin and co-workers have studied the electrochemistry of a model compound (structure **II** in Figure III-6), possessing a customised S-to-S bridge. The presence of the pendant OMe group on the amine group of this S-to-S bridge was intended to mimic possible coordination of H_2O in the catalytic cycle *in vivo*. Thus this ligand offers the possibility of nitrogen-based protonation, as discussed by Hall, Hu and their respective co-workers, but also the possibility that reversible coordination of the OMe group can influence the barriers.

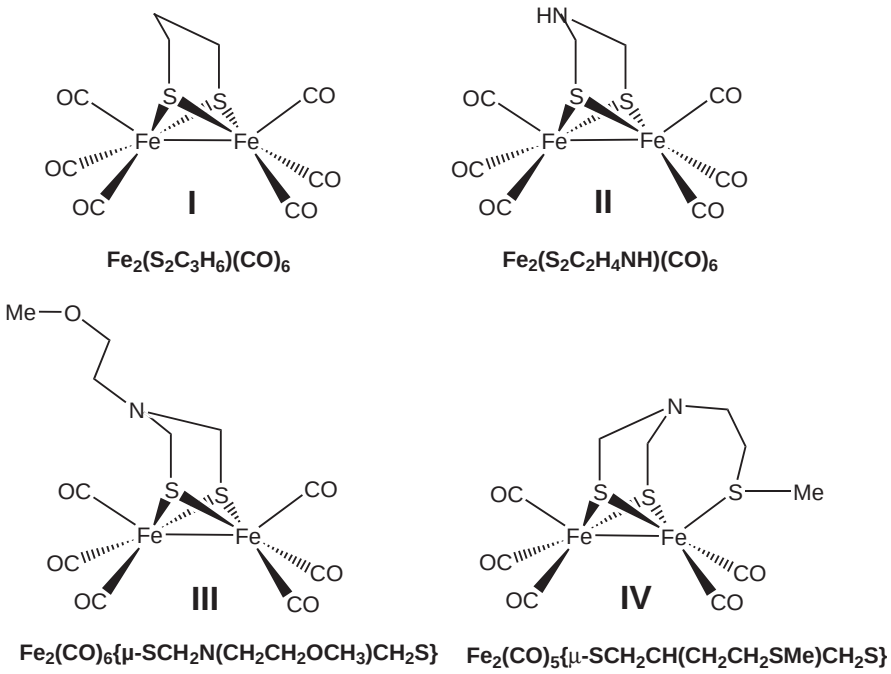

Figure III-6: Structures studied by Talarmin and Rauchfuss and their respective co-workers.

In the neutral $Fe^I{-}Fe^I$ species, however, coordination of the OMe group could not be induced by extraction of CO, as Rauchfuss *et al.* had done with a sulphur analogue, $[Fe_2(CO)_5(\mu{-}SCH_2N(CH_2CH_2SCH_3)CH_2S)]$ (see structure **IV** in Figure III-6).[25] This does not, however, exclude the possibility that the $N(CH_2CH_2OMe)$ group does coordinate at some other oxidation level which is important in the cat-

alytic reduction of protons. The key feature of Talarmin's study is the comparison of the reduction processes of **III**, shown above, with its simpler counterpart, **I**, where the pendant CH_2CH_2OMe group and the amine group are absent, eliminating the possibility of coordination of an additional ligand. Cyclic voltammetry performed under a CO atmosphere (see Figure III-7) suggests that the reduction products take part in subsequent chemical processes, generating daughter products **1'** and **2'** (see Figure III-8). The black line in Figure III-7 has been obtained by following the complete reduction-oxidation process while the red line has been obtained by reversing the current as soon as the first reduction has been reached.

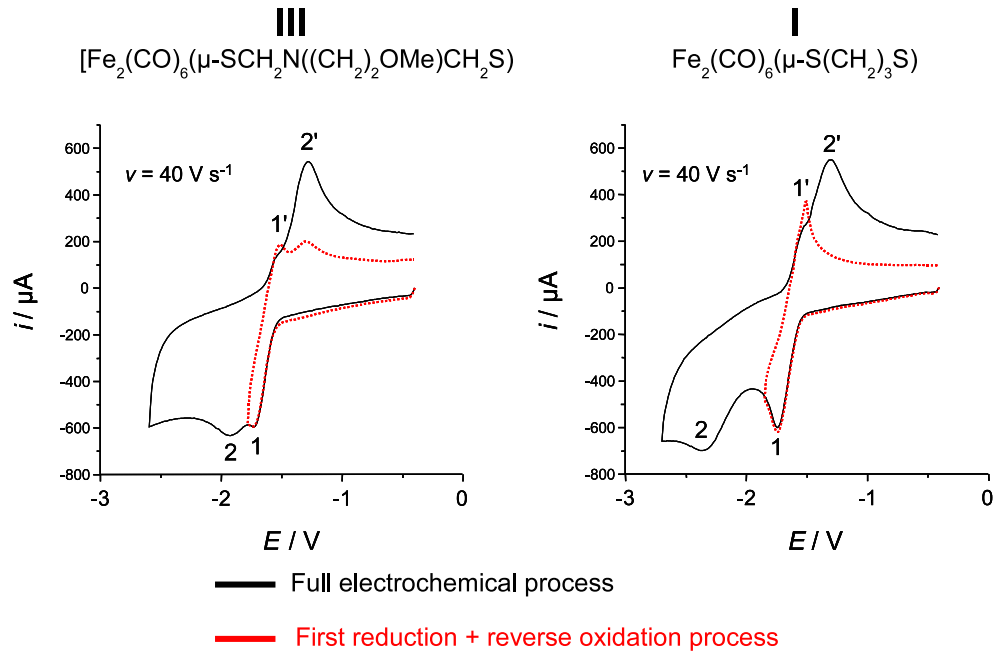

Figure III-7: Cyclic voltammetry of complexes $Fe_2(CO)_6(\mu{-}SRS)$ in MeCN-$[NBu_4]$-$[PF_6]$ under CO at 40 $V.s^{-1}$ scan rate (**III**, R=$CH_2N((CH_2)_2OMe)CH_2$ and **I**, R=$(CH_2)_3$).

Pickett *et al.* also studied the reduction of $[Fe_2(CO)_6(\mu{-}SRS)]$ and found a compound that is the possible analogue of product **2**.[26] This species exhibits two different IR vibrations, one typical of terminal CO coordination ($2032cm^{-1}$), the other of a bridging geometry ($1741cm^{-1}$). On this basis, they proposed the structure shown in Figure III-9. The possibility that Fe-S bonds, rather than Fe-Fe bonds as

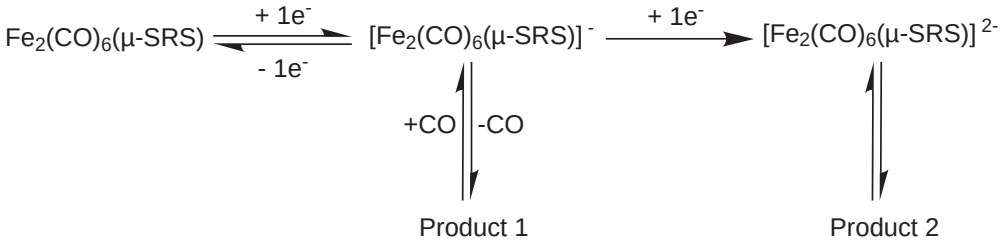

Figure III-8: Reduction reaction and the side products.

shown in Figure III-9, can be cleaved on reduction will be one of the key areas of interest in the results section.

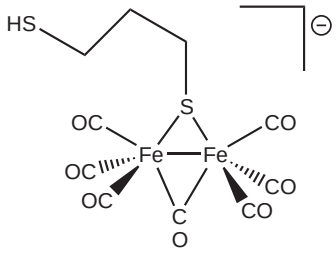

Figure III-9: $[Fe_2(CO)_6(\mu{-}CO)(\mu{-}S(CH_2)_3SH)]^-$ as observed by Pickett *et al.* with IR.

In the absence of CO, Talarmin and co-workers have observed that the identity of the S-to-S linker affects the thermodynamic stability of the anion. The second reduction of **III** occurs at a slightly less negative potential than the first one, which means that the disproportionation of the anion, shown in the following equation, is favoured, the overall reduction to dianion being a 2-electron process.

$$\mathbf{2\,[\,Fe_2(CO)_6(\mu{-}SRS)]^-} \overset{K_{disp}}{\rightleftharpoons} \mathbf{Fe_2(CO)_6(\mu{-}SRS)} + \mathbf{[Fe_2(CO)_6(\mu{-}SRS)]^{2-}}$$

In the case of **I**, in contrast, the potential of the second reduction is more negative than the first one which suggests that the anion is stable with respect to the disproportionation. This also suggests that the nature of the structural changes that accompany reduction is somewhat different in the two systems. The purpose of this chapter is to use density functional theory to explore the nature of the structural changes which occur during these processes, and to identify any potential role played

by the pendant OMe group.

These studies have been divided into two sections: the first deals with validation of our theoretical model; by making comparisons with known crystal structure data, we establish the optimal method to deal with systems of this type. In the second section, we consider the effects of reduction on the two systems, and also on the simple model where the linker is $-CH_2-NH-CH_2-$.

2 - Validation of methodology

Throughout this project, we use DFT as implemented in the Gaussian 03 software.[27] In the first section, we employ different combinations of functionals and basis sets to establish which one provides the best agreement with experimental data. In Table III-1, the optimised structural parameters for the simple model system $[Fe_2(CO)_6(\mu-pdt)]$ (pdt = $S(CH_2)_3S$) are summarised for a range of functionals and basis sets.

The Fe-Fe bond length and the Fe-S bond lengths are highly sensitive to basis set (Table III-1). In particular, the presence of polarisation functions on the sulphur results in a significant contraction and a much better agreement with experiment compared to those where polarisation is absent (6-31G basis set for S). Otherwise most combinations of basis set/functional give very similar results but the number of basis functions differs considerably. Thus, those with the 6-311G* basis set use 432 basis functions, increasing the calculation time significantly compared to the calculations made with the lanl2dz or the SDD basis set. On this basis, we consider that the best compromise between efficiency and structural accuracy is the SDD/6-31G* coupled with B3LYP.(see Table III-1)

Basis Set		**Basis functions**	**Functionals**	**Bond (in Å)**				
				Fe_1-Fe_2	Fe_1-S_3	Fe_1-S_4	Fe_2-S_3	Fe_2-S_4
6-31G*		(326)	B3LYP	2.47	2.30	2.30	2.31	2.31
			mPW1PW91	2.43	2.27	2.27	2.28	2.28
			O3LYP	2.50	2.29	2.29	2.30	2.30
6-311G*		(432)	B3LYP	2.47	2.30	2.30	2.31	2.31
			mPW1PW91	2.43	2.26	2.26	2.27	2.27
			O3LYP	2.49	2.28	2.28	2.29	2.29
LanL2DZ for Fe and	6-31G* for others	(316)	B3LYP	2.48	2.32	2.32	2.32	2.32
			mPW1PW91	2.44	2.27	2.27	2.28	2.28
			O3LYP	2.49	2.30	2.30	2.31	2.31
	6-31G for S 6-31G* for others	(306)	B3LYP	2.47	2.36	2.36	2.37	2.37
SDD for Fe and 6-31G* for others		(344)	B3LYP	2.51	2.31	2.31	2.32	2.32
			mPW1PW91	2.47	2.27	2.27	2.28	2.28
			O3LYP	2.53	2.29	2.29	2.30	2.30
Experiment[28]				*2.5103(11)*	*2.2542(10)*	*2.2491(10)*	*2.2542(10)*	*2.2491(10)*

pdt = propanedithiolate, $S(CH_2)_3S$

Table III-1: Basis set/functional comparison for $[Fe_2(CO)_6(\mu-pdt)]$.

Results

As said earlier, much of the interest in the chemistry of the di-thiolato di-iron systems relates to the role of the bridgehead group. In the context of this study, we wish to understand the impact of the $N(CH_2)_2OMe$ group on the complex structure.

It is clear from Figure III-7 that there is a subtle difference between the reduction of **I** and **III** (different potential between peaks *1* and *2* for one compound compared to the other). The difference between **III** and **I** shown in the cyclic voltamogramms might arise from a difference of disproportionation constant, K_{disp} of the anion species. Normally, two-electron transfers occur where the doubly reduced species is very stable relative to the anion. Thus, Talarmin and co-workers concluded that species **III** might have a disproportionation constant, $K_{disp} > 1$ while voltamogramm for species **I** is more consistent with, $K_{disp} \ll 1$. This situation typically arises if there is a consequent structural rearrangement which allows a more thermodynamically favourable transfer of the second electron than the first. This usually happens when the LUMO has strong σ antibonding character leading to large changes in bond length through reduction. In the bimetallic compounds studied here this LUMO often presents a dominant M-M σ antibonding character. In our case, this would normally leads to an increase of the Fe-Fe bond throughout reduction. However, differences observed earlier in the electrochemical studies suggest that this rearrangement might be influenced by the bridgehead substituent.
To confirm this hypothesis we looked at the impact of the bridgehead on the structural features of compound **I** and **III** as well as for an intermediate compound (possessing nitrogen on the bridgehead), **II** (see Figure III-6).

First, we have compared bond lengths for compound **III** (see Figure III-6) with simplified models **I** and **II** in the neutral state so as to check if the bridgehead has any impact on the structure itself. In Figure III-10 structural features for the three compounds are reported.

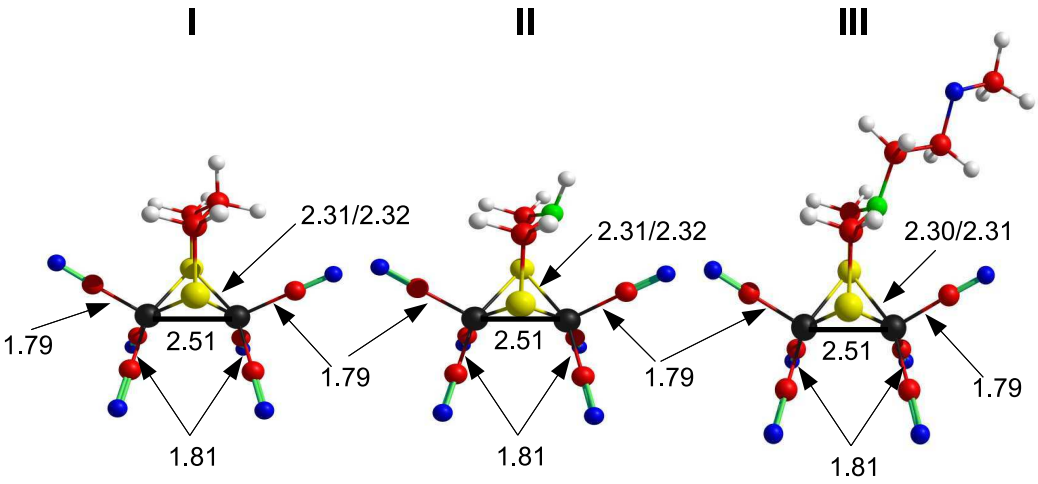

Figure III-10: Comparison of different possible bridgeheads for the neutral species (bond lengths in Å).

Compound **I** has already been extensively studied by other groups, and our optimised structure is fully consistent with earlier studies done by Hall and co-workers (in particular, the optimised Fe-Fe bond length of 2.51 Å is in excellent agreement with experiment).[16]

For the neutral Fe^{I}–Fe^{I} species we observe no significant changes on the most important bond lengths, Fe-Fe, Fe-S and Fe-C(O) stay unchanged regardless of the bridgehead group used. Our results shows that bridgehead has no impact on the structure itself in the initial stage. We now consider whether this remains the case for the more reduced species.

Following the studies done by Hall and co-workers[15] about the better stability of the "rotated" structures, we have searched for minima corresponding to the structures where one CO occupies a bridging position, as in the active site of the enzyme itself. However, in all cases optimisation led to the structure with all terminal CO ligands. In the next section, we consider the structural changes when we reduce the complex.

1 - Reduction of the Fe-Fe core

In light of the previous results, we looked at the possible impact of the bridgehead throughout the reduction of species **I**, **II** and **III**. As we noted previously, it is generally accepted that reduction of such systems causes an elongation of the Fe-Fe bond due to population of the Fe-Fe σ^* orbital. We first examine our three species following this hypothesis (Figure III-11)

As we can see from Figure III-11, the presence of different bridgeheads doesn't have any effect on the reduction of the $Fe_2(CO)_6(\mu-SRS)$ compounds, the Fe-Fe, Fe-S and Fe-C(O) are similar for the three species for both the anion and the dianion (see Figure III-11). We observe as well that no coordination of the OMe part (for the $N(CH_2)_2OMe$ bridgehead) with one of the iron is made, in contrast with the results obtained by Rauchfuss *et al.* for compound **IV** (Figure III-6) where (Me)S-Fe bond is formed.

1.a - Reduction of [(Fe(CO)$_3$)$_2$(μ−(SRS))]

The redox properties are clearly the key to understand the catalytic activity of the complex. This is also where the bridgehead might exert an influence on the system. We have considered the effects of adding one or two electrons to the neutral compound, possessing a $N(CH_2)_2OMe$ pendant on the bridgehead position, which has been described previously (Structure **A** in Figure III-12). One possible result of the reduction process is that the two electrons added enter the Fe-Fe σ^* orbital, and so break this bond. Alternatively, the increase of negative charge at the metal core may lead to the dissociation of one of the sulfide groups (Structures **B** and **C**) as proposed by Talarmin *et al.*.[29] The structure of **C** is reminiscent of the species observed by Pickett and co-workers (Figure III-9),[26] however with one fewer CO ligand in this case. If one of the sulfide ligands does dissociate, the presence of a vacant coordination site may allow the neutral OMe group to bond to the metal.

We have surveyed the potential energy surface for the anions and dianions and

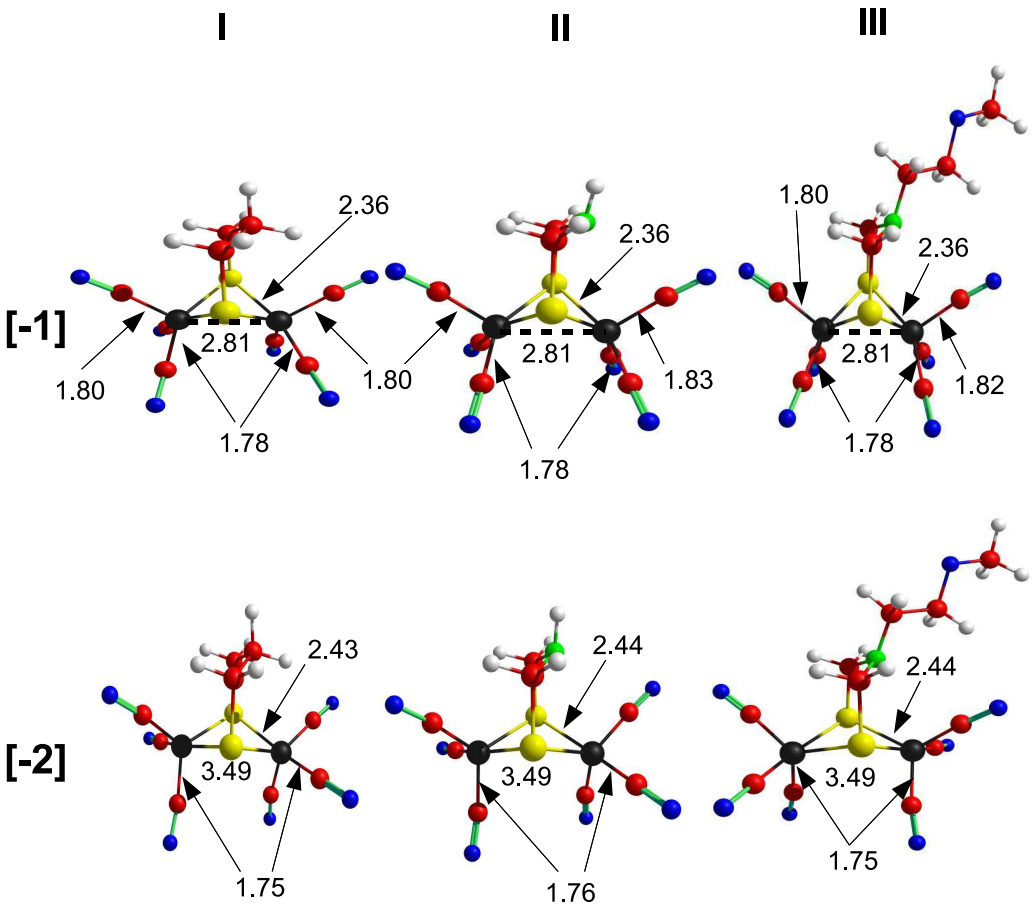

Figure III-11: Comparison of different possible bridgehead for the anion and dianion species (bond lengths in Å).

identified distinct minima corresponding to isomers **A**, **B** and **C** for all three species (CH_2, NH and $N(CH_2CH_2OMe)$ at the bridgehead). The optimised structures for the $N(CH_2CH_2OMe)$ species are shown in Figure III-13. The neutral compound, characterised by X-ray diffraction corresponds to isomer **A**.

For the anion, structure **A** is the most stable, indicating that the first electron enters the Fe-Fe σ^* orbital, and as a result, the Fe-Fe bond length increases to 2.81 Å (compared to 2.51 Å in the neutral compound) upon reduction. Further addition of a second electron to this orbital completely breaks the Fe-Fe bond, which elongates to 3.49 Å. However, for the dianion, unlike the anion, isomer **A** is not the most stable - **B** is lower in energy. The dissociation of one Fe-S bond causes the Fe-Fe distance to contract to 2.61 Å, while one CO ligand moves into a bridging position.

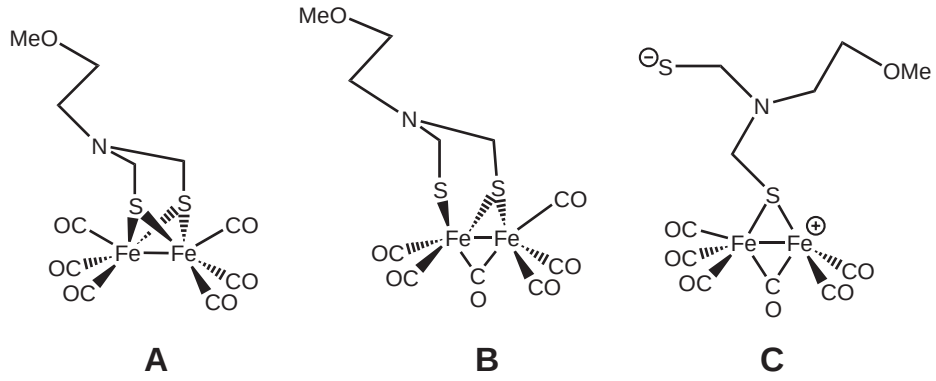

Figure III-12: The isomers **A**, **B** and **C** of $Fe_2(CO)_6(\mu{-}SCH_2N((CH_2)_2OMe)CH_2S)$.

We note, however, that isomer **C** is very close, energetically, to **B** in the case of the dianion. Similarly, the very small difference of energy between isomer **A** and **B** for the anion (1 kcal/mol) indicates a rearrangement thermodynamically favoured between the original anion isomer **A** into the isomer **B** similar to the dianion one.

Charge	Anion			Dianion		
Isomer	**A**	**B**	**C**	**A**	**B**	**C**
R = OMe (**III**)*	**0**	1	25	7	**0**	4
R = NH (**II**)	**0**	5	33	0.6	4	**0**
R = CH_2 (**I**)	**0**	4	43	0.6	**0**	4

*OMe stands for $N(CH_2)_2OMe$

Table III-2: Energies of the different conformations of $Fe_2(CO)_6(\mu{-}SCH_2N((CH_2)_2OMe)CH_2S{-})$ (**A**, **B** and **C**) for different charges (anion and dianion) and different bridgeheads ($N(CH_2)_2OMe$, NH and CH_2) (relative energies in kcal/mol).

Table III-2 shows that the presence of different bridgehead can have an effect on the structure adopted by the dianion species. Isomer **A** is the most stable for the anionic species in all cases, but while isomer **B** is preferred for the dianion species for $N(CH_2)_2OMe$ and CH_2 bridgeheads, isomer **C** becomes the more stable for the

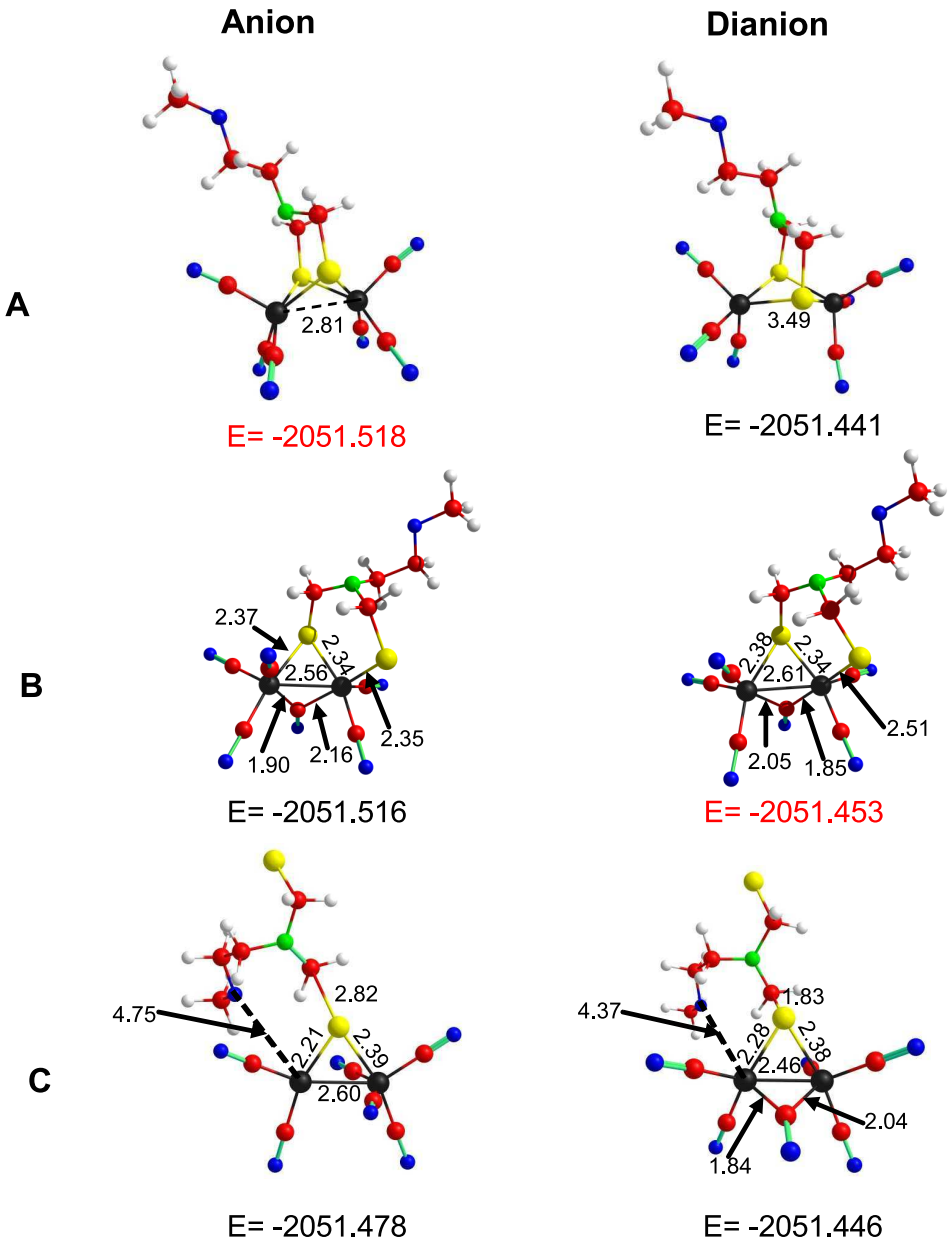

Figure III-13: Comparison of the energies of $[Fe_2(CO)_6(\mu{-}SCH_2N((CH_2)_2OMe)CH_2S)]$ (**III**) for different isomers and redox states (Energies are given in a.u. and bond length in Å).

NH bridgehead species. The relative energies of **B** and **C** remain close in all cases, and it is not possible to make a definitive conclusion regarding the identity of the dianion in solution.

For the anionic species we observe that isomer **C** is generally unstable because the breaking of two Fe-S bonds leads to a loss of three electrons for the Fe_2 core, which is not compensated by the addition of a single electron through reduction.

We have also repeated these calculations with diffuse functions added to both O and S atoms (6-31+G*), but they have no impact on the relative energies of the isomers.

Following the previous results, we can already draw a preferred reduction pathway for the three structures studied (**I**, **II** and **III**). We clearly see that compounds **I** and **III** follow the same pathway: their neutral species adopt the structure **A** which remains intact after the first reduction step. The only structural change is the elongation of the Fe-Fe bond which is to be expected if the LUMO of the system is a Fe-Fe σ antibonding. However, when a second reduction is performed to both species, a change appears in their structure. They adopt structure **B** where the Fe-Fe bond length decreases to a value close to the initial value observed in the neutral species and one of the Fe-S bonds is broken instead. This indicates that electrons are transferred into an Fe-S σ^* orbital instead of the expected Fe-Fe σ^*. This pathway is not followed, however, by species **II**. Although the neutral and anionic species possess the same structural features as species **I** and **III**, its dianion favours structure **C** with the cleavage of not one but but two Fe-S bonds. However, this difference between the dianions of species **I** and **III** and **II** emerges from gas-phase calculations, and we anticipate that the dianion will be more sensitive to solvent than the neutral and anion counterparts. We therefore decided to check if the addition of a solvent environment has any impact on the results.

1.b - Impact of the solvation on the computational model

Solvation effects can be important in the study of model compounds of proteins active core.[30] So, we have also considered the impact of the solvation on the previous

compounds, because some of them (principally the dianion species) are clearly more susceptible to the polar effects of solvents. We used the polarisable continuum model (PCM) of Tomasi and co-workers,[31–33] and used H_2O as well as CH_3CN as solvents (dielectric constants, ϵ: 78.39 and 36.64, respectively). The default model for PCM in Gaussian03 has been used. The cavity were builded up using the United Atom model (UA0), i.e. putting a sphere around each solute heavy atom (hydrogen atoms are enclosed in the sphere of the atom to which they are bonded). The results are summed up in Table III-3.

Solvent	CH_3CN					
Charge	Anion			Dianion		
Isomer	**A**	**B**	**C**	**A**	**B**	**C**
OMe*	**0**	3	19	3	**0**	1
NH	**0**	4	37	8	**0**	4
CH_2	**0**	3	71	2	**0**	3
Solvent	H_2O					
Charge	Anion			Dianion		
Isomer	**A**	**B**	**C**	**A**	**B**	**C**
OMe*	**0**	3	18	2	**0**	1
NH	**0**	4	36	7	**0**	4
CH_2	**0**	4	70	1	**0**	3

*OMe stands for $N(CH_2)_2OMe$.

Table III-3: Relative energies for anion and dianion for the different conformations (**A**, **B** and **C**) solvated (relative energies are in kcal/mol).

As we can see, calculations using solvent confirm the pathways calculated previously for species **I** and **III**: after the first reduction the compound retains the structure **A** but after the second reduction it isomerises to **B**. The real difference

between solvated and gas phase results comes in compound **II**, where the most stable isomer for compound **II** in its dianion state is structure **B**, as was the case for **I** and **III**.

These results suggest that the type of bridgehead has no real structural impact during the reduction of the systems.

1.c - Use of NHC as an electron-donating ligand

The two-electron reduction process we study here requires the dianionic species to be relatively more stable compared to the anion so as to induce a second reduction at a lower potential than the first one. To fulfill this condition Talarmin and coworkers have used an electron-donating ligand, N-heterocyclic carbene (NHC) in place of one of the CO to stabilise the dianion species (see Figure III-14).[29] While Talarmin *et al.* substituted methyl and 2,4,6-trimethylphenyl groups on the N atom of the NHC ligand, we substituted the nitrogen atoms by hydrogen to reduce the calculation time.

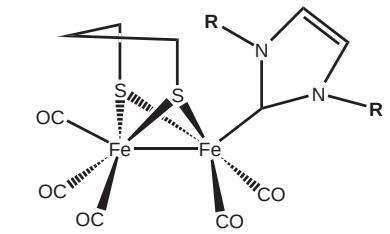

Figure III-14: Structure of $[Fe_2(CO)_5L_{NHC}(\mu-pdt)]$ with L_{NHC} = 2,4,6-trimethylphenyl, methyl or H.

In Table III-4, we report the energies of the optimised structures of the dianion species containing a NHC ligand.

We observe that the use of the NHC electron-donor ligand helps to stabilise isomer **C** over isomer **B**. Thus it appears that the donation of electrons favours the cleavage of two Fe-S bonds.

Isomer	**A**	**B**	**C**
OMe*	20	2	**0**
NH	29	8	**0**
CH_2	16	4	**0**

*OMe stands for $N(CH_2)_2OMe$

Table III-4: Comparison of the stabilisation of the dianion species for different bridgehead by replacing a CO by a NHC ligand (relative energies in kcal/mol).

Table III-5 and Figure III-15 present the main bond lengths for the three possible isomers for the dianion species. In Table III-5 are also presented for comparison the main bond lengths for standard dianion 6-CO structure. The addition of the electron-donating ligand NHC has minimal impact on the bond lengths: the only exception is the Fe-Fe bond length of isomer **A** which decreases to ≈ 2.60 Å. Indeed, when we look at Mulliken charges to understand such a small Fe-Fe bond for isomer **A**, we observe a difference in charges between the irons of the NHC dianionic compound and those of the 6-CO^{2-} parent structure (only dianionic species are considered here). The irons for the 6-CO^{2-} species have both a charge of -1, whereas for isomer $\mathbf{A}^{2-}$ the irons possess different charges: the iron substituted by the NHC ligand has a charge of -2.8 while the other iron possesses a charge of -0.5. Similarly for the dianion of the NHC species isomer $\mathbf{A}^{2-}$ differs from isomers $\mathbf{B}^{2-}$ and $\mathbf{C}^{2-}$: the latter have charges of -1.1 and -0.7 for the iron substituted by NHC and the iron opposite the NHC ligand, respectively.

Although the presence of the electron-donating ligand effectively stabilises the dianion to improve the second reduction, the isomer $\mathbf{B}^{2-}$ is not the most stable anymore: $\mathbf{C}^{2-}$ is the thermodynamically favoured product. Bridgeheads have here again no impact on the structure. With the exception of isomer **A**, all the structures possess the same charge mix on the irons, and are all comparable to 6-CO^{2-} structures. So the replacement of a CO ligand by NHC affects only the stabilisation of the isomer **C** but leave the structure of the complex unchanged (with the exception

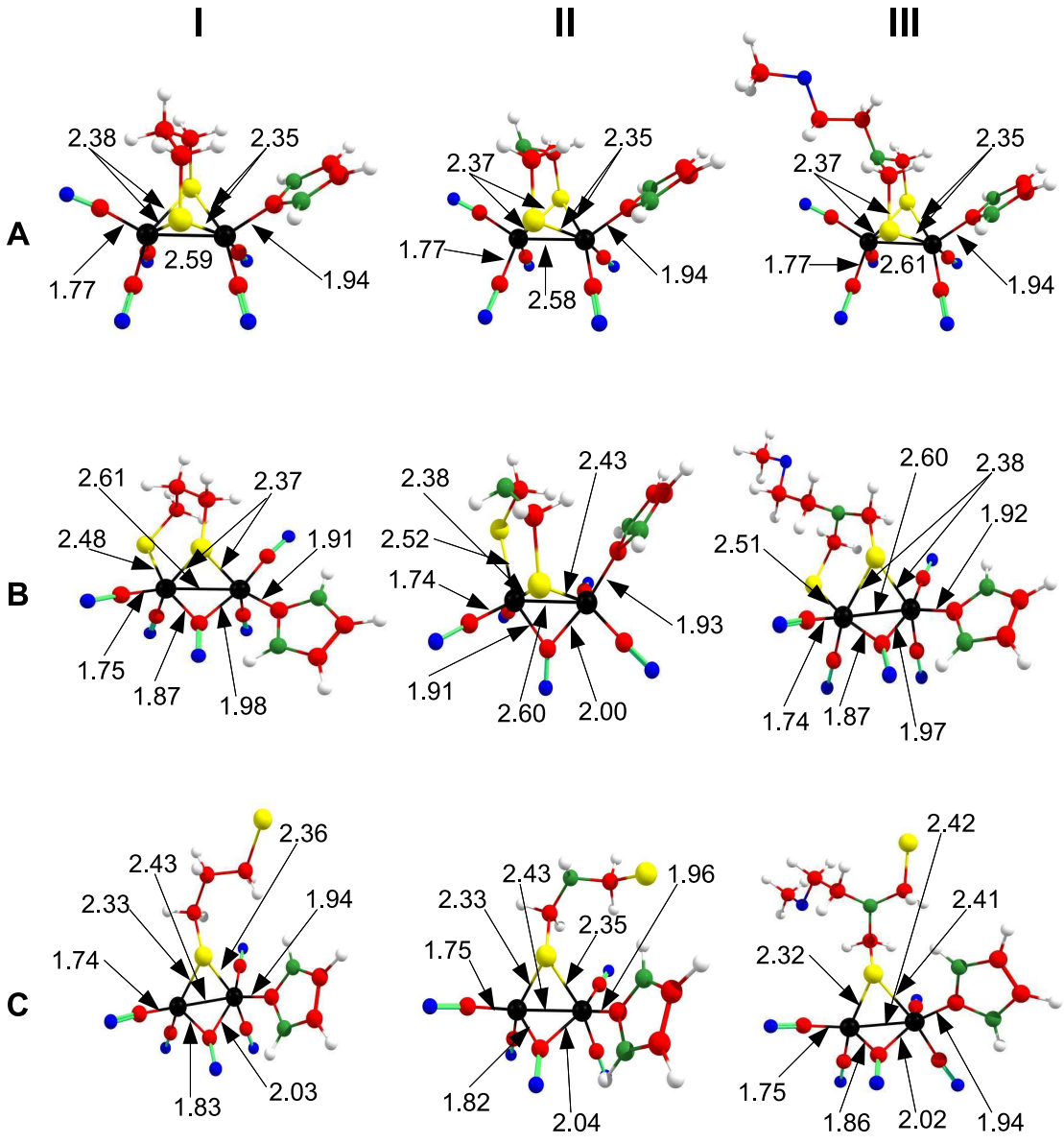

Figure III-15: Comparison of structural parameters for isomers **A**, **B** and **C** for the dianion species of compounds **I**, **II** and **III** where one of the CO is replaced by a NHC ligand (bond lengths in Å).

Charge			dianion		
Isomer			**A**	**B**	**C**
L = NHC	R = CH_2	Fe-Fe	2.59	2.61	2.43
		Fe-S	2.35/2.38	2.37/2.48/4.24‡	2.33/2.36
		Fe-C	1.77/1.94^{n}	1.75/1.91^{n}/1.87†/1.98†	1.74/1.94^{n}/1.83†/2.03†
	R = NH	Fe-Fe	2.58	2.60	2.43
		Fe-S	2.35/2.37	2.38/2.33/2.50/4.27‡	2.33/2.35
		Fe-C	1.77/1.94^{n}	1.75/1.93^{n}/1.91†/2.00†	1.75/1.94^{n}/1.82†/2.04†
	R = OMe*	Fe-Fe	2.61	2.60	2.42
		Fe-S	2.35/2.37	2.38/2.51/4.27‡	2.32/2.41
		Fe-C	1.77/1.94^{n}	1.74/1.92^{n}/1.87†/1.97†	1.75/1.94^{n}/1.86†/2.02†
L = CO	R = CH_2	Fe-Fe	3.49	2.62	2.44
		Fe-S	2.41-2.45	2.33/2.38/2.49/4.27‡	2.30/2.38
		Fe-C	1.75-1.77	1.74-1.78/1.87†/2.05†	1.74-1.78/1.84†/2.06†
	R = NH	Fe-Fe	3.49	2.62	2.45
		Fe-S	2.41-2.46	2.33/2.38/2.50/4.22‡	2.29/2.38
		Fe-C	1.75-1.77	1.74-1.78/1.87†/2.06†	1.74-1.78/1.84†/2.06†
	R = OMe*	Fe-Fe	3.49	2.61	2.46
		Fe-S	2.40-2.45	2.34/2.38/2.51/4.27‡	2.29/2.38
		Fe-C	1.75-1.76	1.74-176/1.87†/2.05†	1.74-1.78/1.84†/2.04†

* stands for $N(CH_2)_2OMe$ bridgehead substituent.

^{n} Fe-C bond length for the NHC ligand.

† Fe-C bond length for the $CO_{bridging}$ ligands.

‡ Fe-S bond length for broken Fe-S bonds.

Table III-5: Bond length comparison for $[Fe_2(CO)_5L(\mu{-}SCH_2RCH_2S)]^{2-}$ (bond length in Å).

of the Fe-Fe bond of the isomer **A**).

The isomer **C** is interesting due to its exceptionally short Fe-Fe bond for the dianion species in contrast to what was expected. The fact that the addition of an electron-donor ligand can stabilise this isomer, e.g. which is a proof of the possible synthesis of a stable complex with the isomer **C**, led us to study this astonishing structure more precisely.

2 - Electronic structure of the dianion in isomer C

The work described above suggests that the breaking of Fe-S bonds may occur in the dianion. Therefore, the electronic structure of **C** is particularly intriguing, as the very short Fe-Fe distance suggests some multiple bonding. The presence of a Fe=Fe double bond in a biological relevant species would be a remarkable observation, and this brought us to further explore the electronic structure of isomer **C**. The dissociation of a bridging RS- group reduces the formal electron count by three, and as a result the 18-electron rule can only be satisfied by formation of an Fe=Fe double bond. Indeed, if we look at compound C^{2-} (see Figure III-13) and consider the 18-electron rule we should obtain 36 electrons for the Fe_2 core. The six CO ligand bring 12 electrons to the overall electron count while the bridging sulphur contributes to 3 more. The irons give 16 electrons which brings the electronic count to 31 electrons. The decoordinated sulfide group carries a 1- charge, meaning that the total count at the core is 32. The presence of an Fe=Fe double bond between the two irons would therefore be consistent with the 18-electron rule. Thus far from breaking the Fe-Fe bond, it appears that two-electron reduction actually strengthen it, while cleaving the two Fe-S bonds of one of the thiolato bridges instead. The electronic unsaturation of the cluster could, in principle, also be reduced by the coordination of the OMe group in the free site occupied by the seventh CO ligand in Pickett's proposed structure (Figure III-9).[26]

The presence of a weak Fe=Fe π bond opens the possibility for a triplet configuration. Indeed, the presence of a potential weak π bond would induced an easy promotion of an electron from the π to the π^* orbital. Thus the triplet state might become more stable than the singlet. The stability might also be improved by the presence of bridges between the metals which decreases the metal-metal bond strength. We have examined this question using the simple model compound, $[Fe_2(CO)_6(\mu{-}SH)]^-$, where the Fe−Fe separation increases from 2.35 Å in the singlet to 2.49 Å in the triplet. Although the two states are close in energy ($\approx$ 9

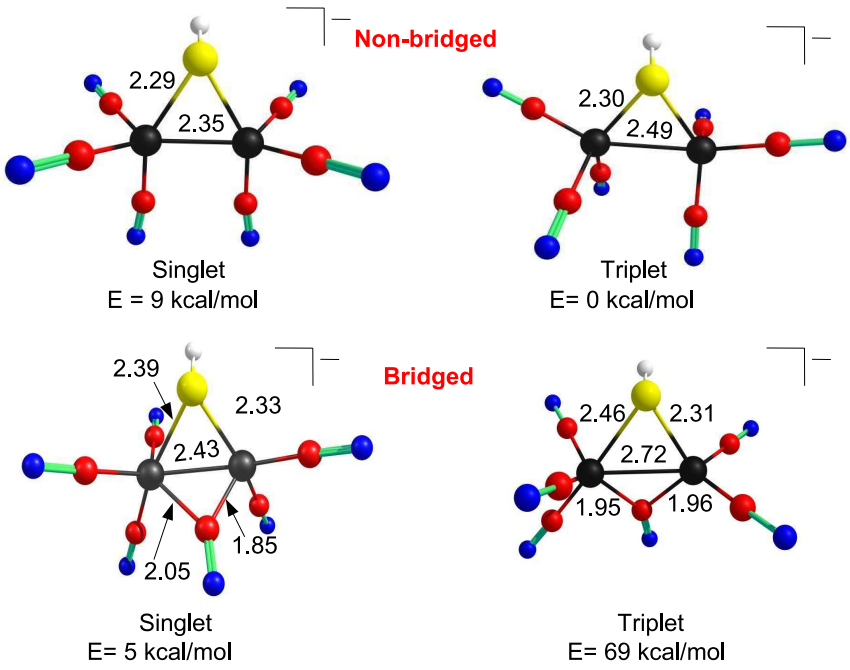

Figure III-16: Calculation of $[Fe_2(CO)_6(\mu{-}SH)]^-$ singlet and triplet for the CO-bridged and non-CO-bridged compounds (energies are given in a.u. and bond length in Å).

kcal/mol difference (see Figure III-16)) the triplet state is the more stable. We have optimised the same compound but this time possessing a CO bridge as in the $\mathbf{C}^{2\text{-}}$ isomer for the OMe-bridgehead. The results show that this time the singlet is the more stable by 64 kcal/mol compared to the triplet. As the species we are interested here correspond to the bridged species we can conclude that the only possibility here is that isomer $\mathbf{C}^{2\text{-}}$ is in its singlet state.

The possible coordination of the OMe group would increase the electron count at the Fe_2 site by 2, and so break the Fe−Feπ bond. To explore this effect, we conducted a scan of the Fe-O coordinate, allowing all other parameters to vary freely (see Table III-6).

We note that the decrease of Fe-O bond results in an increase of the Fe-Fe bond, arguing that Fe-O σ and Fe-Fe π bonding are in competition. The total energy is almost unaffected by this structural change, implying that the surface is very soft.

The energy decreases until a certain value and then increases again. It indicates

Bond length (in Å)				**Energies (in a.u.)**	**Relative energies (in kcal/mol)**
Fe-O	Fe-Fe	Fe-CO	Fe-S	E	E
2.3	2.531	1.86/2.02	2.33/2.38	-2051.4431	1.82
2.4	2.525	1.86/2.02	2.32/2.38	-2051.4437	1.44
2.5	2.516	1.85/2.02	2.31/2.38	-2051.4441	1.19
3.0	2.480	1.84/2.02	2.29/2.39	-2051.4450	0.63
3.5	2.473	1.83/2.04	2.28/2.38	-2051.4455	0.31
4.0	2.464	1.84/2.04	2.28/2.38	-2051.4459	0.06
4.5	**2.458**	**1.84/2.04**	**2.29/2.38**	**-2051.4460**	**0**
5.0	2.454	1.84/2.04	2.28/2.38	-2051.4457	0.19
5.5	2.450	1.84/2.04	2.28/2.38	-2051.4451	0.56

Table III-6: Effects of the reduction/elongation of the Fe-O bond.

that we obtain a minimum. The minimum energy is obtained for a Fe-O bond length of 4.5 Å which is consistent with our most stable structure, which presents a Fe-O bond length of 4.37 Å. It is interesting to notice that after a certain distance the bond length has no more effect on the Fe-S and Fe-CO bonds.

2.a - AIM calculations

The presence of such short Fe-Fe bond for the isomer **C** is quite remarkable for this type of compound, as to the best of our knowledge no such features have ever been noted previously.

To validate the double bond proposal, we decided to explore the electron density using the Atom In Molecule (AIM) method. The AIM approach characterises the chemical bonding of a system based on the topology of the quantum charge density.

Schaefer *et al.* have reported a dichromium compound where the two chromium atoms can be bound by a Cr=Cr double.[34] The optimised Cr-Cr compound in this case is composed of three CO bridges. AIM analysis gives the following topological figure presented in Figure III-18, clearly showing a critical point between the two

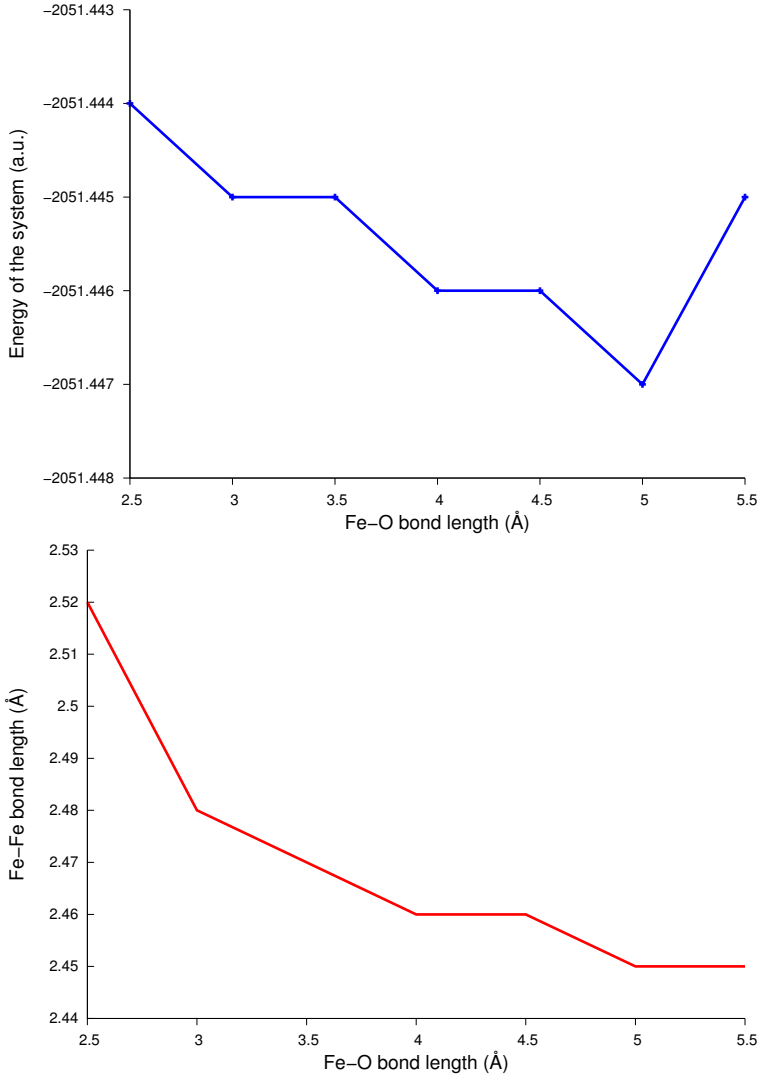

Figure III-17: Evolution of the Fe-Fe bond length and the energy of the system with the increase of the Fe-O bond length.

chromium atoms.

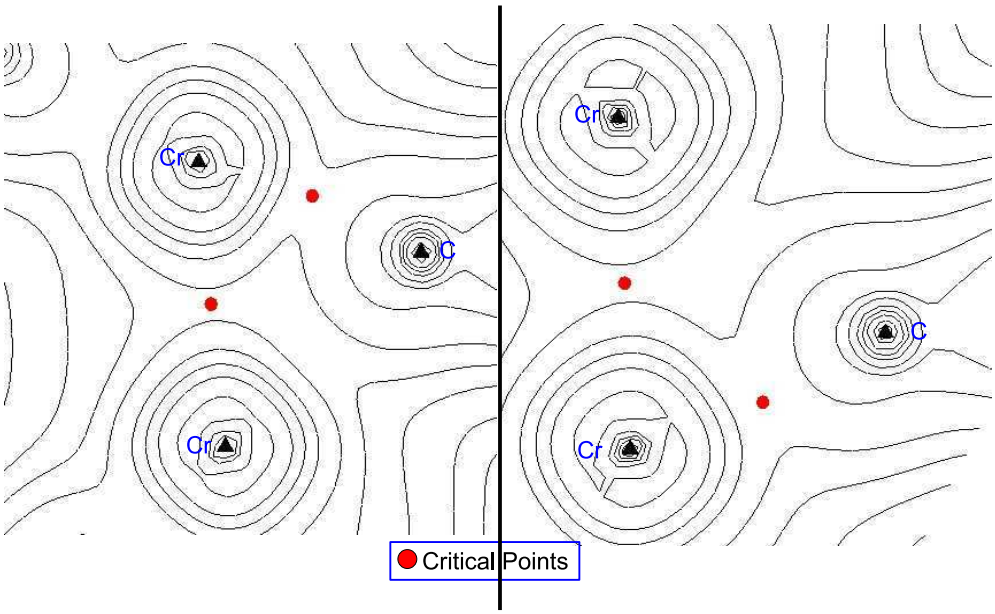

Figure III-18: AIM analysis of the Cr-Cr bond in the two Cr-C simple bond plan

In Figure III-19 we present the results we obtain using AIM calculations for our Fe-Fe compound in its $\mathbf{C}^{2-}$ isomer state. The topological diagram on the left of the figure is taken in the Fe-$C_{bridging}$(O)-Fe plane while the left part of the figure is taken in the Fe-S-Fe plane.

In contrast to the chromium case, we observe no critical point between the two irons that would confirm the presence of even a single bond there. We, however, obtain a critical point for the other bonds (Fe-C, Fe-S) as expected. The link between the Fe centres is not made through the covalent bonding but rather *via* the carbonyl and thiolato bridges. Thus although the formal electron count demands an Fe=Fe double bond, we do not find evidence to support it in electron density map.

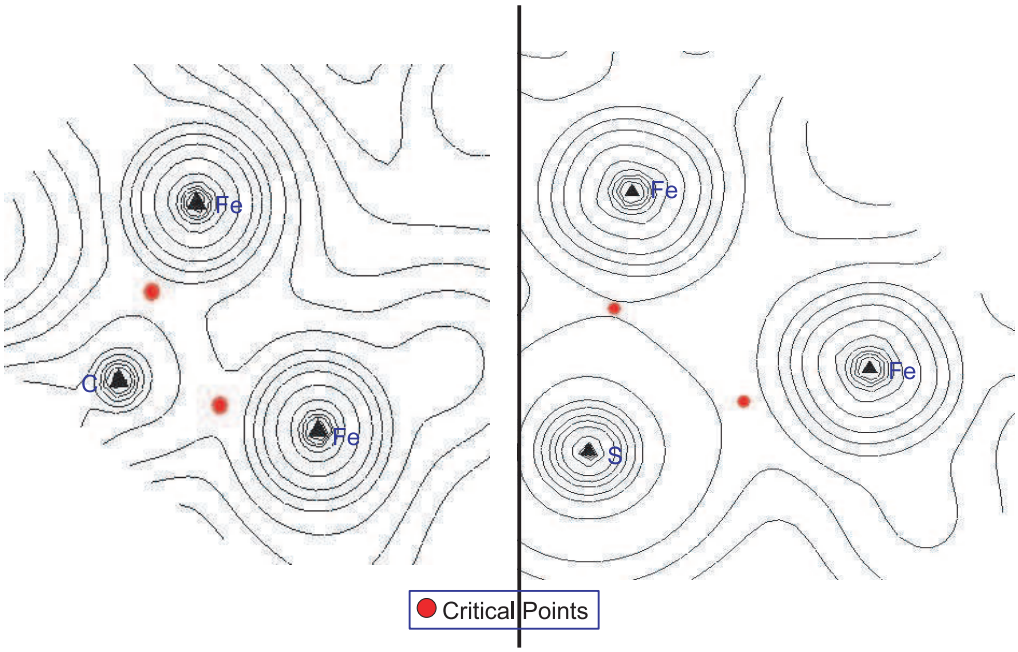

Figure III-19: AIM analysis of the Fe-Fe bond in the Fe-$C_{(bonding)}$-Fe plan and in the Fe-S-Fe plan

3 - Conclusion

We observed that contrary to what was thought first the reduction of $Fe_2(CO)_6$ (μ−$S(CH_2CH_2OMe)S$) doesn't go through the elongation of the Fe-Fe bond but through the breaking of one of the Fe-S bond followed by the bridging of a CO. Although different bridgeheads have experimentally a different impact on the catalytic cycle itself, it is clear from our results that bridgeheads don't influence the structure itself through reduction.

Species **I** and **III** go from isomer **A** for the neutral species, isomer **A** for the anion and **B** for the dianion species. In contrast, species **II** differ on the favoured structure for the dianion. However, when solvation is used all species follow the same pathway: **A**, $\mathbf{A}^-$ and $\mathbf{B}^{2-}$.

We also checked different other effects which would change the final choice of the reduction pathway but none of them induce any change in the final choice of the structure obtain for each charge. We also checked the impact of NHC, electron-withdrawing ligand, on the dianion species (NHC is used experimentally to stabilise

the dianion to facilitate the second reduction). NHC stabilises isomer $\mathbf{C}^{2-}$ over isomer $\mathbf{B}^{2-}$. In parallel we looked more closely on the isomer $\mathbf{C}^{2-}$ and its unique short Fe-Fe bond. However, no definitive answered could be reached from the studies done.

Bibliography

[1] Liu, Z.-P.; Hu, P. *J. Chem. Phys.*, **2002**, *117*, 8177.

[2] Liu, Z.-P.; Hu, P. *J. Am. Chem. Soc.*, **2002**, *124*, 5175.

[3] Popescu, C. V.; Münck, E. J. *J. Am. Chem. Soc.*, **1999**, *121*, 7877.

[4] Fan, H. J.; Hall, M. B. *J. Am. Chem. Soc.*, **2001**, *123*, 3828.

[5] Baik, M.-H.; Ziegler, T.; Schauer, C. K. *J. Am. Chem. Soc.*, **2000**, *122*, 9143.

[6] Bruschi, M.; Greco, C.; Fantucci, P.; De Gioia, L. *Inorg. Chem.*, **2008**, *47*, 6056.

[7] Hsu, S. C. N.; Zheng, Y.-C.; Chen, H.-Y.; Hung, M.-Y.; Kuo, T.-S. *J. Organomet. Chem.*, **2008**, *693*, 3035.

[8] Zampella, G.; Greco, C.; Fantucci, P.; De Gioia, L. *Inorg. Chem.*, **2006**, *45*, 4109.

[9] Fiedler, A. T.; Brunold, T. C. *Inorg. Chem.*, **2005**, *44*, 9322.

[10] Zhou, T.; Mo, Y.; Liu, A.; Zhou, Z.; Tsai, K. R. *Inorg. Chem.*, **2004**, *43*, 923.

[11] Greco, C.; Bruschi, M.; De Gioia, L.; Ryde, U. *Inorg. Chem.*, **2007**, *46*, 5911.

[12] Darensbourg, M. Y.; Lyon, E. J.; Zhao, X.; Georgakaki, I. P. *Proc. Nat. Ac. Sc.*, **2003**, *100*, 3683.

[13] Felton, G. A. N.; Vannucci, A. K.; Chen, J.; Lockett, L. T.; Okumura, N.; Petro, B. J.; Zakai, U. I.; Evans, D. H.; Glass, R. S.; Lichtenberger, D. L. *J. Am. Chem. Soc.*, **2007**, *129*, 12521.

[14] Trohalaki, S.; Pachter, R. *Energy & Fuels*, **2007**, *21*, 2278.

[15] Tye, J. W.; Darensbourg, M. J.; Hall, M. B. *Inorg. Chem.*, **2006**, *45*, 1552.

[16] Cao, Z.; Hall, M. B. *J. Am. Chem. Soc.*, **2001**, *123*, 3734.

[17] Tye, J. W.; Darensbourg, M. Y.; Hall, M. B. *Inorg. Chem.*, **2008**, *47*, 2380.

[18] Georgakaki, I. P.; Thomson, L. M.; Lyon, E. J.; Hall, M. B.; Darensbourg, M. Y. *Coord. Chem. Rev.*, **2003**, *238-239*, 255.

[19] Sun, L.; Åkermark, B.; Ott, S. *Coord. Chem. Rev.*, **2005**, *249*, 1653.

[20] Wang, F.; Wang, M.; Liu, X.; Jin, K.; Dong, W.; Sun, L. *Dalton Trans.*, **2007**, 3812.

[21] Bruschi, M.; Fantucci, P.; De Gioia, L. *Inorg. Chem.*, **2003**, *42*, 4773.

[22] Zampella, G.; Bruschi, M.; Fantucci, P.; Razavet, M.; Pickett, C. J.; De Gioia, L. *Chem. Eur. J.*, **2005**, *11*, 509.

[23] Zilberman, S.; Stiefel, E. I.; Cohen, M. H.; Car, R. *Inorg. Chem.*, **2007**, *46*, 1153.

[24] Justice, A. K.; Zampella, G.; De Gioia, L.; Rauchfuss, T. B.; Van der Vlugt, J. I.; Wilson, S. R. *Inorg. Chem.*, **2007**, *46*, 1655.

[25] Lawrence, J. D.; Li, H.; Rauchfuss, T. B. *Chem. Comm.*, **2001**, 1481.

[26] Borg, S. J.; Behrsing, T.; Best, S. P.; Razavet, M.; Liu, X.; Pickett, C. J. *J. Am. Chem. Soc.*, **2004**, *126*, 16988.

[27] *Gaussian03, D.02*: Frisch, J. A.; Trucks, G. W.; Schlegel, H. B.; Scuseria, G. E.; Robb, M. A.; Cheeseman, J. R.; Montgomery, J. A. Jr; Vreven, T.; Kudin, K. N.; Burant, J. C.; Millan, J. M.; Iyengar, S. S.; Tomasi, J.; Barone, V.; Mennucci, B.; Cossi, M.; Scalmani, G.; Rega, N.; Peterson, G. A.; Nakatsuji, H.; Hada, M.; Ehara, M.; Toyota, K.; Fukuda, R.; Hasegawa, J.; Ishida, M.; Nakajima, T.; Honda, Y.; Kitao, O.; Nakai, H.; Klene, M.; Li, X.; Knox, J. E.; Hratchian, H. P.; Cross, J. B.; Adamo, C.; Jaramillo, J.; Gomperts, R.; Stratmann, R. E.; Yazyev, O.; Austin, A. J.; Cammi, R.; Pomelli, C.; Ochterski, J. W.; Ayala, P. Y.; Mrokuma, K.; Voth, G. A.; Salvador, P.; Dannenberg, J. J.; Zakrzewski, V. G.; Dapprich, S.; Daniels, A. D.; Strain, M. C.; Farkas, O.; Malick, D. K.; Rabuck, A. D.; Raghavachari, K.; Foresman, J. B.; Ortiz, J. V.; Cui, Q.; Baboul, A. G.; Clifford, S.; Cioslowski, J.; Stefanov, B. B.; Liu, G.; Liashenko, A.; Piskorz, P.; Komaromi, I.; Martin, L. R.; Fox, D. J.; Keith, T.; Al-Laham, M. A.; Peng, C. Y.; Nanayakkara, A.; Challacombe, M.; Gill, P. M. W.; Johnson, B.; Chen, W.; Wong, M. W.; Gonzalez, C.; Pople, J. A. Gaussian, Inc. Pittsburgh, 2003.

[28] Lyon, J. E.; Georgakaki, L. P.; Reibenspies, J. H.; Darensbourg, M. Y. *Angew. Chem. Int. Ed.*, **1999**, *38*, 3178.

[29] Capon, J.-F.; Ezzaher, S.; Gloaguen, F.; Pétillon, F. Y.; Schollhammer, P.; Talarmin, J.; Davin, T. J.; McGrady, J. E.; Muir, K. W. *New J. Chem.*, **2007**, *31*, 2052.

[30] Tye, J. W.; Darensbourg, M. Y.; Hall, M. B. *J. Comput. Chem.*, **2006**, *27*, 1454.

[31] Barone, V.; Cossi, M.; Tomasi, J. *J. Comput. Chem.*, **1998**, *19*, 404.

[32] Cossi, M.; Scalmani, G.; Rega, N.; Barone, V. *J. Chem. Phys.*, **2002**, *117*, 43.

[33] Cossi, M.; Crescenzi, O. *J. Chem. Phys.*, **2003**, *19*, 8863.

[34] Li, S.; Richardson, N. A.; Xie, Y.; King, R. B.; Schaefer III, H. F. *Faraday Discuss.*, **2003**, *124*, 315.

CHAPTER IV

Characterisation of iron hydride complexes through the computation of NMR parameters

In chapter II, we have emphasised the importance of iron hydrides, and in particular the binding site of these ligands. Experimentally this is rather hard to determine, as NMR confirms the presence of a hydride, but not its precise environment. One possible way of obtaining this information is to compute NMR parameters for several candidate structures and compare them to experiment. In this chapter, we illustrate how such a process can be used to identify hydride species generated by protonation of an Fe_2 dimer.

1 - Experimental basis

In a recent publication, Schollhammer and co-workers have studied the protonation of an hydrogenase-like compound containing a dppe ligand instead of two CO ligands, $Fe_2(CO)_4(S(CH_2)_3S)$(dppe) (dppe = 1,2-bis(diphenylphosphino)ethane).[1] In this system, the dppe ligand can take two conformations: apical-basal (ap-ba) and basal-basal (ba-ba) (see Figure IV-1). As noted in chapter II, this creates an asymmetry in the compound which helps to control the site of protonation. NMR spectra obtained by Schollhammer and co-workers, at different temperatures, indicate that 4 distinct isomers of the resultant hydride can exist and they have proposed the

structures shown in Figure IV-2. Of the 4 isomers, compound **A** - the only species present at the highest temperature (298K) - has been isolated and characterised structurally, offering an opportunity to calibrate our calculations. The other isomers can be observed at different temperatures: at 203 K the protonation leads to the formation of the isomer **C**, while at 243 K, **A** and **B** are formed. When the protonation is done at 223 K, all 4 species are observed simultaneously, as shown in Figure IV-2.[1]

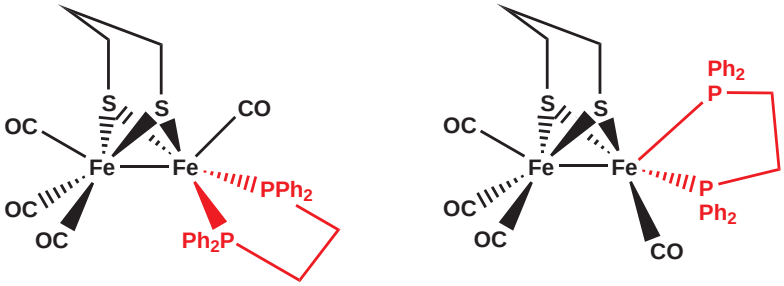

Figure IV-1: Conformations induced by the replacement of 2 CO by a dppe.

On the basis of chemical shifts and coupling constants, Schollhammer *et al.* have proposed the structures **B**, **C** and **D** shown in Figure IV-2 for these peaks. In **C**, the phosphine bearing iron centre is remote from the hydride, so they were unable to define the stereochemistry at this centre.

2 - Structures

The first step in our study was the optimisation of the structures of the compounds proposed (compounds shown in Figure IV-2). We used the B3LYP functional and a combination of SDD (Fe) and SVP or TZVP for the basis set. We observed that the use of TZVP basis set in place of SVP make little difference to the quality of structural results, but, obviously, it makes a difference in term of calculation time. The optimisation of the 4 isomers shows clearly (see Table IV-1) that isomer **A** is the most stable of the 4 species. This is consistent with experiment: **A** is the only species present when the solution is brought back to ambient temperature, and is

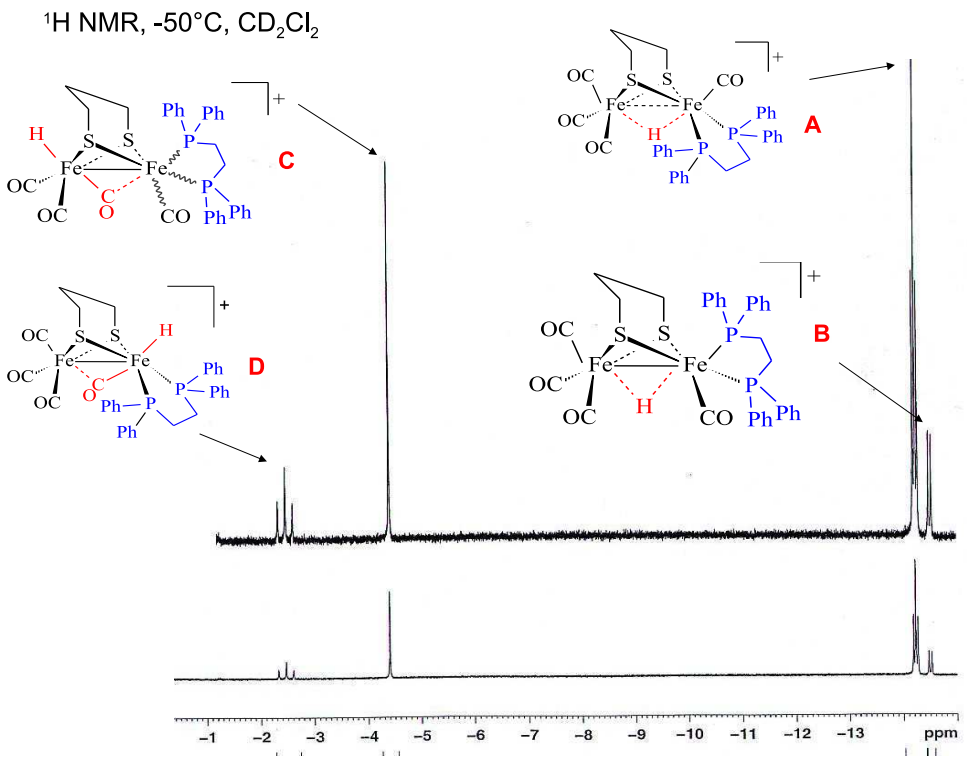

Figure IV-2: NMR spectra obtained by Schollhammer and co-workers and corresponding proposed structures (at 223K).

the only one characterised by X-ray diffraction. Optimised structural parameters for different basis set combinations on the compounds **A**, **B**, **C** and **D** are shown in Table IV-2. The values for isomer **A** obtained by X-ray crystallography are shown for comparison.

Compounds	**Energy (in kcal)**
A	0
B	3
$\mathbf{C}_{basal-basal\ dppe}$	17
$\mathbf{C}_{apical-basal\ dppe}$	20
D	21

Table IV-1: Energies of the different di-iron model isomers (B3LYP and SDD(Fe) / SVP (others)).

We can conclude from Table IV-2 that the Fe-Fe bond are well described using

this method. Fe-S and Fe-P bonds are not as well described but they are still described qualitatively well enough. The only exception are cases where the SDD basis set is applied on either S or P (in fact D95 basis set), in which case the Fe-S (P) bonds are elongated by ≈ 0.04 Å, and are ≈ 0.10 Å larger than experiment.

basis set		SDD all atoms	SDD Fe SVP P,S,C	SDD Fe,S SVP P,C	SDD Fe,P SVP S,C	SDD Fe,C SVP P,S	SDD Fe,S,C SVP P	SDD Fe,P,C SVP S	SDD Fe,P,S SVP C	TZVP all atoms	*Experiment*
Conformer	**Bond**	**Bond lenth (in Å)**									
A	Fe-Fe	2.64	2.62	2.62	2.62	2.62	2.62	2.62	2.62	2.63	*2.581(5)*
	Fe-S	2.35	2.32	2.36	2.32	2.32	2.36	2.32	2.32	2.32	*2.27*
	Fe-$C_{on\ dppe}$	1.76	1.78	1.79	1.78	1.78	1.78	1.78	1.79	1.78	*1.75*
	Fe-C	1.81	1.83	1.83	1.83	1.83	1.83	1.83	1.83	1.83	*1.82*
	Fe-P	2.33	2.28	2.28	2.34	2.28	2.28	2.34	2.34	2.28	*2.234(1)/2.238(1)*
	Fe-H	1.68	1.67	1.67	1.67	1.67	1.67	1.67	1.67	1.67	*1.627(3)/1.640(4)*
B	Fe-Fe	2.61	2.60	2.61	2.60	2.60	2.61	2.60	2.61	2.61	
	Fe-S	2.36	2.33	2.38	2.32	2.33	2.36	2.32	2.36	2.32	
	Fe-$C_{on\ dppe}$	1.78	1.80	1.80	1.80	1.80	1.80	1.80	1.80	1.80	
	Fe-C	1.81	1.84	1.83	1.83	1.83	1.83	1.83	1.83	1.84	
	Fe-P	2.33	2.27	2.27	2.33	2.27	2.27	2.33	2.33	2.27	
	Fe-H	1.65	1.66	1.65	1.65	1.66	1.65	1.65	1.65	1.66	
C	Fe-Fe	2.61	2.63	2.63	2.64	2.64	2.64	2.64	2.64	2.65	
	Fe-S	2.33	2.32	2.34	2.31	2.31	2.34	2.31	2.30	2.30	
	Fe-C_b	1.84/2.33	1.85/2.44	1.85/2.42	1.84/2.46	1.84/2.45	1.85/2.42	1.84/2.46	1.84/2.46	1.85/2.48	
	Fe-$C_{on\ dppe}$	1.76	1.77	1.77	1.77	1.76	1.77	1.76	1.77	1.77	
	Fe-C	1.80	1.81	1.81	1.81	1.81	1.81	1.81	1.81	1.82	
	Fe-P	2.35	2.30	2.29	2.36	2.30	2.30	2.36	2.36	2.30	
	Fe-H	1.51	1.50	1.50	1.50	1.50	1.50	1.50	1.50	1.50	
D	Fe-Fe	2.58	2.59	2.59	2.59	2.59	2.59	2.59	2.59	2.60	
	Fe-S	2.33	2.30	2.34	2.30	2.30	2.34	2.30	2.33	2.30	
	Fe-C_b	1.79/2.51	1.80/2.56	1.83/2.53	1.81/2.56	1.79/2.57	1.80/2.55	1.80/2.57	1.80/2.53	1.80/2.59	
	Fe-C	1.79/1.83	1.80/1.85	1.81/1.85	1.80/1.85	1.80/1.85	1.80/1.85	1.80/1.85	1.80/1.85	1.80/1.85	
	Fe-P	2.30	2.24	2.24	2.31	2.24	2.24	2.31	2.31	2.25	
	Fe-H	1.52	1.52	1.52	1.52	1.52	1.52	1.52	1.52	1.52	

C_b is the carbon bridging the two iron, $C_{on\ dppe}$ is the carbon bonded to the iron substiuted by the dppe ligand

Table IV-2: Comparison between bond lengths obtained computationally (B3LYP functional used) and experimentally (in Å) (TZVP basis set results are given as comparison. Phenyls of the dppe are replaced by hydrogen atoms in our calculation).

3 - Development of the methodology for the calculation of NMR parameters

The first attempt to calculate chemical shifts theoretically comes from Ramsey in 1950 who developed a method using perturbation theory.[2] Subsequently, methods were developed by Hirschfelder and Hornig in 1955[3] and Tillieu and Guy in 1956[4] both of them based on the variational theorem while Das and Bersohn reported later the calculated chemical shift of hydrogen.[5] In 1957 McGarvey reported hydrogen chemical shift in hydrogen halides using an equation which derives from Ramsey equation obtained from first- and second-order perturbation theory.[6] The development of DFT has made those calculations easier and the advances in computer hardware have allowed bigger systems to be studied.

3.a - Brief overview of the theoretical background

NMR chemical shifts and coupling constants are second-order properties and can be expressed as a mixed second derivative of the total electronic energy of the system.

$$\sigma_{st} \propto \left. \frac{\partial^2 E}{\partial X_s \, \partial Y_t} \right|_{\vec{X}=\vec{Y}=0} \qquad \text{(IV-1)}$$

Where $\vec{X}$ corresponds to a magnetic field $\vec{B}$ and $\vec{Y}$ to a nuclear magnetic moment, σ_{st} describes chemical shielding, whereas if $\vec{X}$ and $\vec{Y}$ both correspond to nuclear magnetic moments then σ_{st} describes a spin-spin coupling constant. The chemical shift is obtained by subtracting the calculated chemical shielding of the studied system from the calculated shielding of a reference compound (usually TMS):

$$\delta = \sigma^{ref} - \sigma^{complex} \qquad \text{(IV-2)}$$

The introduction of magnetic fields into the Schrödinger equation requires us to address the 'gauge' problem. To understand what is the "gauge" problem, it is necessary, first, to know that the magnetic field, $\vec{B}$, is not introduced directly

in the Schrödinger equation. It is rather the vector potential, $\vec{A}$ which enters the appropriate equations. $\vec{A}$ is linked to the magnetic field $\vec{B}$ through the following equation:

$$\vec{B} = \nabla \times \vec{A} \tag{IV-3}$$

There is not a unique vector potential, $\vec{A}$ that can describe $\vec{B}$, and although $\vec{B}$ is independent of the choice of origin, $\vec{A}$ is not. NMR parameters being only dependent on the magnetic field $\vec{B}$, results must of course be independent of the choice of the vector potential $\vec{A}$. It is this requirement which is meant if one states that the magnetic field is *gauge invariant*.[7]

An infinite basis set would ensure the gauge invariance, but it is obviously impossible to fulfil this requirement. Alternative strategies have therefore been developed to resolve this gauge problem. Gauge-independent methods aim to compensate the perturbation of the kinetic energy operator created by the magnetic field (the motion of electrons generates magnetic moments). Two types of gauge factor have been developed for the calculation of chemical shifts: the GIAO and IGLO methods. The GIAO - Gauge Including Atomic Orbitals - method was the first method developed by London in 1937.[8] It incorporates the gauge origin into the basis functions themselves and all the matrix elements involving the basis functions can be arranged to be independent of it. The IGLO - Individual Gauge for Localised Orbitals - method has been developed later by Schindler and Kutzelnigg in 1982.[9] Different gauge origins are used for each localised molecular orbital (MO) so as to minimise the error introduced by having the gauge origin far from any particular MO. Of the two methods the modern implementation of GIAO in DFT is to a certain extent more robust but it is still possible to obtain good qualitative results with both of the methods.[10]

3.b - Previous calculations of chemical shifts

i - On light elements: ^{1}H, ^{13}C, ^{31}P, ^{15}N and ^{17}O

The use of DFT associated with more and more accurate functionals and basis sets developed during the last decade has proved a very good method to calculate NMR parameters for light elements. Usually, ^{1}H and ^{13}C, for obvious reasons, are the most studied elements. However, calculations done on ^{1}H are not as numerous as one might think, due to the fact that the proton shift is not very large and effects of solvation can be comparable to the range of the chemical shift itself.[7] Still, several calculations have been done.[11–13] Rablen *et al.* showed that the use of hybrid functionals such as: B3P86, B3PW91 and B3LYP give very accurate results for many organic compounds.[14] Bagno and co-workers also showed that using the B3LYP functional and a reasonably large basis set, chemical shifts can be calculated for ^{1}H and ^{13}C which fit the experimental values with a high degree of precision.[15] Significantly, the geometry chosen is very important because even with very accurate functionals and basis sets the calculated parameters are rather sensitive to geometry. This is important for our purposes, as it means that even rather similar structures should have distinct NMR signals.[7] Other light elements such as N and P have also been calculated, although ^{17}O has proved more problematic.

Gauss and Stanton have stated that the calculations of NMR parameters for ^{17}O present usually a discrepency with experimental results. This is due to a systematic 15 to 20 ppm shift in the experimental ^{17}O NMR scale.[16]

ii - On transition metals and heavier elements

DFT methods can also be used to calculate chemical shifts of heavy elements. However, the calculation of NMR parameters for transition metals or heavy elements in general requires that relativistic effects should be dealt with adequately. Effective core potentials (ECP) are generally used to approximate these effects and shielding calculations have been shown to have some predictive power. The presence of a transition metal next to an organic entity will obviously change the electronic prop-

erties of its ligand, and so, relativistic effects can be important for the ligand too. Here again ECPs are often used to approximate the relativistic effects involved by the presence of metallic entities.[17]

iii - On metal hydrides

Jolibois and co-workers showed that calculations of metal hydride chemical shifts (for $H_2Fe(CO)_4$, $K^+[HFe(CO)_4]^-$ and $HMn(CO)_5$) using DFT-GIAO (PBE0 or B3PW91 hybrid functionals) combined with standard Pople 6-31G(d,p) basis sets are consistent with experimental values. They also showed that if an ECP is used to describe CO ligands, the chemical shielding of the hydrides is overestimated.[18] Computational results obtained by Ziegler *et al.* presented in Table IV-3 also show that DFT-GIAO methods are in agreement with experimental data in most cases, although there are some disparities between experimental and computational results for $HCo(CO)_4$ and $H_2Fe(CO)_4$ systems. Ziegler and Jolibois and their respective co-workers suggest that an efficient core potential on Fe should allow the chemical shift δ of the hydride to be computed with a maximum error of $\pm$ 20%.[18,19]

Jolibois *et al.* have recently presented their computational results based on Ru(L)(H) (dXpm) systems (L= $-H^-$, $-Cl^-$, H_2O; dXpm= di-X-phosphomethane; X= −H, −Me, −Ph). The chemical shifts they obtained using DFT methods are in good agreement with values obtained experimentally (Table IV-3). It shows again the high level of accuracy obtained for chemical shifts by using hybrid-GGA functionals and the ECPs developed by the Stuttgart group and associated basis sets. However, in the study, the values obtained using an ECP on the carbon and oxygen atoms for $K^+[HFe(CO)_4]^-$ and $HMn(CO)_5$ complexes present significant errors for ^1H chemical shifts (-49% and -82%).[18] Gobetto and co-workers in 2003, emphasised the importance of relativistic effects for hydrides of heavy elements. They noted the poor accuracy of the calculated chemical shifts for osmium hydrides relative to experimental data. They computed, for example, for $[Os(bpy)_2(CO)(H)](PF_6)$, a chemical shift of -5.43 ppm (B3LYP/6-31++G(2d) for all atoms) compared to -11.4

System	δ (ppm)		relative error *
	Calculation	Experiment	
Ziegler *et al.*[20]			
$[HCr(CO)_5]^-$	-6.5	-6.9	*+6%*
$[HCr_2(CO)_{10}]^-$	-20.3	-19.5	*-4%*
$HMn(CO)_5$	-6.8	-7.5	*+9%*
$HRe(CO)_5$	-5.2	-5.7	*+9%*
$H_2Fe(CO)_4$	-7.5	-11.1	*+32%*
$HCo(CO)_4$	-5.3	-10.7	*+50%*
Jolibois *et al.*[18]			
$K^+[HFe(CO)_4]^-$	-8.4	-13.3	*-49%* †
$K^+[HFe(CO)_4]^-$	-8.4	-8.75	*+5%* ‡
$H_2Fe(CO)_4$	-13.4	-11.1	*-21%*
$HMn(CO)_5$	-7.5	-14.0	*-82%* †
$HMn(CO)_5$	-7.5	-7.9	*-3%* ‡
$Ru(H)_2(dppm)_2$	-8.9	-7.4	*-20%*
$Ru(H)(Cl)(dppm)_2$	-12.5	-14.0	*+11%*
$[Ru(H)(H_2O)(dppm)_2]^+$	-14.6	-18.8	*+22%*
$cis-Ru(H)_2(dppm)(PPh_3)_2$	-10.3	-7.8	*-32%*
	-11.3	-9.6	*-18%*

* the relative error is calculated as $100(\delta_{theo} - \delta_{exp})/\delta_{exp}$

† basis set I: Stuttgart ECP and associated basis set (Dunnning basis set) on C and O

‡ basis set II: standard Pople 6-31G(d,p) on C and O

Table IV-3: Comparison of Experimental and calculated chemical shift for transition metal hydrides as proposed by Ziegler and Jolibois and their respective co-workers.[18,20]

ppm measured experimentally.[13]

The number of computational NMR studies applied to iron hydrides are very limited. Best *et al.* have considered di-iron systems that are similar to those considered here,[21] while Ziegler and Jolibois have considered $H_2Fe(CO)_4$[18,20] and Ahlberg and co-workers a protonated ferrocene system, [$^2H_{11}$]-ferrocene.[22] Ziegler has shown that for $H_2Fe(CO)_4$, the calculated values obtained are similar to those predicted for other mononuclear systems but are different from experimental values obtain by Cotton *et al.* (calculated:[20] -7.5 ppm, experiment:[23] -11.1 ppm).

In 2007, Best and co-workers calculated NMR parameters of iron hydride systems (similar to the systems studied in this chapter). In this case, all ^1H chemical

shifts were calculated relative to $[HFe(CO)_4]^-$ for which the chemical shift relative to TMS is known from experiment to be -8.81 ppm. This is significant as the reference contains the same elements as the system of interest. We adopt this protocol in this work. As Ahlberg previously, they used the GIAO method and B3LYP functional. However, the basis sets they used in this study are Los Alamos effective core potential for the iron and Dunning basis set for the rest of the atoms. They calculated chemical shifts for systems whose properties have already been determined experimentally: $[HFe(CO)_4]^-$, $(H_2)Fe(CO)_4$, $Fe_2(H)(CO)_5(\mu^2{-}CO)(\mu{-}SCH_2CH_2S)^-$ and $Fe_2(\mu^2{-}H)(CO)_6(\mu{-}SCH_2CH_2S)^-$ (Figure IV-3). The calculated values agreed with those obtained experimentally with an average error of $\approx$ 1.64 ppm. Interestingly, their calculated chemical shift for $(H_2)Fe(CO)_4$ at -9.43 ppm is close to the experimental value obtained by Jones and co-workers,[24] -9.67 ppm.[21] In Figure IV-3, the structures and their hydride chemical shifts are represented.

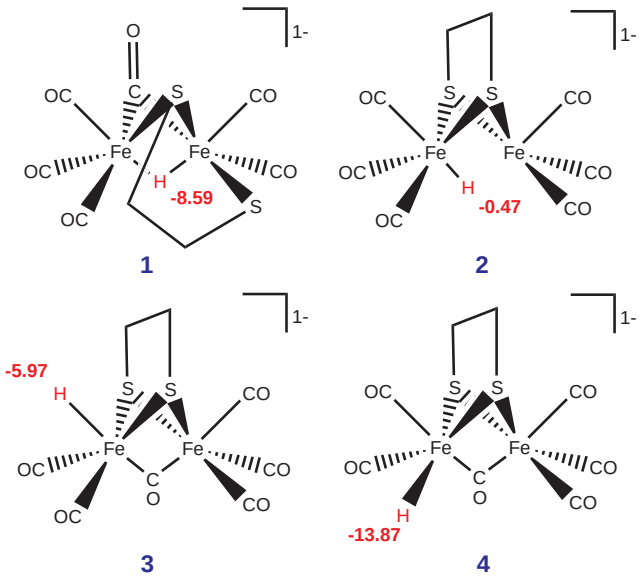

Figure IV-3: Systems for which hydride NMR chemical shift have been calculated by Best *et al.* (hydride chemical shifts in ppm).

Very recently, Jolibois *et al.* reported NMR parameters for $FeH(H_2)(dmpe)_2$, $H_2Fe(CO)_4$ and $K^+[HFe(CO)_4]^-$,[18] compounds that have been characterised experimentally using NMR spectroscopy by Baker, Brunet and Wilkinson and their co-workers.[23,25,26] As seen previously, the ^1H NMR chemical shift of $H_2Fe(CO)_4$

has been studied previously by DFT by Ziegler *et al.* (see Table IV-3).[20] For $K^+[HFe(CO)_4]^-$ the values obtained computationally agreed very well with those found experimentally. However, in the case of $FeH(H_2)(dmpe)_2$, the two chemical shifts calculated for the two different types of hydrogen are underestimated compared to experimental data (-13.9 and -10.4 ppm instead of -17.071 and -11.823 ppm). The work reviewed in this section shows that, in general, computed chemical shifts agree well with experimental results but are sensitive to the structure of the system studied.[7]

3.c - Previous calculations of coupling constant

The calculation of coupling constants, J, is a relatively new development. There are four terms which contribute to J, diamagnetic and paramagnetic spin-orbit terms, a spin-dipole term and a Fermi-contact term. The spin-dipole term is usually neglected because its contribution is small and difficult to compute. The most important part is the Fermi-contact (see Table IV-4) which describes the magnetic interaction between an electron and a nucleus. This induces a small polarisation of the total spin density which is felt by the other nuclei. The calculation of coupling constants is very sensitive to both the functional and the basis set chosen and so more demanding than the calculation of chemical shifts. Koch and Holthausen recommend the use of all-electrons basis sets (such as 6-31G*). However, they emphasise that GTOs do not reproduce the correct cusp condition at nuclei so they recommend the use of special IGLO-II or -III basis sets.[7]

The reduced coupling constant, K is usually adopted in theoretical discussions rather than the ordinary spin-spin coupling constant, J:

$$J(A,B) = \frac{h\,\gamma_A\,\gamma_B\,K(A,B)}{4\pi^2} \qquad \text{(IV-4)}$$

J is proportional to the product of the nuclear gyromagnetic ratios γ and K (J is given in Hz while K is given in SI units ($10^{19} kg.m^{-2}.s^{-2}.A^{-2}$).[29]

Complex	$^2J_{AB}$		Fermi-contact $^2J_{total}$ (Hz)	$^2J_{total}$ (Hz)	Fermi participation in $^2J_{total}$
	A	B			
$O_2H_3^-$	O	O	16.28	17.96	90.64%
$^+H_2OH \cdot NCH$	O	N	34.07	34.12	99.85%
$HOH \cdot NCH$	O	N	1.14	1.16	98.27%
$^+HCNH \cdot NCH$	N	N	32.46	32.52	99.81%
$CNH \cdot NC^-$	N	N	21.47	21.52	99.77%
$CNH \cdot NCH$	N	N	5.60	5.62	99.64%

Table IV-4: Participation of the Fermi-contact part in the ^{2}J coupling constant as reported in Elguero and Alkorta review[27] (results obtained by Del Bene *et al.*[28]).

i - Systems containing a metal

Ziegler and Dickson,[29] report coupling constants for 3d-metal-ligand coupling ($[V(CO)_6]^-$, $Fe(CO)_5$, $[Co(CO)_4]^-$). They were found to present a higher level of error than the coupling constants calculated for the elements of the first 3 rows. However, the error is not greater than 15% which is still acceptable for such calculations. They used both local spin-density (LSDA) and gradient-corrected density (GGA) functionals without seeing any noticeable differences between them (triple-ζ-doubly-polarised basis set).[29]

Ziegler and Khandogin calculated ^{1}K(M X) reduced coupling constants for M = V, Fe, Co, Nb, Mo, Rh, W, Cr, Mn, Tc, Ti, Ni and Pt and for X = C, O, F and P using DFT and non-hybrid functionals. They observed results in good agreement with experiments for 3d- and 4d- transitions metals but results obtained for 5d-transition metals such as W which were far from satisfactory.[30] These bad results for 5d-transition metal coupling constant are due to relativistic effects not being taken into account during calculations. However, relativistic effects can also be significant for the 3d-metals.[19]

Autschbach and Mort have calculated $^2J_{H\text{-}H}$ coupling constants for heavy metal hydride and dihydrogen complexes (for metals Ir, Os, Nb, Re and Ru) using 6-31G(p) or IGLO-III basis sets for the hydrogen bound to the metal (see Table IV-5). They found calculated values in line with those obtained experimentally and conclude that vibrational corrections and H-H distance have an impact on the ^{2}K(H H) coupling

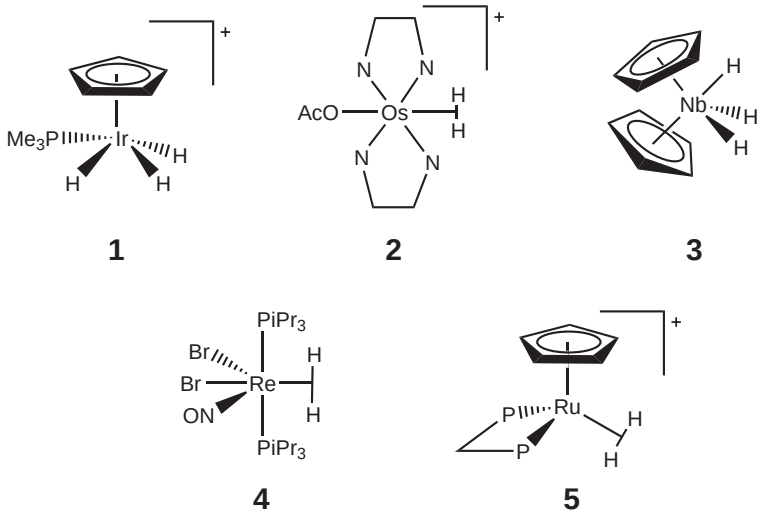

Figure IV-4: Compounds for which $J_{H\text{-}H}$ coupling constants have been calculated by Autschbach and Mort.[31]

constants.[31]

Compounds (see Figure IV-4)	**H-H distances (in Å)**	**Coupling constants (in Hz)**	
		Calc.	**Exp.**
1	1.699	2.76 †	3.9[32]
2	1.263	8.29 †	9[33]
3	1.752	0.66 †	0.9[34]
4	1.343	9.52 ‡	12.8[35]
5	0.892	32.94 *	20.6(3)[36]

† MPW1PW91 and IGLO-III
‡ MPW1PW91 and 6-31G(p)
* B3LYP and IGLO-III

Table IV-5: Calculated coupling constants, $J_{H\text{-}H}$ compared to experimental data for hydrogen and hydride ligands (compound of Figure IV-4) as presented by Autschbach and Mort.[31]

ii - coupling constants involving P: $J_{P\text{-}H}$ and $J_{P\text{-}P}$

In the work that will be described later in this chapter, the coupling constants that have been calculated are $J_{P\text{-}H}$ and $J_{P\text{-}P}$. For this reason, we review calculations in the literature done on these two specific coupling constants.

$J_{P\text{-}P}$: Termaten and co-workers observed a discrepancy between their results and experimental data and they calculated $J_{P\text{-}P}$ coupling constants, for Cp(L)M=PH (L = PH_3 or CO and M = Co, Rh or Ir) system. The calculated values are 117 to 290 % higher than experimental values.[37] Their calculations were performed using the LDA functional, VWN and a triple-zeta basis set. Wasylishen and co-workers have discussed the coupling in the system, $[Ph_3P{-}P{-}Ph_2]^+$ using the same computational method as Termaten *et al.*,[38] and they observed $^1J_{P\text{-}P}$ coupling constants consistent with experimental data. Their closest calculated coupling constant is in perfect agreement with the experimental value (calculation: -340 Hz (for a P-P dihedral angle of 180 °); experiment: -340 Hz (in solution)). Similarly, $^2J_{P\text{-}P}$ coupling constants calculated by Elguero and co-workers for [^{15}N]-phenylamino-[(diphenylphosphinoyl)methyl] present an acceptable agreement with experimental coupling constants.[39] The presence of the transition metal in Termaten's work may therefore be the cause of the over-estimation of the $J_{P\text{-}P}$ coupling constant, and a more accurate functional than LDA may be required to describe such system. Recent work reported by Elguero and Johnson confirmed that B3LYP provides better agreement with experiment.[40,41] The calculation of $J_{P\text{-}P}$ is, however, sensitive to the molecular geometry and in particular to the dihedral angle between the phosphorus centres. For example, Galasso, Cowley and Gray have shown that $J_{P\text{-}P}$ in P_2H_4 varies from from -142 Hz to +35 Hz for $^1J_{P\text{-}P}$ (for P_2H_4) when the dihedral angle, describing the rotation around the P-P bond, goes from 0 ° to 180 °, respectively.[42–46]

$J_{P\text{-}H}$: Coupling constants such as $^2J_{P\text{-}H}$, have been described by Autschbach, and appear to be difficult to calculate accurately.[19] However, a certain number of recent studies have presented calculated coupling constants in satisfactory and even good agreement with experimental data. For example, Chandra *et al.* calculated P-H coupling constants for a series of simple phosphorus species, PH_3, PH_4^+ and P_2H_4 for different basis sets,[47] in apparently good agreement with experiment. They showed that to obtain such agreement, it is necessary to use a double-zeta basis sets with polarisation functions. However, the coupling constants they obtained for a PH_2^- species are far from experimental values. Chandra *et al.* have explained this

discrepancy by arguing that the geometry used for PH_2^- might not be the one giving the lowest energy.[47]

Bagno and co-workers have recently calculated $^3J_{P\text{-}H}$ and $^4J_{P\text{-}H}$ coupling constants for a wide range of organic structures. Their calculations are in very good agreement with experimental values. The maximum difference they observed between experimental and calculated coupling constants is of approximately 5 Hz. In their case the use of the hybrid-GGA functional, B3LYP give far better results than the GGA functional, BP (B88/PW91).[48]

4 - Methodology

It is important to select an appropriate combination of a functional and basis sets that would provide the best compromise between accuracy and computational cost. Moreover, it is not obvious that the optimal method for geometries is necessarily optimal for NMR parameters.

In the previous chapter we have established the best choice of functional for the optimisation of structures and energies but it is not clear that this will necessarily be optimal for the calculation of chemical shifts as well as coupling constants. Results in the literature suggest that polarisation functions are important for the description of NMR parameters.[13,21,49] An example of one of the most precise basis set combination used in literature is the one used by Clot *et al.* who have shown that the IGLO-II basis set - developed especially for NMR calculations - for the organic atoms and Wachters+f[50] for the iron centres is a good combination for the calculation of the chemical shift for compounds containing Fe(CO) fragments.[51] Our aim here is to use the experimental NMR data obtained by Schollhammer for compounds for which the structure is already known as a testing ground to explore the ability of different DFT methodologies to compute NMR parameters. The availability of accurate chemical shifts and coupling constants for a series of closely related compounds offers an ideal

opportunity to benchmark in this way.

Results

1 - Basis set choice

In Table IV-6, we report the results of our calculations of the hydride chemical shifts and the P-H and P-P coupling constants for structures **A** to **D** proposed by Schollhammer *et al.*. In all cases, the chemical shift is given as $\sigma_{(FeH(CO)_4^-)}$ - σ_{complex} + 8.81, where -8.81 ppm is the chemical shift of $FeH(CO)_4^-$ relative to TMS. As a starting point, we can consider isomer **A**, as it is the only one where the structural assignment has been confirmed by crystallography. We have already noted that a SDD(Fe)/SVP basis set combination gives reliable optimised structures. However, NMR calculations using the same basis set combinations are not efficient to describe the NMR parameters correctly. We see in the table that most of the mixed basis sets give good results for the $J_{P\text{-}H}$ coupling constant, but the results are less satisfactory for the chemical shift and the $J_{P\text{-}P}$ coupling constants.

Clot *et al.*,[51] and Bühl *et al.*.[52] have used the Wachters+f basis set for iron centres and IGLO-II basis set for the other atoms.[50] Our results using such basis sets, presented in Table IV-6, suggest that this method gives better agreement with experiment for isomer **A** and all 3 parameters: δH, $J_{P\text{-}H}$ and $J_{P\text{-}P}$ are described accurately.

2 - Chemical shifts for isomers A, B, C and D

In Table IV-6 we reports the values obtained for the calculation of chemical shifts for the isomers **A**, **B**, **C** and **D** for a variety of basis sets.We see in Table IV-6 that the experimental and calculated chemical shifts are closely related for **A**, **C** and **D**, which suggests that the NMR parameters of these compounds are well described computationally compared to experiment. We observe that the values for **A**, **C** and **D** are in the range of expected values for bridging hydrides ($\delta :\approx -10 \rightarrow -17$ ppm) and for terminal hydrides ($\delta :\approx -2 \rightarrow -4$) for this type of dimers.

In the case of **B**, results are out of the expected range for such hydridic system. This suggests that the identity of **B** is in doubt. We see only two possibilities that would explain this difference for the compound **B**: either it is a failure in the methodology or the proposed structure by Schollhammer *et al.* is incorrect. The calculation of the chemical shift of iron hydrides entities is known to be challenging computationally, and Jolibois *et al.* showed that substantial errors can arise due to an over-estimation of the shielding.[18] However, the good results obtained for the other isomers **A**, **C** and **D**, suggest that our chosen methodology is able to describe these systems, and there seems to be no obvious reason why **B** should be poorly described.

Conformation		**A**			**B**			**$C_{basal\text{-}basal}$**			**D**		
Parameters		δH*	J_{P-H}**	J_{P-P}**	δH*	J_{P-H}**	J_{P-P}**	δH*	J_{P-H}**	J_{P-P}**	δH*	J_{P-H}**	J_{P-P}**
Experiment		-14.23	21/21	0	-14.50	26/0	24.3	-4.33	0	0	-2.47	69/69	0
Basis set	**Number of basis functions**												
SDD all	318	-10.46	22/18	20	-19.32	31/22	12	-2.25	5/6	15	4.11	105/119	6.4
SDD Fe / SVP	415	-13.63	20/16	2.4	-17.98	25/20	9	-1.72	3.4/4	4	-0.41	88/106	5.1
SDD Fe,S / SVP	415	-11.01	20/16	3.3	-15.89	24/19	10	0.17	4.3/4.0	5.2	2.59	92/111	6.2
SDD Fe,C / SVP	455	-14.71	20/16	2.3	-18.75	29/18	9	-2.64	3.4/4.0	0.8	-1.26	88/106	4.8
SDD Fe,P / SVP	415	-9.50	20/17	21	-19.05	28/20	14	-0.82	3.7/4.4	17	5.14	105/118	10
SDD Fe,S,C / SVP	455	-13.18	20/16	3.6	-17.71	28/18	10	-1.90	3.6/4.3	2.2	0.68	92/111	6.2
SDD Fe,P,C / SVP	455	-12.63	20/17	20	-20.76	28/20	14	-2.76	3.6/4.3	18	2.25	105/119	8.8
SDD Fe,P,S / SVP	415	-8.68	20/17	21	-17.91	26/19	13	-1.03	3.7/4.4	19	6.46	110/125	9.6
TZVP	491	-13.79	20/17	0.53	-17.93	27/19	7	-1.93	4/5	0.93	-0.54	91/110	1.6
Wachters+f Fe IGLO-II	622	-14.95	23/19	0.4	-18.55	29/22	5.4	-2.36	4.1/4.8	0.2	-1.51	101/123	0.41
Wachters+f Fe IGLO-II Phenyls on dppe		-13.51	11/8	25	-18.97	12/18	14	-3.34	1.3/2.3	12	2.22	36/61	41

* chemical shift are given in ppm
** coupling constant are given in Hz

Table IV-6: NMR calculations with different basis sets (using B3LYP functional) compared to experimental NMR spectra.

3 - Coupling constants for A, B, C and D

The $^{31}P-^{1}H$ coupling constant, clearly seen in the experimental spectra, offer a further dimension to our analysis. The computed coupling constants, J_{PH}, are given in Table IV-6. For compounds **A**, **C** and **D**, the coupling constants are in excellent agreement with the experiment and in range with expected values for bridging ($J_{P\text{-}H}$: ≈ 20 Hz) and terminal ($J_{P\text{-}H}$: $\approx 80 \rightarrow 100$ Hz) hydrides. For **C**, the J_{PH} values are very small because the hydride and phosphorus ligands are on opposite Fe centres. As a result, Schollhammer and co-workers were unable to resolve the dppe position (ap-ba or ba-ba) for structure **C**. As seen previously in Table IV-1, our calculated energies suggest that the compound containing the ba-ba dppe is the more stable of the two.

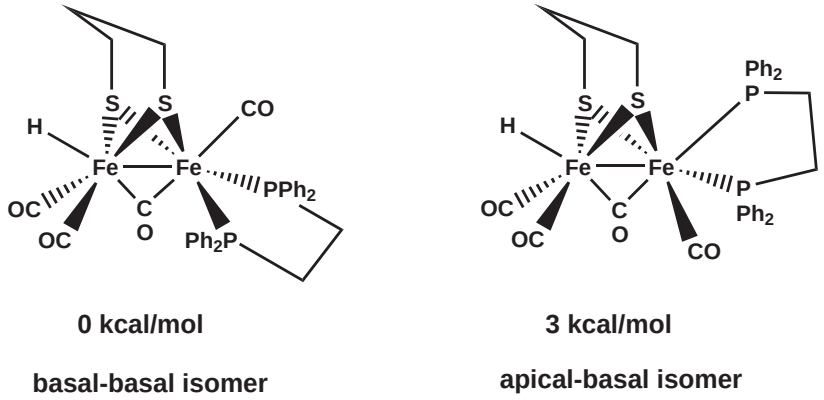

Figure IV-5: Comparison of the stabilities between the two possible isomers for **C**: basal-basal and basal-apical (relative energies given).

For compound **B**, the agreement with experiment is again poor. As we can see in Table IV-6 , calculations for the hypothetical isomer **B** show two distinct coupling constant, one for each of the phosphorus. However, experimentally there is only only one coupling constant observed. Schollhammer has proposed that the signal for **B** appears as a doublet rather than a triplet or doublet of doublet because one of the coupling constants is very small. However, our calculations do not support this: both $J_{P\text{-}H}$ are substantial, and we would predict a doublet of doublets. Our doubts about the geometry of the isomer **B** led us to consider the factor that could

make a difference between the calculated and experimental results. Before making any hypotheses about the possible structure of **B**, we tried to understand what parameters in the molecule could have an important impact on the chemical shielding and coupling constants in the system of interest.

Impact of the position of the phenyls The experiments are done based on compounds containing 4 phenyls attached to the phosphorus of the dppe, while in our initial calculations, the phenyls have been replaced by hydrogens. We therefore decided to include the full phenyl groups in our calculations (Table IV-6). This does result in a reduction in $J_{P\text{-}H}$, but both remain significant, and so it is not clear that a doublet should emerge.

Another possibility is that errors in the geometry optimisation could lead to errors in the computed NMR parameters. To explore this issue, we have varied a number of key structural parameters around their equilibrium values to explore the sensitivity of the computed $J_{P\text{-}H}$ (Table IV-7). In each case, a given structural parameter was fixed, and the remainder re-optimised (B3LYP and SDD(Fe)/SVP) NMR parameters were computed using Wachters+f and IGLO-IIbasis set associated with the B3LYP functional.

We observe that the changes in bond lengths, and angles result in very small energy changes compared to the most stable compound (with a maximum of 22 kcal/mol difference). Otherwise, the parameters which are the most perturbed by these changes are the chemical shift (with a maximum difference of $\approx$ 3 ppm) and even more, the P-P coupling constant (with a maximum difference of $\approx$ 13 Hz). The parameter that has the most impact is the Fe-P distance both on δH and $J_{P\text{-}P}$, while the H-Fe-P angle has an impact mainly on the $J_{P\text{-}P}$ coupling constant. However, the structural variations are not big enough to consider them as a solution to resolve the problem of discrepancy between the values obtained for **B** computationally and experimentally.

Bond length (in Å)				**^{1}H NMR (in ppm)**	**Coupling constants (in Hz)**	**^{31}P NMR (in ppm)**	**Coupling constants (in Hz)**	**Relatives Energies (in kcal.mol^{-1})**
Fe-H	Fe-P	H-Fe-P	P-Fe-P	δH	J_{P-H}	δP	J_{P-P}	
1.55 *	2.27	173	86	-19.63	32/23	287/291	4.5	1
1.65 *	2.26	173	86	-18.55	29/22	284/287	5.4	0
1.75 *	2.25	174	86	-17.42	28/21	278/287	5.6	0.6
1.66	2.16 *	174	87	-15.54	27/22	269/284	13	1.1
1.65	2.26 *	173	86	-18.55	29/22	284/287	5.4	0
1.65	2.36 *	173	85	-21.72	32/23	290/298	1.7	0.7
1.65	2.27	163 *	85	-17.89	32/36	285/288	18	1.2
1.65	2.26	173 *	86	-18.55	29/22	284/287	5.4	0
1.66	2.26	180 *	87	-19.15	28/16	278/288	1.1	0.4
1.65	2.33	92	76 *	-19.65	36/13	302/314	1.2	6
1.65	2.26	173	86 *	-18.55	29/22	284/287	5.4	0
1.67	2.21	168	96 *	-18.56	27/32	273/279	18	6
1.68	2.18	173	106 *	-19.53	31/48	273/281	28	22

* parameter frozen for the calculation

Table IV-7: Effect of bond and angle change on the NMR parameters calculated for isomer **B**.

Impact of the group trans to the hydride Our calculations on the proposed structures for **A** and **B** (bridging hydride) suggest that the chemical shift is very sensitive to the group *trans* to H (CO or PR_3), with a difference of 3.6 ppm. In contrast, the experimental data place the chemical shifts of **A** and **B** within 0.25 ppm of each other, suggesting that the *trans* ligand is probably the same in each case (contrary to Schollhammer's structure for **B**). In order to establish whether this *trans* influence on δH is general, we have considered work reported by Duckett and co-workers.[53]

They synthesised a compound possessing two hydrides, one having a CO group trans, the other a phosphorus (see Figure IV-6) and used NMR spectroscopy to obtain the hydride chemical shifts. The resulting chemical shifts for $\mathbf{H_1}$ and $\mathbf{H_2}$ are -8.80 and -10.24 ppm, respectively.

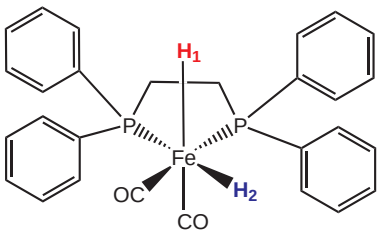

Figure IV-6: Complex containing two iron hydrides with two different groups in trans synthesised and resolved by NMR spectroscopy by Duckett and co-workers.[53]

We performed calculations based on this compound where phenyls are replaced by hydrogens.

In Figure IV-7, there is a clear difference between the cases where CO is trans to the hydride and where a P group is trans to the hydride, the chemical shift for the former one is approximately 2 ppm lower than for the later one. Moreover, the computed results are very close to the experimental data.

Impact of the fluxional process Last but not least, a fluxional process involving exchange between the phosphorus centres of the dppe ligand might be the reason of some of the discrepancies observed between experimental and calculated results in

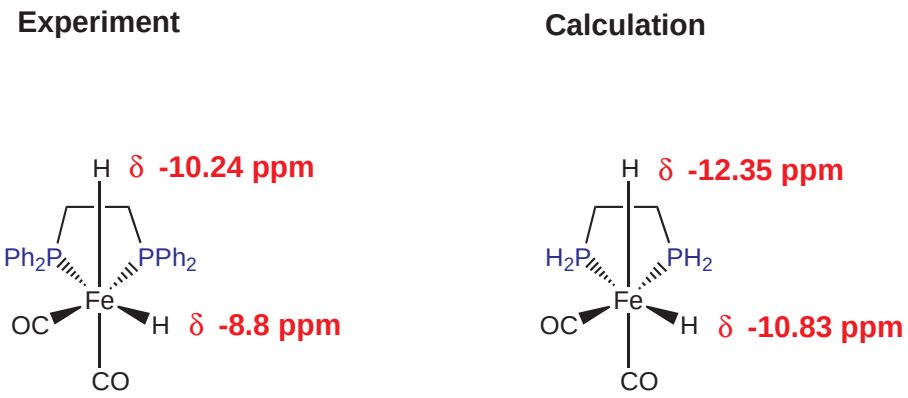

Figure IV-7: Comparison of the chemical shift of hydrides in trans of a CO or P group between experiment done by Duckett *et al.* and our calculations.

species **B**. Specifically, it is possible that exchange of the phosphorus centres would result in an average value of J_{PH}.

4 - Conclusion

The chemical shifts calculated for **A**, **C** and **D** are in good agreement with those obtained experimentally, However the chemical shift of **B** is not in agreement with the NMR spectra proposed experimentally. Coupling constants have also been calculated and are also in good agreement with the experimental values with the obvious exception of **B**. The identity of species **B** remains unclear. We have shown that a fluxional process could account for some of the discrepancies observed between the experimental and computational results. We have also shown that other structural features could account for the observed NMR parameters

Bibliography

[1] Ezzaher, S.; Capon, J.-F.; Gloaguen, F.; Pétillon, F. Y.; Schollhammer, P.; Talarmin, J.; Pichon, R.; Kervarec, N. *Inorg. Chem.*, **2007**, *46*, 3426.

[2] Ramsey, N. F. *Phys. Rev.*, **1950**, *77*, 567.

[3] Hornig, J. F.; Hirschfelder, J. O. *J. Chem. Phys.*, **1955**, *23*, 474.

[4] Tillieu, J.; Guy, G. *J. Chem. Phys.*, **1956**, *24*, 1117.

[5] Das, T. P.; Bersohn, R. *Phys. Rev.*, **1956**, *104*, 849.

[6] McGarvey, B. R. *J. Chem. Phys.*, **1957**, *27*, 68.

[7] Koch, W.; Holthausen, M. C. *A Chemist's Guide to Density Functional Theory.* Wiley-VCH, Weinheim, second edition, **2000**.

[8] London, F. *J. Phys. Radium*, **1937**, *8*, 397.

[9] Schindler, M.; Kutzelnigg, W. *J. Chem. Phys.*, **1982**, *76*, 1919.

[10] Cramer, C. J. *Essentials of Computational Chemistry.* John Wiley & sons, Chichester, **2002**.

[11] Dejaegere, A. P.; Case, D. A. *J. Phys. Chem. A*, **1998**, *102*, 5280.

[12] Jimeno, M. L.; Alkorta, I.; Elguero, J.; Anderson, J. E.; Claramunt, R. M.; Lavandera, J. L. *New J. Chem.*, **1998**, 1079.

[13] Gobetto, R.; Nervi, C.; Romanin, B.; Salassa, L. *Organometallics*, **2003**, *22*, 4012.

[14] Rablen, P. R.; Pearlman, S. A.; Finkbiner, J. *J. Phys. Chem. A*, **1999**, *103*, 7357.

[15] Bagno, A.; Saielli, G. *Theor. Chem. Acc.*, **2007**, *117*, 603.

[16] Gauss, J.; Stanton, J. F. *J. Chem. Phys.*, **1996**, *104*, 2574.

[17] Bühl, M.; Kaupp, M.; Malkina, O. L.; Malkin, V. G. *J. Comp. Chem.*, **1999**, *20*, 91.

[18] del Rosal, I.; Maron, L.; Poteau, R.; Jolibois, F. *Dalton Trans.*, **2008**, 3959.

[19] Kaltsoyannis, N.; McGrady, J. E., Eds. *Principles and Applications of Density Fuctional Theory in Inorganic Chemistry.* Springer-Verlag Berlin Heidleberg, **2004**.

[20] Ruiz-Morales, Y.; Schreckenbach, G.; Ziegler, T. *Organometallics*, **1996**, *15*, 3920.

[21] Borg, S. J.; Tye, J. W.; Hall, M. B.; Best, S. P. *Inorg. Chem.*, **2007**, *46*, 384.

[22] Karlsson, A.; Broo, A.; Ahlberg, P. *Can. J. Chem.*, **1999**, *77*, 628.

[23] Cotton, F. A.; Wilkinson, G. *Chem. Ind.*, **1956**, 1305.

[24] Krusic, P. J.; Jones, D. J.; Roe, D. C. *Organometallics*, **1986**, *5*, 456.

[25] Baker, M. V.; Field, L. D.; Young, D. J. *J. Chem. Soc., Chem. Commun.*, **1988**, 546.

[26] Brunet, J.-J.; Chauvin, R.; Diallo, O.; Kindela, F.; Leglaye, P.; Neibecker, D. *Coord. Chem. Rev.*, **1998**, *178-180*, 331.

[27] Alkorta, I.; Elguero, J. *Int. J. Mol. Sci.*, **2003**, *4*, 64.

[28] Del Bene, J. E.; Perera, S. A.; Bartlett, R. J. *J. Am. Chem. Soc.*, **2000**, *122*, 3560.

[29] Dickson, R. M.; Ziegler, T. *J. Phys. Chem.*, **1996**, *100*, 5286.

[30] Khandogin, J.; Ziegler, T. *Spectrochim. Act. A*, **1999**, *55*, 607.

[31] Mort, B. C.; Autschbach, J. *J. Am. Chem. Soc.*, **2006**, *128*, 10060.

[32] Heinekey, D. M.; Hinkle, A. S.; Close, J. D. *J. Am. Chem. Soc.*, **1996**, *118*, 5353.

[33] Hasegawa, T.; Li, Z.; Parkin, S.; Hope, H.; McMullan, R. K.; Koetzle, T. F.; Taube, H. *J. Am. Chem. Soc.*, **1994**, *116*, 4352.

[34] Heinekey, D. M. *J. Am. Chem. Soc.*, **1991**, *113*, 6074.

[35] Gusev, D.; Llamazares, A.; Artus, G.; Jacobsen, H.; Berke, H. *Organometallics*, **1999**, *18*, 75.

[36] Law, J. K.; Mellows, H.; Heinekey, D. M. *J. Am. Chem. Soc.*, **2002**, *124*, 1024.

[37] Termaten, A. T.; Aktas, H.; Schakel, M.; Ehlers, A. W.; Spek, A. L.; Lammertsma, K. *Organometallics*, **2003**, *22*, 1827.

[38] Gee, M.; Wasylishen, R. E.; Ragogna, O. J.; Burford, N.; McDonald, R. *Can. J. Chem.*, **2002**, *80*, 1488.

[39] López-Leonardo, C.; Alajarín, M.; Llamas-Lorente, P.; Bautista, D.; Jimeno, M. L.; Alkorta, I.; Elguero, J. *Struct. Chem.*, **2003**, *14*, 391.

[40] Fruchier, A.; Vicente, V.; Alkorta, I.; Elguero, J. *Magn. Reson. Chem.*, **2005**, *43*, 471.

[41] Hatnean, J. A.; Raturi, R.; Lefebvre, J.; Leznoff, D. B.; Lawes, G.; Johnson, S. A. *J. Am. Chem. Soc.*, **2006**, *128*, 14992.

[42] Cowley, A. H.; White, D. W. *J. Am. Chem. Soc.*, **1969**, *91*, 1917.

[43] Gray, G. A.; Albright, T. A. *J. Am. Chem. Soc.*, **1976**, *98*, 3857.

[44] Gray, G. A.; Albright, T. A. *J. Am. Chem. Soc.*, **1977**, *99*, 3243.

[45] Galasso, V. *J. Magn. Reson.*, **1979**, *36*, 181.

[46] Galasso, V. *J. Chem. Phys.*, **1984**, *80*, 365.

[47] Chakraborty, D.; Chandra, P. *J. Molec. Struct.*, **1998**, *434*, 75.

[48] Tähtinen, P.; Bagno, A.; Koch, A.; Pihlaja, K. *Eur. J. Org. Chem.*, **2004**, 4921.

[49] Cheeseman, J. R.; Trucks, G. W.; Keith, T. A.; Frisch, M. J. *J. Chem. Phys.*, **1996**, *104*, 5497.

[50] Basis sets were generated using the basis set exchange website: http://gnode2.pnl.gov/bse/portal.

[51] Bolton, P. D.; Clot, E.; Cowley, A. R.; Mountford, P. *Chem. Commun.*, **2005**, 3313.

[52] Šarić, A.; Vrček, V.; Bühl, M. *Organometallics*, **2008**, *27*, 394.

[53] Schott, D.; Callaghan, P.; Dunne, J.; Duckett, S. B.; Godard, C.; Goicoechea, J. M.; Harvey, J. N.; Lowe, J. P.; Mawby, R. J.; Müller, G.; Perutz, R. N.; Poli, R.; Whittlesey, M. K. *Dalton Trans.*, **2004**, 3218.

CHAPTER V

Carbon Phosphorus chemistry

Introduction

In this chapter, we use theory to explore some aspects of main group chemistry and more particularly phosphorus/carbon systems. Work was done in collaboration with Russell and co-workers at the University of Bristol. The work is divided into two distinct sections, but the common theme is the isomerisation of systems featuring multiple bonds to phosphorus into more complex, 3-dimensional structures involving only σ bonds. The relative instability of π bonds involving heavy elements is, of course, well known, but the mechanisms by which they rearrange to more stable 3-dimensional structures is less well established. The first section describes the rearrangement of a P=C bonded species, while the second focuses on P=P bonds.

In order to place this work into context, we first review the chemistry of multiple bonds involving main group heavy elements, with a particular emphasis on systems where C−H groups have been replaced by P atoms. Such systems are very common - so much that phosphorus has been refereed in the literature as "a carbon copy". The phosphorus chemistry is closer to carbon chemistry than was first thought. Silicon has always been thought to be a closer analogue of carbon than phosphorus. The same sort of limited analogy between silicon and carbon is present between nitrogen

and phosphorus (both elements of group 15). In both cases, it is largely due to the fact that silicon and phosphorus easily attain coordination 6 because of their larger covalent radii (C: 0.77, N: 0.70 vs Si: 1.11, P: 1.10 Å). However, carbon and phosphorus possess a similar electronegativity (C: 2.5 vs P: 2.2 eV) which is the factor governing their ability to release or accept electrons and which in turn controls the reactivity of any species containing the element. This observation prompted Dillon and co-authors to note that "*Carbon is more similar to its diagonal relative, phosphorus than to silicon*".[1]

1 - P/C isolobal analogy

In the context of phosphorus-carbon chemistry the isolobal relationship between P and C-H is particularly important.[2] Isolobal means that two fragments possess frontier orbitals of the same symmetry and occupation and similar energies (see Figure V-1). This relationship means that one fragment can be easily replaced by an isolobal one without changing the underlying electronic structure. The most commonly discussed isolobal analogy is between BH fragments and CH^+, but in our studies, we focus on the P/CH isolobal analogy (Figure V-1).

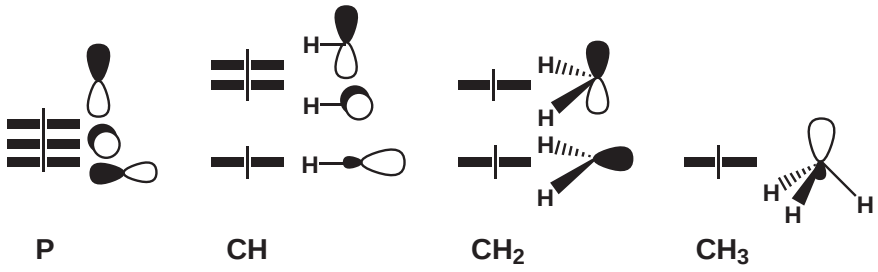

Figure V-1: Frontier molecular orbitals of P, CH, CH_2 and CH_3 fragments.

2 - Multiple bonding in main group heavy elements

A few decades ago, the formation of homo- or hetero-multibonds by heavy elements from groups 14 and 15 (group 14: Si, Ge, Sn; group 15: P, As, Sb) was thought to be impossible due to the instability of π bonds involving these atoms.[3] This impossibility was summarised in the "double bond rule", which states that elements having a principal quantum number greater than 2 should not be able to form π-π bonds with the same element or with other elements.[4] In the 70's the compound $[Sn(CH-(SiMe_3)_2)_2]_2$ was the first to clearly show a double bond (Sn=Sn), and it was later, in the 80s, that the first double bond for an element of group 15 was found ($(t-Bu)_3C_6H_2P=PC_6H_3(t-Bu)_3$).[5] Those discoveries renewed the interest in this type of compound and subsequently numerous compounds possessing a double bond have been isolated (P=As, As=As, P=B, As=B, As=C for example).[6,7]

In this section, silicon multiple bonds will be discussed first as they illustrate the key features of multiple bonding between heavy elements. Phosphorus multiple bonds will be then discussed as they will be the centre of interest of the work described in this chapter. One of the most extensively studied multiple bonded silicon systems are the disilenes, of formula Si_2R_4. Disilene itself, $H_2Si=SiH_2$, has not yet been successfully synthesised, but its electronic structure has been studied using a variety of theoretical methods. Recent computational work shows that, in contrast to C_2H_4, Si_2H_4 adopts a trans-bent structure (see Figure V-2).[8,9]

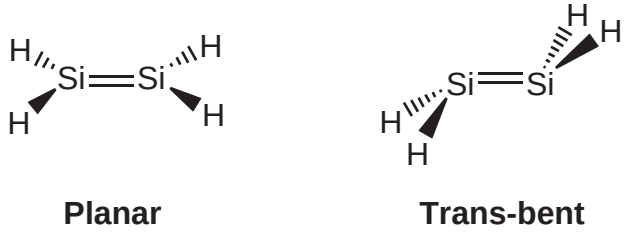

Figure V-2: Description of planar and trans-bent structures.

The formation of trans-bent structure instead of a planar one is due to a relative instability of the silicon π-bonds. The strength of the π bond is defined by the height of the cis-to-trans barrier. For the Si=Si double bond the cis-to-trans isomerisation has been found computationally (using MRD-CI (Multi-Reference Double-Excitation Configuration Interaction) method) to be about 22 kcal/mol[10] which agrees with the value obtained experimentally, 25-30 kcal/mol.[11] This small cis-to-trans barrier is a sign of a not so strong double bond. The strength of Si=Si double bond has also been confirmed by Ziegler and Jacobsen who showed that the Si=Si double bond of $H_2Si{=}SiH_2$ has a total bond energy (TBE) of 250 kJ/mol which is far weaker than the C=C bond in ethylene, where the calculated TBE is 739 kJ/mol.[9] The addition of bulky substituents, in contrast, makes the structure adopt a planar structure which indicates a strengthening of the Si=Si double bond.

There are two main possibilities to interpret the change from the planar $H_2C{=}CH_2$ to the trans-bent $H_2Si{=}SiH_2$ structure. The first, presented by Tranquier and Malrieu, views the bonding in $H_2X{=}XH_2$ (X=Si, Ge, Sn, Pb) systems in terms of the interaction of two carbenic fragments in which the lone pair of one species is partly delocalised into the empty p_π orbital of the other fragment as shown in Figure V-3.[12]

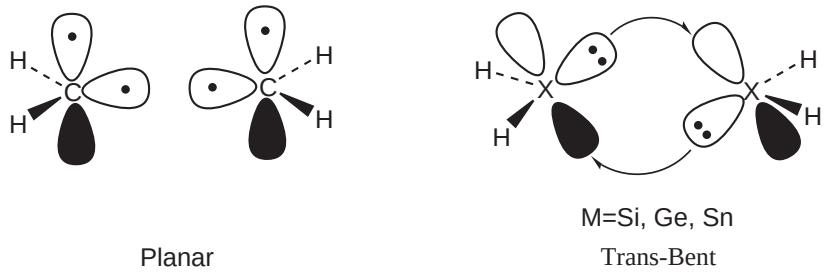

Figure V-3: Comparison of H_2XXH_2 structures for X=C and M=Si,Ge,Sn.

Alternatively, Ziegler and Jacobsen have used the delocalised molecular orbitals to show that when the symmetry is lowered D_{2h} to C_{2h}, the σ^* and the π orbitals (b_{3u} and b_{2u} in D_{2h}) mix because both transform as b_u in the lower symmetry. The mixing of the σ^* and π orbitals gives hybrid π orbitals and weakens the π-bond (see Figure V-4).[9]

The general trend for main group element double bonds to be weak has been explained as a less efficient mixing of the s and p valence orbitals. Physically, this is shown by an increase of the non bonding character of the s orbitals and a gradual transition from π bonded electron pairs to lone pairs in the heavier elements.[7]

The disilyne species, HSi≡SiH, is very similar to its double bonded analogue, i.e. it possesses the same weak bonding due to the mixing of its π and σ^* orbitals (see Figure V-5).[13] This mixing reduces the effective bond order from 3 to somewhere approaching 2. Thus, Si-Si multiple bond in HSiSiH has been described by Andreoni *et al.*[14] as a double bond whereas Frenking and co-workers[15] described it as a triple bond with a donor-acceptor description for the pseudo-π bonds (see Figure V-6). This is an equivalent description of the "π" bonds to the one made by Malrieu *et al.* for $H_2Si{=}SiH_2$ (Figure V-3).[12]

Silicon also forms double bonds to carbon forming compounds called silenes, Si=C. These compounds possess a stronger double bond than disilene systems; their π-bond strength, measured by the bond rotational barrier, is $\approx$ 37-40 kcal/mol ($H_2Si{=}CH_2$) compared to a value of $\approx$ 22 kcal/mol for disilenes ($H_2Si{=}SiH_2$).[16–18] As previously seen with disilene species, the silene compounds can adopt two different conformations: a planar and a twisted biradical (see Figure V-7). However, it is the planar structure that is the most stable.[18]

The stabilisation of the planar structure indicates the presence of a double bond similar in composition to the C=C double bond.

3 - Multiple bonds to phosphorus

As said previously, the first compound synthesised containing a double bond between two group 15 elements was the compound of Yoshifuji *et al.*, $((t{-}Bu)_3C_6H_2P{=}PC_6H_3(t{-}Bu)_3)$.[5] This compound composed of a P=P double bond is of the diphosphene family.

The simplest compound of the diphosphene family, P_2H_2 possesses 3 constitu-

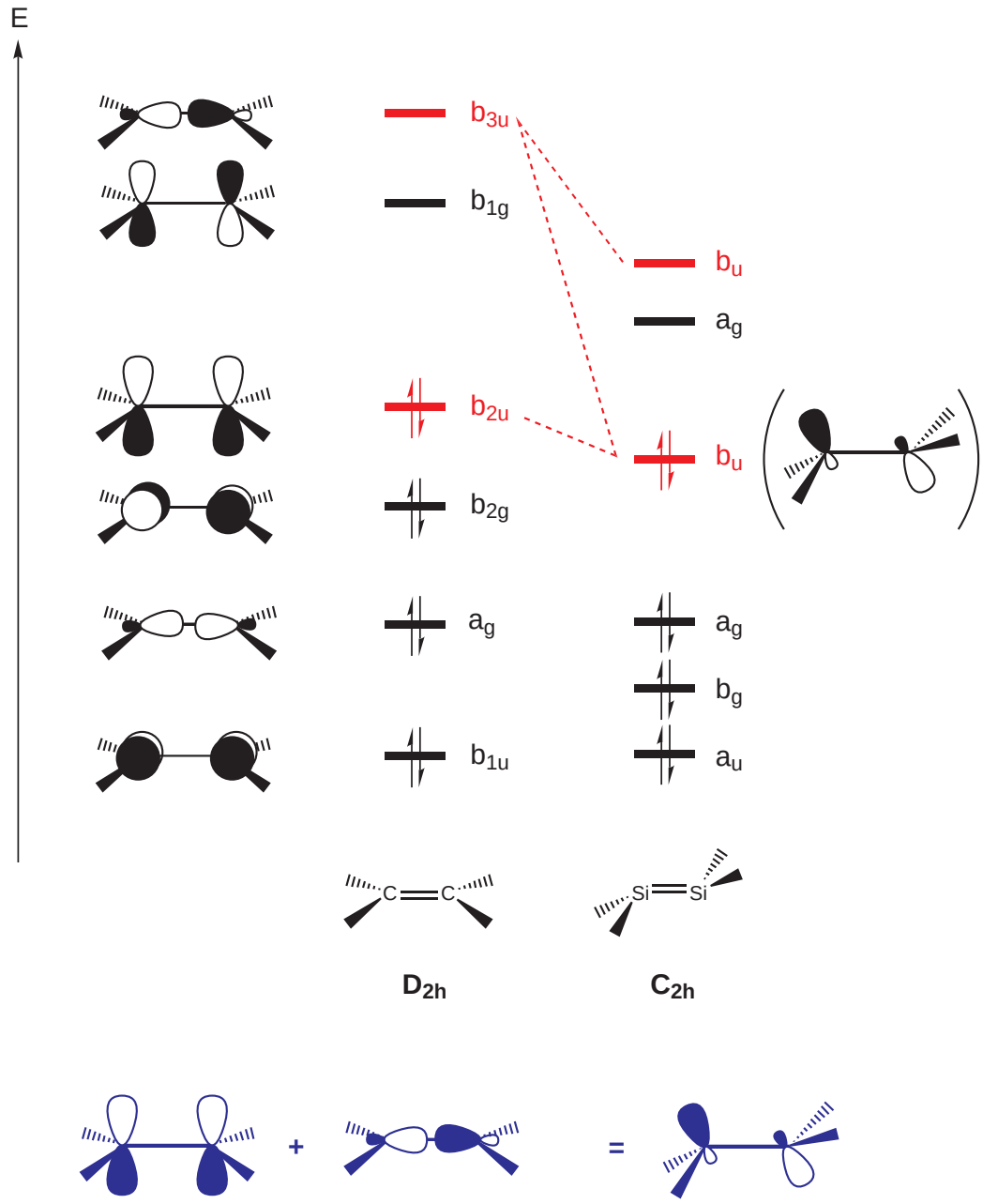

Figure V-4: Orbital diagram presenting the switch from alkene (D_{2h}) to disilene (D_{2h} or C_{2h} for $H_2Si{=}SiH_2$) species.

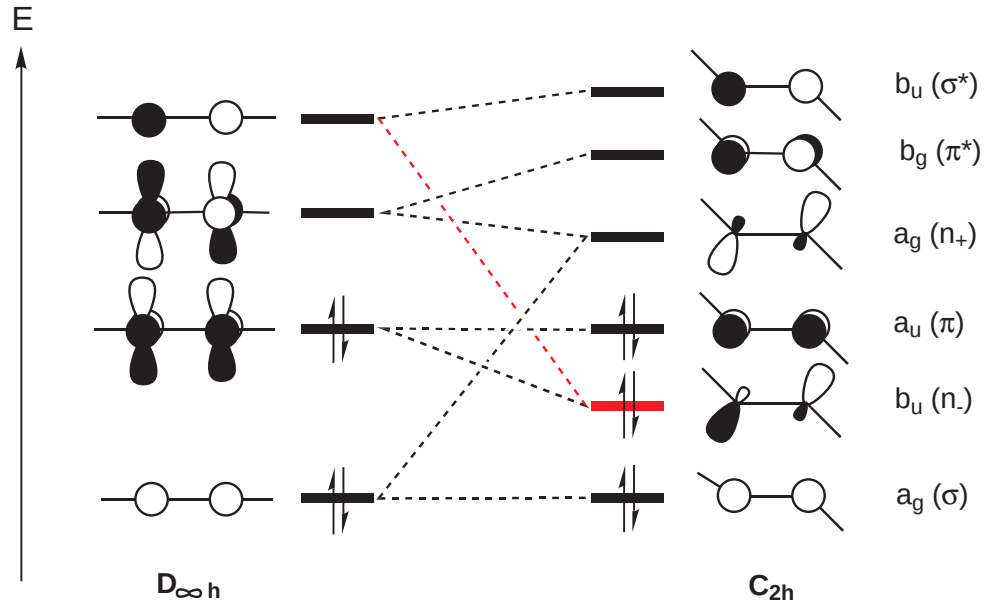

Figure V-5: Orbital diagram presenting the switch from alkyne ($D_{\infty h}$) to disilyne (C_{2h}) species.

tional isomers: a *cis* or a *trans* diphosphene or a phosphinophosphinidene (see Figure V-8). Computational studies have shown that the trans-HPPH structure is the most stable conformation (see Table V-1).[19–21]

In contrast to silicon multiple bonds, phosphorus multiple bonds are rather more similar to those of carbon: there is less hybridisation of the orbitals than for silicon and so the P=P double bonds are made up of classical σ and π components.[22] The homonuclear π-bond strength is also increased in group 15 as a result of their

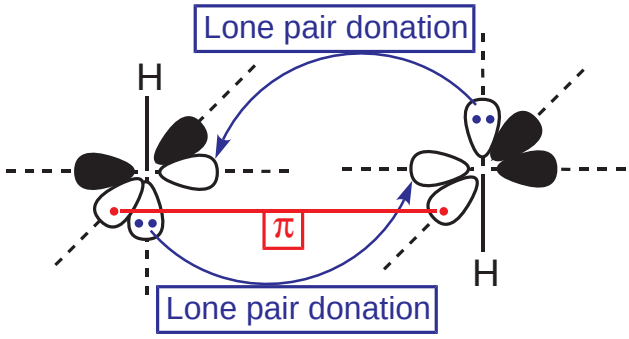

Figure V-6: Donor-acceptor system to describe the Si≡Si triple bond as proposed by Frenking *et al.*.[15]

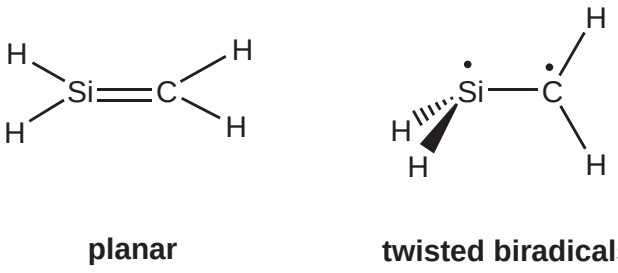

Figure V-7: Two possible conformations a silene can adopt.

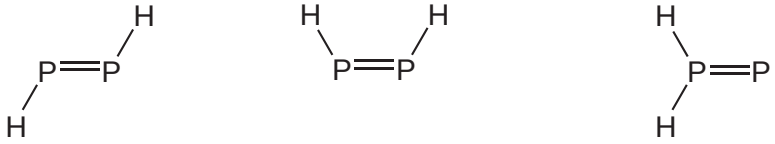

Figure V-8: The three possible isomers that a compound of formula P_2H_2 can adopt.

smaller size.[6] However, despite the similarities between P=P and C=C bonds, the P-P π-bonds remain weaker than C-C ones.[6] Indeed, Gordon[19] and Walsh[10] and their respective co-workers have calculated a π-bond strength of 35 kcal/mol for P=P compared to a calculated value of 62 kcal/mol for C=C (experimentally 65 kcal/mol[23]). The fact that P-P double bonds are somewhat similar to carbon double bonds in their σ:π bond strength ratio, (48:34) for P=P and (81:62) for C=C confirms that the P-P double bond can be regarded as a full-fledged double bond. However, their weakness can be explained by comparing their frontier orbitals with those of stable N=N double bond (63.5 kcal/mol[19]). Figure V-9 shows the frontier orbitals of HN=NH, HP=NH and HP=PH systems as calculated by Nagase and Ito.[24] While the HN=NH and HP=NH HOMO and HOMO-1 are lone pairs and

Structure	Relative energy (kcal/mol)
trans HP=PH (C_{2h})	0
cis HP=PH (C_{2v})	3
H_2P=P (C_{2v})	28

Table V-1: Comparison of the stability of different possible conformation for P_2H_2 as calculated by Allen *et al.*.[21]

π orbitals, respectively, the situation is reversed in HN=NH. The lone pair-π orbitals switch has also been confirmed computationally by Galasso[25] and by Elbel *et al.* using photoelectron spectroscopy.[26] In all cases, however, the LUMO are π^* orbitals. The HOMO-LUMO gaps for HP=PH, HP=NH and HN=NH systems have also been calculated to be approximately 9.9, 11.7 and 14.7 eV. It seems that the reduction of the HOMO-LUMO gap is the reason of the greater instability of the P-P double bond. The loss of bond strength is also confirmed by Elbel *et al.* who showed a reduction of electron density in the bonding region for the heavier species.

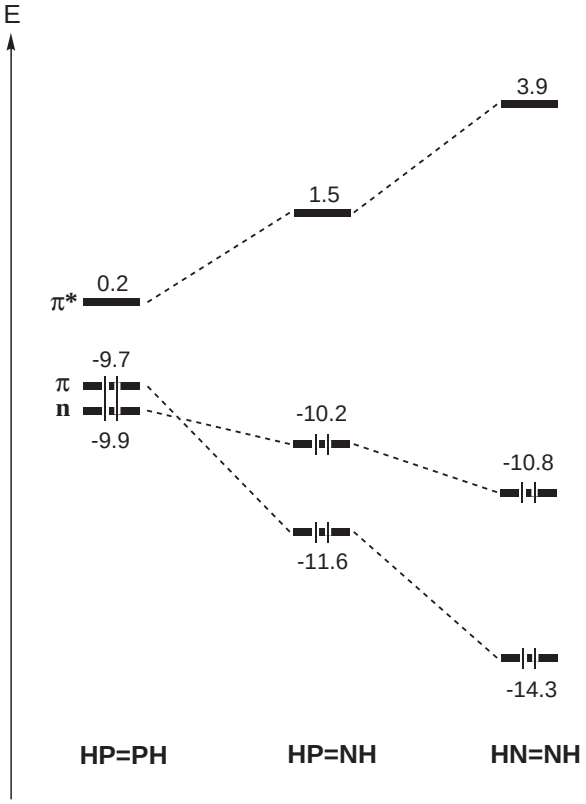

Figure V-9: Comparison of frontier orbitals for double bond between same elements of group 15 (N=N and P=P).

As was the case for silicon-carbon double bond, the P=C double bond in $R^1R^2C{=}PR^3$ is not as strong compared to C=C and C=N double bonds.[27] Figure V-10 summarises the differences between the HOMOs and HOMO-1s of C=N and C=P bonds. While in C=N double bonds the HOMO corresponds to the lone pair and the HOMO-1 corresponds to the π-bonding orbital, these two are reversed for the C=P bond.

As a result the P=C double bond is very reactive and as the lone pair lies only at 0.4 eV lower than the HOMO, it can also play a key role in the chemistry. The inversion of the lone pair and the π orbitals seems to be typical of a bond partially or fully constituted by a phosphorus or a silicon (see Figure V-11) and there is, therefore, a competition between the lone pair reactivity and the double bond reactivity in $-$C=P$-$ species.[1]

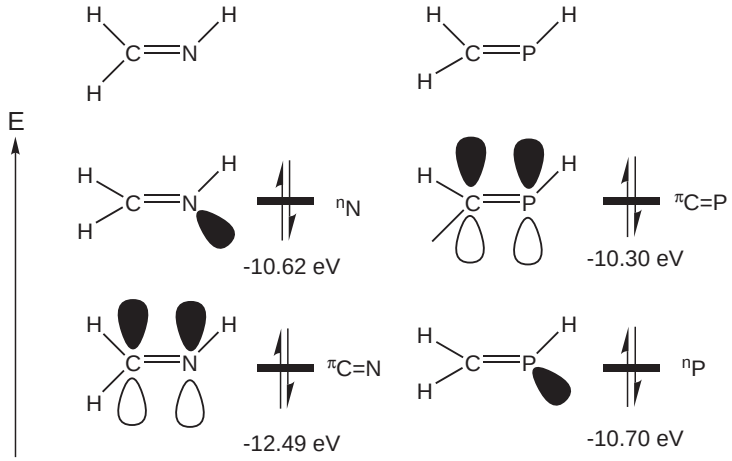

Figure V-10: Highest occupied molecular orbitals of imine and phosphaethylene as described by Lacombe *et al.*.[28]

The first example of a phosphaalkyne, HC≡P was reported by Gier in 1961. It was obtained among other products of the reaction of PH_3 in the middle of graphite electrodes, but it was highly unstable.[29] In these systems, the two degenerate π-orbitals are far above the sp hybridised P lone pair, suggesting that the lone pair will be almost inert and that most of the reactions will take place at the triple bond.[1] As a result of the small HOMO-LUMO gap, phosphaalkynes are both better electron donors and better electron acceptors compared to the all-carbon species.

Another category of multiple bonded phosphorus compounds, the aromatic C/P systems, can be divided in two categories: the phosphinines and the phospholes. Phosphinines have one or more P fragment replacing the CH fragment in a benzene ring. The phospholes are based on a cyclopentadiene ring, where one or more of the CH fragments has been replaced by phosphorus. Phosphinine, C_5H_5P is structurally very similar to benzene: C-C bond lengths in phosphinines, 1.38-1.41 Å can be com-

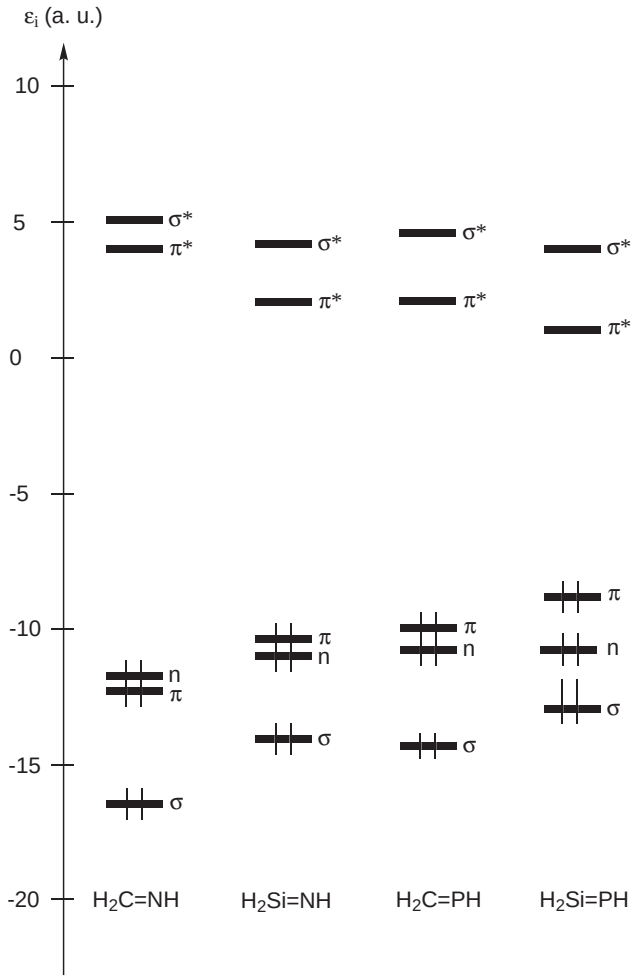

Figure V-11: Comparison of the HOMOs and LUMOs for structurally close double bonded systems.

pared to those in benzene, 1.395 Å. C_5H_5P also has a planar ring.[30,31] However, the resonance energy of phosphinine has been estimated to be only 88% of that of benzene.[31] In phosphinine, the P lone pair is rather stable (it is the HOMO-3),[32] but the π system acts as a good π-acceptor ligand due to the stabilised LUMO.[33] Again here, the phosphorus electronegativity has an important impact on the system: Mulliken population analysis shows that phosphorus carries a positive charge whereas the carbon ring is negatively charged (contrary to benzene where all carbons are positively charged).[34]

Different isomers of phosphinine, diphosphinine, triphosphinine and hexaphosphinine have been studied by Narahari Sastry,[35] Hiberty,[36] Hofmann[37] and Nagase[38]

and their co-workers (Figure V-12). In table V-2 the results of their calculations are presented. The energies are an average of the values obtained for the different possible conformations for each isomer (depending on the number of phosphorus atoms in the compound this can range from 1 to 26 for a given isomer). The most stable isomer for the phosphinines, diphosphinines and triphosphinines is also the planar structure (**B**) but for the hexaphosphinines species the benzvalene structure, **V**, is preferred.

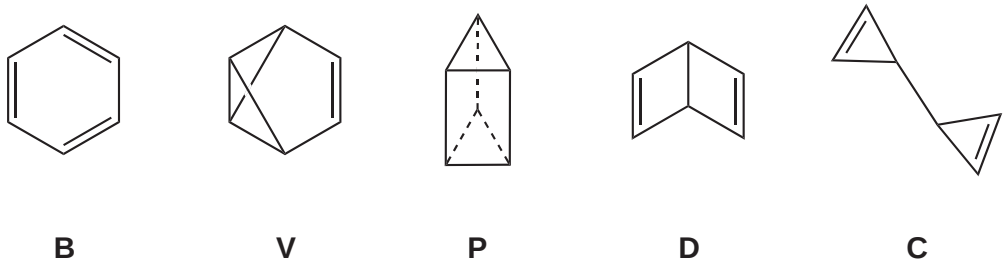

Figure V-12: Potential isomeric structures for benzene and phosphinine structures: Benzene (**B**), Benzvalene (**V**), Prismane (**P**), Dewar benzene (**D**) and Bicyclopropenyl (**C**).[35]

	Relative energies (kcal/mol)*				
Isomers	Phosphinines†,[35]	Diphos.†,[36]	Triphos.†,[37]	Hexaphos.‡,[39]	Benzene†,[39]
B	**0**	**0**	**0**	30.9	**0**
V	52.07	36.31	18.6	**0**	75
D	61.0	47.85	33.03	18.0	81
P	87.4	63.17	39.47	6.5	118
C	103.3	81.6	57.02	20.6	126

* the values are an average of the values reported for each conformation for each isomer
† functional: MP2, basis set: 6-31G*
‡ functional: SCF, basis set: 6-31G*

Table V-2: Stability comparison between the different potential isomer for phosphinines and benzene species.

The phospholes are the equivalent of cyclopentadiene structures with one or more P replacing one or more of the original CH fragments. Contrary to phosphinine, only two different conformations have been considered for phospholes, the planar and the pyramidal structure. Indeed, it has been shown experimentally by Mislow and Quin

and their respective co-workers that the structure of phospholes is pyramidal (see Figure V-13).[40,41] However, this trend only applies to phospholes containing from one to four P. For pentaphosphole, P_5H, the more stable conformation becomes the planar geometry as we will see in the following paragraphs.

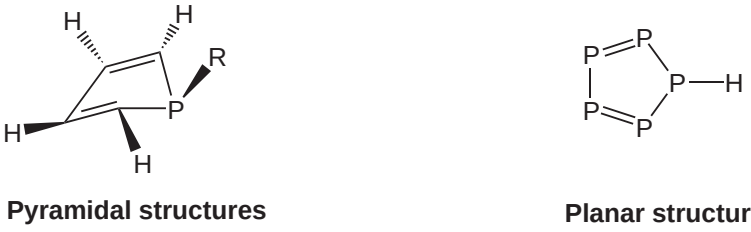

Figure V-13: The pyramidal and planar phosphole conformations (R= $CH_2(C_6H_5)$[40] or $CH(CH_3)_2$[41,42]).

Nyulászi and co-workers have shown that increasing the number of phosphorus atoms in the 5 membered ring forces the ring to become more planar.[43–45] Schleyer *et al.* have confirmed this tendency by showing that unlike phosphole (C_4H_4PR, $1 \leq n \leq 4$), pentaphosphole (P_5H) is planar.[46] The pyramidalisation of the phosphole has raised questions about the aromaticity of the structure. The presence of aromaticity in pyramidal phosphole can be estimated through the barrier to pyramidal inversion.[42] This inversion barrier is low in phosphole system due to the $(2p\text{-}3p)_\pi$ conjugation (measured experimentally to be 16 kcal/mol) in the transition state.[42] Mislow *et al.* have argued that the low barrier to pyramidal inversion in phospholes is an indication of heteroaromaticity in the planar conformation and that the pyramidal ground state of these systems retain the same aromaticity.[47] Calculations by Nyulászi *et al.* also showed that the ring planarity is directly related to the electronic delocalisation (or aromaticity) and a planar ring is predicted to be strongly aromatic. Moreover, Dransfeld *et al.* have shown that the replacement of $-CH=$ units by $-P=$ in phospholes increases the aromatic character due to the decrease of pyramidality of the tricoordinate phosphorus when more P are present.

In light of the instability of P=C and P=P bonds, it is unsurprising that they tend to rearrange to more stable 3-D structures with a so-called ‘3-D aromaticity”.

In a recent paper, McGrady, Pantazis *et al.* surveyed all possible isomers for the isoelectronic systems $C_5H_5^+ \longrightarrow P_5^+$ and showed that the all-carbon species adopt a planar structure, but the presence of even a single P atom causes a switch to 3-D cluster-like structures.[50] The basis for understanding the structures of such electron-deficient clusters has been put in place by Wade and Mingos.

4 - Theories of cluster bonding

In 1971 Wade established rules to rationalise the electronic structures of main-group clusters.[48] These rules were then further developed by Mingos in 1984 to give the well known "Wade/Mingos" rules that rationalise cluster geometries.[49] The rules were originally developed to predict structures of borane and carborane cluster compounds that adopt deltahedral geometries. Such structures can be classified as *closo*-, *nido*-, *arachno*- or *hypho*-, based on whether they represent a complete deltahedron (*closo*-), or a deltahedron missing one (*nido*-), two (*arachno*-) or three (*hypho*-) vertices (see Figure V-14).

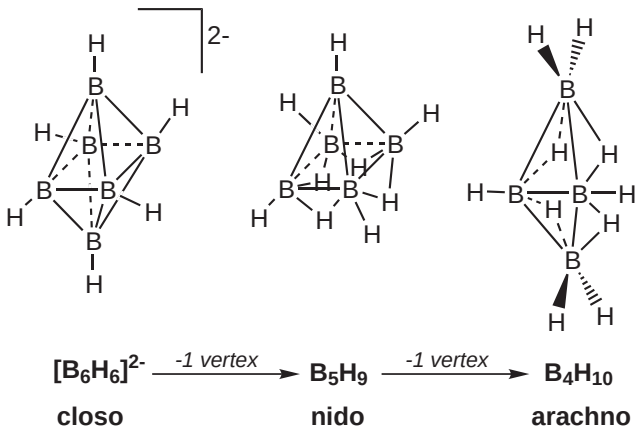

Figure V-14: Borane examples of *closo*, *nido* and *arachno* deltahedra.

Electron counting works in the following way. The total number of valence electrons is established from the configuration of the atoms (for some examples see Figure V-1). Then 2 electrons per vertex are removed to account for radial pairs (i.e. those sticking out of the cluster) which can be lone pairs or C−H or B−H bonds. The remaining electrons can be used to bind the cluster. If there are *n+1*

pairs remaining (n represents the number of vertices) the system adopts a "closo" structure, *n+2* pairs a 'nido" structure, *n+3* pairs an "arachno" structure and *n+4* pairs an "hypho" structure.

These rules can be extended to transition elements by noting the isolobal analogies between main group and transition metal fragments (see Figure V-15).

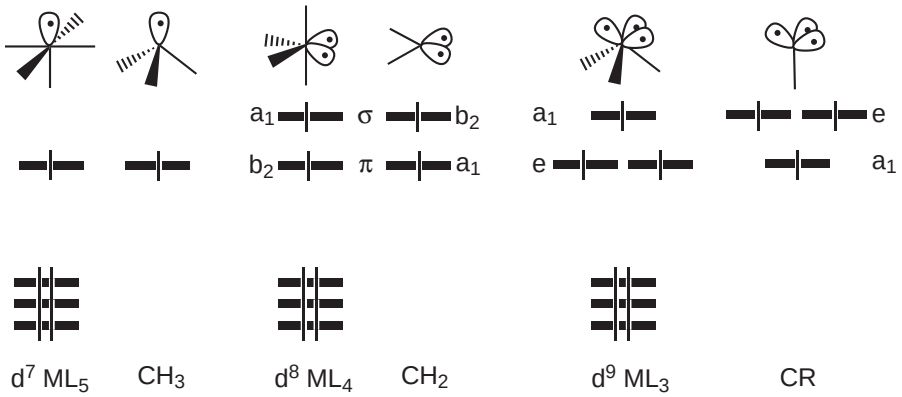

Figure V-15: Isolobality between organic and organometallic fragments.

Results

1 - 2D vs 3D isomerisation in P/C rings

In previous work, McGrady, Russell *et al.* have explained the properties of the cluster $(RC)_2P_3^+$ which adopts a square pyramidal structure with one P atom at the apex.[50] This species is isoelectronic with the cyclopentadienyl cation, $C_5H_5^+$, which instead adopts a planar structure due to the stronger C=C π bonds. A full survey of the possible isomers of $(CH)_xP_{5-x}^+$, x= 1 $\rightarrow$ 5, suggests that the presence of even a single P atom is sufficient to cause a switch to a square pyramidal geometry. In this section we use theory to explore the possibility that planar isomers might be favoured by the addition of substituents on the $P_3(CR)_2^+$ framework. In particular we consider the effect of incorporating the (C-C) unit into an aromatic ring, where the additional delocalisation should disfavour a 3-dimensional structure.

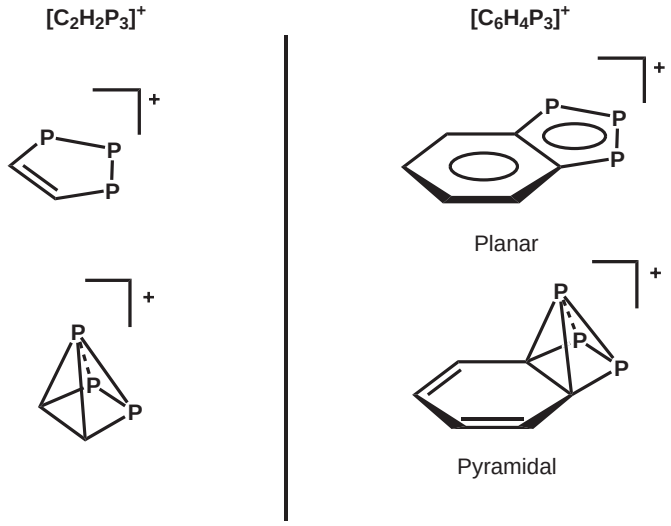

Figure V-16: Pyramidal and planar structure of $[H_2C_2P_3]^+$ and $[C_6H_4P_3]^+$.

1.a - The aim of our work

Following the previous work done on clusters of formula $[C_nH_nP_{5-n}]^+$, the aim of our work was to study the effect of adding a benzene ring to a C_2P_3 cluster. We stud-

ied the interconversion between pyramidal cluster to planar ring, with the aim of assessing how the ring influences the balance between planar and three dimensional structures.

1.b - Validation of methodology

Throughout this project, we use DFT as implemented in the Gaussian 03 software. In both cases we tried different functional and basis set combinations from the commonly used (B3LYP/6-31G*) to more complicated combinations of functionals/basis set. For the CP-cluster case, we decided to focus on B3LYP and PBE1PBE functionals combined with a 6-311G(2df)/6-311G(d) (for P and C/H atoms respectively) basis set. The PBE1PBE/6-311G(2df/d) method has already been proven to describe very well the type of systems studied here as shown in a previous publication from our group.[50] We observe no difference between the structures except for the cluster distortion in B3LYP which will be discussed later.

Results

A potential energy surface describing the interconversion of the planar structure to the three-dimensional form is shown in Figure V-17. Using the PBE1PBE functional we locate two minima for $(C_6H_4)P_3^+$, **A** and **B**. **A** is a planar species with a 5-membered P_3C_2 ring, while **B** is a cluster with a symmetric C_2P_3 square pyramid. The difference of energy between the two is 21 kcal/mol, indicating that the cluster structure remains the most stable, as was the case for $[C_2H_2P_3]^+$. At the same level of theory, the energy difference between planar and cluster forms of $[C_2H_2P_3]^+$ is 41 kcal/mol (the "planar" form in fact being a transition state[50]) indicating that the benzene ring does stabilise structure **A**, by approximately 20 kcal/mol but this is not sufficient to reverse the order of stability. We have also located a transition state connecting **A** and **B** ($\mathbf{TS_{AB}}$), 24 kcal/mol above **A**, where the C_2P_3 adopts

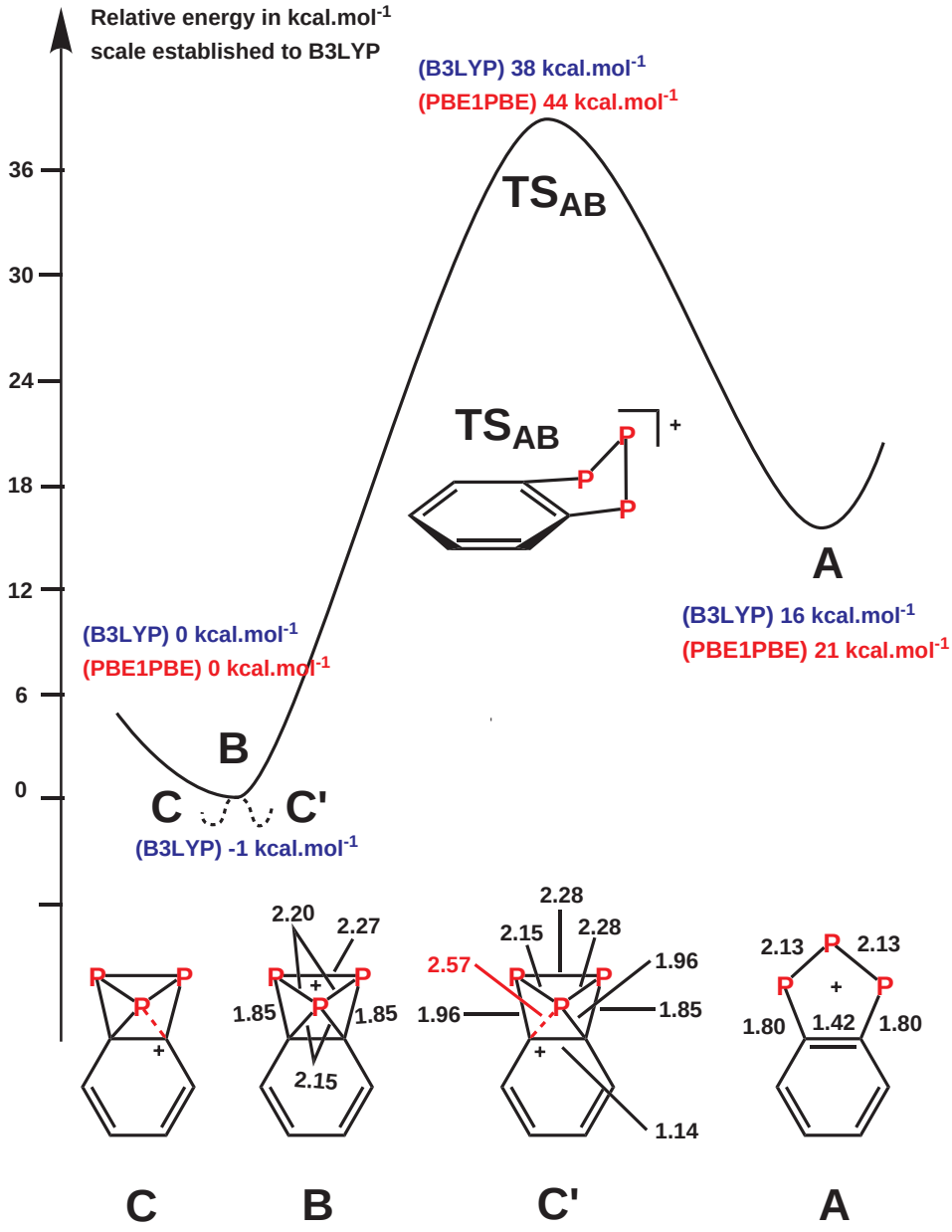

Figure V-17: The total potential energy surface for the isomerisation of $C_6H_4P_3$ (bond length in Å).

an envelope conformation.

For the B3LYP functional, the shape of the potential energy surface is very similar to the PBE1PBE one, with the exception that structure **B**, the square pyramidal cluster, is no longer a minimum, but instead is a transition state with an imaginary frequency at 66 cm^{-1}. This imaginary frequency leads to two enantiomeric isomers, **C** and **C′**, where the $[C_2P_3]^+$ unit is distorted such that one P_{apical}−C bond is longer than the other in the C-P pyramid. These two minima, **C** and **C′**, lie only 1 kcal/mol below **B**, suggesting that the C_2P_3 unit structure will oscillate between the two isomers. The easy distortion of the cluster can be understood by the presence of two resonance forms as shown in Figure V-18, which differ in the distribution of their positive charge. The B3LYP functional clearly favours the localisation of the positive charge on a single carbon centre, causing the observed distortions, while PBE1PBE stabilises a more delocalised charge distribution.

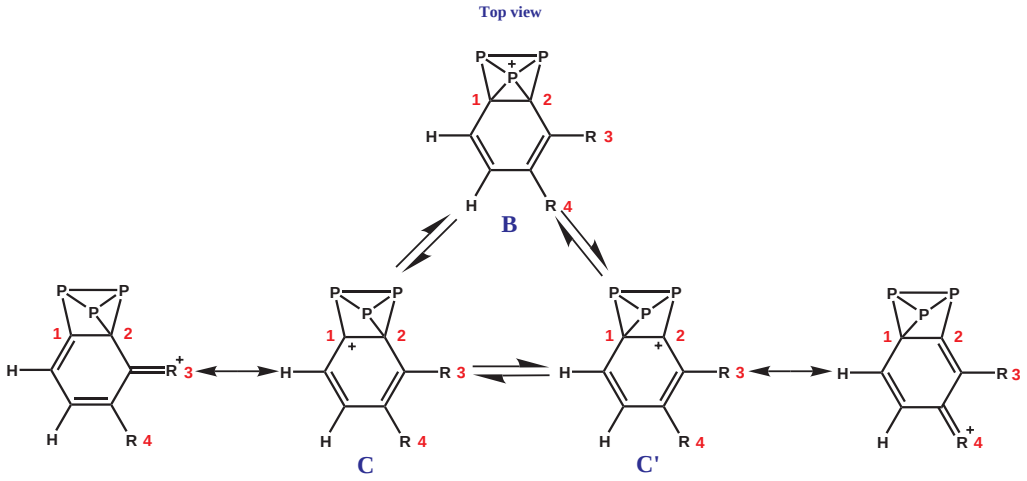

Figure V-18: Distortion mechanism of the original structure, **B** and the potential positions for substituents (position 3 and 4).

1.c - Influence of substitution

The different distribution of positive charge in **B** and **C** suggests that it might be possible to force the structure from one geometry to the other by introducing

substituents on the benzene ring, in either position 3 or 4 (see Figure V-18). We use different substituents; π-electron-donors: F, OH and NH_2 and a π-electron acceptor: NO_2. Calculations have been done using the PBE1PBE functional. For electron-donating substituents, the cluster always adopts a distorted structure, **C** or **C′** (see Figure V-19) regardless of the position of substitution. The positive charge is localised at position 1 (structure **C** Figure V-18) when the substituent occupies the position 3 (adjacent to a C-P bond), whereas the positive charge is localised at position 2 (structure **C'** Figure V-18) when the substituent occupies the position 4. These differences can be understood in terms of contributions from the resonance forms shown in Figure V-18. At this level of theory (PBE1PBE functional) the unsubstituted cluster is undistorted (structure **B**), so the presence of electron donors clearly stabilises the distorted form, where the positive charge is localised on the C_6 ring, relative to the undistorted cluster, where it is localised on P, and also controls the direction of the distortion.

As we observe in Figure V-19, whatever electron-donor substituent is used the bond lengths are quite similar from one species to another (for a substituent in a given position (position 3 or 4)). The only difference is the length of the C_1-P or the C_2-P bonds and consequently the length of C_2-P or C_1-P opposite bonds, respectively. Otherwise, the other bonds don't undergo any change. Compounds with electron-donor substituents in position 3 are the exact image of compounds possessing a substituent in position 4. So the sole effect induced by adding electron-donor substituents on the phenyl ring is the control of the compound symmetry, more precisely the switching (from one side to another) of the C_2P_3 pyramidal fragment.

In contrast, electron-withdrawing groups destabilise the positive charge on the benzene ring (structure **C**), relative to structure **B**, where it is on the phosphorus centre. As a result, the NO_2 substituted species adopts a symmetric cluster structure, **B**, regardless of the position of substitution. This is shown by the equivalence of the C-P bond lengths.

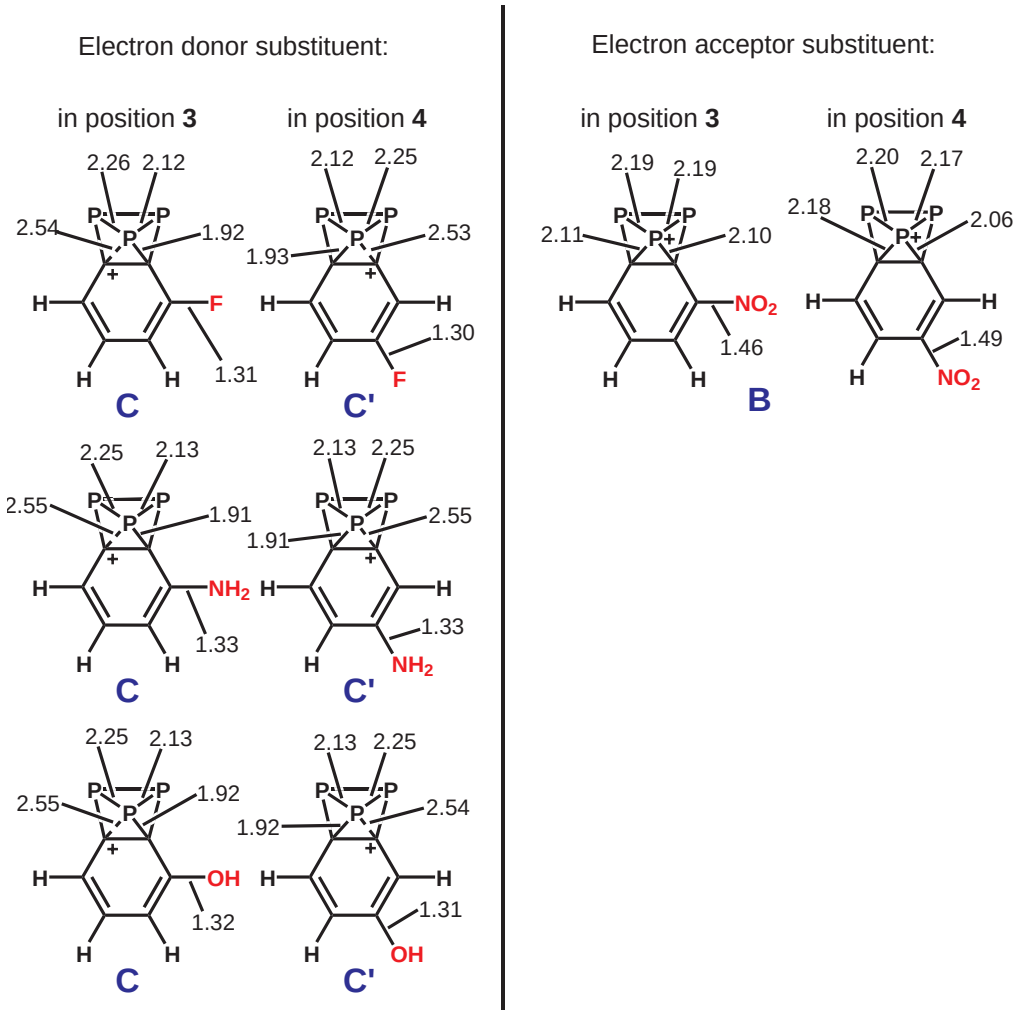

Figure V-19: Optimised structures of substituted species $[R{-}C_6H_3P_3]^+$ (PBE1PBE/6-311G(2df) on P and 6-311G(d) on other).

1.d - Conclusion

We have shown that although the pyramidal structure remains more stable than the planar form in all cases, the presence of benzene ring stabilises the latter by ≈ 20 kcal/mol. When the pyramidal structure is optimised with B3LYP we observe a distortion of the pyramidal cluster away from C_s symmetry. This distortion is also observed in presence of electron donating substituents on the aromatic ring. In contrast, electron-withdrawing substituents favour the symmetric structure. Subtle changes in electronic structure of the framework can therefore exert a significant influence on these species.

2 - Rearrangement of P=P bonds

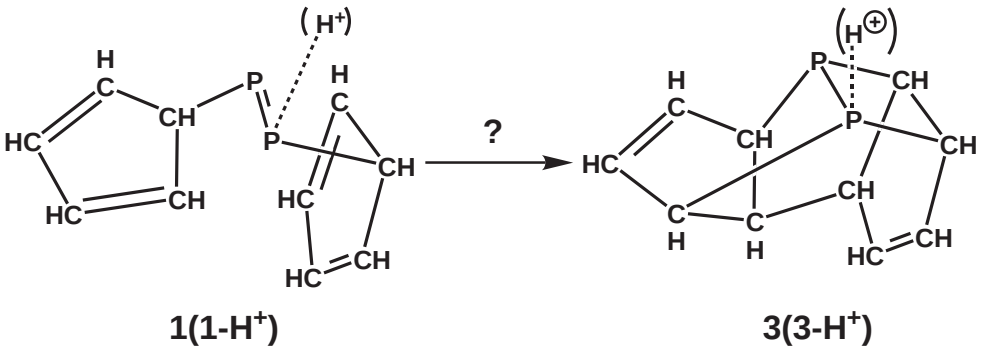

Figure V-20: Conversion of **1** (**1-H**$^+$) into **3** (**3-H**$^+$).

In 1986 Jutzi and co-workers reported a rare example of a stable compound containing a P=P double bond. Experimentally, the system is stabilised by cyclopentadiene substituents at the P centres, but it is not clear whether its stability is kinetic due to the bulk of the substituents, or thermodynamic. More recently, Russell *et al.* have observed that the addition of group 13 halides, InCl or GaI to $C_5Me_5PCl_2$ results in the formation of a diphosphorus cage, $[C_{10}Me_{10}P_2X]^+$, whose core is isomeric to the compound synthesised by Jutzi *et al.*, $C_5Me_5P{=}PC_5Me_5$.[51,52] However, the nature of the bonding in the two cases is different. Previous studies done by Cowley and co-workers[53,54]on the reaction of Inamoto's diphosphene, mes*P=Pmes* (mes* = 2,4,6-tri-*tert*-butylphenyl)[5] (precursor of P-P multiple bonds studies) with HBF_4 leading to the formation of a phosphacycle encouraged Russell *et al.* to study the possible rearrangement of Jutzi's compound by addition of an acid into a cage species (Figure V-20).[55] The rearrangement is clearly a complex one, involving the replacement of one P=P and two C=C π bonds, by two P-C and one C-C σ bonds. In this section, we use DFT to explore the mechanism of this process, and the role of acid in catalysing it. In Figure V-20, and in this whole section, compounds **1** and **3** represent the original planar and cage structures (non protonated) while **1-H**$^+$ and **3-H**$^+$ represent the same structures but protonated on one of the phosphorus. Notation such as **1** + **H**$^+$ represents the original compound in presence of the proton (the proton comes from the triflic acid, CF_3SO_3H) but not protonated.

The aim of our work was to understand why compound **1** is stable in the absence of acid and why when protons are present we observe a rapid rearrangement from **1-H**$^+$ into **3-H**$^+$. Russell and coworkers have proposed the following mechanism (Figure V-21), based on the initial protonation of a phosphorus centre.

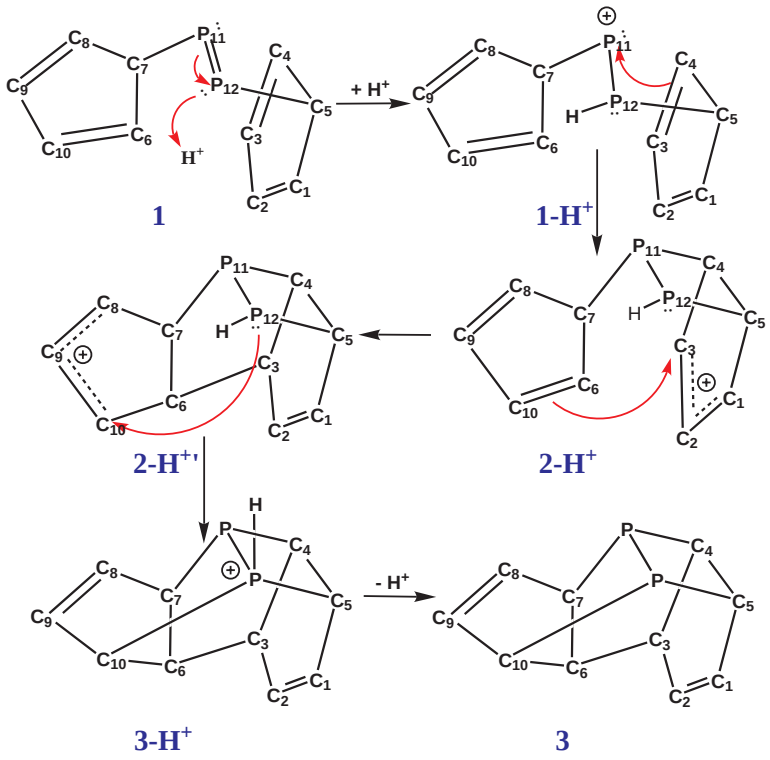

Figure V-21: Mechanism proposed by Russell *et al.*.

The mechanism involves initial attack of the C=C π system on the positive phosphorus centre which leads to the intermediate **2-H**$^+$ which contains an allyl cation. Formation of C_3-C_6 and $C_{10}-P_{12}$ bonds then follow, leading to the protonated product **3-H**$^+$. We use this as a framework for our computational studies.

2.a - Validation of methodology

All calculations in this section were done with the B3LYP functional and a 6-31G* basis set. A simple Cp ring was used instead of Cp* for computational expedience.

Bond	Computation B3LYP/6-31G*	Experiment
$P_{11}-P_{12}$	2.28	2.230(2)
$P_{11}-C_7$	1.94	1.905(6)
$P_{11}-C_4$	1.91	1.933(7)
$P_{12}-C_5$	1.95	1.896(7)
$P_{12}-C_{10}$	1.94	1.888(6)
C_3-C_6	1.54	

Table V-3: Comparison of the bond length (in Å) obtained through computational optimisation with experimental results for compound **3**.

Results

In our initial survey we optimised each of the structures shown in Figure V-21 following the proposed mechanism going from **1** (**1-H**$^+$) to **3** (**3-H**$^+$). Then we searched for transition states between each possible step, and then followed each transition state to confirm the link between minima and transition states. The potential energy surfaces for the reactions with and without protons are shown in Figure V-22. Compound **2** in our calculations is a mix between **2** and **2'** as our calculations show that the formation of bonds C_3-C_6 and $C_{10}-P_{12}$, involved in **2** and **2'**, respectively, happen at the same stage of the rearrangement.

We clearly observe a huge difference between the barriers for the last step showing that when an H^+ is added the reaction is feasible compared to the same system without H^+, where the barrier is 32 kcal/mol. Those results are in agreement with what has been found experimentally, but what is the origin of this difference?

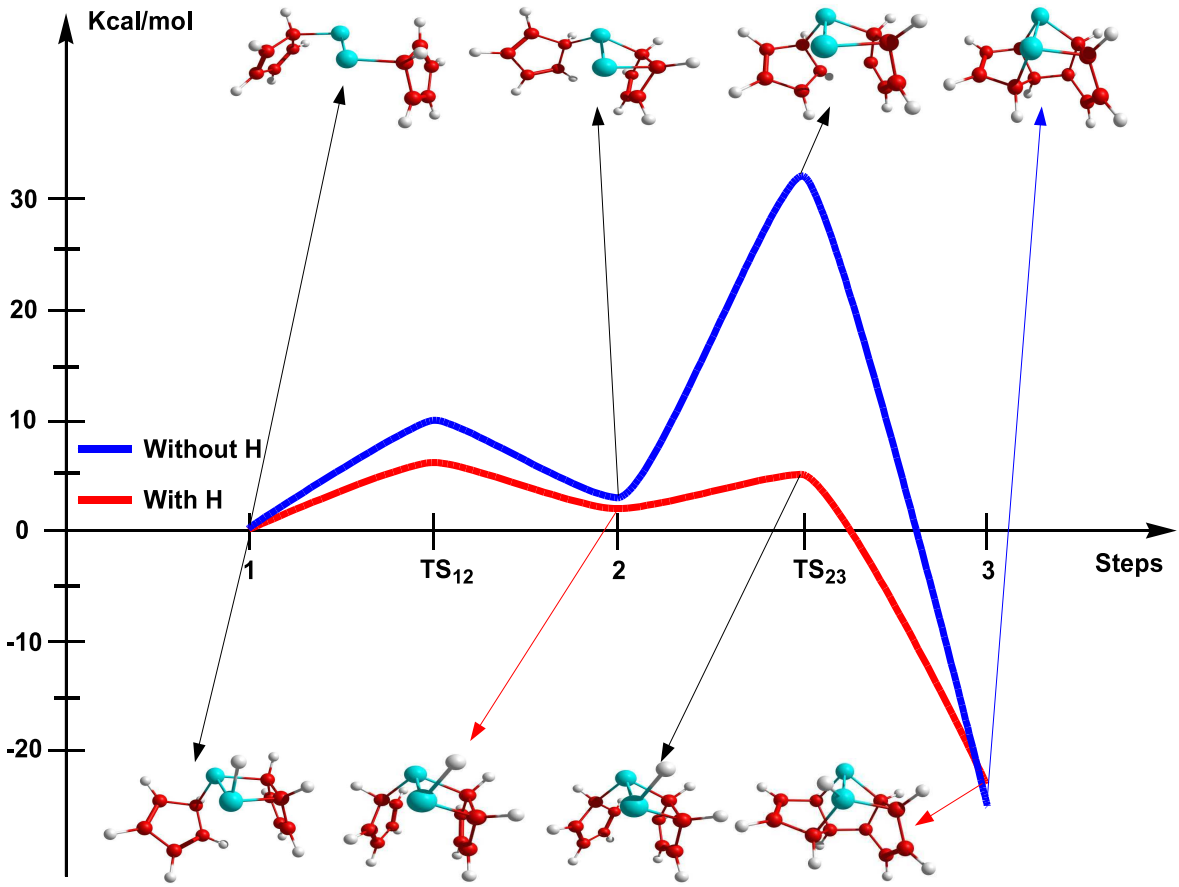

Figure V-22: Potential energy surface of the rearrangement reaction.

2.b - Mechanism in absence of proton

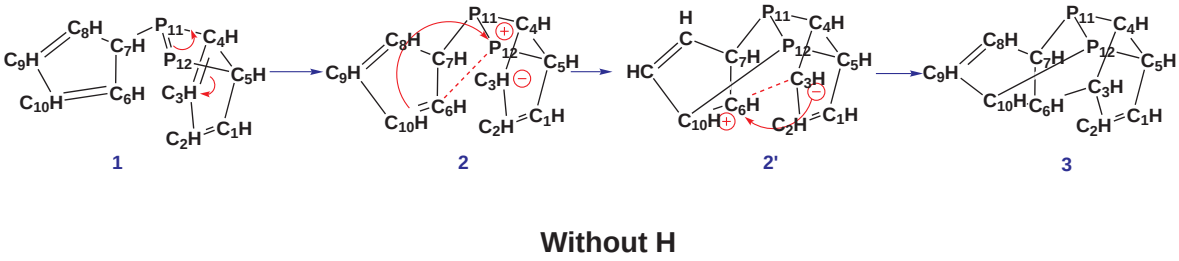

Figure V-23: Proposed mechanism of the potential rearrangement from compound **1** to **3**.

In the initial stage (**1** to **2**), the C_4−P_{11} bond is formed (compound 2), resulting in the formation of an allyl *anion* delocalised on C_1, C_2 and C_3 and a phosphonium cation delocalised on P_{12} (see Figure V-24). In the second step, the C_3−C_6 and C_{10}−P_{12} bonds are formed in a single concerted step (as described from the two step process proposed in Figure V-23). This process can be considered as an attack on the P^+ by the C_6=C_{10} double bond, followed by a nucleophilic attack by the allyl *anion* (localised on C_3) on C_6. The rate-limiting step in the process is clearly the rearrangement from **2** to **3**, with a large barrier of approximately 30 kcal/mol which is consistent with the stability of **1** in the absence of acid. The transition state between compound **2** and **3** ($\mathbf{TS_{23}}$) shows that both C_{10}−P_{12} and C_3−C_6 are significantly formed in $\mathbf{TS_{23}}$, as shown through the bond length evolution in Figure V-25, and this large structural rearrangement clearly causes the high energetic barrier.

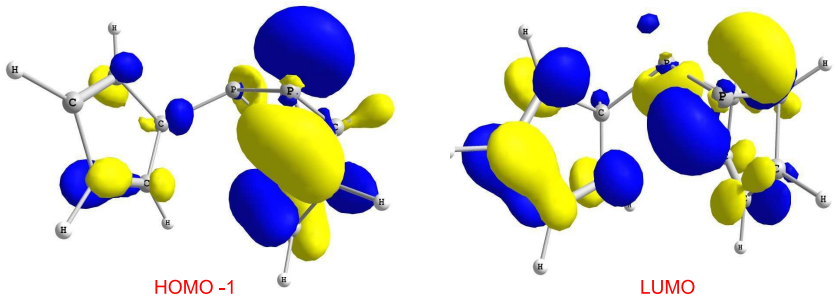

Figure V-24: Representation of the HOMO-1 (C_1, C_2 and C_3 delocalisation) and the LUMO (localisation on the P_{12}) for the compound **2** in absence of H^+.

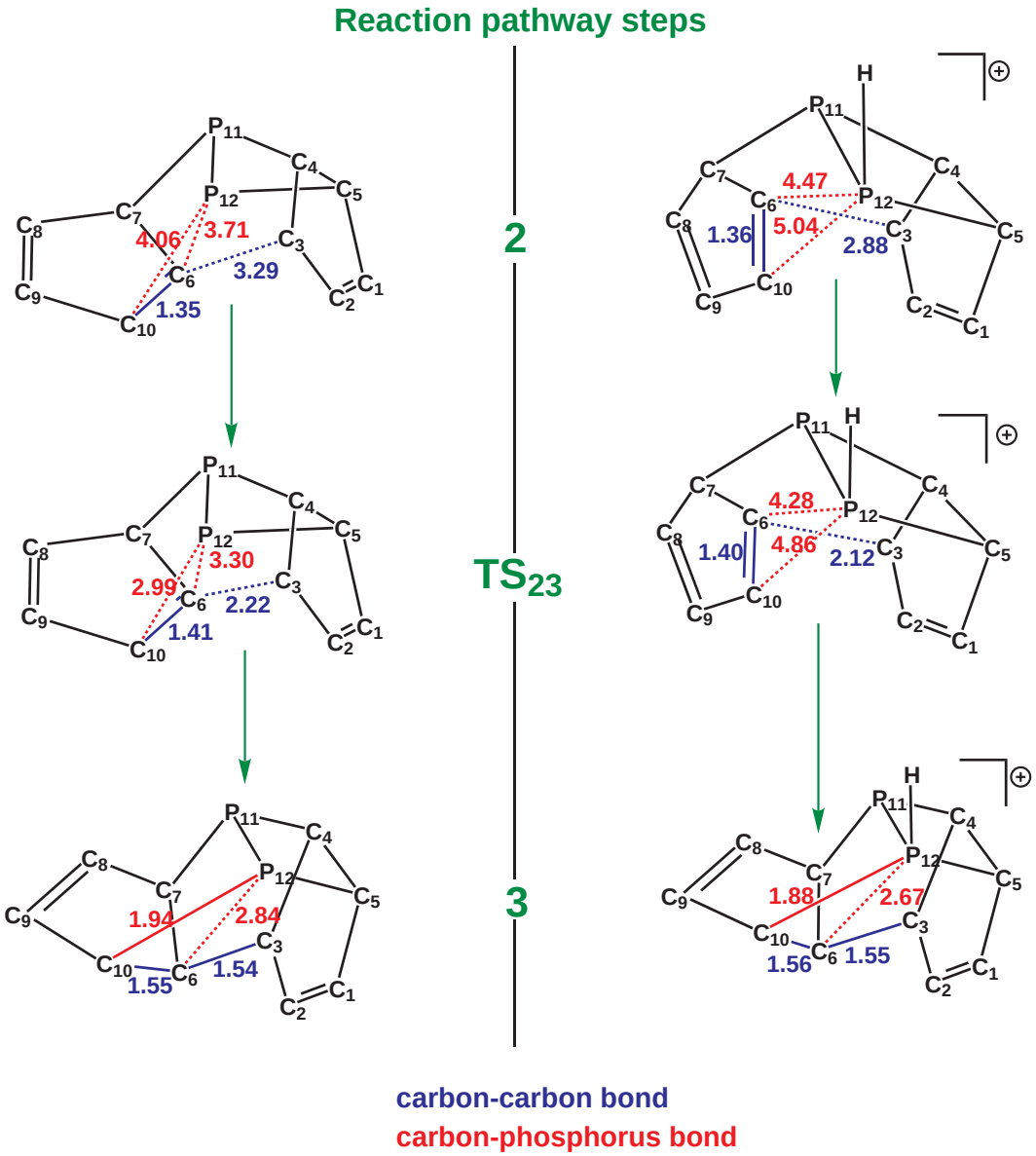

Figure V-25: Evolution of the C_3-C_6 and $C_{10}-P_{12}$ bond lengths during the transition state between **2** and **3**.

2.c - Mechanism in presence of proton

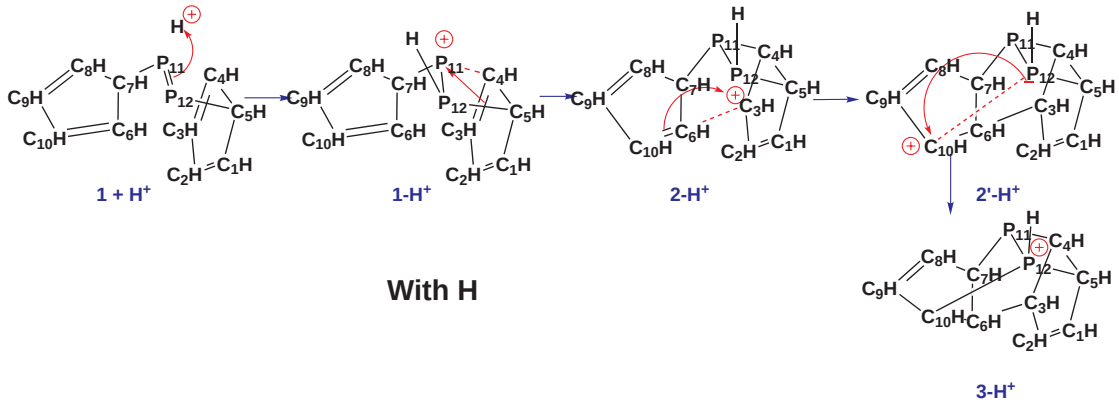

Figure V-26: Possible rearrangement from **1** to **3** deduced from calculations.

The profile in the presence of H^+ is rather different, with a much lower barrier for $\mathbf{TS_{23}}$. This lower barrier is consistent with the rapid reaction of **1** in acidic conditions. The presence of H^+ changes the nature of the electron transfer involved in the different steps. The first step (**1** to **2**) now involves a nucleophilic attack on the P^+ centre, leading to an allyl *cation* (in contrast to the mechanism in the absence of H^+) localised on C_1, C_2 and C_3. The second step (from **2** to **3**) involves a second nucleophilic attack of the C_6=C_{10} double bond on the allyl cation (localised on C_3), followed by P_{12}−C_{10} bond formation (as described in Figure V-26). The critical feature is that at the $\mathbf{TS_{23}}$ step the C_3−C_6 bond is substantially formed, while P_{12}−C_{10} remains very large, and the 2 Cp rings almost parallel (shown through the bond lengths in Figure V-25). The very different nature of the electron redistribution gives a much lower barrier.

2.d - Solvation

In Figure V-27 the solvated (CH_2Cl_2 solvent) and gas phase calculated reaction pathways are represented. All energies along the solvated and gas phase pathways are reported relative to **1** + $\mathbf{CF_3SO_3H}$, which is set to zero.

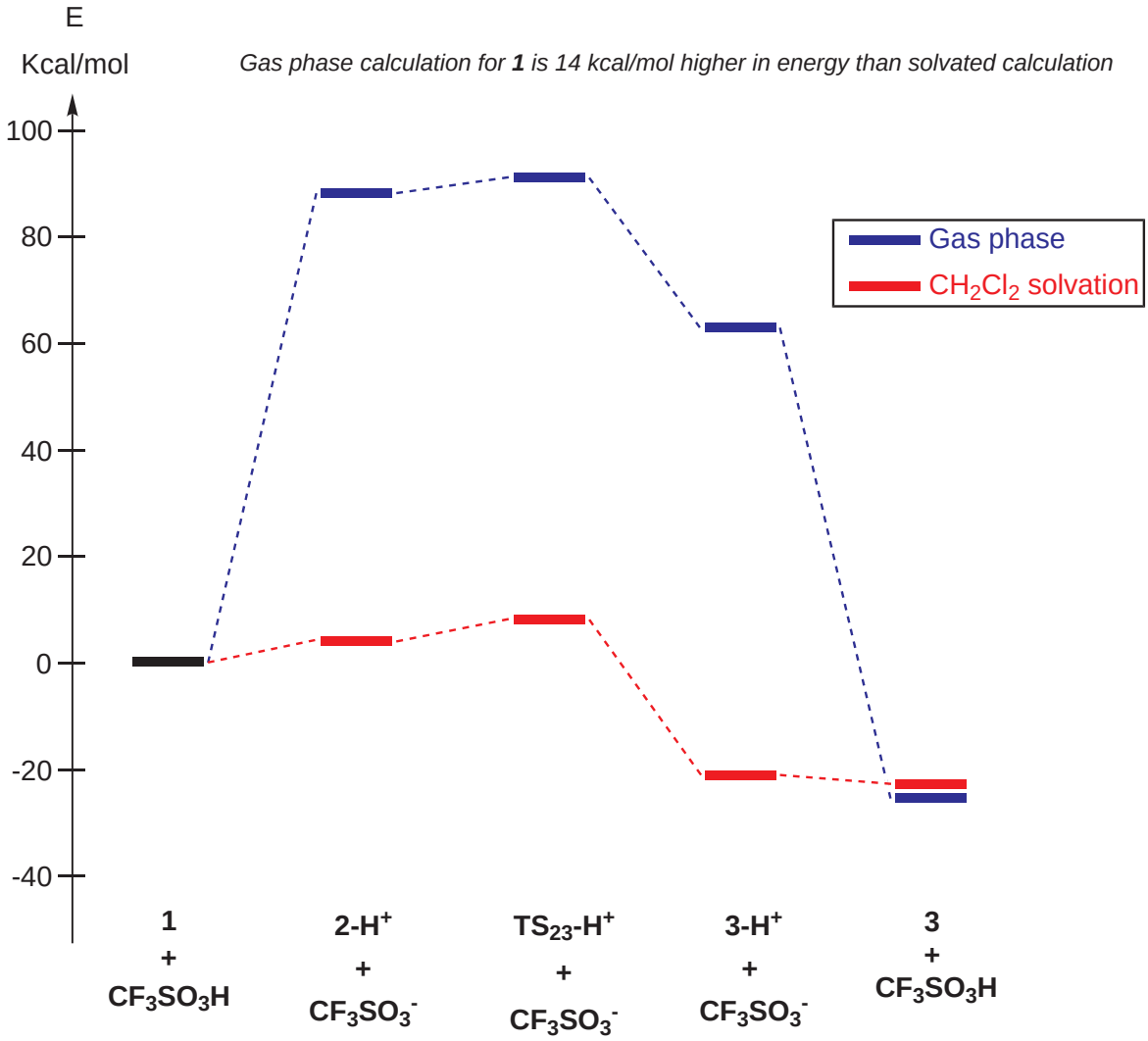

Figure V-27: Comparison between solvated and gas phase pathway including the non-protonated starting and ending compound (Energies are relative to step **1** + $\mathbf{CF_3SO_3H}$).

As we can see the solvation of the protonated forms doesn't change the shape of the pathway from **2-H$^+$ + CF$_3$SO$_3^-$** to **3-H$^+$ + CF$_3$SO$_3^-$**: the energy barrier for the rearrangement is increased only by 1 kcal/mol under solvation. However, we observe a huge reduction of the gap between **1 + CF$_3$SO$_3$H** and **2-H$^+$ + CF$_3$SO$_3^-$** when the species are solvated. This small gap between the non-protonated and the protonated form ($\approx$ 4 kcal/mol) is in better agreement with what have been observed experimentally: the reaction is instantaneous when the acid is inserted in the mix even at low temperature (-78 $^\circ$C).

2.e - Conclusion

Computational chemistry helped us here understand the impact of an hydrogen on a rearrangement pathway. We saw that by adding a proton in the mix the pathway is more or less inverted compared to the hypothetical pathway which was not working. So we found what was making one pathway feasible while the other was impossible. On a minor scale, we also showed that solvation has no effect on the cage rearrangement pathway, but take all its importance when an acid is involved.

Bibliography

[1] Dillon, K. B.; Mathey, F.; Nixon, J. F. *Phosphorus: the carbon copy.* New York Chichester, John Wiley, **1998**.

[2] Mathey, F. *Chem. Rev.*, **1992**, *92*, 1839.

[3] Guselnikov, L. E.; Nametkin, N. S. *Chem. Rev.*, **1979**, *79*, 529.

[4] Jutzi, P. *Angew. Chem. Int. Ed. Engl.*, **1975**, *14*, 232.

[5] Yoshifuji, M.; Shima, I.; Inamoto, N.; Hirotsu, K.; Higuchi, T. *J. Am. Chem. Soc.*, **1981**, *103*, 4587.

[6] Power, P. P. *J. Chem. Soc., Dalton Trans.*, **1998**, 2939.

[7] Power, P. P. *Chem. Rev.*, **1990**, *99*, 3463.

[8] Dolgonos, G. *Chem. Phys. Lett.*, **2008**, *466*, 11.

[9] Jacobsen, H.; Ziegler, T. *J. Am. Chem. Soc.*, **1994**, *116*, 3667.

[10] Olbrich, G.; Potzinger, P.; Reimann, B.; Walsh, R. *Organometallics*, **1984**, *3*, 1267.

[11] Raabe, G.; Michl, J. *Chem. Rev.*, **1985**, *85*, 419.

[12] Trinquier, G.; Malrieu, J.-P. *J. Am. Chem. Soc.*, **1987**, *109*, 5303.

[13] Power, P. P. *Organometallics*, **2007**, *26*, 4362.

[14] Pignedoli, C.; Curioni, A.; Andreoni, W. *ChemPhysChem*, **2005**, *6*, 1795.

[15] Frenking, G.; Krapp, A.; Nagase, S.; Takagi, N.; Sekiguchi, A. *ChemPhysChem*, **2006**, *7*, 799.

[16] Schmidt, M. W.; Gordon, M. S.; Dupuis, M. *J. Am. Chem. Soc.*, **1985**, *107*, 2585.

[17] Ahlrichs, R.; Heinzmann, R. *J. Am. Chem. Soc.*, **1977**, *99*, 7452.

[18] Dobbs, K. D.; Hehre, W. J. *Organometallics*, **1986**, *5*, 2057.

[19] Schmidt, M. W.; Gordon, M. S. *Inorg. Chem.*, **1986**, *25*, 248.

[20] Yoshifuji, M.; Hashida, T.; Inamoto, N.; Hirotsu, K.; Horiuchi, T.; Higuchi, T.; Ito, K.; Nagase, S. *Angew. Chem. Int. Ed. Engl.*, **1985**, *24*, 211.

[21] Allen, T.; Schneier, A. C.; Yamaguchi, Y.; Schaefer III, H. F. *Chem. Phys. Lett.*, **1985**, *121*, 154.

[22] Nagase, S.; Suzuki, S.; Kurakake, T. *J. Chem. Soc., Chem. Commun.*, **1990**, 1724.

[23] Douglas, J. E.; Rabinovitch, B. S.; Looney, F. S. *J. Chem. Phys.*, **1955**, *23*, 315.

[24] Nagase, S.; Ito, K. *Chem. Phys. Lett.*, **1986**, *126*, 531.

[25] Galasso, V. *Chem. Phys.*, **1984**, *83*, 407.

[26] Elbel, S.; Ellis, A.; Niecke, E.; Egsgaard, H.; Carlsen, L. *J. Chem. Soc., Dalton Trans.*, **1985**, 879.

[27] von Ragué Schleyer, P.; Kost, D. *J. Am. Chem. Soc.*, **1988**, *110*, 2105.

[28] Lacombe, S.; Gonbeau, D.; Cabioch, J.-L.; Pellerin, B.; Denis, J.-M.; Pfister-Guillouzo, G. *J. Am. Chem. Soc.*, **1988**, *110*, 6964.

[29] Gier, T. E. *J. Am. Chem. Soc.*, **1961**, *83*, 1769.

[30] Wong, T. C.; Bartell, L. S. *J. Chem. Phys.*, **1974**, *61*, 2840.

[31] Jonas, V.; Frenking, G. *Chem Phys. Lett.*, **1993**, *210*, 211.

[32] Oehling, H.; Schweig, A. *Phosphorus*, **1971**, *1*, 203.

[33] Waluk, J.; Klein, H.-P.; Ashe III, A. J.; Michl, J. *Organometallics*, **1989**, *8*, 2804.

[34] Nyulászi, L.; Keglevich, G. *Heteroatom Chem.*, **1994**, *5*, 131.

[35] Deva Priyakumar, U.; Dinadayalane, T. C.; Narahari Sastry, G. *Chem. Phys. Lett.*, **2001**, *336*, 343.

[36] Colombet, L.; Volatron, F.; Matre, P.; Hiberty, P. C. *J. Am. Chem. Soc.*, **1999**, *121*, 4215.

[37] Hofmann, M.; von Ragué Schleyer, P.; Regitz, M. *Eur. J. Org. Chem.*, **1999**, 3291.

[38] Nagase, S.; Ito, K. *Chem. Phys. Lett.*, **1986**, *126*, 43.

[39] Warren, D. S.; Gimarc, B. M. *J. Am. Chem. Soc.*, **1992**, *114*, 5378.

[40] Coggon, P.; Engel, J. F.; McPhail, A. T.; Quin, L. D. *J. Am. Chem. Soc.*, **1970**, *92*, 5779.

[41] Egan, W.; Tang, R.; Zon, G.; Mislow, K. *J. Am. Chem. Soc.*, **1970**, *92*, 1442.

[42] Rauk, A.; Allen, L. C.; Mislow, K. *Angew. Chem. Int. Ed. Engl.*, **1970**, *9*, 400.

[43] Nyulászi, L.; Várnai, P.; Veszprémi, T. *J. Mol. Struct.*, **1995**, *358*, 55.

[44] Nyulászi, L. *J. Phys. Chem.*, **1995**, *99*, 586.

[45] Nyulászi, L. *J. Phys. Chem.*, **1996**, *100*, 6194.

[46] Glukhovtsev, M. N.; Dransfeld, A.; von Ragué Schleyer, P. *J. Phys. Chem.*, **1996**, *100*, 13447.

[47] Andose, J. D.; Rauk, A.; Mislow, K. *J. Am. Chem. Soc.*, **1974**, *96*, 6904.

[48] Wade, K. *Chem. Comm.*, **1971**, *549*, 792.

[49] Mingos, D. M. P. *Acc. Chem. Res.*, **1984**, *17*, 311.

[50] Pantazis, D. A.; McGrady, J. E.; Lynam, J. M.; Russell, C. A.; Green, M. *Dalton Trans.*, **2004**, 2080.

[51] Jutzi, P.; Wippermann, T. *J. Organomet. Chem.*, **1985**, *287*, C5.

[52] Jutzi, P.; Meyer, U.; Krebs, B.; Dartmann, M. *Angew. Chem. Int. Ed. Eng.*, **1986**, *25*, 919.

[53] Cowley, A. H.; Kilduff, J. E.; Norman, N. C.; Pakulski, M.; Atwood, J. L.; Hunter, W. E. *J. Am. Chem. Soc.*, **1983**, *105*, 4845.

[54] Cowley, A. H.; Kilduff, J. E.; Norman, N. C.; Pakulski, M. *J. Chem. Soc., Dalton Trans.*, **1986**, 1801.

[55] Presly, O. C.; Davin, T. J.; Green, M.; Kilby, R. J.; Mansell, S. M.; McGrady, J. E.; Russell, C. A. *Eur. J. Inorg. Chem.*, **2008**, 4511.

Appendix: Publications submitted up to this date

Electrochemical and theoretical investigations of the reduction of $[Fe_2(CO)_5L\{\mu\text{-}SCH_2XCH_2S\}]$ complexes related to [FeFe] hydrogenase†

Jean-François Capon,[a] Salah Ezzaher,[a] Frédéric Gloaguen,[a] François Y. Pétillon,[a] Philippe Schollhammer,[a] Jean Talarmin,*[a] Thomas J. Davin,[b] John E. McGrady*[b] and Kenneth W. Muir[b]

Received (in Montpellier, France) 19th June 2007, Accepted 18th July 2007
First published as an Advance Article on the web 17th August 2007
DOI: 10.1039/b709273c

The complexes $[Fe_2(CO)_6\{\mu\text{-}SCH_2N(R)CH_2S\}]$ (R = $CH_2CH_2OCH_3$, **1a**; R = ^{i}Pr, **1b**) and $[Fe_2(CO)_6(\mu\text{-pdt})]$ **2** (pdt = $S(CH_2)_3S$) are structural analogues of the $[2Fe]_H$ subsite of $[FeFe]H_2$ases. Electrochemical investigation of **1** and **2** in MeCN–$[NBu_4][PF_6]$ under Ar and under CO has demonstrated that the reduction can be resolved into two one-electron transfer steps by using fast scan cyclic voltammetry. At slow scan rates the reduction of **1** tends towards a two-electron process owing to the fast disproportionation of the anion, while the two-electron reduction of **2** is clearly favoured in the presence of CO. Substitution of a CO ligand in **2** by a N-heterocyclic carbene results in the destabilisation of the anion. Thus, in MeCN–, thf- or CH_2Cl_2–$[NBu_4][PF_6]$, the electrochemical reduction of $Fe_2(CO)_5L_{NHC}(\mu\text{-pdt})]$ **3** (L_{NHC} = 1,3-bis(methyl)-imidazol-2-ylidene, **3a**; 1,3-bis(2,4,6-trimethylphenyl)-imidazol-2-ylidene, **3b**) occurs in a single-step, two-electron process at moderate scan rates; under appropriate conditions this process can be separated into two one-electron steps. Density Functional Theory calculations successfully rationalize the effects of the S-to-S linkage on the electrochemistry of the complexes.

1. Introduction

The structural characterization of the functional centre of iron-only hydrogenase,[1] the H-cluster (Scheme 1), has led to a renewed interest in diiron dithiolate complexes of general formula $[Fe_2(CO)_{6-n}(L)_n(\mu\text{-}SR)_2]$[2] because of their resemblance to the organometallic [2Fe] sub-site of the H-cluster that catalyses the $2H^+ + 2e \leftrightarrow H_2$ reaction.

Most of the recently published work concerns {2Fe2S} or {2Fe3S} species that are either all-CO or substituted derivatives with cyanide, phosphine, isocyanide, or N-heterocyclic carbene ligands (NHC); they may also differ in the nature of the bridging atoms (S or P) and the link between them.[2–15] Electrochemical studies have focused on the reduction of the $[Fe_2(CO)_{6-n}(L)_n(\mu\text{-dithiolate})]$ complexes in acidic media. Little, however, is known at this stage about their intrinsic electrochemical properties,[4a,6,7a,15] but the nature of the S-to-S link seems to play a key role in controlling the electron transfer processes. For the all-CO complexes, the μ-sdt derivative (sdt = sulfurdithiolate, SCH_2SCH_2S) reduces through the transfer of two electrons (*i.e.* two reversible one-electron steps with $E_2^\circ - E_1^\circ > 0$)[15] while conflicting results have appeared concerning the reduction of the μ-pdt analogue (pdt = propanedithiolate, $S(CH_2)_3S$) which has been assigned as either a one-electron (Fe^I–$Fe^I \rightarrow Fe^I$–Fe^0)[3a,16] or a two-electron process.[17,18] Recent reports indicate that one electron is involved on the short cyclic voltammetric timescale while bulk electrolysis under CO consumes two electrons per molecule.[4a,6b] Similar ambiguity surrounds the electrochemistry of the closely related complex $[Fe_2(CO)_6(\mu\text{-}SCH_2C_6H_4CH_2S)]$, which may involve either one[3a] or two electrons.[7a] The nature of the dithiolate bridge also seems to affect the reversibility of the electrode processes: while the reduction of $[Fe_2(CO)_6(\mu\text{-sdt})]$ is reversible[15] and that of $[Fe_2(CO)_6(\mu\text{-pdt})]$ partially reversible,[3a,4a,18] the one-electron reduction of $[Fe_2(CO)_6(\mu\text{-adt})]$ (adt = azadithiolate, $SCH_2N(R)CH_2S$; R = C_6H_4Br,[8a] $C_6H_4NH_2$ [8b]) is apparently irreversible.

In addition to the intrinsic interest in resolving these questions, deeper understanding of the effects of specific changes in the coordination sphere of the metal centres on the electrochemistry of dinuclear thiolate-bridged complexes would facilitate the design of more efficient catalysts. Here we focus

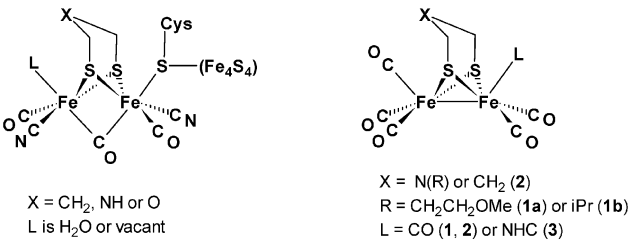

Scheme 1 Schematic representations of the H-cluster of [FeFe] hydrogenases (left) and of the model complexes **1–3** (right).

[a] *UMR CNRS 6521 « Chimie, Electrochimie Moléculaires et Chimie Analytique », UFR Sciences et Techniques, Université de Bretagne Occidentale, CS 93837, 29238 Brest-Cedex 3, France. E-mail: jean.talarmin@univ-brest.fr*
[b] *WestCHEM, Department of Chemistry, University of Glasgow, Glasgow, UK G12 8QQ*

† Electronic supplementary information (ESI) available: Cyclic voltammograms (Fig. S1, S3–S6), scan rate dependence of the current function for **2** (Fig. S2), average lengths and angles (Table S1) and cartesian coordinates and total energies (Table S2) and NR conformations (Fig. S7). See DOI: 10.1039/b709273c

on the primary reduction of $[Fe_2(CO)_{6-n}(L)_n(\mu\text{-SRS})]$ complexes under either argon or CO in an attempt to assess the effects of different constituents on the mechanism of electrochemical reduction. To this end we compare the electrochemistry of $[Fe_2(CO)_6\{\mu\text{-}SCH_2N(R)CH_2S\}]$ (R = $CH_2CH_2OCH_3$, **1a**; R = ^{i}Pr , **1b**) with that of $[Fe_2(CO)_6(\mu\text{-pdt})]$ **2** (Scheme 1) under the same experimental conditions to examine the effects of the S-to-S linkage. The CH_2CH_2OMe arm in **1a** has been designed to mimic the presence of solvent, which may bind to the metal centre at various stages in the electrochemical cycle, thereby protecting any vacant coordination site generated by cleavage of Fe–Fe or Fe–CO bonds. We also reinvestigate the reduction of $[Fe_2(CO)_5(L_{NHC})(\mu\text{-pdt})]$ where L_{NHC} is the N-heterocyclic carbene ligand 1,3-bis(methyl)-imidazol-2-ylidene, **3a**, which we previously assigned as a one-electron process[7b] in contrast to the report on the two-electron reduction of the analogue with L_{NHC} = 1,3-bis(2,4,6-trimethylphenyl)-imidazol-2-ylidene, **3b**.[3f] Comparison of the reduction mechanisms of **2** and **3** provides important information regarding the effects of substituting a CO by an electron-releasing NHC ligand. In all three systems, **1–3**, we show that the electrochemical reduction can be split into two separate one-electron steps under appropriate cyclic voltammetric conditions.

Density functional theory has proved very useful in exploring the electronic structure of hydrogenase and its mimics, and also the intimate mechanism of hydrogen formation.[3–6,19–26] We therefore also report a complementary computational study which explores possible candidates for the various redox events observed in the cyclic voltammograms.

2. Results and discussion

2.1 Synthesis of $[Fe_2(CO)_6\{\mu\text{-}SCH_2N(R)CH_2S\}]$ (R = $CH_2CH_2OCH_3$, 1a; R = ^{i}Pr, 1b) and X-ray crystal structure of 1a

Complexes **1a** and **1b** were obtained by treatment of $[Fe_2(CO)_6(\mu\text{-S})_2]^{2-}$ with *N*,*N*-di(chloromethyl)-2-methoxyethylamine or *N*,*N*-di(chloromethyl)-2-isopropylamine, respectively, following a known procedure[5a,c] (Experimental). We note that the synthesis of a close analogue of **1a** has appeared during the course of our work.[9b] The formulation of **1a** as a bis(μ-thiolato) complex was confirmed by X-ray analysis of a single crystal obtained from hexane–dichloromethane solution. This reveals, as expected, a distorted $S_2(CO)_3$ square-pyramid at each 18-electron iron centre (Fig. 1) and the well-established butterfly structure found in other $[Fe_2(CO)_6\{\mu\text{-}SCH_2N(R)CH_2S\}]$ diiron complexes. Distances and angles in **1a** are unexceptional: for example, the Fe–Fe and mean Fe–S and S–C distances of 2.513(1), 2.249(2) and 1.832(3) Å are barely distinguishable from the corresponding mean values of 2.507, 2.256 and 1.847 Å for all 18 structurally characterised $[Fe_2(CO)_6\{\mu\text{-}SCH_2N(R)CH_2S\}]$ molecules (see Table S1†).[5a,c,d,8a–c,e–g,9a,b,12b,27] The single Fe–Fe bond in **1a** is bridged by both sulfur atoms of the azapropanedithiol ligand, thereby forming boat and chair FeSCNCS rings. Here it is the Fe2–S1–C7–N1–C8–S2 ring which adopts a chair conformation and the methoxyethyl substituent on N1 is in an equatorial position. However, the

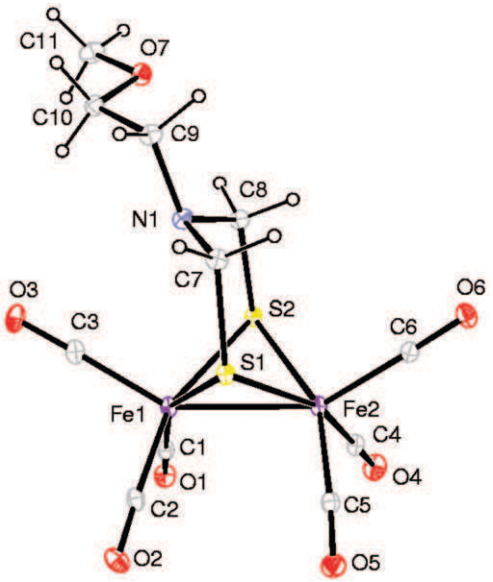

Fig. 1 A view of a molecule of **1a** showing 20% ellipsoids. Selected distances and angles (Å & °): Fe–S 2.245(1)–2.256(1), C7–N1 1.443(2), C8–N1 1.446(2), C9–N1 1.478(2), C7–N1–C8 112.1(2), C7–N1–C9 111.8(1), C8–N1–C9 112.6(1), S1–C7–N1–C9 161.3(1), S2–C8–N1–C9 −161.4(1), Fe2–S1–C7–N1 68.1(1), Fe2–S2–C8–N1 −67.8(1).

N(R) substituent is axial in the closely analogous R = CH_2CH_2OH species.[9b] The N-substituents in $[Fe_2(CO)_6\{\mu\text{-}SCH_2N(R)CH_2S\}]$ complexes show in general almost equal preference for axial and equatorial positions: axial conformations typically have S–CH_2–N–R torsion angles of 83–101° and near trigonal planar coordination at N whereas equatorial conformations are characterised by S–C–N–R torsion angles of 157–168° and more obviously pyramidal nitrogen coordinations (**1a** being typical, see Fig. S7†). DFT calculations suggest that the axial conformer is prefered when R = H but is less stable than the equatorial conformer when R = Me.[9c] The equatorial position of the R = CH_2CH_2OMe substituent in **1a** implies that the nitrogen lone pair points towards Fe1 and the Fe1···N1 and C3···N1 distances [3.279(1) & 3.015(2) Å] seem short. In contrast, the axial H atoms on C7 and C8 do not interact significantly with Fe2 or the C6–O6 carbonyl ligand. The slight (0.03 Å) lengthening of the exocyclic N–CH_2 bond in **1a** relative to the endocyclic N–CH_2 bonds is found in all similar $[Fe_2(CO)_6\{\mu\text{-}SCH_2N(R)CH_2S\}]$ complexes.

We have previously noted that the CH_2CH_2OMe arm was introduced into **1a** in order to mimic possible coordination of a water molecule to a vacant site created by Fe–Fe bond

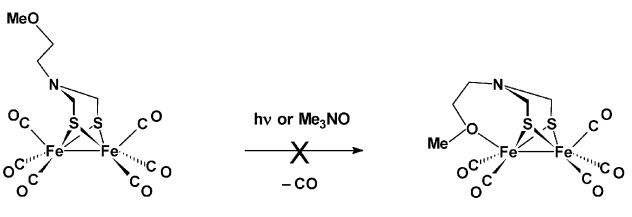

Scheme 2

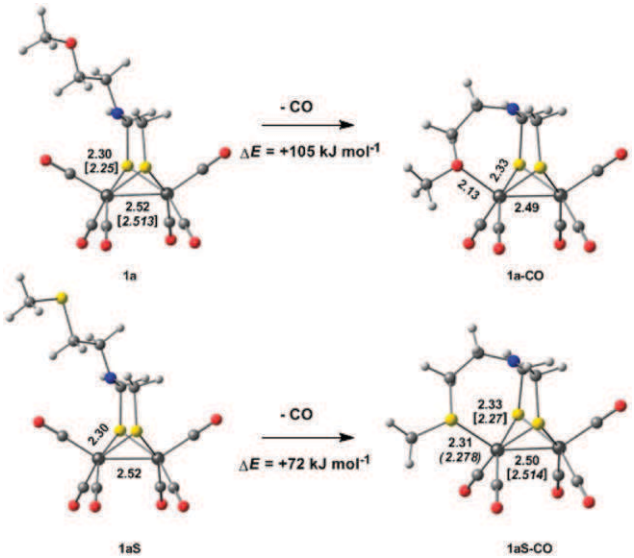

Fig. 2 Optimised structures of **1a** and its decarbonylated derivative, **1a–CO**, along with the thioether analogues (**1S** and **1S–CO**). Crystallographic data for **1a** and **1aS–CO** are given in italics.

cleavage or CO dissociation (Scheme 2). Rauchfuss has described a similar process in the analogue of **1a** with a thioether arm, where CO abstraction using Me_3NO leads to the coordination of the sulphur donor.[5a] However, all attempts to force the coordination of the pendant ether group in **1a** by treatment with Me_3NO, heating in refluxing toluene or irradiation have proved unsuccessful, yielding only a black insoluble material.

The apparent failure of this reaction in the case of **1a** caused us to question whether the weaker electron donating ability of the OMe group relative to SMe was sufficient to prevent coordination to the metal centre. To explore this issue, we used density function theory to probe the energetics of the reaction shown in Scheme 2 for **1a** and its thioether analogue, **1aS**. Structural parameters and total energies of the different species are summarised in Fig. 2. The optimised Fe–Fe bond length in **1a** is in excellent agreement with experiment (2.52 Å *vs.* 2.513(1) Å), as is that in the decarbonylated thioether analogue **1aS–CO** (2.50 Å *vs.* 2.514 Å) which has been crystallographically characterised by Rauchfuss and co-workers.[5a] The loss of CO is endothermic in both cases, but when the subsequent reaction of CO with Me_3NO to form Me_3N + CO_2 ($\Delta E = -320$ kJ mol^{-1} at the same level of theory) is taken into account, it is clear that the relatively minor changes on going from SMe to OMe should not prevent coordination of the pendant arm, at least on thermodynamic grounds. The failure to form the decarbonylated species **1a–CO** shown in Scheme 2 must therefore reflect either an alternative decomposition route or a substantial kinetic barrier to CO loss.

2.2 Electrochemical reduction of the diiron hexacarbonyl dithiolate-bridged complexes $[Fe_2(CO)_6\{\mu\text{-}SCH_2N(R)CH_2S\}]$ (R = $CH_2CH_2OCH_3$, 1a; R = ^{i}Pr, 1b) and $[Fe_2(CO)_6(\mu\text{-pdt})]$, 2 under Ar or CO

2.2.1 Cyclic voltammetry studies. The electrochemical reduction of **1** was investigated by cyclic voltammetry (CV) in MeCN–$[NBu_4][PF_6]$ under Ar and under CO. Complex **2** was examined under the same conditions for comparison. Reproducible CV curves were obtained provided the vitreous carbon disc was polished on a wet felt tissue with alumina. In the present study, this operation was repeated before each individual CV scan.

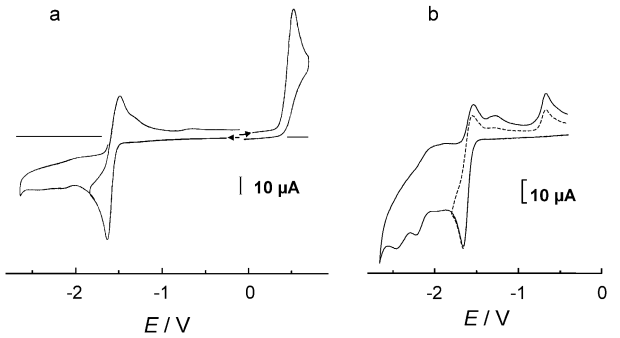

Fig. 3 Cyclic voltammetry of (a) $[Fe_2(CO)_6\{\mu\text{-}SCH_2N(CH_2CH_2OMe)\text{-}CH_2S\}]$ **1a** (0.83 mM) and (b) $[Fe_2(CO)_6\{\mu\text{-}S(CH_2)_3S\}]$ **2** (*ca.* 1.5 mM) under Ar in MeCN–$[NBu_4][PF_6]$ (v = 0.2 V s^{-1}; vitreous carbon electrode; potentials are in V *vs.* Fc^+/Fc).

The CV of **1a** (Fig. 3a, Table 1) shows a partially reversible reduction that is also present at similar potentials in **1b** (Fig. S1†). The partial reversibility of this reduction stands in sharp contrast to recent reports of the irreversible reduction of several analogues of **1**.[8a,b,9b] The reduction of **2** was also found to be partially reversible under Ar at moderate scan rate (Fig. 3b): the peak current ratio $[(i_p^a/i_p^c)^{red1}]$[28,29] increases from 0.5 to 0.7 when the scan rate is increased from 0.1 V s^{-1} to 1 V s^{-1}, in agreement with previous studies of this complex.[18] A comparison of the CVs in Fig. 3 and S1† clearly shows that the reduction of the complexes with an azadithiolate bridge (**1a**, **1b**) is chemically more reversible than that of the propanedithiolate analogue. In all cases the occurrence of follow-up reactions is indicated by the presence of several product peaks at potentials more negative than that for the primary reduction of the complexes and on the return scan. A detailed investigation of the products formed upon reduction of **2** has been published.[4a]

The reduction of **1** and **2** was examined by cyclic voltammetry at scan rates up to 60 V s^{-1} in order to separate the primary electron transfer steps from the ensuing chemistry. The current function $[(i_p^c)^{red1}/v^{1/2}]$ associated with the first reduction of the complexes over the range 0.02 V s^{-1} $\leq v \leq$ 60 V s^{-1} deviates markedly from linearity at slow scan rates (Fig. 4 and Fig. S2†), which demonstrates that the electrode process tends towards a two-electron transfer on the longer time scale. Comparison of the current function measured under Ar and under CO for **1a** and **2** shows that the two-electron pathway is favoured under CO. This was confirmed in the case of complex **2** by comparing its reduction peak current $[i_p^{red1}]$ with the peak current $[(i_p^a)^{ox}]$ of the one-electron oxidation of $[Fe_2Cp_2(CO)_2(\mu\text{-}SMe)_2]$[31–33] present in solution at the same concentration as **2**. The peak current ratio $[i_p^{red1}/(i_p^a)^{ox}]$ decreases from 1.5 (Ar) and ~1.7 (CO) to 1.2 (Ar or CO) upon increasing the scan rate from 0.02 V s^{-1} to 20 V s^{-1}. The effect of CO will be discussed below. Our results are consistent with

Table 1 Redox data[a] of the diiron complexes measured by CV under Ar (vitreous carbon electrode; potentials are in V *vs.* Fc^+/Fc)

Complex[b]	Solvent	v/V s^{-1}	$E_{1/2}^{red1}$/mV	ΔE_p^{red1}/mV	$E_{1/2}^{red2}$/mV	ΔE_p^{red2}/mV
$Fe_2(CO)_6\{\mu\text{-}SCH_2N\{R\}CH_2S\}$ **1a**	MeCN	0.2	−1.56	130	—	—
		40	−1.62	200	−1.60	650
R = CH_2CH_2OMe		60	−1.62	240	−1.61	690
$Fe_2(CO)_6\{\mu\text{-}SCH_2N(R)CH_2S\}$ **1b**	MeCN	0.2	−1.58	155	—	—
		10	−1.64	140	−1.63	410
R = ^{i}Pr		20	−1.65	140	−1.63	490
$Fe_2(CO)_6\{\mu\text{-}S(CH_2)_3S\}$ **2**	MeCN	0.2	−1.60	110	—	—
		20	−1.62	170	−1.80	870
		40	−1.62	230	−1.81	980
$Fe_2(CO)_5{}^1L_{NHC}\{\mu\text{-}S(CH_2)_3S\}$ **3a**	MeCN	0.2	−2.01	60	—	—
		40	−2.1	240	−2.1	590
		60	−2.1	280	−2.1	670
	THF	0.2	−2.16	130	—	—
	CH_2Cl_2	0.2	−2.24 (irr)	—	—	—
$Fe_2(CO)_5{}^2L_{NHC}\{\mu\text{-}S(CH_2)_3S\}$ **3b**	MeCN	0.2	−2.07 (irr)	—	—	—

[a] v, scan rate; ΔE_p, peak separation; irr, irreversible. [b] $^1L_{NHC}$ = 1,3-bis(methyl)-imidazol-2-ylidene; $^2L_{NHC}$ = 1,3-bis(2,4,6-trimethylphenyl)-imidazol-2-ylidene.

previous work on the reduction of complex **2**.[4a,18] However, our conclusion that the electrochemical reduction of **1** is an overall two-electron process at slow scan rate contradicts reports that analogues of **1** undergo one-electron reductions[8,9] under similar experimental conditions (solvent + supporting electrolyte, scan rate) to those used here.

The CV curves obtained for 0.04 V $s^{-1} \leq v \leq$ 40 V s^{-1} under Ar (Fig. 5) demonstrate that two separate one-electron steps can be observed for the reduction of **1** and **2** at fast scan rates (for **1b** see Fig. S3†). CVs of **1a** and **2** recorded under CO but under otherwise identical conditions are shown in Fig. S4.† That the second reduction peak (peak 2, i_p^{red2}, Fig. 5, S3 and S4†) is due to the reduction of the anion to the dianion rather than to formation of a daughter product is demonstrated by the increase of the peak current ratio $[i_p^{red2}/i_p^{red1}]$ upon increasing v. Similarly, the oxidation peak of the dianion (peak 2′, Fig. 5, S3 and S4†) can be separated from that of the anion (peak 1′) at fast scan rates. It should be noted that the oxidation of the dianion takes place at a more positive potential than that of the anion (peaks 2′ and 1′, respectively) so that the latter is thermodynamically unstable at the potential of the oxidation of the dianion. Therefore, the oxidation peak 2′ corresponds to the two-electron oxidation of the dianion, eqn (1) [X = CH_2 or N(R), R = CH_2CH_2OMe or ^{i}Pr].

$$[Fe_2(CO)_6\{\mu\text{-}SCH_2XCH_2S\}]^{2-} - 2e \rightarrow [Fe_2(CO)_6\{\mu\text{-}SCH_2XCH_2S\}] \quad (1)$$

To the best of our knowledge, this is the first time that the two one-electron reduction steps of $[Fe_2(CO)_6(\mu\text{-dithiolate})]$ compounds have been clearly separated. Very detailed analyses of electrochemical kinetic discrimination of the successive one-electron steps of an overall two-electron process (EE) have

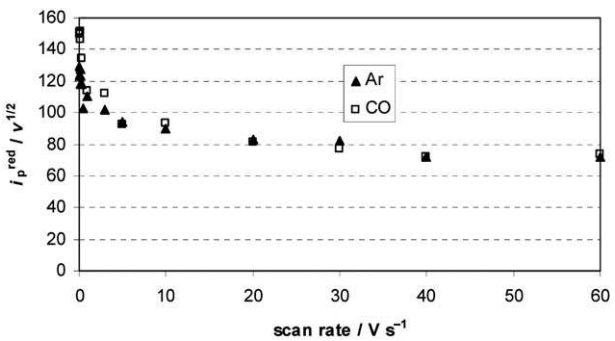

Fig. 4 Scan rate dependence of the current function for the reduction of $[Fe_2(CO)_6\{\mu\text{-}SCH_2N(CH_2CH_2OMe)CH_2S\}]$ **1a** (1.3 mM) under Ar and under CO in MeCN–$[NBu_4][PF_6]$ (vitreous carbon electrode).

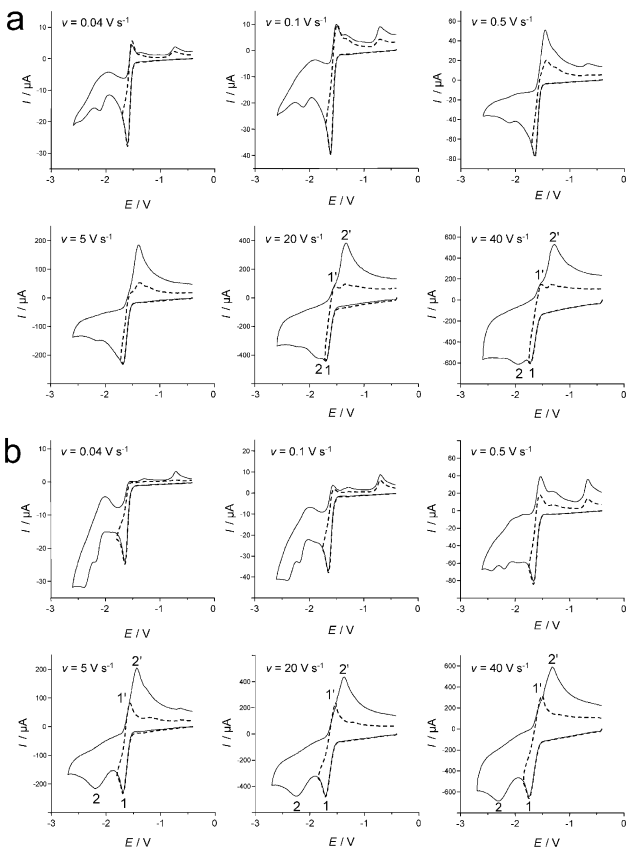

Fig. 5 Cyclic voltammetry of complexes (a) **1a** and (b) **2** in MeCN–$[NBu_4][PF_6]$ under Ar at different scan rates (vitreous carbon electrode; potentials are in V *vs.* Fc^+/Fc).

been reported by several groups and parameters defining conditions under which wave-splitting is observable have been identified.[34,35] The central parameters are the separation of the formal potentials of the individual electron transfer steps (ΔE°), the relative rates of the heterogeneous electron transfers k_s, and the occurrence and rate of homogeneous electron transfer reactions. Wave-splitting was not observed for the two-electron reduction of $[Fe_2(CO)_6(\mu\text{-sdt})]$ or $[Fe_2(CO)_6(\mu\text{-bdt})]$ complexes for which the second heterogeneous rate constant k_s^{red2} was, respectively larger than, or similar to, k_s^{red1}.[7a,15]

In the present case, the second reduction step is much slower than the first one, as shown by the magnitude of the peak-to-peak separations, ΔE_p^{red2}: these increase from 460 mV (v = 20 V s^{-1}) to 690 mV (v = 60 V s^{-1}) for **1a**, from 490 mV (v = 20 V s^{-1}) to 720 mV (v = 60 V s^{-1}) for **1b** and from 540 mV (v = 3 V s^{-1}) to 1080 mV (v = 60 V s^{-1}) for **2**.[36] Previous studies have shown that disproportionation of the intermediate species in an overall two-electron transfer has a strong influence on the shape of CV curves[34,38] and on the extent of wave-splitting.[34] The redox potentials of the successive one-electron reductions of the complexes in MeCN–$[NBu_4][PF_6]$ (Table 1) lead to disproportionation constants, K_{disp}, of 4 ± 3 (**1a**); 2 ± 1 (**1b**) and $(2.4 \pm 2)\ 10^{-3}$ (**2**). At 298 K, the ratio of K_{disp} for **1a** : **2** ($4 : 2.4 \times 10^{-3}$) indicates a difference of approximately 18 kJ mol^{-1} in ΔG for the disproportionation reaction. The thermodynamically favourable disproportionation in **1a** and **1b** is confirmed by the presence of the oxidation peak of $\mathbf{1a}^{2-}$ and $\mathbf{1b}^{2-}$ (peak 2′, return scan) in the CVs limited to the first reduction (Fig. 5a, and S4a,† dotted line). Moreover, the persistence of this peak for scan rates up to 40 V s^{-1} demonstrates that the disproportionation of $\mathbf{1a}^{-}$ and $\mathbf{1b}^{-}$ are fast reactions. The rapid and thermodynamically favourable disproportionation of the one-electron reduced species therefore offers a simple explanation for the 2-electron nature of the reduction of **1a** and **1b**, where $K_{disp} > 1$. The basic reduction mechanism of **1** is summarised in the upper part of Scheme 3 where the heterogeneous steps are complemented by the disproportionation of the anion.

In contrast to the CV of **1a**, the oxidation peak 2′ is completely absent in the CVs of **2** recorded under the same conditions (Fig. 5b, dotted line), consistent with the much smaller disproportionation constant for **2** ($K_{disp} \ll 1$). Simple disproportionation of the anion cannot, therefore, account for the two-electron nature of the reduction of **2** at slow scan rates under Ar (Fig. S2†). We return to this point when we consider the nature of possible daughter products of the primary reduction.

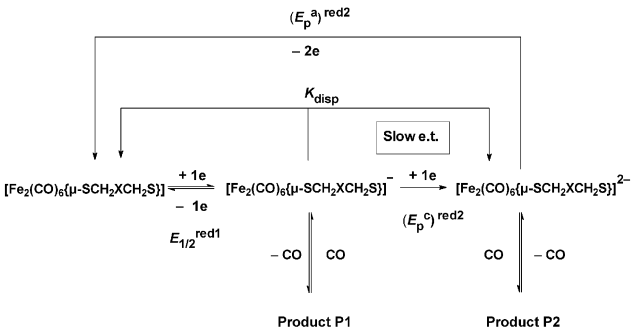

Scheme 3 X = CH_2 or NR; R = CH_2CH_2OMe or ^{i}Pr (Product **P2** was not detected for X = N^{i}Pr).

2.2.2 Electronic structure of the reduced products. The previous paragraphs have highlighted both the rich electrochemistry of these diiron dithiolate complexes and the multiplicity of reduction products that can be formed under different conditions. The subtle differences between **1** and **2**, the most obvious of which is the change in disproportionation constant, K_{disp}, indicate that the substituent, R, on the amine bridgehead plays some role in the reaction. Overall two-electron transfers occur where the doubly reduced species is very stable relative to the anion, in which case the disproportionation constant, $K_{disp} > 1$. Typically, this situation arises where there is a substantial structural rearrangement that makes the transfer of a second electron thermodynamically more favourable than the first.[44–47] This is often the case when the LUMO of the complex (the SOMO of the reduced analogue) has strong σ antibonding character, leading to dramatic changes in bond length through the reduction process. Numerous calculations have confirmed that the LUMO in bimetallic complexes such as **1a**, **1b** and **2** has dominant M–M σ* character. Furthermore, the critical role of the bridging ligands in controlling the kinetics and thermodynamics of concerted two-electron transfer and metal–metal bond cleavage has been demonstrated for $[M_2(\mu\text{-}PPh_2)_2(CO)_8]^{0/2-}$ (M = Mo or W).[45e] Structural rearrangement therefore seems likely to be the cause of the two-electron behaviour observed for the reduction of **1** and **2**. The rather different electrochemical responses of **1a**, **1b** and **2** highlighted above, however, suggest that the extent of this rearrangement may depend on the nature of the R group.

In order to explore the nature of the reduction process in more detail, we have extended our density functional calculations on **1a** and **2** to include their 1- and 2-electron reduced analogues. Optimised structures of the neutral species, **2**, along with those of its 1- and 2-electron reduced analogues, are shown in Fig. 6, and key structural parameters for these and the corresponding species derived from reduction of **1a** and **2** are collected in Table 2. The electronic structure of complex **2** has been extensively studied by other groups, and our optimised structure is fully consistent with these earlier studies. In particular, the optimised Fe–Fe bond length of 2.51 A is very similar to those reported by Hall and co-workers.[19b,d]

The structural consequences of one- and two-electron reduction of **2** have also been discussed previously,[6b,23e] but we reiterate the key features here as they provide a logical reference point for the subsequent discussion of the role of the pendant CH_2CH_2OMe group in **1a**. The structural parameters summarised in Table 2 confirm that reduction of **2** does indeed populate the Fe–Fe σ* orbital, causing a significant elongation of both Fe–Fe (2.81 Å) and Fe–S (2.36 Å) bonds. The basic butterfly $Fe_2(\mu\text{-}SR)_2$ architecture is, however, retained, and the optimised structure of the core is very similar to that proposed by Borg *et al.* for the same species based on their infra-red spectroelectrochemical data.[4a] At the dianionic level ($\mathbf{2}^{2-}$) we have located three quite distinct local minima (**A**, **B** and **C**) on the potential energy surface, separated by less than 20 kJ mol^{-1}. Isomer **A** retains the butterfly structure

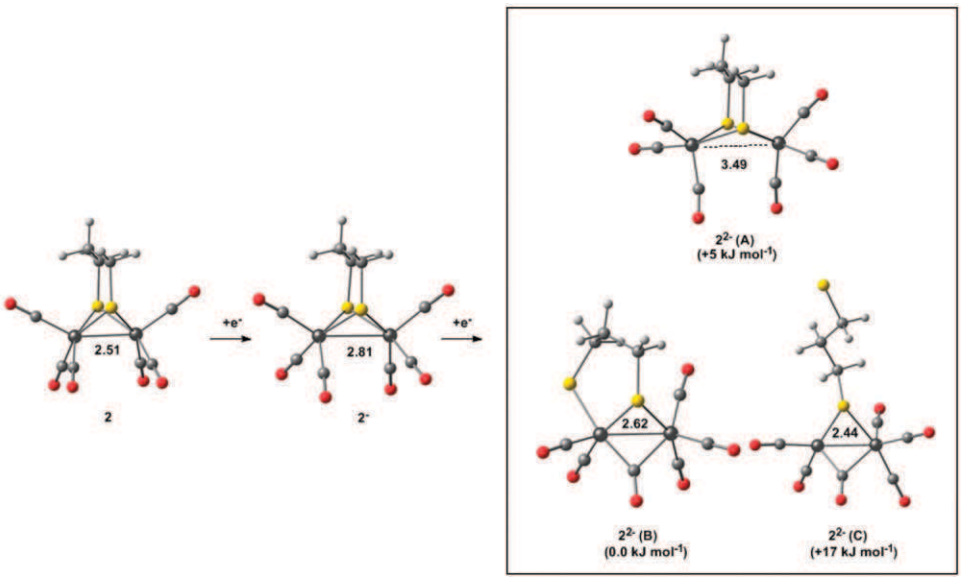

Fig. 6 Optimised structures of **2**, $\mathbf{2}^-$ and $\mathbf{2}^{2-}$ (isomers **A**, **B** and **C**).

of the $Fe_2(\mu\text{-}SR)_2$ core found in **2** and $\mathbf{2}^-$, but the very long Fe–Fe distance (3.49 Å) is consistent with double occupation of the σ^* orbital. The core is therefore considerably flatter than in either the neutral or anionic structures, but the constraints of the chelating architecture prevent it from adopting the electronically preferred planar diamond structure. We have also located two further minima on the potential energy surface of $\mathbf{2}^{2-}$, corresponding to cleavage of either one (isomer **B**) or two (isomer **C**) Fe–S bonds. The tendency to cleave Fe–S bonds at the doubly reduced level is a natural consequence of the build up of negative charge at the metal core. The structure of isomer **C**, where one of the thiolate ligands is completely removed from the bimetallic core, is very similar to that proposed for $[Fe_2(CO)_6(\mu\text{-}CO)\{\mu\text{-}S(CH_2)_3SH\}]^-$,[4a] albeit with one fewer carbonyl ligand. The nature of the metal–metal bonding in isomers **B** and **C** merits some comment. Cleavage of one or two Fe–S bonds in isomers **B** and **C**, respectively, reduces the total electron count at the metal core by two/four, hence requiring the formation of single (**B**) or double (**C**) Fe–Fe bonds to restore the 18-electron configuration at each metal. The very short Fe–Fe separation in isomer **C** (2.44 Å *cf.* 2.51 Å in **2**) provides clear evidence for some multiple character to the Fe–Fe bond. We find isomer **B** to be the global minimum in this case, lying 5 kJ mol^{-1} below the unrearranged structure, isomer **A**. Borg *et al.* computed a difference of 13 kJ mol^{-1} for the closely related species with one fewer CH_2 group in the dithiolate bridge.[6b]

Table 2 Key optimised bond lengths (Å) of **1a**, **2** and their one- and two-electron reduced derivatives, along with relative energies of the different isomers of the dianions

	Fe–Fe/Å	Fe–S/Å	E_{rel}/kJ mol^{-1}
2	2.51	2.31, 2.31, 2.31, 2.31	—
$\mathbf{2}^-$	2.81	2.36, 2.36, 2.36, 2.36	—
$\mathbf{2}^{2-}$ (A)	3.49	2.42, 2.43, 2.45, 2.45	+5
$\mathbf{2}^{2-}$ (B)	2.62	2.33, 2.38, 2.48, 4.27	0
$\mathbf{2}^{2-}$ (C)	2.44	2.30, 2.38. 7.11, 7.28	+17
1a	2.51	2.31, 2.31, 2.31, 2.31	—
$\mathbf{1a}^-$	2.81	2.36, 2.36, 2.36, 2.38	—
$\mathbf{1a}^{2-}$ (A)	3.49	2.40, 2.42, 2.43, 2.45	+31
$\mathbf{1a}^{2-}$ (B)	2.61	2.35, 2.38, 2.51, 4.26	0
$\mathbf{1a}^{2-}$ (C)	2.46	2.29, 2.38, 7.08, 7.42	+18

A survey of the potential energy surface of $\mathbf{1a}^-$ and $\mathbf{1a}^{2-}$ reveals a series of minima that are very similar in structure to those derived from **2**. In all cases the Fe···OMe distance remains long, indicating that coordination of the pendant arm (as observed in **1a–CO**) plays no role in stabilising the primary reduction products. In the context of the electrochemistry, the most significant observation is that the elongation of the Fe–Fe bond at the singly reduced level is identical for **1a** and **2**. Thus, although the stabilisation of the SOMO as a result of this elongation will undoubtedly play a role in lowering the potential of the second electron transfer (*i.e.* the tendency towards 2-electron behaviour in both **1a** and **2** at slow scan rates), it *cannot* account for the subtle differences between **1a** and **2**. At the dianionic level, however, differences between the two systems do emerge that may account for the contrasting electrochemical behaviour. For both $\mathbf{2}^{2-}$ and $\mathbf{1a}^{2-}$, isomer **B** is the most stable of the three, but in the former it lies only 5 kJ mol^{-1} below **A**, indicating that the driving force for Fe–S bond cleavage is relatively weak. In $\mathbf{1a}^{2-}$, in contrast, isomer **B** lies 31 kJ mol^{-1} below **A**, suggesting that cleavage of the Fe–S bonds is much more favourable in this case. Our calculations suggest that the pendant OMe group is entirely innocent in this process, and so the difference between **2** and **1a** must reflect the stabilising inductive effect of the nitrogen substituent in the bridge, a hypothesis that would also explain the similar electrochemical behaviour of **1a** and **1b**. Calculations on a generic model system with an NH group at the bridgehead confirm a strong (25 kJ mol^{-1}) preference for **B** over **A**.

Whatever the origin of the preference for Fe–S bond cleavage in **1a**, it is clear that the additional stabilisation of the dianion may have a significant impact on the

disproportionation of the anion, and hence on the electrochemical response. In the absence of any Fe–S bond cleavage at the dianionic level (*i.e.* considering only the butterfly isomer **A** in each redox state), the energies for the disproportionation reactions ($2\ X^{1-} \rightarrow X + X^{2-}$) are almost identical for **1a** and **2**. The additional stabilisation of $\mathbf{1a}^{2-}$ as a result of Fe–S bond cleavage (forming isomer **B**) makes the disproportionation more favourable by 31 kJ mol^{-1} (compared to a difference of 18 kJ mol^{-1} (ΔG) obtained from the electrochemical measurements). By Hammond's postulate, we would also anticipate that the greater driving force for Fe–S bond cleavage in $\mathbf{1a}^{2-}$ will reduce the barrier for rearrangement of isomer **A** to **B**, hence leading to the faster reduction of $\mathbf{1a}^{-}$ compared to $\mathbf{2}^{-}$, consistent with $k_s^{red2}(\mathbf{1}) > k_s^{red2}(\mathbf{2})$.[36]

2.2.3 The effect of CO on the reduction of 1 and 2. We have noted above that under Ar the reduction of the complexes with an azadithiolate bridge (**1a**, **1b**) is chemically more reversible than that of the propanedithiolate analogue (Fig. 3). Under CO, in contrast, significant return peaks even at slow scan rates indicate that the reduction of both **1a** and **2** becomes reversible. These results suggest that a reduced species undergoes CO loss, a well-known reaction for diiron carbonyl complexes.[3,4a,18,39] The daughter product (Product **P1** in Scheme 3) detected by a peak around −2.1 V (**1a**) or −2.2 V (**1b** and **2**) under Ar is absent under CO (compare Fig. 5†). The persistence of this peak for scan rates up to 10 V s^{-1} for **1a** confirms that reversible CO loss is a fast reaction.

We have already confirmed that the first reduction is a two-electron process at slow scan rates, so it is not clear, *a priori*, whether loss of CO occurs from the anion or the dianion. We favour the former for the following reasons:

(i) for **1**, both $(i_p^c)^{red1}$ and $(i_p^a)^{red1}$ measured at slow scan rates are larger under CO than under Ar.[40] The increase of $(i_p^c)^{red1}$ is consistent with more extensive disproportionation due to the stabilisation of $\mathbf{1}^{-}$ under CO.

(ii) for complex **2**, the kinetic stabilisation of the anion under CO is also revealed by the detection of its reduction peak around −1.9 V, which was absent under Ar (Fig. S4).

We therefore propose that the peak around −2.1 V (**1a**) or −2.2 V (**1b** and **2**) is due to reduction of a species, Product **P1**, derived from loss of a CO ligand from the anion, either directly or following subsequent reactions (Scheme 3).[41]

On the basis of infra-red spectroelectrochemical results, Borg *et al.* have proposed that CO loss from $\mathbf{2}^{-}$ is followed by a ligand redistribution reaction and recoordination of CO to form a dianionic species containing four metal centres (Fig. 7).[4a,6] This has been later confirmed by the full characterisation of this dianion generated by chemical reduction of **2**.[13b] The initial step in this process is clearly loss of CO to vacate a coordination site, so we have used DFT to explore the thermodynamic and structural effects of CO loss from the anions $\mathbf{1a}^{-}$ and $\mathbf{2}^{-}$. Optimised structures of the anions and their decarbonylated products ($\mathbf{1a}^{-}$**–CO**, $\mathbf{2}^{-}$**–CO**) are summarised in Fig. 7, along with the energies of CO loss. In $\mathbf{2}^{-}$, loss of CO results in a substantial redistribution of electron density, such that the additional electron moves from the Fe–Fe σ antibonding orbital into an orbital localised on the CO-deficient iron. The net result, in structural terms, is that the Fe–Fe bond contracts back to a value typical of an Fe–Fe single bond. The structural and energetic changes associated with CO loss from $\mathbf{1a}^{-}$ are very similar, with a significant contraction of the Fe–Fe bond. There is again no indication of coordination of the OMe group to the metal (Fe–O = 4.02 Å) but the pendant arm in **1a** does have a significant impact on the geometry at the CO-deficient iron centre. The CH_2CH_2OMe group lies directly over the vacant coordination site, with a relatively short Fe–(H–C) separation of 2.63 Å suggesting the presence of a weak stabilising interaction between the metal and alkyl chain. Whilst the preference for interaction with a C–H group, rather than OMe may seem somewhat surprising, it is consistent with the high electron density at the metal, and also explains the very similar behaviour of the ^{i}Pr analogue, **1b**, where a methyl group is similarly placed to block the vacant coordination site. In the context of the electrochemistry, the pendant arm in both **1a** and **1b** effectively blocks the dimerisation process that causes the loss of reversibility.

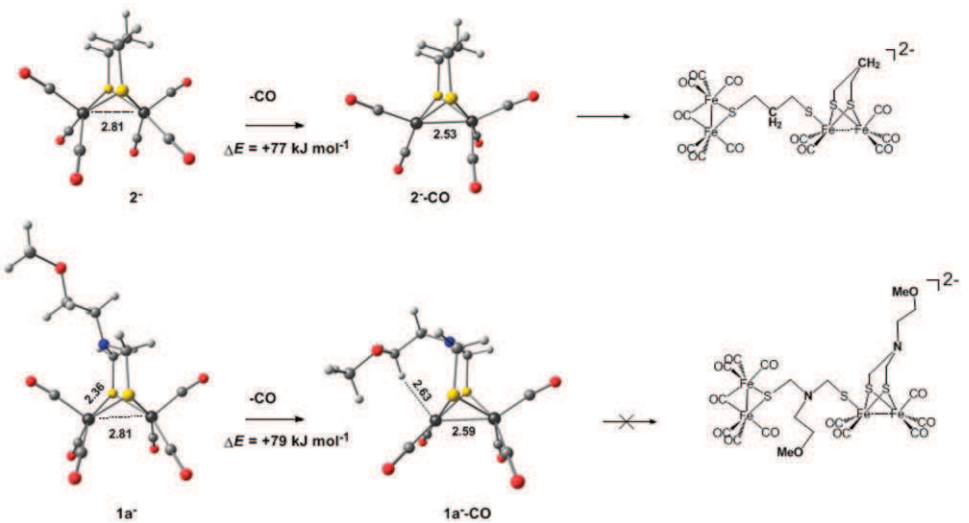

Fig. 7 Optimised structures of the anions, $\mathbf{1a}^{-}$ and $\mathbf{2}^{-}$, along with their decarbonylated products.

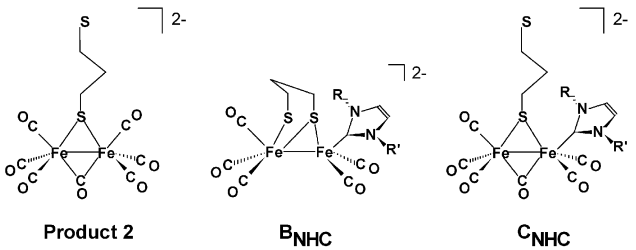

Scheme 4 Proposed structure of the doubly reduced carbonylated daughter products of **2** and **3a**.

In the CVs shown in Fig. 5, an additional quasi-reversible reduction peak around −2.4 V must also result from chemical reactions subsequent to the reduction of **1a** and **2** (this product was not detected in the accessible potential window in the case of **1b**). However, unlike the daughter peak at −2.1 V assigned to Product **P1** in Scheme 3, the peak at −2.4 V is observed under both Ar and CO, and can therefore reasonably be assigned as resulting from the decay of the dianion rather than anion (Product **P2** in Scheme 3). The fact that Product **P2** is observed under CO while the primary reduction maintains substantial chemical reversibility when the potential scan is reversed around −1.8 V (Fig. S4) suggests that the follow-up reaction is reversible. From the mechanism in Scheme 3, electrolysis of **1a** and **2** performed in the presence of CO should afford Product **P2** with a charge consumption of 2 F mol^{-1} **2**. Pickett and co-workers have shown that bulk electrolysis of **2** in MeCN under CO does indeed consume *ca.* 2 F mol^{-1} **2** to produce $[Fe_2(CO)_6(\mu\text{-}CO)\{\mu\text{-}S(CH_2)_3SH\}]^-$ [4a] where one of the two Fe–S bonds has been cleaved, and it seems likely that Product **P2** (Scheme 4) is analogous. The core structure of this species is very similar to isomer **C** of the dianion discussed in Fig. 6, except that it features an additional CO ligand. It seems reasonable, therefore, to suggest that excess CO drives the redox equilibria in Scheme 3 to the right by coordinating to the dianion. The net effect will therefore be to stabilise the dianion relative to the anion, and hence favour a two-, rather than one-electron process.

In summary, a two-electron reduction process requires that the dianion is relatively stable compared to the anion, allowing the second electron transfer to occur at or below the potential of the first. Our experiments and calculations have highlighted two ways in which this might happen. In $\mathbf{1a}^{2-}$, the presence of an electron-withdrawing NR substituent stabilises the negative charge by promoting cleavage of the Fe–S bond, and this is sufficient to drive a disproportionation reaction and hence two-electron reduction. In $\mathbf{2}^{2-}$, in contrast, cleavage of the Fe–S bonds is much less favourable unless excess CO is available to bind to the coordinatively unsaturated diiron core.

2.3 Electrochemical reduction of $[Fe_2(CO)_5L_{NHC}(\mu\text{-pdt})]$, 3a–b

[**a**: L_{NHC} = 1,3-bis(methyl)-imidazol-2-ylidene; **b**: L_{NHC} = 1,3-bis(2,4,6-trimethylphenyl)-imidzol-2-ylidene].

2.3.1 Reduction of 3 under Ar. Cyclic voltammetry of complex **3a** (Fig. 8a) shows partially reversible reduction ($E^{red}_{1/2}$ = −2.01 V, v = 0.2 V s^{-1}, Table 1)[7b] and oxidation ($E^{ox}_{1/2}$ = 0.11 V) processes in MeCN–$[NBu_4][PF_6]$ under Ar. The presence of several minor reduction and oxidation peaks (E^{red2}_p = −2.46 V; E^{ox}_p = −1.5 V; E^{ox}_p = −1.15 V) indicates that the reduction is followed by chemical reaction(s). The reduction of **3b** (E^{red}_p = −2.07 V) under the same conditions shows no sign of chemical reversibility at moderate scan rate, in agreement with the results reported by Darensbourg.[3f] The CV of **3a** was also briefly investigated in thf- and CH_2Cl_2–$[NBu_4][PF_6]$ (Fig. S5 and S6†). In thf, the electrochemical reduction of **3a** is similar to that in MeCN (Table 1; product peaks at E^{red}_p = −2.66 V; E^{ox}_p = −1.65 V; E^{ox}_p = −1.24 V), while the oxidation involves several steps, with only the first one partially reversible ($E^{ox}_{1/2}$ = 0.22 V) at v = 0.2 V s^{-1}. In CH_2Cl_2, the reduction is irreversible (Table 1; product peaks at $E^{red2}_p \sim -2.5$ V; $E^{ox}_p \sim -1.8$ V; E^{ox}_p = −1.14 V), but the oxidation is a fully reversible one-electron process on the CV time scale with $E^{ox}_{1/2}$ = 0.15 V (Fig. S6†). Comparison of the reduction peak current $(i^c_p)^{red1}$ with the current of the reversible one-electron oxidation of the complex, $[(i^c_p)^{red1}/(i^a_p)^{ox}$ = 1.95 for v = 0.05 V s^{-1}; 1.7 for v = 1 V s^{-1}], demonstrated unambiguously that the reduction involves the transfer of two electrons in CH_2Cl_2 at slow to moderate scan rates. This conclusion contradicts our previous report that the reduction of **3a** in MeCN–$[NBu_4][PF_6]$ was a one-, rather than two-electron process,[7b] so we decided to revisit the reduction of **3a** in MeCN by CV at variable scan rates to establish whether

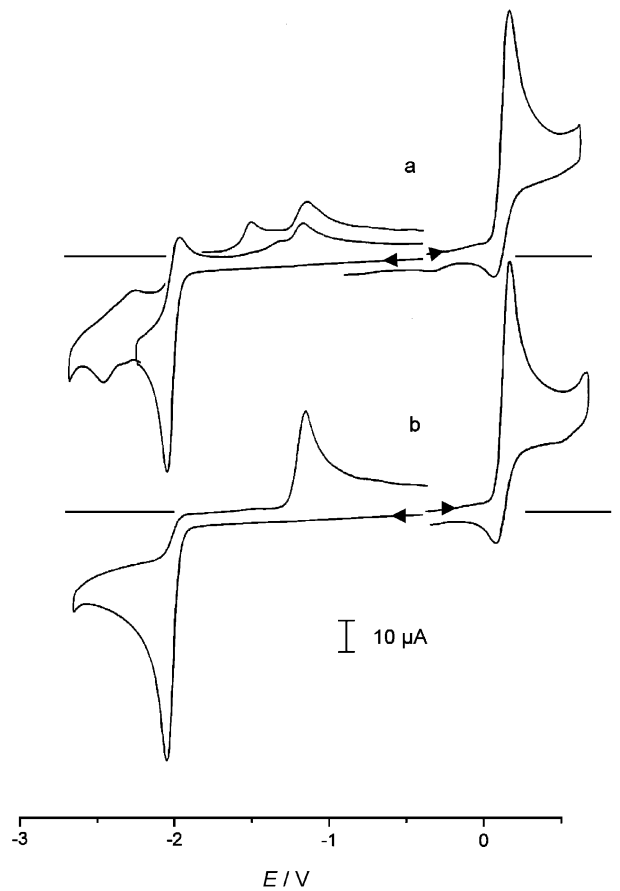

Fig. 8 Cyclic voltammetry of **3a** (a) under Ar, and (b) under CO in MeCN–$[NBu_4][PF_6]$ (vitreous carbon electrode; v = 0.2 V s^{-1}; potentials are in V *vs.* Fc^+/Fc).

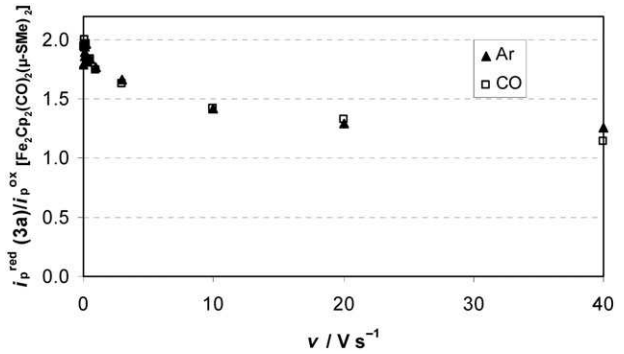

Fig. 9 Scan rate dependence of the ratio of the cyclic voltammetric reduction peak current of **3a** (1 mM) to the peak current of the one-electron oxidation of $[Fe_2Cp_2(CO)_2(\mu\text{-}SMe)_2]$ (1 mM) in MeCN–$[NBu_4][PF_6]$ (vitreous carbon electrode).

wave-splitting could be observed. The scan rate dependence of the current function $[i_p^{red1}/v^{1/2}]$, and the comparison of the current of the first reduction of **3a** with that of the first one-electron oxidation of an equimolar solution of $[Fe_2Cp_2(CO)_2(\mu\text{-}SMe)_2]$[32] at different scan rates (Fig. 9) demonstrate that at slow scan rate, the reduction of **3a** in MeCN–$[NBu_4][PF_6]$ is clearly a *two-electron* process (as is that of the analogue **3b**)[3f] but at faster rates two separate reduction steps can be detected, both with $E_{1/2}^{red} \sim -2.1$ V (Fig. 10). Thus wave-splitting does emerge in these systems, albeit much less distinctly than for **1a** and at faster scan rates. The scan rate dependence of the peak-to-peak separation for both reductions (Table 1) also suggests that the second electron transfer is again slower than the first one. Comparison with complex **2** shows that the substitution of a CO ligand by a N-heterocyclic carbene results in the expected negative shift of the redox potentials, but the potential shift is more pronounced for the first reduction step ($\Delta E_{1/2}^{red1} \sim 0.5$ V) than for the second one ($\Delta E_{1/2}^{red2} \sim 0.3$ V). Thus, the substituted anion is thermodynamically less stable than the parent and disproportionation of the anion, still detectable at $v = 60$ V s^{-1} (Fig. 10b, solid line) is responsible for the transition from a one- to a two-electron process, as illustrated by the scan rate dependence of the current function. The basic reduction mechanism of **3a** may also be represented as shown in Scheme 3 (with one of the CO ligands replaced by L_{NHC}).

2.3.2 Reduction of 3 under CO. The effect of CO on the CV of **3a** (Fig. 8b, S5b and S6b†) is strikingly different from that described above for **1** and **2**. In the all-carbonyl species, an atmosphere of CO made the reduction more reversible but in **3a** precisely the opposite is found and the reduction becomes totally irreversible ($E_p^{red} = -2.04$ V in MeCN). The product peaks observed under Ar at −2.46 V and −1.5 V for **3a**, and at $E_{1/2} = -2.4$ V and $E_p^{ox} = -1.53$ V for **3b**, are absent under CO and only a single oxidation peak is observed on the return scan at −1.15 V (**3a**) (Fig. 8b) or −1.32 V (**3b**). The comparison of the CVs of **3a** recorded at fast scan rates under Ar and under CO demonstrates that the CO effect arises from the reaction of the dianion with CO, since the oxidation peak of $\mathbf{3a}^{2-}$ (peak 2′) is replaced by one at −1.15 V when CO is present (Fig. 10). This reaction is quite fast since it is still observed at scan rates

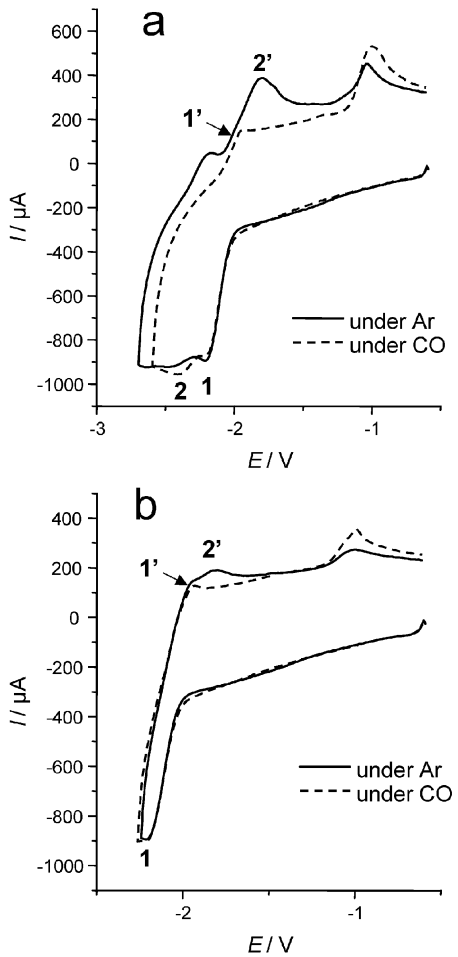

Fig. 10 Cyclic voltammetry of **3a** (1.1 mM) in MeCN–$[NBu_4][PF_6]$ under Ar (solid line) and under CO (broken line); in panel a the potential scan covers both reduction events, and only the first one in panel b ($v = 60$ V s^{-1}; vitreous carbon electrode; potentials are in V *vs.* Fc^+/Fc).

up to 60 V s^{-1}. The *removal* of the dianion $\mathbf{3a}^{2-}$ under CO suggests that coordination of CO must be involved, which in turn suggests the presence of a vacant coordination site at the metal in the doubly reduced species. We can eliminate dissociation of the NHC ligand as a potential source of the vacant site because the oxidation peak observed on the return scan under CO occurs at different potentials for **3a** (–1.15 V) and for **3b** (–1.32 V), indicating that the NHC ligand remains attached to the metal core. Alternatively, two-electron reduction of the NHC-substituted complexes **3a** and **3b** may result in the cleavage of one or more Fe–S bonds, in a process precisely analogous to that which generates isomers **B** and **C** in the all-carbonyl species (Fig. 6). In the presence of excess CO, coordination of an additional ligand to the coordinatively unsaturated intermediate obtained by reduction of **3a** and **3b** would lead to compounds $\mathbf{B_{NHC}}$ or $\mathbf{C_{NHC}}$ shown in Scheme 4, where $\mathbf{C_{NHC}}$ is a substituted analogue of the $[Fe_2(CO)_6\{\mu\text{-}CO\}(\mu\text{-}S(CH_2)_3SH\}]^-$ species observed by Borg *et al.* upon bulk electrolysis of **2**.[4a]

The very different behaviour of **3a** and **2** may result from a combination of factors: first, the formation of the NHC

analogue of Product **P1** would be hindered if the CO ligands are less labile in the $[Fe_2(CO)_5L_{NHC}(\mu\text{-pdt})]^-$ anion than in its hexacarbonyl parent; secondly, it is expected that the Fe–S bonds in the $[Fe_2(CO)_5L_{NHC}(\mu\text{-pdt})]^{2-}$ dianion will cleave more easily than those in $\mathbf{2}^{2-}$, and the subsequent binding of CO to the more electron-rich site appears to be irreversible.

Conclusion

In this paper we have shown that the two one-electron reduction steps of different $[Fe_2(CO)_5L(\mu\text{-dithiolate})]$ complexes are discernible by cyclic voltammetry at fast scan rates. The nature of the S-to-S link affects the reduction of the hexacarbonyl complexes in that the potentials of the redox steps are inverted only for those containing an azadithiolate bridge so that E° (or $E_{1/2}$) for the second reduction is less negative than that of the first, while it is more negative for the pdt complex. Therefore, the reduction of $[Fe_2(CO)_6\{\mu\text{-}SCH_2N(R)CH_2S\}]$ tends towards a two-electron process at lower scan rates owing to the disproportionation of the anion. Density functional theory suggests that the addition of the first electron leads to a substantial lengthening of the Fe–Fe bond, but 2-electron reduction gives two structures with very similar energy, where either the Fe–Fe or an Fe–S bond is cleaved. The presence of the azadithiolate bridge promotes cleavage of the Fe–S bond, and this structural reorganisation may provide the driving force for the disproportionation reaction.

The substitution of a N-heterocyclic carbene ligand for CO in the complex with a propanedithiolate bridge was found to alter the reduction both thermodynamically and kinetically. The substitution leads to a negative shift of the redox potentials that is larger for the first reduction than for the second, and thus to a thermodynamically less stable anion for the substituted derivative. The two-electron reduction of the NHC-substituted complex **3a** is thus due to disproportionation of the anion rather than to simultaneous electron uptake by the Fe–Fe core and the NHC ligand as in the case of the analogue **3b**.[3f] On the other hand, the increased electron density at the metal core in the $[Fe_2(CO)_5L_{NHC}(\mu\text{-pdt})]^{n-}$ species makes the CO ligands less labile in the anion and facilitates Fe–S bond cleavage in the dianion as well as the subsequent binding of a CO ligand.

The overall two-electron reduction of azadithiolate hexacarbonyl complexes and the ensuing Fe–S bond cleavage may have consequences on the mechanisms of proton reduction by these compounds. Further studies are in progress in our laboratory to examine this question.

Experimental section

Methods and materials

All the experiments were carried out under an inert atmosphere, using Schlenk techniques for the syntheses. Tetrahydrofuran (THF) was purified as described previously.[48] Acetonitrile (Merck, HPLC grade) was used as received. $[Fe_2(\mu\text{-}S)_2(CO)_6]$ was prepared according to reported methods.[49,50] *N*,*N*-di(chloromethyl)-2-methoxyethylamine and *N*,*N*-di(chloromethyl)-2-isopropyl amine were obtained from reaction of paraformaldehyde with either 2-methoxyethylamine or isopropylamine, followed by chlorination with thionyl chloride, according to a reported procedure.[5a] All other chemicals were used as purchased (Sigma-Aldrich).

The preparation and the purification of the supporting electrolyte $[NBu_4][PF_6]$ were described previously.[48] The electrochemical equipment consisted in a GCU potentiostat (Tacussel/Radiometer) driven by a PAR 175 Universal Programmer, CV traces were recorded with a SEFRAM TGM 164 X-Y recorder. Fast scan CV were obtained with a PGSTAT 12 or a μ-AUTOLAB (Type III) driven by a GPES software. All the potentials (text, tables, figures) are quoted against the ferrocene–ferrocenium couple; ferrocene was added as an internal standard at the end of the experiments. 1H NMR spectra were recorded on a Bruker AC300 spectrophotometer. Shifts are relative to tetramethylsilane as an internal reference. The infrared spectra were recorded on a Nicolet Nexus Fourier transform spectrometer. Chemical analyses were made by the Service de Microanalyses I.C.S.N., Gif sur Yvette (France).

Syntheses

Synthesis of $[Fe_2(CO)_6\{\mu\text{-}SCH_2N(CH_2CH_2OCH_3)CH_2S\}]$ (1a). The addition of 2 molar equivalents of $LiBEt_3H$ (6 mL, 6 mmol) to a solution of $[Fe_2(\mu\text{-}S)_2(CO)_6]$ (1 g, 2.9 mmol) at −78 °C gave a green solution of the dianion $[Fe_2(\mu\text{-}S)_2(CO)_6]^{2-}$. To this was added dropwise a THF solution (10 mL) of *N*,*N*-di(chloromethyl)-2-methoxyethylamine $(ClCH_2)_2N(CH_2)_2OCH_3$ (0.525 g, 3.1 mmol). The reaction mixture turned red and was stirred for 2 h at room temperature. Solvent was removed under vacuum, leaving a red oil which was extracted with 3 × 50 mL of Et_2O. The combined solution was evaporated to dryness under vacuum. The crude product was chromatographed on silica gel. An orange band was eluted with a dichloromethane–hexane (25 : 75) mixture and gave only the starting material. A second red band collected with dichloromethane gave compound **1**. 100 mL of hexane were added to compound **1** and the solution obtained was concentrated to 5 mL under vacuum. A red powder of complex **1a** (0.57 g, yield 44%) was recovered after filtration.

N,N-Di(chloromethyl)-2-methoxyethylamine. ^{1}H NMR (300 MHz, $CDCl_3$): δ 5.25 (s, 4H, $N(CH_2)_2S_2$), 3.59 (t, J_{HH} = 5.1 Hz, 2H, $NCH_2CH_2OCH_3$), 3.37 (s, 3H, OCH_3), 3.18 ppm (t, J_{HH} = 5.1 Hz, 2H, $NCH_2CH_2OCH_3$).

1a. ^{1}H NMR (300 MHz, $CDCl_3$): δ 3.64 (s, 4H, $N(CH_2)_2S_2$), 3.23 (t, J_{HH} = 5.4 Hz, 2H, $NCH_2CH_2OCH_3$), 3.20 (s, 3H, OCH_3), 2.86 (t, J_{HH} = 5.4 Hz, 2H, $NCH_2CH_2OCH_3$). IR (CH_2Cl_2): ν_{CO} = 2073, 2034, 1996 cm^{-1}. Anal. Calcd for $C_{11}H_{11}Fe_2NO_7S_2$: C, 29.69; H, 2.49; N, 3.15. Found: C, 29.42; H, 2.55; N, 3.29.

Synthesis of $[Fe_2(CO)_6\{\mu\text{-}SCH_2N(^iPr)CH_2S\}]$ (1b). To a solution of $[Fe_2(\mu\text{-}S)_2(CO)_6]$ (0.5 g, 1.45 mmol) in tetrahydrofuran (50 mL) was added dropwise 2 equiv. of $LiBEt_3H$ (2.9 mL, 2.9 mmol) at −78 °C. After 30 min stirring, the solution turned from red to green. To this was added at −78 °C a solution of chloramine (0.272 g, 1.74 mmol) in

tetrahydrofuran (5 mL). The reaction mixture turned red and was stirred for 2 h until the temperature of the solution raised to 25 °C. Solvent was then removed under vacuum, giving a red oil that was extracted with 3 × 15 mL of diethylether. The combined extracts were evaporated to dryness, and the crude product, dissolved in hexane, was chromatographed on silica gel. Elution with hexane–dichloromethane (9 : 1) gave a red band, that after evaporation of the volatiles afforded a brick-red powder of complex **1b** (125 mg, 20% yield).

N,N-Di(chloromethyl)-2-isopropylamine. ^{1}H NMR (300 MHz, $CDCl_3$): δ 5.30 (s, 4H, $N(CH_2)_2S_2$), 3.41 (spt, J_{HH} = 6.6 Hz, 1H, $NCH(CH_3)_2$), 1.27 ppm (d, J_{HH} = 6.6 Hz, 6H, $NCH(CH_3)_2$).

1b. ^{1}H NMR (300 MHz, $CDCl_3$): δ 3.22 (s, 4H, $N(CH_2)_2S_2$), 2.82 (spt, J_{HH} = 7.4 Hz, 1H, $NCH(CH_3)_2$), 0.92 ppm (d, J_{HH} = 7.4 Hz, 6H, $NCH(CH_3)_2$). IR (CH_2Cl_2): ν_{CO} = 2073(w), 2034(s), 1996(s) cm^{-1}. Anal. Calcd for $C_{11}H_{11}Fe_2NO_6S_2$: C, 30.79; H, 2.58; N, 3.26. Found: C, 30.37; H, 2.62; N, 3.16.

Crystal structure analysis of 1a

Crystal data. $C_{11}H_{11}Fe_2NO_7S_2$, M = 445.03, triclinic, space group $P\bar{1}$ (no. 2), a = 7.4291(4), b = 9.8933(6), c = 11.8779(7) Å, α = 73.116(3), β = 78.757(3), γ = 86.088(4)°, U = 819.3(1) Å^3, Z = 2, ρ_{calcd} = 1.804 g cm^{-3}, T = 100 K. Mo-K$_\alpha$ X-rays, λ = 0.71073 Å, μ = 2.057 mm^{-1}, θ_{max} = 30.1°, red plate 0.50 × 0.30 × 0.10 mm, 14 673 intensity measurements from thick-slice ϕ or ω scans, transmission factors 0.614–0.815, all 4735 unique reflections (R_{int} = 0.06) gave $R(F)$ = 0.039, w$R(F^2)$ = 0.080 when 209 parameters were refined on F^2, $|\Delta\rho| < 0.58$ e Å^{-3}, riding model for H atoms, only CH_3 orientation refined.[51]‡

Details of calculations. All calculations were performed with Gaussian 03 package,[52] using the hybrid B3LYP functional[53] in conjunction with the SDD basis set and associated effective core potential for Fe[54] and 6-31G(d,p) basis sets for all other atoms. Fully unconstrained geometry optimisations were performed and the resultant stationary points were confirmed as minima through vibrational analysis.

Acknowledgements

This work was supported by CNRS (France, Programme "Energie", PRI-4.1) and ANR (Programme "PhotoBioH2"). EPSRC (UK), Université de Bretagne Occidentale and Glasgow University are acknowledged for financial support.

References

1 (*a*) J. W. Peters, W. N. Lanzilotta, B. J. Lemon and L. C. Seefeldt, *Science*, 1998, **282**, 1853–1858; (*b*) Y. Nicolet, C. Piras, P. Legrand, C. E. Hatchikian and J. C. Fontecilla-Camps, *Structure*, 1999, **7**, 13–23; (*c*) Y. Nicolet, A. L. de Lacey, X. Vernede, V. M. Fernandez, C. E. Hatchikian and J. C. Fontecilla-Camps, *J. Am. Chem. Soc.*, 2001, **123**, 1596–1602; (*d*) B. J. Lemon and J. W. Peters, *Biochemistry*, 1999, **38**, 12969–12973.

2 For recent reviews, see: (*a*) I. P. Georgakaki, L. M. Thomson, E. J. Lyon, M. B. Hall and M. Y. Darensbourg, *Coord. Chem. Rev.*, 2003, **238–239**, 255–266; (*b*) M. Y. Darensbourg, E. J. Lyon, X. Zhao and I. P. Georgakaki, *Proc. Natl. Acad. Sci. U. S. A.*, 2003, **100**, 3683–3688; (*c*) D. J. Evans and C. J. Pickett, *Chem. Soc. Rev.*, 2003, **32**, 268–275; (*d*) T. B. Rauchfuss, *Inorg. Chem.*, 2004, **43**, 14–26; (*e*) L.-C. Song, *Acc. Chem. Res.*, 2005, **38**, 21–28; (*f*) V. Artero and M. Fontecave, *Coord. Chem. Rev.*, 2005, **249**, 1518–1535; (*g*) S. P. Best, *Coord. Chem. Rev.*, 2005, **249**, 1536–1554; (*h*) M. Bruschi, G. Zampella, P. Fantucci and L. De Gioia, *Coord. Chem. Rev.*, 2005, **249**, 1620–1640; (*i*) X. Liu, S. K. Ibrahim, C. Tard and C. J. Pickett, *Coord. Chem. Rev.*, 2005, **249**, 1641–1652; (*j*) L. Sun, B. Akermark and S. Ott, *Coord. Chem. Rev.*, 2005, **249**, 1653–1663; (*k*) J.-F. Capon, F. Gloaguen, P. Schollhammer and J. Talarmin, *Coord. Chem. Rev.*, 2005, **249**, 1664–1676; (*l*) P. Vignais, *Coord. Chem. Rev.*, 2005, **249**, 1677–1690, and references cited therein.

3 (*a*) D. Chong, I. P. Georgakaki, R. Mejia-Rodriguez, J. Sanabria-Chinchilla, M. P. Soriaga and M. Y. Darensbourg, *Dalton Trans.*, 2003, 4158–4163; (*b*) E. J. Lyon, I. P. Georgakaki, J. H. Reibenspies and M. Y. Darensbourg, *Angew. Chem., Int. Ed.*, 1999, **38**, 3178–3180; (*c*) E. J. Lyon, I. P. Georgakaki, J. H. Reibenspies and M. Y. Darensbourg, *J. Am. Chem. Soc.*, 2001, **123**, 3268–3278; (*d*) X. Zhao, I. P. Georgakaki, M. L. Miller, R. Mejia-Rodriguez, C.-H. Chiang and M. Y. Darensbourg, *Inorg. Chem.*, 2002, **41**, 3917–3928; (*e*) R. Mejia-Rodriguez, D. Chong, J. H. Reibenspies, M. P. Soriaga and M. Y. Darensbourg, *J. Am. Chem. Soc.*, 2004, **126**, 12004–12014; (*f*) J. W. Tye, J. Lee, H.-W. Wang, R. Mejia-Rodriguez, J. H. Reibenspies, M. B. Hall and M. Y. Darensbourg, *Inorg. Chem.*, 2005, **44**, 5550–5552.

4 (*a*) S. J. Borg, T. Behrsing, S. P. Best, M. Razavet, X. Liu and C. J. Pickett, *J. Am. Chem. Soc.*, 2004, **126**, 16988–16999; (*b*) M. Razavet, S. C. Davies, D. L. Hughes, J. E. Barclay, D. J. Evans, S. A. Fairhurst, X. Liu and C. J. Pickett, *Dalton Trans.*, 2003, 586–595; (*c*) A. Le Cloirec, S. P. Best, S. Borg, S. C. Davies, D. J. Evans, D. L. Hughes and C. J. Pickett, *Chem. Commun.*, 1999, 2285–2286; (*d*) M. Razavet, S. C. Davies, D. L. Hughes and C. J. Pickett, *Chem. Commun.*, 2001, 847–848; (*e*) M. Razavet, S. J. Borg, S. J. George, S. P. Best, S. A. Fairhurst and C. J. Pickett, *Chem. Commun.*, 2002, 700–701; (*f*) S. J. George, Z. Cui, M. Razavet and C. J. Pickett, *Chem.–Eur. J.*, 2002, **8**, 4037–4046.

5 (*a*) J. D. Lawrence, H. Li and T. B. Rauchfuss, *Chem. Commun.*, 2001, 1482–1483; (*b*) M. Schmidt, S. M. Contakes and T. B. Rauchfuss, *J. Am. Chem. Soc.*, 1999, **121**, 9736–9737; (*c*) J. D. Lawrence, H. Li, T. B. Rauchfuss, M. Bénard and M.-M. Rohmer, *Angew. Chem., Int. Ed.*, 2001, **40**, 1768–1771; (*d*) H. Li and T. B. Rauchfuss, *J. Am. Chem. Soc.*, 2002, **124**, 726–727; (*e*) F. Gloaguen, J. D. Lawrence and T. B. Rauchfuss, *J. Am. Chem. Soc.*, 2001, **123**, 9476–9477; (*f*) F. Gloaguen, J. D. Lawrence, M. Schmidt, S. R. Wilson and T. B. Rauchfuss, *J. Am. Chem. Soc.*, 2001, **123**, 12518–12527; (*g*) F. Gloaguen, J. D. Lawrence, T. B. Rauchfuss, M. Bénard and M.-M. Rohmer, *Inorg. Chem.*, 2002, **41**, 6573–6582; (*h*) C. A. Boyke, T. B. Rauchfuss, S. R. Wilson, M.-M. Rohmer and M. Bénard, *J. Am. Chem. Soc.*, 2004, **126**, 15151–15160; (*i*) J. D. Lawrence, T. B. Rauchfuss and S. R. Wilson, *Inorg. Chem.*, 2002, **41**, 6193–6195.

6 (*a*) M. H. Cheah, S. J. Borg, M. I. Bondin and S. P. Best, *Inorg. Chem.*, 2004, **43**, 5635–5644; (*b*) S. J. Borg, J. W. Tye, M. B. Hall and S. P. Best, *Inorg. Chem.*, 2007, **46**, 384–394; (*c*) M. H. Cheah, S. J. Borg and S. P. Best, *Inorg. Chem.*, 2007, **46**, 1741–1750.

7 (*a*) J.-F. Capon, F. Gloaguen, P. Schollhammer and J. Talarmin, *J. Electroanal. Chem.*, 2004, **566**, 241–247; (*b*) J.-F. Capon, S. El Hassnaoui, F. Gloaguen, P. Schollhammer and J. Talarmin, *Organometallics*, 2005, **24**, 2020–2022; (*c*) P. Das, J.-F. Capon, F. Gloaguen, F. Y. Pétillon, P. Schollhammer and J. Talarmin, *Inorg. Chem.*, 2004, **43**, 8203–8205; (*d*) J.-F. Capon, F. Gloaguen, P. Schollhammer and J. Talarmin, *J. Electroanal. Chem.*, 2006, **595**, 47–52.

8 (*a*) S. Ott, M. Kritikos, B. Åkermark, L. Sun and R. Lomoth, *Angew. Chem., Int. Ed.*, 2004, **43**, 1006–1009; (*b*) T. Liu, M. Wang, Z. Shi, H. Cui, W. Dong, J. Chen, B. Åkermark and L. Sun, *Chem.–Eur. J.*, 2004, **10**, 4474–4479; (*c*) W. Gao, J. Liu, C. Ma, L. Weng, K. Jin, C. Chen, B. Åkermark and L. Sun, *Inorg. Chim. Acta*, 2006, **359**, 1071–1080; (*d*) Z. Wang, J. Liu, C. He, S. Jiang, B. Åkermark and L. Sun, *Inorg. Chim. Acta*, 2007, **360**,

‡ CCDC reference number 244692. For crystallographic data in CIF or other electronic format see DOI: 10.1039/b709273c

2411–2419; (*e*) F. Wang, M. Wang, X. Liu, K. Jin, W. Dong, G. Li, B. Åkermark and L. Sun, *Chem. Commun.*, 1999, **1**, 3221–3222; (*f*) S. Ott, M. Kritikos, B. Åkermark and L. Sun, *Angew. Chem., Int. Ed.*, 2003, **42**, 3285–3288; (*g*) S. Jiang, J. Liu, Y. Shi, Z. Wang, B. Åkermark and L. Sun, *Dalton Trans.*, 2007, 896–902, and references therein.

9 (*a*) S. Jiang, J. Liu and L. Sun, *Inorg. Chem. Commun.*, 2006, **9**, 290–292; (*b*) H.-G. Cui, M. Wang, W.-B. Dong, L.-L. Duan and L.-C. Sun, *Polyhedron*, 2007, **26**, 904–910; (*c*) L. Duan, M. Wang, P. Li, Y. Na, N. Wang and L. Sun, *Dalton Trans.*, 2007, 1277–1283.

10 (*a*) L. Schwartz, J. Ekström, R. Lomoth and S. Ott, *Chem. Commun.*, 2006, 4206–4208; (*b*) L. Schwartz, G. Eilers, L. Eriksson, A. Gogoll, R. Lomoth and S. Ott, *Chem. Commun.*, 2006, 520–522.

11 (*a*) J. Hou, X. Peng, J. Liu, Y. Gao, X. Zhao, S. Gao and K. Han, *Eur. J. Inorg. Chem.*, 2006, 4679–4686; (*b*) J. Hou, X. Peng, Z. Zhou, S. Sun, X. Zhao and S. Gao, *J. Organomet. Chem.*, 2006, **691**, 4633–4640.

12 (*a*) L.-C. Song, Z.-Y. Yang, H.-Z. Bian and Q.-M. Hu, *Organometallics*, 2004, **23**, 3082–3084; (*b*) L.-C. Song, M.-Y. Tang, F.-H. Su and Q.-M. Hu, *Angew. Chem., Int. Ed.*, 2006, **45**, 1130–1333.

13 (*a*) J. L. Nehring and D. M. Heinekey, *Inorg. Chem.*, 2003, **42**, 4288–4292; (*b*) I. Aguirre de Carcer, A. DiPasquale, A. L. Rheingold and D. M. Heinekey, *Inorg. Chem.*, 2006, **45**, 8000–8002.

14 G. Hogarth and I. Richards, *Inorg. Chem. Commun.*, 2007, **10**, 66–70.

15 J. Windhager, M. Rudolph, S. Bräutigam, H. Görls and W. Weigand, *Eur. J. Inorg. Chem.*, 2007, 2748–2760.

16 R. E. Dessy, F. E. Stary, R. B. King and M. Waldrop, *J. Am. Chem. Soc.*, 1966, **88**, 471–476.

17 R. Mathieu, R. Poilblanc, P. Lemoine and M. Gross, *J. Organomet. Chem.*, 1979, **165**, 243–252.

18 (*a*) A. Darchen, H. Mousser and H. Patin, *J. Chem. Soc., Chem. Commun.*, 1988, 968–970; (*b*) H. Mousser, *Thesis*, University of Rennes, France, 1987.

19 (*a*) H.-J. Fan and M. B. Hall, *J. Am. Chem. Soc.*, 2001, **123**, 3828–3829; (*b*) Z. Cao and M. B. Hall, *J. Am. Chem. Soc.*, 2001, **123**, 3734–3742; (*c*) J. W. Tye, M. Y. Darensbourg and M. B. Hall, *J. Mol. Struct.: THEOCHEM*, 2006, **771**, 123–128; (*d*) J. W. Tye, M. Y. Darensbourg and M. B. Hall, *Inorg. Chem.*, 2006, **45**, 1552–1559.

20 S. Motiu, D. Dogaru and V. Gogonea, *Int. J. Quantum Chem.*, 2006, **107**, 1248–1252.

21 M.-H. Baik, T. Ziegler and C. K. Schauer, *J. Am. Chem. Soc.*, 2000, **122**, 9143–9154.

22 (*a*) Z.-P. Liu and P. Hu, *J. Am. Chem. Soc.*, 2002, **124**, 5175–5182; (*b*) Z.-P. Liu and P. Hu, *J. Chem. Phys.*, 2002, **117**, 8177–8180.

23 (*a*) M. Bruschi, P. Fantucci and L. De Gioia, *Inorg. Chem.*, 2002, **41**, 1421–1429; (*b*) M. Bruschi, P. Fantucci and L. De Gioia, *Inorg. Chem.*, 2003, **42**, 4773–4781; (*c*) G. Zampella, M. Bruschi, P. Fantucci, M. Razavet, C. J. Pickett and L. De Gioia, *Chem.–Eur. J.*, 2005, **11**, 509–520; (*d*) G. Zampella, C. Greco, P. Fantucci and L. De Gioia, *Inorg. Chem.*, 2006, **45**, 4109–4118; (*e*) C. Greco, G. Zampella, L. Bertini, M. Bruschi, P. Fantucci and L. De Gioia, *Inorg. Chem.*, 2007, **46**, 108–116; (*f*) A. K. Justice, G. Zampella, L. De Gioia, T. B. Rauchfuss, J. I. van der Vlugt and S. R. Wilson, *Inorg. Chem.*, 2007, **46**, 1655–1664.

24 (*a*) T. Zhou, Y. Mo, A. Liu, Z. Zhou and K. R. Tsai, *Inorg. Chem.*, 2004, **43**, 923–930; (*b*) T. Zhou, Y. Mo, Z. Zhou and K. Tsai, *Inorg. Chem.*, 2005, **44**, 4941–4946.

25 (*a*) A. T. Fiedler and T. C. Brunold, *Inorg. Chem.*, 2005, **44**, 1794–1809; (*b*) A. T. Fiedler and T. C. Brunold, *Inorg. Chem.*, 2005, **44**, 9322–9334.

26 (*a*) S. Zilberman, E. I. Stiefel, M. H. Cohen and R. Car, *J. Phys. Chem. B*, 2006, **110**, 7049–7057; (*b*) S. Zilberman, E. I. Stiefel, M. H. Cohen and R. Car, *Inorg. Chem.*, 2007, **46**, 1153–1161.

27 F. H. Allen, *Acta Crystallogr., Sect. B: Struct. Sci.*, 2002, **58**, 380–388.

28 The parameters i_p and E_p are, respectively the peak current and the peak potential of a redox process; $E_{1/2} = (E_p^a + E_p^c)/2$; E_p^a, i_p^a and E_p^c, i_p^c are, respectively the potential and the current of the anodic and of the cathodic peak of a reversible process; $\Delta E_p = E_p^a - E_p^c$; k_s (in cm s^{-1}) is the rate constant of the heterogeneous electron-transfer. CV stands for cyclic voltammetry; v (V s^{-1}) is the scan rate in CV experiments.

29 The peak current ratio was measured according to the procedure of Nicholson, see ref. 30.

30 R. S. Nicholson, *Anal. Chem.*, 1966, **38**, 1406.

31 P. Madec, K. W. Muir, F. Y. Pétillon, R. Rumin, Y. Scaon, P. Schollhammer and J. Talarmin, *J. Chem. Soc., Dalton Trans.*, 1999, 2371–2383.

32 We chose to calibrate the peak currents using $[Fe_2Cp_2(CO)_2(\mu\text{-}SMe)_2]$ rather than ferrocene as a reference one-electron couple, making the reasonable assumption that $[Fe_2Cp_2(CO)_2(\mu\text{-}SMe)_2]$, $[Fe_2(CO)_6\{\mu\text{-}SCH_2XCH_2S\}]$ (**1**, **2**), and $[Fe_2(CO)_5L_{NHC}(\mu\text{-pdt})]$ (**3**) have similar diffusion coefficients. $D^{1/2}$ for ferrocene is about 1.6 times larger than for $[Fe_2Cp_2(CO)_2(\mu\text{-}SMe)_2]$.[33] This method was preferred to coulometry to determine the number of electrons involved in the reduction because of the existence of follow-up reactions that may be prominent on the longer time scale of bulk electrolyses; the following chemistry is thus susceptible to affect the coulometrically measured n value;[34] controlled-potential electrolysis of **1b** at −1.65 V led to extensive decomposition of the complex after the passage of *ca.* 2 F mol^{-1} **1b**.

33 T. Gennett, W. E. Geiger, B. Willett and F. C. Anson, *J. Electroanal. Chem. Interfacial Electrochem.*, 1987, **222**, 151–160.

34 D. T. Pierce and W. E. Geiger, *J. Am. Chem. Soc.*, 1992, **114**, 6063–6073, and references cited therein.

35 A. J. Downard, A. M. Bond, A. J. Clayton, L. R. Hanton and D. A. McMorran, *Inorg. Chem.*, 1996, **35**, 7684–7690.

36 (*a*) The peak to peak separation for the first reduction of **1** and **2** also increases with increasing v (Table 1), which is partly due to uncompensated solution resistance. The heterogeneous electron transfer rate constants k_s calculated from ΔE_p^{red2} following the procedure of Nicholson[36b] (k_s^{red2}(**1**) ∼6 × 10^{-4} cm s^{-1}; k_s^{red2}(**2**) ∼4 × 10^{-5} cm s^{-1}), were in reasonable agreement with those estimated (k_s^{red2}(**3a**) ∼8 × 10^{-4} cm s^{-1}; k_s^{red2}(**2**) ∼4 × 10^{-5} cm s^{-1}) by digital simulations of CV curves using DigiElch 2.0[37] with Cdl = 1.5 μF and Ru = 85 Ω; the diffusion coefficients for **3a** and **2** used in the calculations of k_s and in the simulations were worked out from the CV peak current i_p^{red1} at scan rates such that the first reduction of the complexes is a reversible one-electron transfer ($v \geq 10$ V s^{-1}). The diffusion coefficients of the anion and dianion were assumed to be identical to those of the neutral complexes **3a** and **2**; (*b*) R. S. Nicholson, *Anal. Chem.*, 1965, **37**, 1351.

37 For detailed information concerning DigiElch, see www.elchsoft.com and the following publications: (*a*) M. Rudolph, *J. Electroanal. Chem.*, 2003, **543**, 23–29; (*b*) M. Rudolph, *J. Electroanal. Chem.*, 2004, **571**, 289–307; (*c*) M. Rudolph, *J. Comput. Chem.*, 2005, **26**, 619–632; (*d*) M. Rudolph, *J. Comput. Chem.*, 2005, **26**, 633–641; (*e*) M. Rudolph, *J. Comput. Chem.*, 2005, **26**, 1193–1204.

38 M. D. Ryan, *J. Electrochem. Soc.*, 1978, **125**, 547–555.

39 F. Robin, R. Rumin, J. Talarmin, F. Y. Pétillon and K. W. Muir, *Organometallics*, 1993, **12**, 365–380.

40 For complex **2**, the reduction current measured at slow scan rate is also larger under CO than under Ar as shown in Fig. S2†.

41 (*a*) In the case of $[Fe_2(CO)_5(PTA)(\mu\text{-pdt})]$ (PTA = 1,3,5-triaza-7-phosphaadamantane, $P(CH_2)_6N_3$), a product peak that is suppressed in the presence of CO was attributed to the neutral MeCN-substituted derivative formed from the parent anion in an ETC process.[3e] In the present case, it is unlikely that product **P1** is $[Fe_2(CO)_5(CH_3CN)\{\mu\text{-}SCH_2XCH_2S\}]$. The ^{t}BuNC-substituted derivative electrogenerated from **1a** by replacement of one CO by a ^{t}BuNC ligand in an ETC process reduces at E_p^{red} = −1.83 V.[41b] From the reduction potentials of **1a** and of the ^{t}BuNC-substituted complex, and from the ligand parameter P_L[42] for MeCN (P_L = −0.58 V[42]), CO (P_L = 0 V[42]) and ^{t}BuNC (P_L = −0.44 V[43]), the reduction of $[Fe_2(CO)_5(CH_3CN)\{\mu\text{-}SCH_2N(R)CH_2S\}]$ is expected to occur around −1.9 V, a potential ∼0.2 V less negative than that of product **P1**. On the other hand, complex **3a** which derives from **2** by replacement of one carbonyl by a N-heterocyclic carbene ligand reduces at −2 V (see text), and it has been reported that $[Fe_2(CO)_5(CH_3CN)\{\mu\text{-}S(CH_2)_3S\}]$ undergoes an irreversible reduction at −1.68 V.[10a] Taken together, these results suggest that the reduction around −2.1 V is most probably due to an anionic species rather than to the neutral $[Fe_2(CO)_5(NCCH_3)\{\mu\text{-}SH_2XCH_2S\}]$. It is

therefore reasonable that product **P1** is the dianion with two bridged {Fe–Fe} units that was shown to form from $\mathbf{2}^{-}$,[4a,13b] and that was suggested[13b] as a reduction product of an analogue of **3a**. However, our DFT calculations suggest that this reaction will be hindered by the bulky R substituent of the N bridgehead atom in **3a**; (*b*) J.-F. Capon, F. Gloaguen, F. Y. Pétillon, P. Schollhammer and J. Talarmin, unpublished results.

42 J. Chatt, C. T. Khan, G. J. Leigh, C. J. Pickett and D. R. Stanley, *J. Chem. Soc., Dalton Trans.*, 1980, 2032–2038.

43 A. J. L. Pombeiro, C. J. Pickett and R. L. Richards, *J. Organomet. Chem.*, 1982, **224**, 285–294.

44 (*a*) For leading references, see W. E. Geiger, *Prog. Inorg. Chem.*, 1985, **33**, 275–352; (*b*) D. H. Evans and K. M. O'Connell, in *Electroanalytical Chemistry*, ed. A. J. Bard, M. Dekker, New York, 1986, vol. 14, pp. 113–207; (*c*) F. Y. Pétillon, P. Schollhammer and J. Talarmin, in *Encyclopedia of Electrochemistry*, ed. A. J. Bard and M. Stratman, Wiley-VCH, Weinheim, vol. 7, 2006, pp. 565–590, and references therein.

45 (*a*) B. Zhuang, J. W. McDonald, F. A. Schultz and W. E. Newton, *Organometallics*, 1984, **3**, 943–945; (*b*) B. Zhuang, J. W. McDonald, F. A. Schultz and W. E. Newton, *Inorg. Chim. Acta*, 1985, **99**, L29–L31; (*c*) D. A. Smith, B. Zhuang, W. E. Newton, J. W. McDonald and F. A. Schultz, *Inorg. Chem.*, 1987, **26**, 2524–2531; (*d*) J. B. Fernandes, L. Qun Zhang and F. A. Schultz, *J. Electroanal. Chem. Interfacial Electrochem.*, 1991, **297**, 145–161; (*e*) D. Uhrhammer and F. A. Schultz, *J. Phys. Chem. A*, 2002, **106**, 11630–11636.

46 (*a*) J. Courtot-Coupez, M. Guéguen, J. E. Guerchais, F. Y. Pétillon, J. Talarmin and R. Mercier, *J. Organomet. Chem.*, 1986, **312**, 81–95; (*b*) M. El Khalifa, F. Y. Pétillon, J.-Y. Saillard and J. Talarmin, *Inorg. Chem.*, 1989, **28**, 3849–3855.

47 J. P. Collman, R. K. Rothrock, R. G. Finke, E. J. Moore and F. Rose-Munch, *Inorg. Chem.*, 1982, **21**, 146–156.

48 J. Y. Cabon, C. Le Roy, K. W. Muir, F. Y. Pétillon, F. Quentel, P. Schollhammer and J. Talarmin, *Chem.–Eur. J.*, 2000, **6**, 3033–3042.

49 L. E. Bogan, Jr, D. A. Lesch and T. B. Rauchfuss, *J. Organomet. Chem.*, 1983, **250**, 429–438.

50 D. Seyferth, G. B. Womack and R. S. Henderson, *Organometallics*, 1986, **5**, 1568–1575.

51 Programs used: (*a*) G. M. Sheldrick, *SHELXL-97, Program for refinement of crystalstructures*, University of Göttingen, Germany, 1997; G. M. Sheldrick, *SHELXS-97, Program for solution of crystal structures*, University of Göttingen, Germany, 1997; (*b*) L. J. Farrugia, WINGX-A Windows Program for Crystal Structure Analysis, *J. Appl. Crystallogr.*, 1999, **32**, 837; (*c*) DENZO-SCALEPACKZ. Otwinowski and W. Minor, in *Methods in Enzymology Macromolecular Crystallography*, ed. C. W. Carter, Jr and R. M. Sweet, Academic Press, 1997, vol. 276 Part A, pp. 307–326.

52 M. J. Frisch, G. W. Trucks, H. B. Schlegel, G. E. Scuseria, M. A. Robb, J. R. Cheeseman, J. A. Montgomery, Jr., T. Vreven, K. N. Kudin, J. C. Burant, J. M. Millam, S. S. Iyengar, J. Tomasi, V. Barone, B. Mennucci, M. Cossi, G. Scalmani, N. Rega, G. A. Petersson, H. Nakatsuji, M. Hada, M. Ehara, K. Toyota, R. Fukuda, J. Hasegawa, M. Ishida, T. Nakajima, Y. Honda, O. Kitao, H. Nakai, M. Klene, X. Li, J. E. Knox, H. P. Hratchian, J. B. Cross, V. Bakken, C. Adamo, J. Jaramillo, R. Gomperts, R. E. Stratmann, O. Yazyev, A. J. Austin, R. Cammi, C. Pomelli, J. Ochterski, P. Y. Ayala, K. Morokuma, G. A. Voth, P. Salvador, J. J. Dannenberg, V. G. Zakrzewski, S. Dapprich, A. D. Daniels, M. C. Strain, O. Farkas, D. K. Malick, A. D. Rabuck, K. Raghavachari, J. B. Foresman, J. V. Ortiz, Q. Cui, A. G. Baboul, S. Clifford, J. Cioslowski, B. B. Stefanov, G. Liu, A. Liashenko, P. Piskorz, I. Komaromi, R. L. Martin, D. J. Fox, T. Keith, M. A. Al-Laham, C. Y. Peng, A. Nanayakkara, M. Challacombe, P. M. W. Gill, B. G. Johnson, W. Chen, M. W. Wong, C. Gonzalez and J. A. Pople, *GAUSSIAN 03 (Revision D.02)*, Gaussian, Inc., Wallingford, CT, 2004.

53 (*a*) A. D. Becke, *J. Chem. Phys.*, 1993, **98**, 5648–5652; (*b*) P. J. Stevens, J. E. Devlin, C. F. Chabalowski and M. J. Frisch, *J. Phys. Chem.*, 1994, **98**, 11623–11627; (*c*) C. Lee, W. Yang and R. G. Parr, *Phys. Rev. B*, 1988, **37**, 785–789.

54 M. Dolg, U. Wedig, H. Stoll and H. Preuss, *J. Chem. Phys.*, 1987, **86**, 866–872.

DOI: 10.1002/ejic.200800766

A Proton-Triggered Cascade Reaction Involving a Heavy p-Block Multiple Bond: Transformation of the Diphosphene $C_5Me_5P{=}PC_5Me_5$ into the Cationic Cage $[C_{10}Me_{10}P_2H]^+$

Oliver C. Presly,[a] Thomas J. Davin,[b] Michael Green,*[a] Richard J. Kilby,[a] Stephen M. Mansell,[a] John E. McGrady,[b] and Christopher A. Russell*[a]

Keywords: Cascade / Heavy p-block multiple bonds / Phosphorus / Cage compounds

Protonation of one of the phosphorus centers of the diphosphene $C_5Me_5P{=}PC_5Me_5$ triggers a remarkable cascade reaction leading to the direct formation of a $C_{10}P_2$ cage. Calculations suggest that the key mechanistic feature is the proximity of a C=C π-system to a developing positive charge on one of the phosphorus centers.

Yoshifuji and Inamoto's seminal report of the synthesis and isolation of the diphosphene mes*P=Pmes* (**A**, mes* = 2,4,6-tri-*tert*-butylphenyl)[1] exploded the myth that such bonds could not exist under ambient conditions. Much effort over the past quarter of a century has aimed to explore the reactivity of this unusual class of compound, but the simple classification of reactivity in the way that has been achieved in organic chemistry has been hampered by the lack of mechanistic insight. Our own interest in this topic derived from our recent report[2] that the addition of the low oxidation state group 13 halides InCl or "GaI" to $C_5Me_5PCl_2$ (**1**) results (Scheme 1) in the quantitative and stereoselective formation of the diphosphorus cages $[C_{10}Me_{10}P_2X]^+[MX_nCl_{4-n}]^-$ (**2**, M = Ga, X = I, n = 0–4; **3**, M = In, X = Cl). We were intrigued by the fact that the cores of **2** and **3** are isomeric with the well-known diphosphene $C_5Me_5P{=}PC_5Me_5$ (**4**),[3,4] although the nature of the bonding in the two cases is clearly completely different. The $(CR)_{10}P_2$ unit is also isolobal with the hydrocarbon $C_{12}H_{12}$, the isomers of which have been the subject of numerous studies, both experimental and theoretical.[5]

The cage species **2** and **3** can be viewed, at least formally, as adducts of a neutral $C_{10}P_2$ unit with a Cl^+ ion, and this led us to wonder whether it might be possible to access the isolated cage by triggering a cascade reaction[6] through protonation of the P=P double bond in **4**. In this respect we were encouraged by the previous reports that Inamoto's mesityl diphosphene, **A**, reacts with HBF_4 to form a phosphacycle[7,8] and is also methylated by $MeOSO_2CF_3$,[9] although strongly forcing conditions in the form of a 35-fold excess of the methylating reagent are required to drive this.

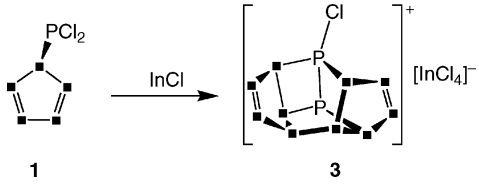

Scheme 1. ■ = CMe.

Reaction of a bright yellow CH_2Cl_2 solution of **4** with an equimolar amount of triflic acid (CF_3SO_3H) at 0 °C results in a yellow/brown solution of **5**. The reaction is quantitative and essentially instantaneous even when the temperature is reduced to –78 °C. The ^{31}P NMR spectrum of the reaction mixture showed two resonances resulting from an HP–P unit [δ = 24.0 (dd, $^1J_{PP}$ = 179, $^1J_{PH}$ = 425 Hz), 14.6 (dd, $^1J_{PP}$ = 179, $^2J_{PH}$ 15 Hz) ppm],[10] both of which are shifted considerably upfield from that of **4** (singlet at δ = 504.0 ppm). The ^{31}P NMR spectrum of the resulting product is also wholly different from that of the methylation product of **A**[1] reported by Grützmacher et al.[9] [δ = 237.0 (d), 332.2 (d) ppm, $^1J_{PP}$ = 633 Hz],[9] and from that of the phosphacycle synthesised by Cowley et al.[7,8] by protonation of **A**. The ^{31}P and ^1H NMR spectra were, however, highly reminiscent of the corresponding spectra of **2** and **3** [for **2**: δ = 68.7 (d), 29.0 (d) ppm, $^1J_{PP}$ = 231 Hz; for **3**: δ = 126.5 (d), 24.7 (d) ppm, $^1J_{PP}$ = 246 Hz; both show ten separate signals for methyl groups in their respective ^1H NMR spectra].[2] This led us to speculate that the product **5** might be $[C_{10}Me_{10}P_2H]^+[OSO_2CF_3]^-$ (Scheme 2) containing a $C_{10}P_2$ cage similar to that found[2] in **2** and **3**. Initial attempts to obtain crystals of **5** suitable for an X-ray crys-

[a] School of Chemistry, University of Bristol, Cantock's Close, Bristol, BS8 1TS, UK
Fax: +44-117-929-0509
E-mail: Chris.Russell@bristol.ac.uk
[b] WestCHEM, University of Glasgow, Joseph Black Building, Glasgow, G12 8QQ, UK
Supporting information for this article is available on the WWW under http://www.eurjic.org or from the author.

tallographic study were unsuccessful, but the relationship between **3** and **5** was confirmed by reduction $\{P^V/P^{III}\}$ of **3** using $HSiCl_3$ and Et_3N,[11] which afforded a quantitative yield of the neutral cage compound $C_{10}Me_{10}P_2$ (**6**). Subsequent protonation of **6** with triflic acid (0 °C, CH_2Cl_2) led to the selective formation of **5** in analytically quantitative yield; this reaction is reversible as treatment of **5** with NEt_3 leads to the quantitative reformation of **6**.

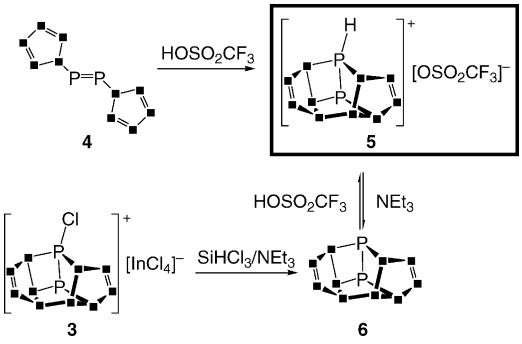

Scheme 2. ■ = CMe.

The neutral cage compound **6**, which is air- and moisture-stable, was characterised by EI mass spectrometry which gave a molecular ion peak at 332 amu and by ^{31}P NMR spectroscopy which showed two doublets characteristic of the P–P bonded cage (δ = 15.9, –13.3 ppm, $^1J_{PP}$ = 148 Hz). Unequivocal confirmation of the structure was provided by a single-crystal X-ray diffraction experiment (see Figure 1). Complex **6** crystallises in the centrosymmetric space group *P*2(1)/*n*, and the diffraction data, although of modest quality, clearly showed the core structure of **6** to be closely related to the cationic cages of **2** and **3**, with the only notable differences being that the P–P and P–C bond lengths to the phosphorus atom of the P–X unit in **2** and **3** are somewhat shorter than the analogous bonds in **6** as a result of the formal positive charge at phosphorus atoms in the cationic cages.[2]

Thus, the experimental data suggests that protonation of the diphosphene **4**, which is isolobal with an alkene, leads to a cascade reaction and the selective formation of the cage compound **5**. Although cascade reactions have played, and will undoubtedly continue to play, an important role in natural product syntheses, the reaction **4** → **5** (Scheme 2) represents a new type of process where a homonuclear heavy p-block multiple bond is an integral component of the process, allowing the construction, in *one* synthetic operation, of the $C_{10}P_2$ cage structure present in **5**; this provides an interesting contrast with the multistep syntheses of the corresponding hydrocarbon systems.[12] Within the wider context of cascade reactions in inorganic chemistry, we note the report by Driess and co-workers of the formation of a phosphonium cage through methylation of a phosphanylidene.[13]

The overall reaction **4** → **5** involves the formation of three strong bonds (two P–C and one C–C), steps that are usually associated with a significant activation barrier. The

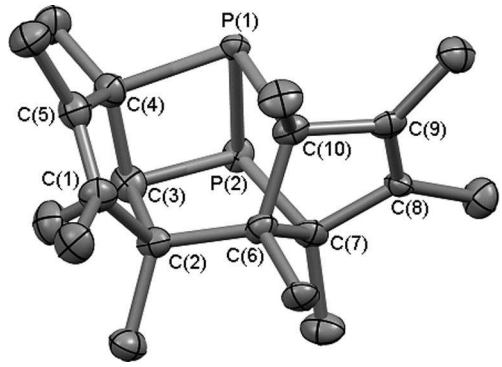

Figure 1. Molecular structure of **6**. Thermal ellipsoids are shown at the 50% probability level. All hydrogen atoms have been removed for clarity. Selected bond lengths [Å] and angles [°]: P(1)–P(2) 2.230(2), P(1)–C(10) 1.888(6), P(1)–C(4) 1.896(7), P(2)–C(7) 1.905(6), P(2)–C(3) 1.933(7), C(7)–C(8) 1.512(9), C(7)–C(6) 1.544(9), C(5)–C(1) 1.532(9), C(5)–C(4) 1.584(9), C(5)–C(6) 1.596(9), C(9)–C(8) 1.336(9), C(9)–C(10) 1.504(9), C(6)–C(10) 1.561(9), C(3)–C(2) 1.489(9), C(3)–C(4) 1.527(10), C(1)–C(2) 1.323(10); C(10)–P(1)–C(4) 93.6(3), C(10)–P(1)–P(2) 92.6(2), C(4)–P(1)–P(2) 78.1(2), C(7)–P(2)–C(3) 101.9(3), C(7)–P(2)–P(1) 89.9(2), C(3)–P(2)–P(1) 77.4(2), C(8)–C(7)–C(6) 103.5(5), C(8)–C(7)–P(2) 99.1(4), C(71)–C(7)–P(2) 112.0(5), C(6)–C(7)–P(2) 108.5(4), C(1)–C(5)–C(4) 101.5(5), C(1)–C(5)–C(6) 110.9(5), C(4)–C(5)–C(6) 106.3(5), C(8)–C(9)–C(10) 109.1(6), C(7)–C(6)–C(10) 97.2(5), C(7)–C(6)–C(5) 115.8(5), C(10)–C(6)–C(5) 108.2(5), C(9)–C(10)–C(6) 103.6(5), C(9)–C(10)–P(1) 106.0(4), C(6)–C(10)–P(1) 101.9(4), C(9)–C(8)–C(81) 127.8(6), C(9)–C(8)–C(7) 109.4(6), C(2)–C(3)–C(4) 105.3(5), C(2)–C(3)–P(2) 112.3(5), C(4)–C(3)–P(2) 97.3(4), C(3)–C(4)–C(5) 101.1(5), C(3)–C(4)–P(1) 99.0(4), C(5)–C(4)–P(1) 108.4(4), C(2)–C(1)–C(5) 111.2(6), C(1)–C(2)–C(3) 110.6(6).

fact that the reaction is instantaneous at –78 °C, with no observable intermediates, prompted us to use density functional theory to explore available pathways for the cascade reaction leading to **5**. For computational expedience we have replaced the methyl groups with hydrogen atoms, and these model compounds are labelled with a prime (′) to distinguish them from the methylated compounds labelled **3**–**6**.

A potential energy surface for the reaction is summarised in Figure 2, along with the optimized structures of the various stationary points. The optimised structure of the cage compound **6′** is in excellent agreement with experiment, with a P–P bond length of 2.28 Å compared to 2.230(2) Å in the X-ray structure. Test calculations using the fully methylated species **6**, confirm that, although the methyl groups increase the steric crowding to some extent, they have no significant impact on the bond lengths of the cage itself. Protonation of **6′** at P(1) to form **5′** causes a contraction of the P–P σ-bond from 2.28 Å to 2.21 Å, but the structure of the remainder of the cage remains largely unchanged. Very similar changes in the carbon/phosphorus cage architecture emerge from a comparison of the crystallographically characterised species **6** and **3**, which are related by formal addition of a Cl^+ ion. Protonation at the other phosphorus center in **6′**, P(2), gives a minimum that lies some 4 kcal mol^{-1} above **5′**, confirming P(1) as the more basic site.

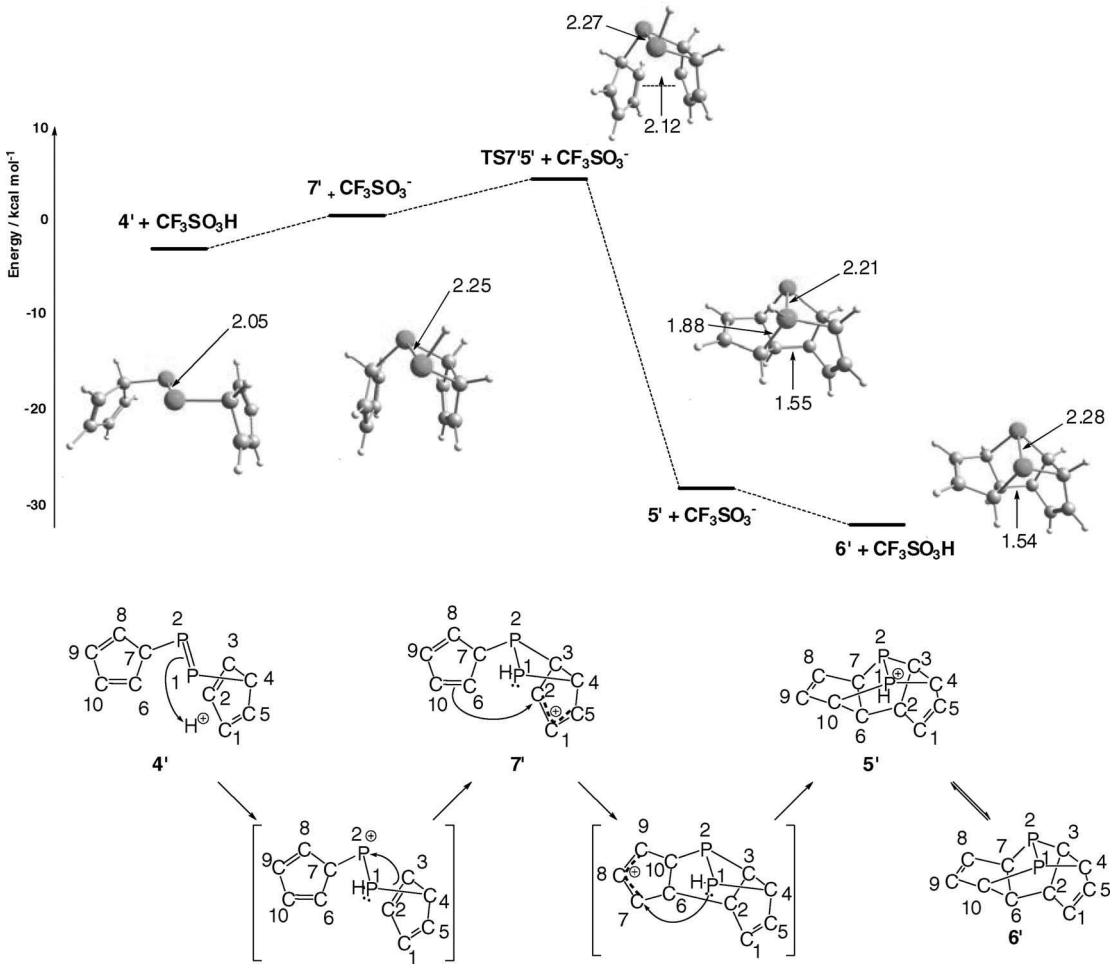

Figure 2. Potential energy surface for the cascade reaction connecting **4′** to **5′**. In the schematic diagrams shown in the bottom half of the figure, the transformations **4′** → **7′** and **7′** → **5′** are broken down into separate steps for clarity, although computationally we find both to be concerted; in addition, CH hydrogen atoms have been omitted for clarity in this part of the figure.

Turning to the overall thermodynamics of the reaction, the cage compound **6′** is 28 kcal mol^{-1} more stable than its P=P double-bonded diphosphene precursor **4′**, indicating that the stability of Jutzi's compound, **4**, in the absence of acid must have kinetic rather than thermodynamic origins. Inclusion of the methyl groups on the five-membered rings reduces the energetic separation (**4** → **6**) to only 5 kcal mol^{-1}, reflecting the greater steric crowding in the cage compound, but the conclusion that the latter is the thermodynamic product remains secure. The energetics of the protonation (**4′** → **7′**) and deprotonation (**5′** → **6′**) steps are referenced to the corresponding reaction of CF_3SO_3H: thus, the reaction **4′** + CF_3SO_3H → **7′** + $CF_3SO_3^-$ is calculated to be endothermic by 4 kcal mol^{-1}, whereas the deprotonation of **5′** is exothermic by the same amount. On this basis, we conclude that, in the presence of triflic acid, protonation/deprotonation will be facile, and in the remainder of the discussion we focus on the course of the reaction *after* the initial protonation step. The most striking observation is that protonation of **4′** at one of the two equivalent phosphorus centers does *not* yield the stable phosphenium cation intermediate shown in square brackets in Figure 2; instead, facile nucleophilic attack by the $C^2{=}C^3$ double bond on the developing cationic phosphorus center leads to intermediate **7′** where the four-membered P_2C_2 ring of **5′** is already formed and the positive charge is delocalized over the allylic unit C^2–C^1–C^5. Critically, then, once protonation occurs, formation of a P–C bond is barrierless. The second step (**7′** → **5′**) then involves nucleophilic attack of a $C^6{=}C^7$ double bond from the other five-membered ring on the allylic cation, leading to formation of both the C^6–C^2 and P^1–C^7 bonds (in Figure 2, the hypothetical structure that would result from formation of only the C^6–C^2 bond is shown in square brackets, but only **7′** and **5′** correspond to stationary points on the potential energy surface). The barrier to this reaction is very low (3 kcal mol^{-1}, **TS5′7′**) because a simple rotation about the P^2–C^{10} bond is all that is required to bring the two five-membered rings into an almost parallel conformation, where the π-systems can overlap and so form the C^6–C^2 bond.

The importance of H^+ in accelerating the cage-forming reaction is illustrated very clearly by the stability of the diphosphene **4** under aprotic conditions, despite the steep thermodynamic gradient leading to the cluster compound

6. An assessment of the potential energy surface in the absence of protons reveals a more complex mechanism involving electrophilic, rather than nucleophilic, attack by one of the C_5 rings on the P=P double bond leading to a zwitterionic intermediate. This substantial charge separation imposes a much larger barrier to isomerisation (32 kcal mol^{-1}), effectively retarding the process.

In summary, protonation of one of the phosphorus centers of the diphosphene **4** triggers a remarkable cascade reaction leading to the $C_{10}P_2$ cage, the key feature being the proximity of a C=C π-system to a developing positive charge on one of the phosphorus centers.

Experimental Section

General: All experimental procedures were performed under N_2 by using standard Schlenk line and glovebox techniques.

5: Trifluoromethanesulfonic acid, $HOSO_2CF_3$ (0.013 mL, 0.15 mmol) was added dropwise to a solution of $C_5Me_5P{=}PC_5Me_5$ (**4**, 0.05 g, 0.15 mmol) in dichloromethane (4 mL) at 0 °C. The intense yellow color of the starting material immediately dissipated to yield a yellow/brown solution. Compound **5** was produced quantitatively according to ^{31}P NMR spectroscopy. $^{31}P\{^1H\}$ NMR (121.4 MHz, $CDCl_3$, 25 °C): δ = 24.0 (d, J_{PP} = 178.6 Hz), 14.6 (d, J_{PP} = 178.6 Hz) ppm. ^{31}P NMR (162.0 MHz, dichloromethane, 25 °C): δ = 24.0 (dd, J_{PP} = 179, $^1J_{PH}$ = 425 Hz), 14.6 (dd, J_{PP} = 179, $^2J_{PH}$ = 15 Hz) ppm.

6: $SiHCl_3$ (0.51 mL, 5 mmol) was added dropwise to a solution of $[C_{10}Me_{10}P_2Cl][InCl_4]$ (**3**, 5 mmol, 0.5 M in CH_2Cl_2) at room temperature. This was followed by the addition of NEt_3 (0.70 mL, 5 mmol), also dropwise and at room temperature. This caused an immediate color change from deep red to yellow. The solvent was removed in vacuo and the product extracted into *n*-hexane (20 mL). The resulting pale yellow solution was filtered (porosity 3 sinter with Celite), reduced in volume and left to crystallise at –18 °C. **6** was produced quantitatively according to ^{31}P NMR spectroscopy and was isolable in a 55% crystalline yield. M.p. 138–142 °C (to form a yellow oil). $^{31}P\{^1H\}$ NMR (121.4 MHz, $CDCl_3$, 25 °C): δ = 15.9, (d, J_{PP} = 148 Hz), 13.3 (d, J_{PP} = 148 Hz) ppm. EI-MS: *m*/*z* = 332 [M$^+$]. $C_{20}H_{30}P_2$ (332): calcd. C 72.27, H 9.10; found C 72.47, H 9.09.

Single-Crystal X-ray Diffraction Data for 6: $C_{20}H_{30}P_2$, M_r = 332.38 g mol^{-1}, crystal dimensions 0.2 × 0.1 × 0.05 mm, monoclinic, space group $P2(1)/n$, a = 7.958(2) Å, b = 16.827(3) Å, c = 13.471(3) Å, β = 92.55(3)°, V = 1802.1(6) Å^3, Z = 4, $\rho_{calcd.}$ 1.225 Mg/m^3, μ = 0.237 mm^{-1}, θ = 1.94–27.48°, measured reflections 20248, independent reflections 4133, R_{int} = 0.0780, R_1 ($I > 2\sigma$) = 0.1323, wR_2 (all data) = 0.2936. Diffraction data were collected at 100(2) K with a Bruker SMART APEX CCD diffractometer using Mo-K_α radiation (λ = 0.71073 Å). The structure was solved by direct methods and refined by full-matrix least squares using the SHELX suite of programs.[14] All non-hydrogen atoms were refined anisotropically. Despite repeated attempts, only poor-quality crystals were available, and hence the data set is relatively weak. CCDC-691307 contains the supplementary crystallographic data for this paper. These data can be obtained free of charge from the Cambridge Crystallographic Data Center via www.ccdc.cam.ac.uk/data_request/cif.

Computational Methodology: Full geometry optimizations were performed with the B3LYP functional[15] using 6-31G* basis sets on all atoms.[16] Transition states were located with the STQN algorithm[17] and all stationary points were characterized as minima or first order saddle points by their harmonic vibrational frequencies. All calculations were carried out with the Gaussian03 series of programs.[18] Total energies include solvation contributions (CH_2Cl_2 solvent) computed with the PCM approach at the gas-phase optimised structures.[19]

Supporting Information (see footnote on the first page of this article): Energies and cartesian coordinates for all stationary points reported in Figure 2.

Acknowledgments

We thank the University of Bristol (M. G., C. A. R., S. M. M., O. C. P.) and the EPSRC (R. J. K.) for financial support.

[1] M. Yoshifuji, I. Shima, N. Inamoto, K. Hirotsu, T. Higuchi, *J. Am. Chem. Soc.* **1981**, *103*, 4587–4589.
[2] O. C. Presly, M. Green, J. C. Jeffery, E. Leiner, M. Murray, C. A. Russell, M. Scheer, U. Vogel, *Chem. Commun.* **2006**, 4542–4544.
[3] P. Jutzi, U. Meyer, B. Krebs, M. Dartmann, *Angew. Chem. Int. Ed. Engl.* **1986**, *25*, 919–921.
[4] P. Jutzi, T. Wippermann, *J. Organomet. Chem.* **1985**, *287*, C5–C7.
[5] J. D. Dunitz, G. Fillipini, A. Gavezzotti, *Helv. Chim. Acta* **2000**, *83*, 2317–2335.
[6] For a general review, see: K. C. Nicolaou, D. J. Edmonds, P. G. Bulger, *Angew. Chem. Int. Ed.* **2006**, *45*, 7134–7186.
[7] A. H. Cowley, J. E. Kilduff, N. C. Norman, M. Pakulski, J. L. Atwood, W. E. Hunter, *J. Am. Chem. Soc.* **1983**, *105*, 4845–4846.
[8] A. H. Cowley, J. E. Kilduff, N. C. Norman, M. Pakulski, *J. Chem. Soc., Dalton Trans.* **1986**, 1801–1808.
[9] S. Loss, C. Widauer, H. Grützmacher, *Angew. Chem. Int. Ed.* **1999**, *38*, 3329–3331.
[10] The same ^{31}P NMR spectrum is observed when using a solution of HBF_4 in diethyl ether as the reagent, but no reaction is observed when using HCl in diethyl ether. Attempts to use other electrophiles, e.g. by reaction of **4** with MeOTf, resulted in a multitude of products whose identity we have not been able to discern.
[11] This reaction must proceed by broadside attack at the cationic phosphorus center.
[12] C. H. Lee, S. L. Liang, T. Haumann, R. Boese, A. Demeijere, *Angew. Chem. Int. Ed. Engl.* **1993**, *32*, 559–561.
[13] M. Driess, N. Muresan, K. Merz, M. Päch, *Angew. Chem. Int. Ed.* **2005**, *44*, 6734–6737.
[14] G. M. Sheldrick, *Acta Crystallogr.* **2008**, *A64*, 112–122.
[15] a) A. D. Becke, *J. Chem. Phys.* **1993**, *98*, 5648–5652; b) P. J. Stevens, J. F. Devlin, C. F. Chabalowski, M. J. Frisch, *J. Phys. Chem.* **1994**, *98*, 11623–11627; c) C. Lee, W. Yang, R. G. Parr, *Phys. Rev. B* **1988**, *37*, 785–789.
[16] a) P. C. Hariharan, J. A. Pople, *Mol. Phys.* **1974**, *27*, 209–214; b) M. M. Francl, W. J. Petro, W. J. Hehre, J. S. Binkley, M. S. Gordon, D. J. DeFrees, J. A. Pople, *J. Chem. Phys.* **1982**, *77*, 3654–3665.
[17] C. Peng, P. Y. Ayala, H. B. Schlegel, M. J. Frisch, *J. Comput. Chem.* **1996**, *17*, 49–56.
[18] M. J. Frisch, G. W. Trucks, H. B. Schlegel, G. E. Scuseria, M. A. Robb, J. R. Cheeseman, J. A. Montgomery Jr, T. Vreven, K. N. Kudin, J. C. Burant, J. M. Millam, S. S. Iyengar, J. Tomasi, V. Barone, B. Mennucci, M. Cossi, G. Scalmani, N. Rega, G. A. Petersson, H. Nakatsuji, M. Hada, M. Ehara, K. Toyota, R. Fukuda, J. Hasegawa, M. Ishida, T. Nakajima, Y. Honda, O. Kitao, H. Nakai, M. Klene, X. Li, J. E. Knox, H. P. Hratchian, J. B. Cross, V. Bakken, C. Adamo, J. Jaramillo, R. Gom-

perts, R. E. Stratmann, O. Yazyev, A. J. Austin, R. Cammi, C. Pomelli, J. W. Ochterski, P. Y. Ayala, K. Morokuma, G. A. Voth, P. Salvador, J. J. Dannenberg, V. G. Zakrzewski, S. Dapprich, A. D. Daniels, M. C. Strain, O. Farkas, D. K. Malick, A. D. Rabuck, K. Raghavachari, J. B. Foresman, J. V. Ortiz, Q. Cui, A. G. Baboul, S. Clifford, J. Cioslowski, B. B. Stefanov, G. Liu, A. Liashenko, P. Piskorz, I. Komaromi, R. L. Martin, D. J. Fox, T. Keith, M. A. Al-Laham, C. Y. Peng, A. Nanayakkara, M. Challacombe, P. M. W. Gill, B. Johnson, W. Chen, M. W. Wong, C. Gonzalez, J. A. Pople, *Gaussian 03*, Revision D.02, Gaussian, Inc., Wallingford CT, **2004**.

[19] M. T. Cancès, B. Mennucci, J. Tomasi, *J. Chem. Phys.* **1997**, *107*, 3032–3041.

Received: July 31, 2008
Published Online: September 4, 2008

